APPLICATION OF ROTORCRAFT FLIGHT SIMULATION PROGRAM (C81) TO PREDICT ROTOR PERFORMANCE AND BENDING MOMENTS FOR A MODEL FOUR-BLADED ARTICULATED ROTOR SYSTEM

F. D. Freeman, et al

Bell Helicopter Company

Prepared for:

Army Air Mobility Research and Development Laboratory

November 1974

EUSTIS DIRECTORATE POSITION STATEMENT

This report has been reviewed by the Eustis Directorate, U. S. Army Air Mobility Research and Development Laboratory and is considered to be technically sound. The purpose of this program was to verify the capability of the Rotorcraft Flight Simulation Program (C-81) to predict rotor performance and load through correlation with model rotor data. Results are inconclusive due to problems apparently related to three-dimensional and/or unsteady effects, which are especially significant for model scale rotors and which are not fully understood in the state of the art.

The program was conducted under the technical management of Edward E. Austin of the Technology Applications Division.

Unclassified
SECURITY CLASSIFICATION OF THIS PAGE (When Data Entered)

REPORT DOCUMENTATION PAGE	READ INSTRUCTIONS BEFORE COMPLETING FORM
1. REPORT NUMBER: USAAMRDL-TR-74-70	2. GOVT ACCESSION NO.
3. RECIPIENT'S CATALOG NUMBER: AD/A-004015	
4. TITLE (and Subtitle): APPLICATION OF ROTORCRAFT FLIGHT SIMULATION PROGRAM (C81) TO PREDICT ROTOR PERFORMANCE AND BENDING MOMENTS FOR A MODEL FOUR-BLADED ARTICULATED ROTOR SYSTEM	5. TYPE OF REPORT & PERIOD COVERED: Final, Jan73 - Jul74
	6. PERFORMING ORG. REPORT NUMBER: 299-099-691
7. AUTHOR(s): F. D. Freeman, K. L. Bennett	8. CONTRACT OR GRANT NUMBER(s): Contract DAAJ02-72-C-0086
9. PERFORMING ORGANIZATION NAME AND ADDRESS: Bell Helicopter Company, P. O. Box 482, Ft. Worth, Tex. 76101	10. PROGRAM ELEMENT, PROJECT, TASK AREA & WORK UNIT NUMBERS: Project 1F163204D157
11. CONTROLLING OFFICE NAME AND ADDRESS	12. REPORT DATE: November 1974
	13. NUMBER OF PAGES: 260
14. MONITORING AGENCY NAME & ADDRESS (if different from Controlling Office): Eustis Directorate, U. S. Army Air Mobility Research & Development Laboratory, Fort Eustis, Va. 23604	15. SECURITY CLASS. (of this report): Unclassified
	15a. DECLASSIFICATION/DOWNGRADING SCHEDULE

16. DISTRIBUTION STATEMENT (of this Report)

Approved for public release; distribution unlimited.

17. DISTRIBUTION STATEMENT (of the abstract entered in Block 20, if different from Report)

DDC
DISTRIBUTED
JUL 23 1975
DISTRIBUTED
D

18. SUPPLEMENTARY NOTES

19. KEY WORDS (Continue on reverse side if necessary and identify by block number)

Aerodynamics, Simulation, Dynamics, Aeroelasticity, Helicopter Rotors

20. ABSTRACT (Continue on reverse side if necessary and identify by block number)

Four sets of model H-34 helicopter rotor blades were built and tested by the Sikorsky Aircraft Corporation. Rotorcraft Flight Simulation Program with Aeroelastic Rotor Representation, Program C81, was used to predict rotor performance and blade bending moments for comparison with the test results. Performance predictions made using the steady-state two-dimensional airfoil data (GFE) supplied by the Army for the model airfoils showed stall

DD FORM 1 JAN 73 1473 EDITION OF 1 NOV 65 IS OBSOLETE

Unclassified
SECURITY CLASSIFICATION OF THIS PAGE (When Data Entered)

characteristics at much lower rotor lift levels than recorded in the tunnel test. Application of unsteady aerodynamic and yawed flow effects did not sufficiently improve the performance correlation. The lift and stall characteristics of the model rotor in the tunnel were found to be very similar to full-scale (R_N = 12 x 10^6) 0012 airfoil properties.

Accordingly, a modified airfoil table was used to predict bending moments. The modified airfoil table employed a full-scale 0012 lift table, the GFE model drag table with an increment of C_D = 0.003 added to all values, and a null pitching moment table.

Bending moment correlation was made using the modified airfoil tables in the calculations. These comparisons are presented as time histories and as harmonic analyses. Calculated loads show good agreement with measured loads for the fiberglass blade set having -8 degrees of twist. The other blade set computations are less satisfactory. Generally, calculated loads are lower in magnitude than measured loads and do not have the higher harmonic content of the measured bending moments.

A correlation criterion and a sensitivity analysis were developed to analyze the results of the correlation study. The correlation criterion was applied to the performance comparisons. Applications to the loads comparisons were not made because it became evident in the latter stages of the project that the method did not represent load differences in a useful manner.

TABLE OF CONTENTS

LIST OF ILLUSTRATIONS

LIST OF TABLES

DESCRIPTION OF COMPUTER PROGRAM

Rotor performance and loads for this project were calculated by Rotorcraft Flight Simulation with Aeroelastic Rotor Representation, Program C81. This program was delivered to the U. S. Army under Contract DAAJ02-70-C-0063. The program is completely described in Reference (1). Following is a brief summary of the program.

Program C81 is a general-purpose rotorcraft flight simulation program capable of analyzing an entire rotorcraft in level or maneuvering flight. However, for the purposes of this study, only the rotor simulation capability was used. The rotor simulation is divided into a trim procedure and a loads calculation portion. The trim procedure iterates on the independent variables (collective pitch, fore and aft and lateral cyclic pitch, and fore and aft and lateral flapping angles) to balance the forces and moments acting on the rotor. For this project, the program trim procedure was modified to iterate to those control positions necessary to give zero fore and aft and lateral flapping. After a trimmed flight condition is obtained, the rotor loads calculations are performed as described below.

The rotor loads procedure is a fully coupled time-variant aeroelastic analysis based on the modal technique. Modes and natural frequencies must be calculated in a separate program and input into Program C81. The modes and natural frequencies used in this study were generated by a program based on the Myklestad procedure.

For a specified rotor speed, the Myklestad program generates a set of fully coupled modes having beam, chord, and torsional components as a function of control system stiffness; blade twist; beam, chord, and torsional stiffness; weight distribution; beam and chord moments of inertia; neutral axis and center-of-gravity locations at twenty radial stations; centrifugal stiffening; centrifugal restoring torsional moment; and hub impedance.

Rotor airloads are calculated by C81 at 20 radial stations for each azimuth location as a function of the local angle of attack and local Mach number to include the effects of stall and compressibility. The effects of both rigid body and elastic displacements and velocities are included in these calculations. Also included at the user's option are nonsteady aerodynamic and yawed flow effects. Airfoil lift, drag, and pitching moment coefficients may be input as tables of discrete values or in equation form.

Inertia forces due to the unsteady motion of the frame of reference and calculated airloads are summed to form the forcing function portion of the modal equations. The total time-variant response of the blade is then obtained by summing the response of each input mode shape. Bending moments are computed by summing the products at each radial station of modal bending moment coefficients and modal participation factors. The bending moment coefficients for each mode are computed as a function of blade mass, rotor speed, mode shape, and mode natural frequency by considering the moments generated by the inertia forces and centrifugal forces.

Rotor performance and blade bending moment information is presented at the end of each Program C81 simulation. The performance information is given in both dimensional and nondimensional form. Bending moments are presented as sine and cosine harmonic analysis components. A complete time history of any rotor performance and load calculations may be obtained by entering the maneuver portion of the program. This section numerically integrates the equations of motion to give the time history, which may be plotted either as printer plots or as CALCOMP plots.

DESCRIPTION OF BLADE PROPERTIES

The blade dynamic and aerodynamic data were obtained by Sikorsky Aircraft Corporation under Contract DAAJ02-72-C-0026. The complete description of the experimental techniques is described in Reference (2). These data are summarized below.

DYNAMIC PROPERTIES

The model rotor blades examined in this project were scaled from the Sikorsky H-34 helicopter rotor system. The geometric scale factor applied was 6.109. The four blades are described as follows:

1. Fiberglass spar, zero twist
2. Fiberglass spar, -8° uniform twist
3. Fiberglass spar, zero twist with 5° trailing-edge flap (over aft 20% of chord)
4. Aluminum spar, zero twist

All blade sets had the same nominal weight and inertia distributions. The aluminum blades, however, were approximately three times stiffer than the fiberglass blades. Blade stiffness, inertia, and geometry information are given in Tables 1 through 4.

The tabulated blade stiffness and inertia properties were apportioned in twenty equal segments to match the input format of Program C81. These equal segment length data are shown in Tables 5, 6, and 7. Calculated frequencies and generalized inertias are given in Table 8. Blade inertia and center of gravity values were apportioned on a pro rata basis. The unequal segment length stiffness values were combined into equal segment length values by using the following relation:

$$\frac{\ell_1 + \ell_2 + \cdots + \ell_{n-1} + \ell_n}{EI_{EQ}} = \frac{\ell_1}{EI_1} + \frac{\ell_2}{EI_2} + \cdots + \frac{\ell_n}{EI_n} \quad (1)$$

where

I_{EQ} = an equivalent area moment of inertia for a beam composed of n subsequents having different area moments of inertia, I_1, I_2, ..., I_n, and lengths ℓ_1, ℓ_2, ..., ℓ_n.

This procedure yields an equivalent beam segment which rotates an amount equal to that of a beam made up of the n subsegments when both beams are subjected to the same moment.

AERODYNAMIC PROPERTIES

Two sets of aerodynamic data are presented for this project. These are the model two-dimensional airfoil data and the modified airfoil data used for loads predictions (explained and presented in the Model Rotor Aerodynamic Investigation section of this report).

The model lift, drag, and pitching moment coefficients are presented in Figures 1, 2, and 3 for the symmetrical (unflapped) blade section and in Figures 4, 5, and 6 for the blade section having the 5° trailing-edge flap. The full-scale 0012 lift table characteristics used in the modified airfoil table are presented in the Model Rotor Aerodynamic Investigation section of this report.

PRETEST PREDICTIONS

PRELIMINARY CALCULATIONS

The two baseline conditions for performance calculation were chosen to be (1) $\mu = 0.30$, $M = 0.40$, and $C_L/\sigma = 0.082$, and (2) $\mu = 0.40$, $M = 0.438$, and $C_L/\sigma = 0.045$. These baseline points were selected because they appeared to be representative of the conditions contained in Reference (3).

Computer Program C81 was used to make initial performance calculations. The results obtained are shown in Figure 7, which illustrates that the predicted stall is much below the scheduled $C_L/\sigma = 0.082$. As a result of these calculations, the scheduled C_L/σ values were reduced by 40 percent. The baseline conditions were then $C_L/\sigma = 0.049$ and $C_L/\sigma = 0.027$. Also shown in Figure 7 are calculations made using the full-scale 0012 airfoil tables contained in C81 and measured results for the fiberglass blade with -8° twist. These two items will be discussed later in the text.

VARIATIONS ABOUT BASELINE CONDITIONS

One hundred sixty-two C81 trim cases were completed to match the scheduled wind-tunnel test points. These cases were performed about the baseline trim points for the fiberglass blade with -8° twist to determine the sensitivity of performance and loads to variations ($\pm 2^\circ$) in mast tilt, collective pitch, longitudinal and lateral cyclic pitch. These cases are analyzed in the Initial Rotor Performance Correlation section of this report. The baselines for the fiberglass, -8° twist blade are given in Figure 8.

Additional cases were calculated for each baseline condition for the three other sets of blades which were not included in the 162 cases. These additional trim cases are presented in Figures 9, 10, and 11.

CORRELATION CRITERION

A correlation criterion must exist to judge comparisons of experimental data and calculated predictions. This section describes the criterion used to quantify the results of this project.

Performance and bending moment data may be compared point to point or statistically, using curve fits to relate results. Each method has its benefits and drawbacks. Point-to-point comparisons yield readily understandable results for each set of points examined, but they do not indicate trends. A statistical representation compacts large amounts of information and describes trends; but, when taken alone, it tends to hide individual deviations. Therefore, use of both procedures is advisable.

A quality factor, abbreviated q, is used with the point-to-point and statistical comparisons. For point-to-point comparisons, a percentage of difference is used, given by

$$q = \frac{|\text{measured} - \text{computed}|}{\text{measured}} \times 100\% \qquad (2)$$

The statistical approach involves a different definition, which is given later in this section. Ranges of q are given in Table 9 . These values were picked from experience considering the ranges of accuracy needed by the designer.

The basis of the statistical method is to plot like quantities (having the same independent parameters, μ, $M_{1,90}$, $\theta_{3/4}$, and α_m) of measured data versus computed predictions and to fit a first-order least-squared error criterion curve fit through the points. The correlation criterion may then be applied to the parameters describing the fitted line. The line has three properties which describe its relation to the data. These are its slope, intercept, and the scatter of data about the line. If measured data (y) is plotted against computed predictions (x), a line fitted through the points using the least-squared error criterion will have the following form:

$$y' = ax + b \qquad (3)$$

where

y' = the predicted value of y

$$a = \frac{\Sigma xy - n\bar{x}\bar{y}}{\Sigma x^2 - n\bar{x}^2} \tag{4}$$

$$b = \frac{\bar{y}\,\Sigma\, x^2 - \bar{x}\,\Sigma\, xy}{\Sigma x^2 - n\bar{x}^2} \tag{5}$$

and

$$n = \text{the number of samples} \tag{6}$$

A correlation coefficient may be defined as

$$r^2 = 1 - \frac{S_e^2}{S_y^2} \tag{7}$$

where

$$r = \text{the linear correlation coefficient} \tag{8}$$

$$S_e^2 = \Sigma \frac{(y-y')^2}{n-1}\text{ , the variance of the estimate} \tag{9}$$

$$\bar{y} = \frac{\Sigma y}{n}\text{ , the mean of the data} \tag{10}$$

$$S_y^2 = \Sigma \frac{(y-\bar{y})^2}{n-1}\text{ , the variance of the data about its mean.} \tag{11}$$

The quantity r^2 may be interpreted as the percentage of the variance (S_y^2) which is contributed by the fitted linear relation for y'. It is, therefore, a statistic which describes the usefulness of the fitted line for estimating purposes.

Perfect correlation, according to the preceding definitions, is represented by a = 1, b = 0, and r = 1. The terms a and r are independent of the magnitude of the variables; however, b is magnitude dependent. Therefore, b is normalized by the average value of the independent variable and subtracted from one so that unity will continue to represent perfect correlation. The term b is replaced by

$$b' = 1 - b/\bar{x} \tag{12}$$

The quality factor may now be defined (in a percentage of error sense) to be

$$q_a = (1-a) \times 100\% \text{ for } a < 1$$

or

$$q_a = (a-1) \times 100\% \text{ for } a > 1 \qquad (13)$$

$$q_b = (1-b') \times 100\% = b/\bar{x} \times 100\% \qquad (14)$$

$$q_r = (1 - r) \times 100\% \qquad (15)$$

The quality factory, q, may then be judged by the stated criteria given in Table 9.

The procedure described here follows Hoel, "Introduction to Mathematical Statistics" (Reference 4).

INITIAL ROTOR PERFORMANCE CORRELATION

Because of the large quantity of data, and the possibility that the actual wind tunnel test points would not match those used in the previous calculations, statistical techniques were used to analyze the data. The following data were subjected to a multiple correlation analysis:

Independent Variables	Dependent Variables
μ, M, α_{mast}, $\theta_{3/4}$, a_1, b_1	C_L/σ, C_D/σ, C_Y/σ
A_1, B_1, α_{TPP}	C_l/σ, C_m/σ, C_n/σ

For a specified dependent variable, the multiple correlation analysis picks, in order of descending importance, the independent variables that may be used in a linear combination to express the dependent variable. Within the 162 computer cases run, the rotor lift can be statistically represented by

$$C_L/\sigma_{calc} = .00824 + .004\,\alpha_{TPP} + .00693\,\theta_{3/4} \qquad (16)$$

The multiple correlation coefficient for the above equation is r = 0.951, which means that $(.951)^2 \times 100 = 90.5\%$ of all variations of C_L/σ can be represented by variation in α_{TPP} and $\theta_{3/4}$. The standard error is $S_e = 0.009$, which can be interpreted as a confidence limit that the computed C_L/σ will be within +0.009 of the value predicted by the above equation in 65 percent of the cases and within $\pm 2x(0.009) = \pm 0.018$ in 95 percent of the cases.

All measured data for the fiberglass -8° twist blade were also subjected to the multiple correlation analysis. The results were

$$C_L/\sigma_{meas} = .01854 + .00456\,\alpha_{TPP} + .0066\,\theta_{3/4} \qquad (17)$$

with a correlation coefficient of r = 0.911

The calculated and measured lift coefficients may be compared by examination of the above relations. The partial derivatives giving the rate of change of lift with respect to tip path plane attack angle and collective setting are within 12 percent. The difference between the constant terms is

due to the low values of $C_{L_{max}}$ in the 2-D wind tunnel data.

The analysis was performed on the calculated and measured power. The results were as follows:

$$C_P/\sigma_{meas} = 0.00006 + .00069\ \theta_{3/4} + .00010\ \alpha_{TPP} \qquad (18)$$
$$r = 0.928$$

$$C_P/\sigma_{calc} = 0.00020 + .00061\ \theta_{3/4} + .00015\ \alpha_{TPP} \qquad (19)$$
$$r = 0.960$$

It should be recalled that the correlation analysis is based on linear theory and, therefore, any nonlinear relationship among the variables is deleted. Since the multiple correlation analysis is free to select any of nine independent variables, it is significant that collective pitch and tip path angle of attack were always selected as the best predictors of rotor thrust and power. The fact that these selections were made for both the measured and calculated values tends to validate the mathematical model of the rotor.

The statistical representation of the measured and calculated gross rotor performance is shown in Figures 11 and 12. The computed results used in this analysis are tabulated in Table 9. The computer subroutines used in the multiple regression analysis are described in Reference (5).

SENSITIVITY ANALYSIS

An analysis was developed to relate the sensitivity of predicted results to input parameter variations. Twenty-six individual variations of significant input parameters were made for the two baseline correlations ($C_L/\sigma = 0.049$ and $C_L/\sigma = 0.027$) using the model aerodynamic data. However, as explained in the Performance Comparisons Section of this report, the program could not accurately represent the model rotor tunnel behavior using the model steady aerodynamic data. This fact, coupled with apparent discrepancies in the model two-dimensional data apart from any program considerations, made the sensitivity analysis calculations generally suspect. Consequently, these calculations are not presented in this report. However, the mathematical procedure for the sensitivity study is considered valid and very useful for future studies. Therefore, the analysis is presented here for information only.

If the standard deviation for an input, x_i, is σ_i, then the standard deviation of an output quantity, y, may be written

$$\sigma_y^2 = \sum_{i=1}^{n} \left(\frac{\partial y}{\partial x_i} \sigma_i \right)^2 \tag{20}$$

where

$$n = \text{number of input variables, } x \tag{21}$$

$$\frac{\partial y}{\partial x_i} = \text{rate of change output, y, with respect to input, } x_i. \tag{22}$$

To employ this method, a value must be assigned to each input parameter standard deviation. These values should be assigned from the results of a large sample test of the values of each quantity. Lacking this information, a judgment must be made to relate the standard deviation to confidence levels (given in plus and minus percent error about a nominal value).

If, after the determination of σy, the computed value and measured value of y are compared and are such that

$$\left| y - y_{measured} \right| < 2\sigma y \tag{23}$$

then there is a 95 percent probability that the variation between the measured and computed values is due to input parameter variation.

The method given here follows Bendat and Piersol (Reference 6).

POSTTEST PERFORMANCE CORRELATION

Performance comparisons of calculated and measured results were made for the following cases:

	μ	$M_{1,90}$
Fiberglass blade, -8° twist, $\delta_F = 0^\circ$	0.299	0.408
	0.400	0.435
	0.502	0.467
Fiberglass blade, 0° twist, $\delta_F = 0^\circ$	0.299	0.408
Fiberglass blade, 0° twist, $\delta_F = 5^\circ$	0.299	0.408

Comparisons of measured and calculated results are shown in Figures 14 through 33. All calculated results shown in these figures were made using the model airfoil data. Performance comparisons for the aluminum, 0° twist blade are not shown since the analysis used in this portion of the study is a quasi-static analysis (using steady and 1/rev blade response) which does not yield results different from those for the fiberglass, 0° twist blade. Basic comparisons are presented as plots of lift versus control plane angle of attack, power versus lift, measured lift versus calculated lift, and measured power versus calculated power. Measured lift versus calculated lift and measured power versus calculated power are not shown for the fiberglass, -8° twist blade at the $\mu = 0.502$, $M_{1,90} = 0.467$ condition because insufficient measured data were available for a statistical analysis.

Examination of the plots shows that measured and calculated lift values are in close agreement at low collective values. Calculated power is generally lower than measured. As collective pitch increases, the calculated lift shows stall characteristics at a much lower pitch angle than the measured lift. These stall characteristics are best compared in the power versus lift plots. These figures show calculated stall to be extremely abrupt. For instance, in Figure 15 a maximum calculated lift coefficient of $C_L/\sigma = 0.07$ has been reached while calculated power increases asymptotically. Calculated stall is most severe for the blade set with the 5° trailing-edge flap (Figure 31), as expected. The measured stall characteristic for this case is hardly in evidence, no more so than for the unflapped blade at the same condition (Figure 27). Figures 18 and 19 illustrate the effect of the Program C81 unsteady aerodynamic and yawed flow representations on the calculated lift and power for the fiberglass blade with -8°

twist (compare with Figures 14 and 15). Though these effects increase the calculated lift at high collective settings, stall still occurs much more abruptly than in the measured results. Table 10 presents quantitative comparisons of measured and calculated lift and power and also grades the correlation according to the correlation criteria given in Table 9.

Because the measured data examined in this portion of the study showed such delayed stall characteristics when compared with the calculated results using the model data, further investigation was indicated. This investigation took the form of a brief correlation study for a full-scale rotor system and a consideration of the aerodynamics of model rotors. The results of these studies are given in the next two sections.

FULL-SCALE COMPARISONS

Program C81 was used to predict performance and bending moments for a full-scale H-34 rotor system. The experimental data for this comparison are published in USAAVLABS Technical Report 68-3 (Reference 3) and NASA TND-4632 (Reference 7). All blade dynamic properties for these comparisons were estimated from the figures and plots given in TR68-3. The aerodynamic properties were those of standard 0012 tables used at Bell Helicopter.

Performance comparisons for various mast tilt angles are given in Figures 34 through 39. Figures 34 through 36 compare measured and calculated lift, drag, and horsepower with collective pitch as the independent parameter, while Figure 37 shows measured and calculated power versus lift. As may be seen, the calculated performance parameters show very good qualitative agreement with the measured data. Lift error is a maximum of 900 lb for the 0° mast tilt case at $\theta_{3/4} = 2°$, amounting to 18 percent of the measured, and decreases with increasing collective pitch. Drag error is about 500 lb or approximately 30 percent of measured for the 10° mast tilt case. Maximum power error is approximately 200 hp or about 16 percent of measured. Figure 37 illustrates that the full-scale rotor stall characteristics are predicted very accurately.

Figures 38 and 39 compare experimental lift to calculated lift and experimental power to calculated power. This method of presentation allows application of the correlation method described previously. First-order least-squared error criterion prediction lines for each of these plots are described by

$$C_L/\sigma_{meas} = 0.0118 + 0.923\ C_L/\sigma_{calc} \tag{24}$$

with $r = 0.989$ and $C_L/\sigma = 0.061$

and

$$C_P/\sigma_{meas} = 0.0000583 + 1.014\ C_P/\sigma_{calc} \tag{25}$$

with $r = 0.957$ and $C_P/\sigma = 0.00239$.

The quantities a(a'), b(b'), and r (slope, normalized intercept, and correlation coefficient as defined previously) for lift and power may be expressed as

Lift:

$$a = 0.923 \quad (q = 7.8\%) \tag{26}$$

$$b' = 1 - \left(\frac{b}{\bar{C}_L/\sigma}\right) = \left(1 - \frac{0.0118}{0.061}\right) = 0.807 \qquad (27)$$

$(q = 19.3\%)$

$$r = 0.989 \ (q = 1.1\%) \qquad (28)$$

Power:

$$a = 1.014 \ (q = 1.4\%) \qquad (29)$$

$$b' = \left(1 - \frac{b}{\bar{C}_P/\sigma}\right) = \left(1 - \frac{0.0000583}{0.00239}\right) = 0.976 \qquad (30)$$

$(q = 2.44\%)$

$$r = 0.957 \ (q = 4.3\%) \qquad (31)$$

Application of the correlation criterion stated in Table 9 grades the lift slope correlation as good, lift intercept as poor, and lift correlation coefficient as excellent. Application of the criterion to power grades the power slope as excellent, power intercept as excellent, and power correlation as excellent.

Figures 40 and 41 compare measured and computed bending stresses. The Program C81 beamwise stress predictions are higher in the midspan region than the measured, but are in good agreement inboard of r/R = 0.35 and outboard of r/R = 0.70. However, the predicted chordwise stresses are low in the inboard regions and quite good outboard of approximately r/R = 0.40.

MODEL ROTOR AERODYNAMIC INVESTIGATION

This section presents a brief examination of the performance correlation problems described in the Posttest Performance Correlation section. The model rotor aerodynamics were examined and a modified airfoil developed which produced reasonable performance correlation.

Rotor stall characteristics are compared in Figures 42 and 43. Figure 42 presents measured power, computed power (using model data tables), and measured oscillatory moment (at r/R = 0.20) plotted against lift. The case presented is at $\alpha_m = 2^\circ$ to represent a forward flight condition. The plotted power figures are modified by removal of induced power and parasite power to isolate aerodynamic effects. These terms are approximated by simple momentum theory and are not exact. They are

$$\text{Induced power coefficient} = C_{P_i}/\sigma = (C_L/\sigma)^2 \, \sigma/2\mu$$

$$\text{Parasite power coefficient} = C_{P_p}/\sigma = \mu(C_x/\sigma)$$

(where C_x/σ is the rotor x-force coefficient in the wind axes).

Figure 42 clearly illustrates that measured power and measured torsional moment "break" together, further evidence that the phenomenon observed is stall. The computed power breaks well before the measured power. This observation is considered further evidence that computations made with the model airfoil tables do not represent the rotor as it behaves in the tunnel. Figure 43 is another power versus lift plot which presents comparisons of measured data and predictions computed using Program C81 and Program F-35 (Ref. 8), a Bell Helicopter rotor performance program. Both computations were made using the model airfoil data tables to check the programs against each other. As may be seen, both programs compute essentially the same stall characteristics.

The results described above, the stall characteristics observed in the Posttest Performance Correlation, and the full-scale comparisons all suggest that the performance correlation problems were caused by the stall characteristics of the model airfoil data. It is well known that the Reynolds number and the Mach number can have significant effects on blade aerodynamic coefficients. The 2-D airfoil tests performed by Sikorsky were designed specifically to obtain the necessary steady-state data to be used in the flight simulation program. These data are presented in Figures 1, 2, and 3. Of particular interest is the maximum lift coefficient $C_{L_{max}}$ as a function of Mach number shown in Figure 44. Also shown for comparison are values of

$C_{L_{max}}$ from synthesized airfoil tables developed from a Bell in-house hovering rotor test and a Sikorsky hovering rotor test (Reference 9). The Bell test was conducted with a two-bladed 2.25 in. chord, 14 in. radius blade. Three twist combinations and three tip Mach numbers were examined and two-dimensional data were developed that correlated the measured performance for all three rotors at all three Mach numbers. This approach has been used by NACA (Reference 10) to synthesize airfoil data from test results. Both sets of synthesized data contain significantly higher maximum lift coefficient values when compared to the model two-dimensional data. The conclusion must be that the model data is unreasonably low or that unusual effects caused the synthesized data to be unexpectedly high.

The model two-dimensional airfoil data was used to predict performance at $\mu = 0.299$, $M_{1,90} = 0.408$ and $\alpha_m = 0^\circ$ as shown in Figure 7. When the model data are used, stall occurs at approximately $C_L/\sigma = 0.075$. These values are considerably below the measured lift values shown for this condition. If full-scale 0012 airfoil data are used, the stall point is increased to 0.106. Comparison between the measured and full-scale lift values indicates that the full-scale data more nearly approximates the behavior of the rotor in the tunnel.

The exact reason for the discrepancy between measured and calculated results is not well understood; however, it may be related to "centrifugal pumping". Centrifugal pumping refers to the tendency for the centrifugal force to push the turbulent boundary layer, which occurs with blade stall, out of the blade. As the turbulent volume is removed, the flow reattaches to the airfoil and thus the stall conditions are removed. The effect may be more significant for model rotors than for full-scale rotors because of the increased centrifugal force field.

Since the model behavior in the tunnel seemed to be best described by full-scale rotor aerodynamic characteristics, a modified airfoil table was assembled to permit bending moment calculations to be made. The table used for the three blades without the trailing edge flap contained a full-scale ($R_N = 12 \times 10^6$) lift table, the model drag table with an increment added uniformly to all values ($\Delta C_D = 0.003$), and a null pitching moment table. Figure 45 presents the lift characteristics of the full-scale 0012 tables used in the modified tables. Drag characteristics may be obtained from the model drag properties shown in Figure 2 by adding the increment. Figures 46 through 50 present representative effects of the modified airfoil on performance calculations. Different increments were used for the flapped airfoil. These were $\Delta C_L = 0.15$ added to the full-scale lift table and $\Delta C_D = 0.005$ added to the model drag table.

The fitted lines relating the measured and calculated lift and power in Figures 49 and 50 have the following values for a, b', and r:

Lift:

$$a = 0.944 \quad (q = 5.6\%)$$

$$b' = 1 - \frac{b}{\bar{C}_L/\sigma} = 1 - \frac{0.00179}{0.0608} = 0.971 \quad (q = 2.94\%)$$

$$r = 0.952 \quad (q = 4.8\%)$$

Power:

$$a = 0.884 \quad (q = 11.6\%)$$

$$b' = 1 - \frac{b}{\bar{C}_P/\sigma} = 1 - \frac{0.000229}{.0026} = 0.912 \quad (q = 8.81\%)$$

$$r = 0.992 \quad (q = 0.8\%)$$

Applying the standards presented in Table 9, the lift correlation is graded as good, excellent, and excellent for its slope, intercept, and correlation coefficient. Similarly, power correlation is graded as fair, good, and excellent on its slope, intercept, and correlation coefficient.

The modified airfoil was used because it allowed the calculation of reasonable performance parameters. A general technique for adjusting two-dimensional model airfoil data to represent actual operating airfoil characteristics has yet to be developed.

POSTTEST ROTOR BENDING MOMENT CORRELATION

Load comparisons were made by computing blade response at certain specified conditions for all four blade sets. The conditions were selected to present a range of lift and μ, $M_{1,90}$ combinations. The cases examined were designated in the Sikorsky wind-tunnel test as Conditions 25, 44, and 68. Because each condition number represents slightly different operating conditions for each blade, the values of lift and power coefficients corresponding to each blade set are listed in Table 11. This table also shows the computed lift and power for each condition and blade.

Load computations were made using the modified airfoil table discussed in the Model Rotor Aerodynamic Investigation section of this report. For each blade set and condition, the computed lift and first harmonic flapping components were brought as close as practicable to the measured lift and flapping. A collective sweep using a quasi-static analysis (steady and first harmonic blade response only) was made to obtain the value of lift required by the target condition. The Program C81 quasi-static procedure will automatically iterate to zero first harmonic flapping component values. However, when a fully elastic computation is made, the values of lift and flapping angles computed in the quasi-static analysis are changed slightly due to aeroelastic effects (principally changes in blade angle of attack due to local blade velocity). These changes required a succession of simulations to obtain the desired lift and flapping angles. Consequently, the computed values do not exactly match the measured. Also, because the modified airfoil characteristics do not represent the model behavior adequately in all regimes, there is frequently a mismatch between computed and measured power.

A choice of rotor blade elastic modes was necessitated by a Program C81 input limit of six modes. Properties of the modes used are shown in Table 8. Computations for the fiberglass blades were made using one rigid-body beamwise mode, one rigid-body chordwise mode, two elastic beamwise modes, and two elastic chordwise modes. For these blades, the selection of the second elastic chordwise mode at approximately 7.5/rev precluded the use of an elastic beamwise mode existing at approximately 6.7/rev. This choice was made to provide a possibility of higher frequency chordwise response. Computations for the aluminum blades were made using the first existing six modes. Torsion modes were omitted for all calculations because the modified airfoil had no pitching moment table. Modes were calculated for a rotor speed of 730 rpm and a root collective pitch of 12°. The boundary conditions applied for mode shape calculations were those of a pinned out-of-plane hinge and a pinned in-plane hinge located at r = 3 inches. The effect of

the inplane lead-lag damper was represented in Program C81 by a damping force, proportional to inplane velocity, applied at r/R = 0.10. Based on the damper rate of 17 in.-lb-sec/rad, the Program C81 damper input was 37.5 lb-sec/ft.

Measured and calculated beam and chord bending moments are compared by time histories and by harmonics at five radial stations (r/R = 0.20, r/R = 0.35, r/R = 0.45, r/R = 0.65, and r/R = 0.80). Figures 51 through 74 present the time histories for the twelve cases examined. These are followed by Figures 75 through 98 which present the harmonic analyses of the same cases. The harmonics are given in magnitude and phase form as explained below. Tables 12 through 35 present the measured and calculated bending moments as sine and cosine harmonic components.

Measured and calculated load harmonics are presented in Figures 75 through 98 as magnitudes and phases plotted against radial station. A load, M, may be represented as Fourier series sine and cosine components in the form

$$M(n\Omega t,r) = \sum_{n=0}^{\infty} (A_n \sin n\Omega t + B_n \cos n\Omega t) \qquad (32)$$

where
- M = load magnitude
- n = harmonic number
- Ω = rotor speed
- t = time
- r = blade radial station
- $A_n = A_n(r)$, the sine component of the load at radial station r
- $B_n = B_n(r)$, the cosine component of the load at radial station r.

The above relation may also be written as a magnitude and phase in the form

$$M(n\Omega t,r) = \sum_{n=0}^{\infty} C_n \cos (n\Omega t - \phi_n) \qquad (33)$$

where
$$C_n^2 = A_n^2 + B_n^2$$
$$\phi_n = \tan^{-1} (A_n/B_n)$$

Of the twelve cases examined, calculations using the -8° twist blade produced the best results. Examination of Figures 57 and 58 shows oscillatory magnitudes to be quite good for Condition 25. The beam traces for this condition show good magnitude and phase relationships for the entire span. Chordwise loads are good from r/R = 0.35 to r/R = 0.80. However, there is a decided difference in magnitude at the 20-percent radius. This effect is very evident in the plots of the chord load harmonics (Figure 82), where good correlation is seen for 1/rev loads from r/R = 0.35 to r/R = 0.80, and for the 2/rev and 3/rev chord load components for the entire span. The most noticeable difference is seen in the 1/rev chord loads at r/R = 0.20, where the calculated load is approximately 50 percent of the measured. Calculated beam and chord load magnitudes for Condition 44 are low. Phase relationships are good for the 1/rev beam bending moments over the entire span and improve for the 2/rev loads toward the tip. Once again, a large jump in chord 1/rev load is observed at the 20-percent radius. Condition 44 measured chordwise moments show a very high 4/rev harmonic content which is not calculated and also not seen in either Condition 25 or Condition 68 for this blade. Oscillatory magnitudes for Condition 68 are low over the entire span for both beam and chord loads. Calculated beam harmonics are low at all frequencies. Calculated chord 1/rev magnitude again shows a very large discrepancy at the 20 percent radius but shows continuing improvement in magnitude and phase with blade radial station. Calculated chord 2/rev load is low at the 20% radius, but shows almost perfect magnitude correlation from r/R = 0.45 to the blade tip. Calculated chord 3/rev and 4/rev magnitudes are low over the entire span.

Calculated loads for the fiberglass blade with 0° twist are lower than measured for all three conditions. The measured loads also exhibit high harmonic content not seen in the calculated loads. The measured chordwise loads for Conditions 25 and 68 show large excursions in the fourth quadrant of the rotor azimuth which are indicative of stall. These are not accompanied by a calculated stall prediction.

Calculated loads for the remaining two-blade sets, the fiberglass blade with the trailing-edge flap and the untwisted aluminum blade, are considerably lower than the measured loads. Generally calculated loads do not show the higher harmonic content of the measured loads, and calculated stall indications are absent.

Calculated loads are characterized by the absence of higher harmonic content and, excepting the fiberglass, -8° twist blade at Condition 25, generally low magnitudes. Measured 1/rev chordwise loads seem to be always increasing in the inboard direction, toward the hinge. This tendency would seem to indicate some moment carryover at the lead-lag hinge. The high harmonic content of the measured loads may indicate the presence of blade interaction effects which are not presently modeled in Program C81.

EFFECT OF CYCLIC RESOLUTION

Another factor which may influence the bending moment correlation is the effects of the cyclic pitch in the resolution angle between the shaft reference system and the blade reference system. Referring to the description of the mathematical model, it can be seen that the blade bending moments are formed by summing the bending moments produced by each mode. At the beginning of each computer run, the input mode shapes are used to calculate the in-plane and out-of-plane bending moment coefficients for each mode. During the time variant aeroelastic rotor analysis, the response of each mode or the participation factor is obtained from the numerical integration of the equations of motion.

These participation factors are multiplied by the previously mentioned in-plane and out-of-plane bending moments. The bending moments are then resolved through the steady geometric pitch angle (collective pitch plus structural twist) to obtain the beam and chord bending moments which have been presented in this report. Thus the cyclic pitch is not included in the resolution angle. Later versions of C81 have been modified to include the cyclic pitch angle in the resolution angle.

Figures 99 and 100 illustrate the effect of the cyclic resolution angle on loads. The calculations shown in these figures were made using a version of Program C81 which incorporates the cyclic pitch angle in the angle of resolution. The results shown are typical for beam and chord bending moments. The most noticeable effect is a general increase of beamwise moments in the midspan and outer regions of the blade.

EFFECT OF UNSTEADY AERODYNAMICS AND YAWED FLOW

The Program C81 unsteady aerodynamics were employed to compute the bending moments presented in Figures 101 and 102 for the fiberglass blade with 0° twist at Condition 25. These figures should be compared with Figures 51 and 52, which present computed results without the unsteady aerodynamics. Load magnitudes are not affected significantly in either the beam o-

chord moments. The effect does produce a damping effect which is seen as a lagging phase shift (moving the calculated loads toward the measured).

Unsteady aerodynamics and the yawed flow simulation were used to produce the representative time history trace shown in Figure 103. The effects do not modify the load amplitudes appreciably. However, the introduction of the yawed flow representation does tend to shift the calculated phase in the leading direction, cancelling the phase shift of the unsteady aerodynamics effect.

EFFECT OF TORSIONAL MOMENT CALCULATIONS

The effect of incorporating a torsional mode shape and a pitching moment table is presented in Figure 104 for the fiberglass blade with -8° of twist at Condition 44. The inclusion of the 7.36/rev torsional mode required the removal of a chordwise mode at 7.56/rev due to the Program C81 input limit of six modes. The pitching moment table used was the model 0012 table. Figure 104 shows that this effect does not appreciably affect results. This figure is representative of the order-of-magnitude difference seen at all radial stations.

EFFECT OF IN-PLANE SPRING

Since the calculated 1/rev chordwise moments at r/R = 0.20 were consistently lower than the measured values, the possibility of excessive moment carryover at the lead-lag hinge was considered. The Sikorsky data package for this program states that possibly 15 percent of the in-plane lead-lag damper value could be considered as a spring component. Assuming 1/rev as the basis for calculating this spring component gives a value of approximately 0.3 ft-lb/deg. Modes and natural frequencies incorporating this in-plane spring value were used to compute the representative time history trace shown in Figure 105. The effect of the spring is to shift the mean value of the moments to a slightly higher level. The higher 1/rev chordwise moments may also be due to moment carryover by the lead-lag hinge bearings.

AERODYNAMIC REPRESENTATION

Correlation problems encountered are believed to be due mainly to an inadequate aerodynamic representation. The modified airfoil used for load predictions apparently did not represent the airfoil well in lift and drag and contained no pitching moment table since there was no method for determining moment coefficient values.

MEASURED DATA

Some problems were observed in the data used for comparison in this project. Figures 106 and 107 show representative time histories of measured model beamwise and chordwise moments. The chordwise moments contain strong noninteger per/rev components which may affect comparisons. The beamwise moment time history is more consistent but still contains components which may be significant at high frequencies. Though non-harmonic response may occur naturally due to various causes, this behavior is believed to be primarily related to inplane moments generated by the rotor drive system. Though the time histories presented herein are averages of measurements made for 40 revolutions, the illustrated behavior may still significantly affect results. The nature of the data indicates that measured results should be analyzed to detect and identify noninteger per/rev responses.

CONCLUSIONS

1. The Rotorcraft Flight Simulation Program (C81) can predict performance and bending moments for full-scale rotors.

2. Since the Rotorcraft Flight Simulation has been shown to correlate well for a similar, but full-scale, rotor system, the problems experienced are likely due to unsteady and/or Reynolds number and/or other scale effects which are not accounted for in the program.

3. The measured model rotor performance is not compatible with the model two-dimensional aerodynamic coefficients.

4. Mathematical modeling techniques, derived for full-scale rotor aerodynamics, may not be valid for model rotors.

5. The sensitivity analysis which was performed is not valid due to limitations in the input data and/or the computer program.

6. Simple harmonic analysis of measured data may lead to erroneous conclusions because of its inability to detect the noninteger, or transient, components.

7. The correlation criterion developed for rotor performance behavior is not applicable to model rotor bending moment correlation.

8. The difficulties associated with model rotors should not preclude the careful use and orderly development of the analysis.

RECOMMENDATIONS

1. A similar program should be repeated using a full-scale rotor system.

2. Measured and computed results should be analyzed using auto- and cross-correlation techniques.

3. The wind-tunnel test conditions should be statistically designed to ensure the maximum usable data.

4. Further basic research should be conducted to understand the aerodynamics of model rotors.

REFERENCES

1. Davis, John M., ROTORCRAFT FLIGHT SIMULATION WITH AEROELASTIC ROTOR AND IMPROVED AERODYNAMIC REPRESENTATIONS, Bell Helicopter Company, Fort Worth, Texas; USAAMRDL Technical Report 74-10A, B, C, Eustis Directorate, U. S. Army Air Mobility Research and Development Laboratory, Fort Eustis, Virginia, June 1974.

2. Niebanck, C., MODEL ROTOR TEST DATA FOR VERIFICATION OF BLADE RESPONSE AND ROTOR PERFORMANCE CALCULATIONS, Sikorsky Aircraft Division of United Aircraft Corporation, Stratford, Connecticut, USAAMRDL Technical Report 74-29, Eustis Directorate, U. S. Army Air Mobility Research and Development Laboratory, Fort Eustis, Virginia, May, 1974.

3. Paglino, Vincent M., and Logan, Andrew H., AN EXPERIMENTAL STUDY OF THE PERFORMANCE AND STRUCTURAL LOADS OF A FULL-SCALE ROTOR AT EXTREME OPERATING CONDITIONS, United Aircraft Corporation, Sikorsky Aircraft Division, Stratford, Connecticut, USAAVLABS Technical Report 68-3, U. S. Army Aviation Materiel Laboratories, Fort Eustis, Virginia, July 1968, AD674187.

4. Hoel, Paul G., INTRODUCTION TO MATHEMATICAL STATISTICS, John Wiley & Sons, Inc., New York, New York, 1947.

5. IBM System 360 Scientific Subroutine Package (GH20-0205-4), Version 3, page 36 (International Business Machines Corporation, New York), September 1971.

6. Bendat, Julius S., and Piersol, Allan G., MEASUREMENT AND ANALYSIS OF RANDOM DATA, John Wiley & Sons, Inc., New York, New York, 1966.

7. McCloud, John L. III, et al, AN INVESTIGATION OF FULL-SCALE HELICOPTER ROTORS AT HIGH ADVANCE RATIOS AND ADVANCING TIP MACH NUMBERS, jointly by Ames Research Center and Army Aeronautical Research Laboratory, NASA Technical Note NASA TN D-4632, National Aeronautics and Space Administration, Washington, D. C. July 1968.

8. Livingston, Charles L., ROTOR AERODYNAMIC CHARACTERISTICS PROGRAM F35(J), Bell Helicopter Company, Fort Worth, Texas; Report No. 599-004-900, June 1967.

9. Rabbott, J. P., Jr., COMPARISON OF THEORETICAL AND EXPERIMENTAL MODEL HELICOPTER ROTOR PERFORMANCE IN FORWARD FLIGHT, SER-50129, Sikorsky Aircraft Division of United Aircraft Corporation, Stratford, Connecticut;

USAAVLABS Technical Report 61-103, U. S. Army Aviation Materiel Laboratories, Fort Eustis, Virginia, July 1961.

10. Powell, Robert D. and Paul J. Carpenter: "Lift and Profile Drag Characteristics of an NACA 0012 Airfoil Section as Derived from Measured Helicopter-Rotor Hovering Performance," NACA TN 4357, 1958.

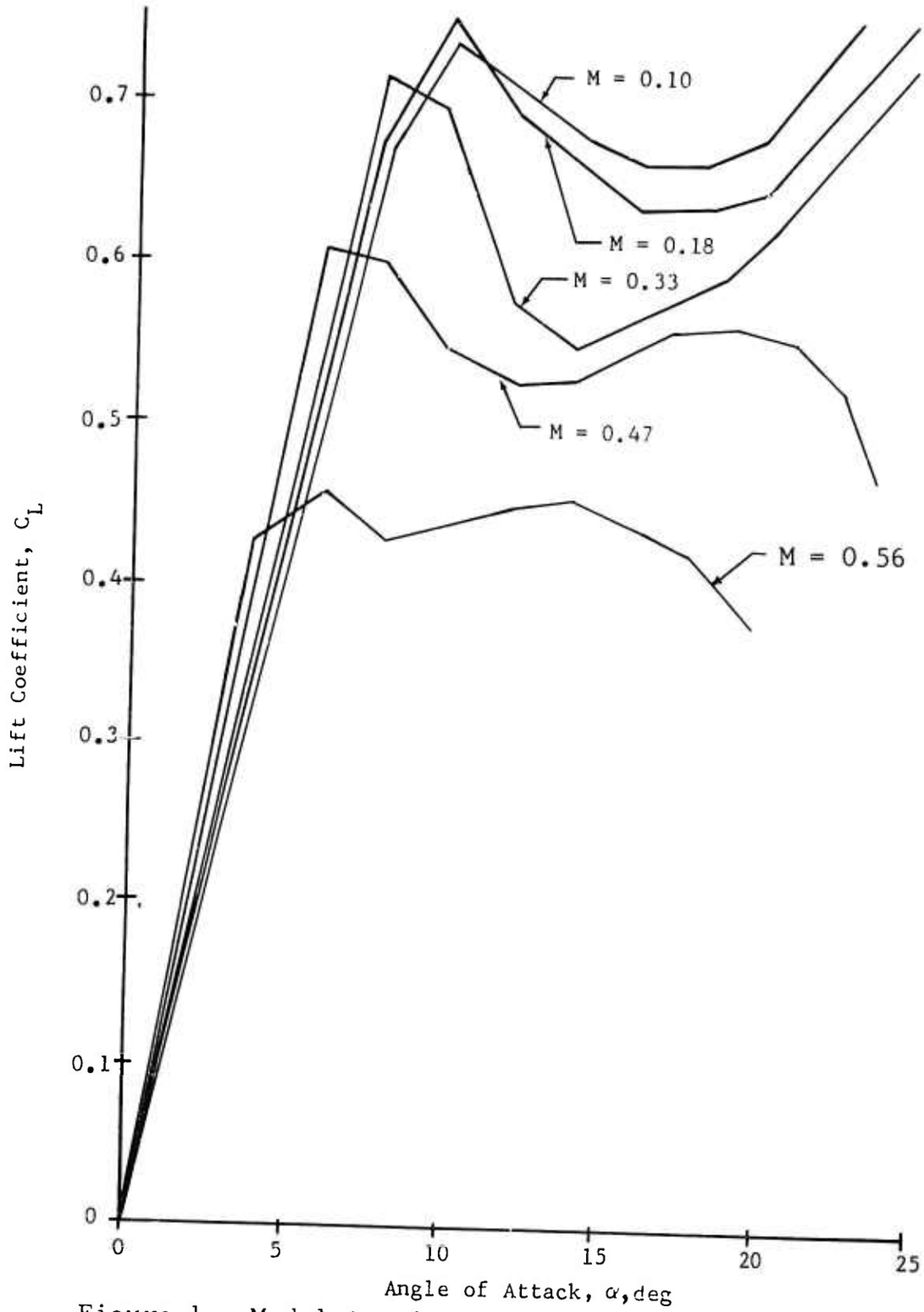

Figure 1. Model Aerodynamic Lift Coefficient vs. Angle of Attack.

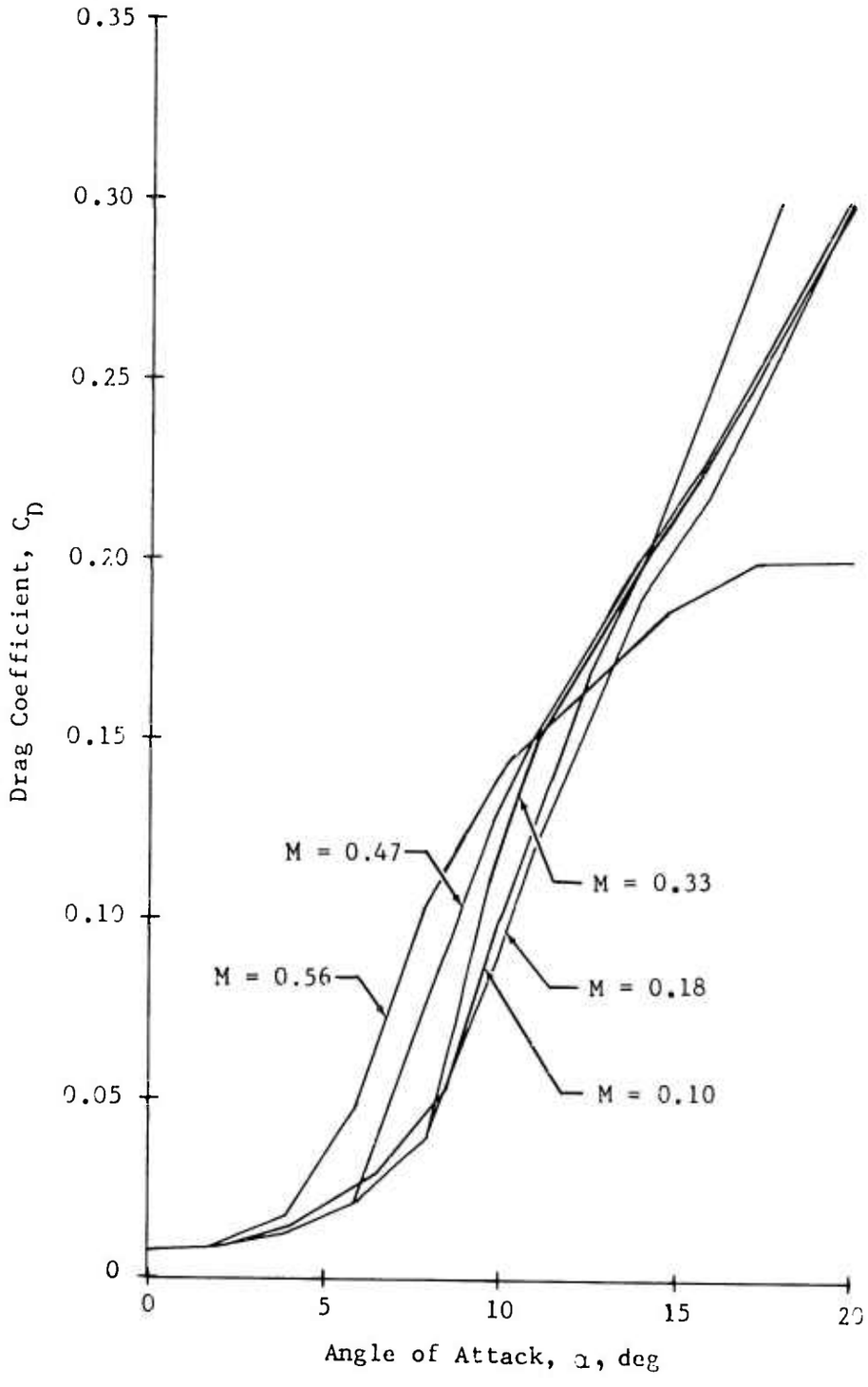

Figure 2. Model Airfoil Drag Coefficient vs. Angle of Attack.

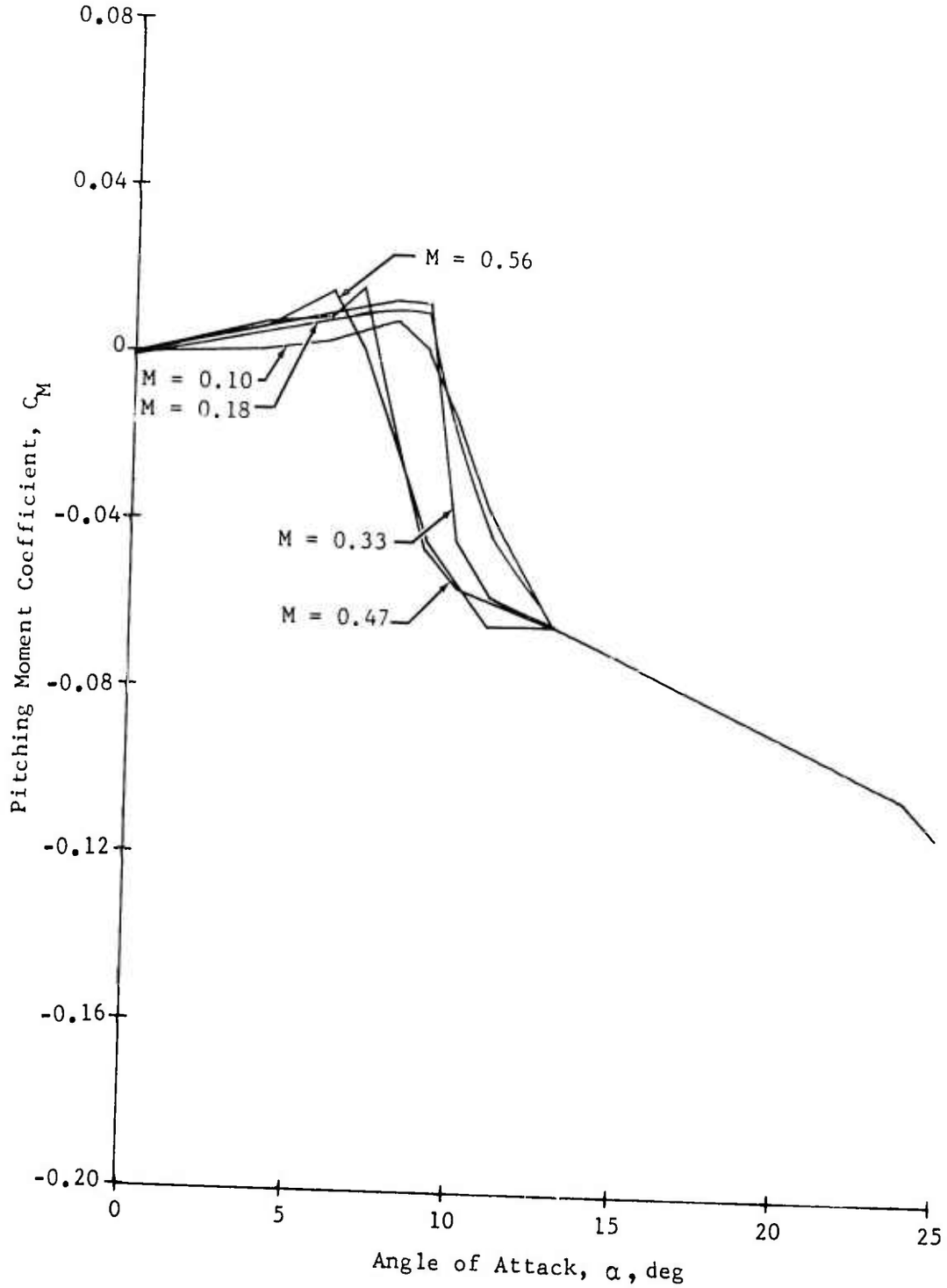

Figure 3. Model Airfoil Pitching Moment Coefficient vs. Angle of Attack.

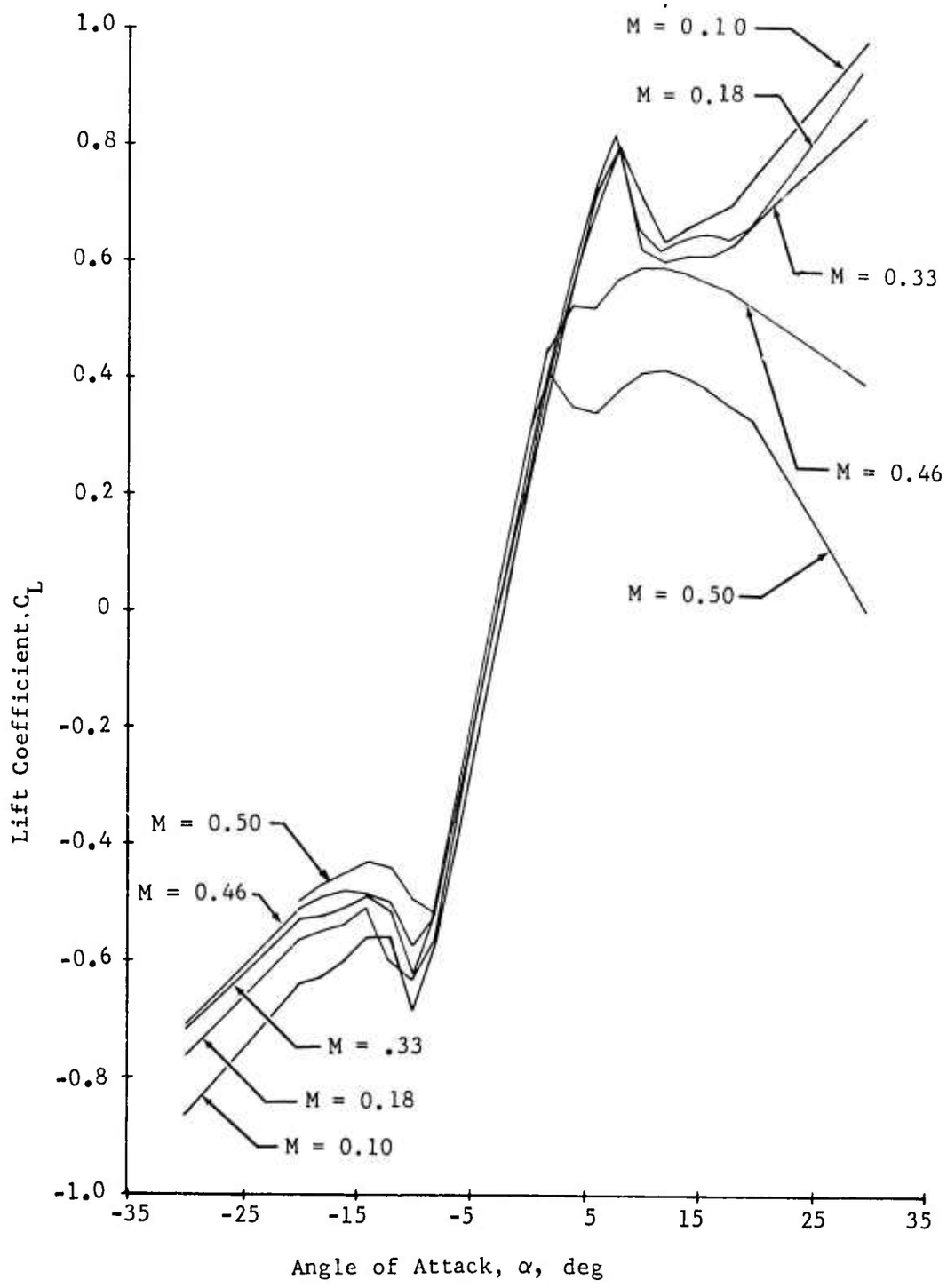

Figure 4. Model Aerodynamic Lift Coefficient vs. Angle of Attack for Flapped Airfoil.

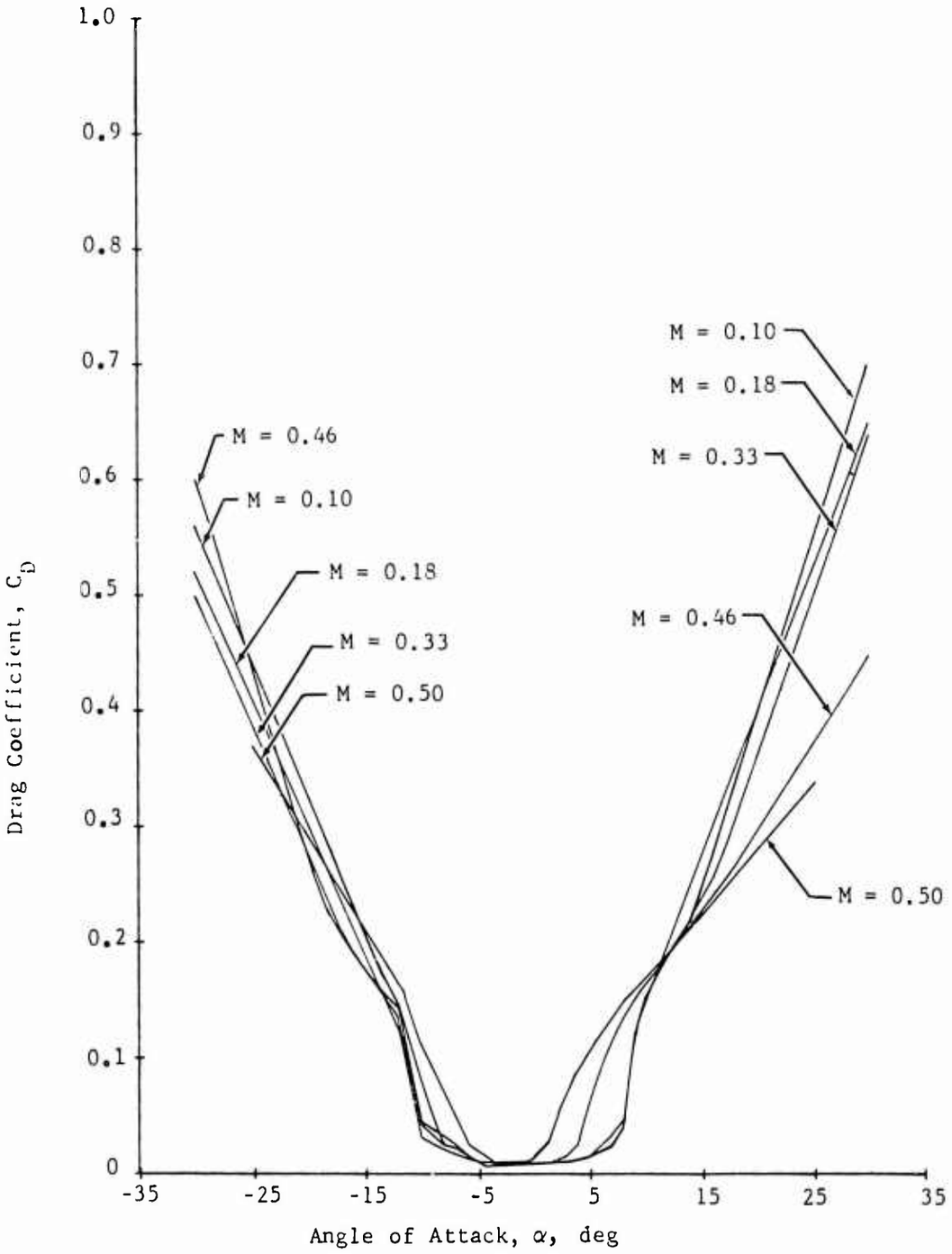

Figure 5. Model Aerodynamic Drag Coefficient vs. Angle of Attack for Flapped Airfoil.

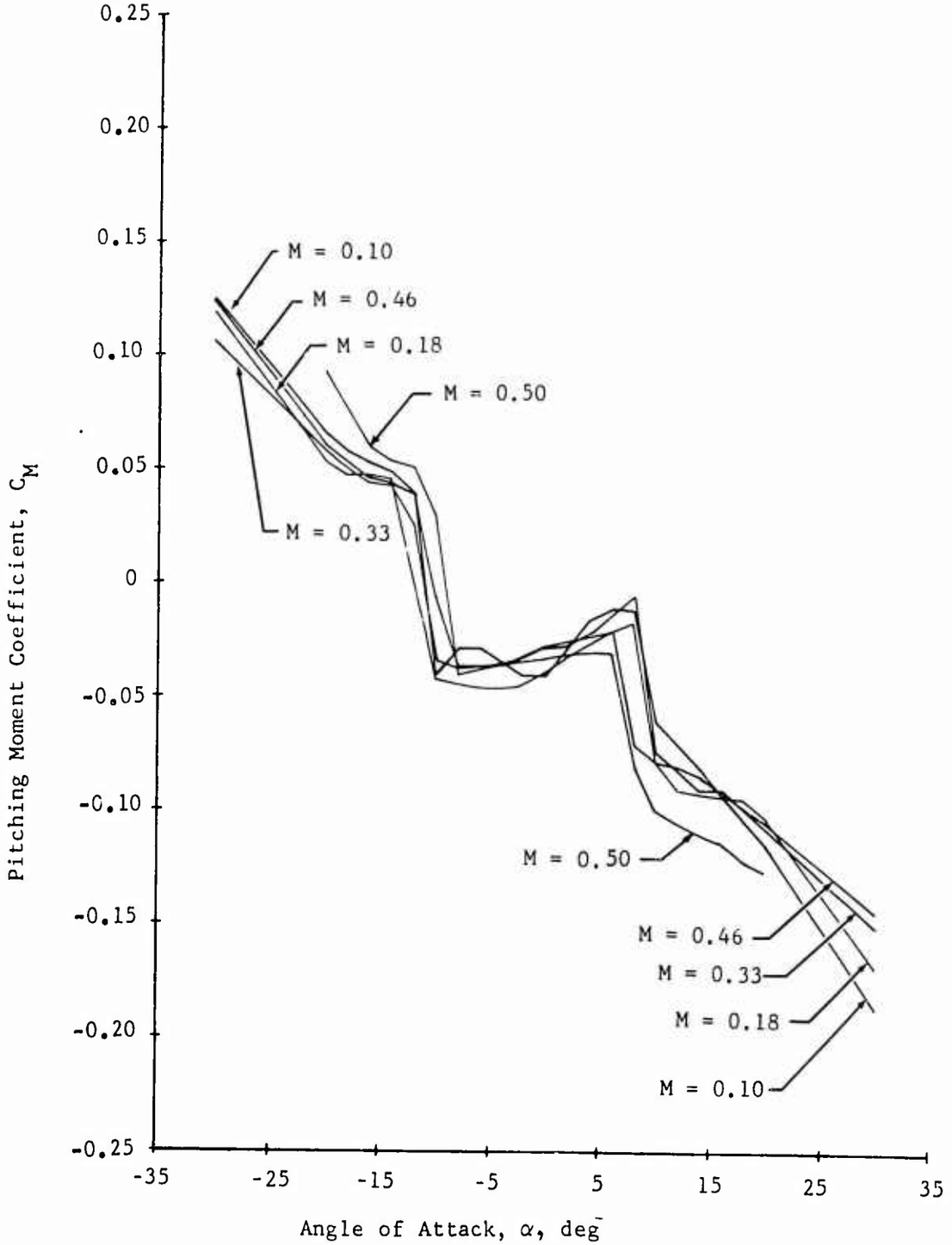

Figure 6. Model Aerodynamic Pitching Moment Coefficient vs. Angle of Attack for Flapped Airfoil.

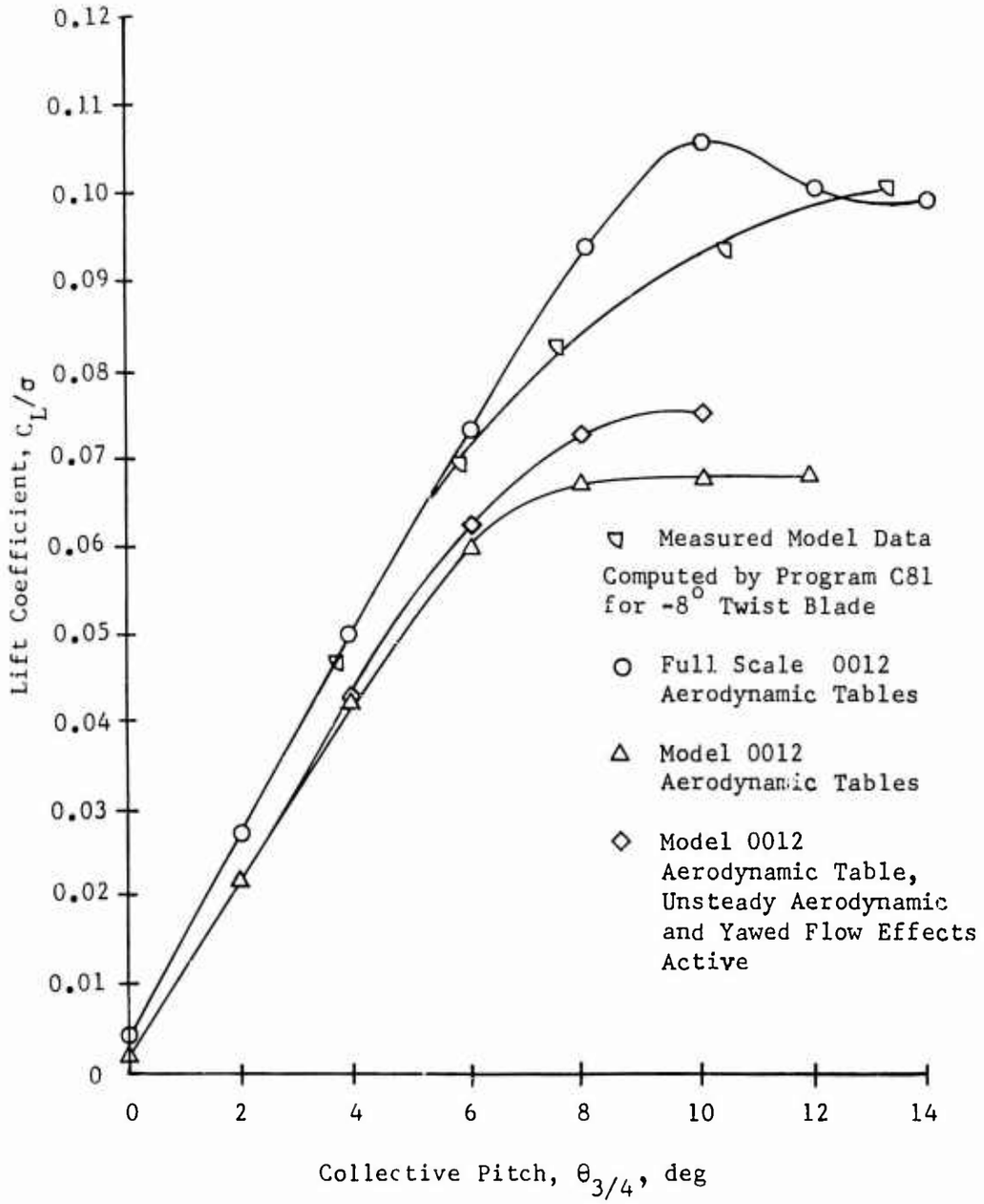

Figure 7. Lift vs. Collective Pitch for Full-Scale and Model Data Tables, μ=0.299, $M_{1,90}$=0.408, α_m=0°.

BELL HELICOPTER COMPANY
ROTORCRAFT FLIGHT SIMULATION PROGRAM ANAL7213
COMPUTED 06/27/73

1 73062606 VARIATIONS STARTING FROM BASELINE CT/SIGMA=0.027
MODEL ROTOR SET 'A',FIBERGLASS WITH 8 DEG WASHOUT TWIST
NO CYCLIC DETUNING, CT/SIGMA = 0.027 VARIATIONS

ROTOR CONTROLS		ROTOR PARAMETERS		TUNNEL PARAMETERS		PROGRAM OPTIONS	
COLLECTIVE PITCH	10.300 DEG	ROTOR SPEED	734.00 RPM	FORWARD SPEED	82.90 KTS	NO INPUT MODES	6
F/A CYCLIC PITCH	3.511 DEG	SOLIDITY	0.0625	ADVANCE RATIO	0.3983	MAX YAW FLOW ANG	0.0 DEG
LAT CYCLIC PITCH	-0.657 DEG	BLADE RADIUS	4.57 FT	ADV TIP MACH NO	0.440	AERODYNAMICS	TABLE
TOT CYC FEATHER	3.572 DEG	CHORD	2.69 IN	SIGMA PRIME	1.000	TORSION	ON
DELTA 3	0.0 DEG	PRECONE	0.0 DEG	MAST TILT ANGLE	2.50 DEG	NON STEADY AERO	OFF
F/A FLAP ANGLE	-0.078 DEG	CONING	3.170 DEG	TPP ANG OF ATTACK	-2.58 DEG	FLAP ITERATION	ON
LAT FLAP ANGLE	0.137 DEG	TWIST	-8.00 DEG	CNT PL ANG OF ATTACK	-6.01 DEG	FREQUENCY CHANGE	OFF
TOTAL FLAP ANGLE	0.158 DEG	TIP SWEEP	0.0 DEG	ROTOR TIP SPEED	351.3 FT/SEC	ELASTIC PYLON	OFF

* * * * * * FORCES AND MOMENTS * * * * * *

	WIND AXIS SYSTEM DIMENSIONLESS HELICOPTER	WIND AXIS SYSTEM DIMENSIONLESS FIXED-WING	WIND AXIS SYSTEM DIMENSIONAL		SHAFT AXIS SYSTEM DIMENSIONLESS HELICOPTER	SHAFT AXIS SYSTEM DIMENSIONLESS FIXED-WING	SHAFT AXIS SYSTEM DIMENSIONAL
LIFT FORCE	0.0284244	0.2814113	34.18 LBS	THRUST	0.0284179	0.2813470	34.17 LBS
DRAG FORCE	-0.0004709	-0.0046625	-0.57 LBS	H FORCE	0.0007694	0.0076170	0.93 LBS
LAT FORCE	-0.0003157	-0.0031253	-0.38 LBS	Y FORCE	-0.0003157	-0.0031253	-0.38 LBS
ROLL MOMENT	-0.0004553	-0.0022540	-2.50 FT-LBS	ROLL MOMENT	-0.0003715	-0.0018391	-2.04 FT-LBS
PITCH MOMENT	0.0000748	0.0003703	0.41 FT-LBS	PITCH MOMENT	0.0000748	0.0003703	0.41 FT-LBS
YAW MOMENT	0.0019112	0.0094607	10.50 FT-LBS	YAW MOMENT	0.0019292	0.0095500	10.60 FT-LBS
				POWER	0.0019292	0.0479513	1.48 HP

* * * * * * ROTOR LOADS * * * * * *

BEAM LOADS (IN-LBS)			CHORD LOADS (IN-LBS)		TORSION LOADS (IN-LBS)		
R/R	MEAN	OSC /MAX AZ/MIN AZ	MEAN	OSC /MAX AZ/MIN AZ	R/R	MEAN	OSC /MAX AZ/MIN AZ
.20	0.57	2.42 / 0. / 120.	1.93	1.73 / 70. / 350.	.20	1.22	1.39 / 170. / 240.
.35	-0.04	2.04 / 0. / 120.	1.96	2.53 / 70. / 350.	.35	1.19	1.35 / 170. / 240.
.45	-0.65	2.28 / 0. / 110.	1.82	2.74 / 70. / 350.	.45	1.14	1.30 / 170. / 240.
.65	-1.32	2.92 / 250. / 100.	1.15	2.21 / 60. / 350.	.65	1.01	1.14 / 170. / 240.
.80	-1.25	2.37 / 240. / 90.	0.48	1.14 / 60. / 350.	.80	0.88	1.00 / 170. / 240.

Figure 8. Baseline Case Fiberglass Blade with -8° Twist, $\mu = 0.398$, $M_{1,90} = 0.440$, $C_L/\sigma = 0.027$.

BELL HELICOPTER COMPANY
ROTORCRAFT FLIGHT SIMULATION PROGRAM ANAL7213
COMPUTED 06/27/73

1 73062605 VARIATIONS STARTING FROM BASELINE CT/SIGMA=0.049
MODEL ROTOR SET 'A',FIBERGLASS WITH 8 DEG WASHOUT TWIST
NO CYCLIC DETUNING

ROTOR CONTROLS		ROTOR PARAMETERS		TUNNEL PARAMETERS		PROGRAM OPTIONS	
COLLECTIVE PITCH	10.687 DEG	ROTOR SPEED	734.00 RPM	FORWARD SPEED	62.10 KTS	NO INPUT MODES	6
F/A CYCLIC PITCH	3.749 DEG	SOLIDITY	0.0625	ADVANCE RATIO	0.2984	MAX YAW FLOW ANG	0.0 DEG
LAT CYCLIC PITCH	-1.325 DEG	BLADE RADIUS	4.57 FT	ADV TIP MACH NO	0.408	AERODYNAMICS	TABLE
TOT CYC FEATHER	3.976 DEG	CHORD	2.69 IN	SIGMA PRIME	1.000	TORSION	ON
DELTA 3	0.0 DEG	PRECONE	0.0 DEG	MAST TILT ANGLE	0.0 DEG	NON STEADY AERO	OFF
F/A FLAP ANGLE	-0.081 DEG	CONING	4.885 DEG	TPP ANG OF ATTACK	-0.08 DEG	FLAP ITERATION	ON
LAT FLAP ANGLE	0.108 DEG	TWIST	-8.00 DEG	CNT PL ANG OF ATTACK	-3.75 DEG	FREQUENCY CHANGE	OFF
TOTAL FLAP ANGLE	0.135 DEG	TIP SWEEP	0.0 DEG	ROTOR TIP SPEED	351.3 FT/SEC	ELASTIC PYLON	OFF

* * * * * * FORCES AND MOMENTS * * * * * *

	WIND AXIS SYSTEM DIMENSIONLESS HELICOPTER	WIND AXIS SYSTEM DIMENSIONLESS FIXED-WING	WIND AXIS SYSTEM DIMENSIONAL		SHAFT AXIS SYSTEM DIMENSIONLESS HELICOPTER	SHAFT AXIS SYSTEM DIMENSIONLESS FIXED-WING	SHAFT AXIS SYSTEM DIMENSIONAL
LIFT FORCE	0.0512240	0.9037533	61.59 LBS	THRUST	0.0512240	0.9037533	61.59 LBS
DRAG FORCE	0.0000863	0.0015230	0.10 LBS	H FORCE	0.0000863	0.0015230	0.10 LBS
LAT FORCE	-0.0007022	-0.0123887	-0.84 LBS	Y FORCE	-0.0007022	-0.0123887	-0.84 LBS
ROLL MOMENT	-0.0003828	-0.0033772	-2.10 FT-LBS	ROLL MOMENT	-0.0003828	-0.0033772	-2.10 FT-LBS
PITCH MOMENT	0.0000760	0.0006705	0.42 FT-LBS	PITCH MOMENT	0.0000760	0.0006705	0.42 FT-LBS
YAW MOMENT	0.0022529	0.0198744	12.38 FT-LBS	YAW MOMENT	0.0022529	0.0198744	12.38 FT-LBS
				POWER	0.0022529	0.1332148	1.73 HP

* * * * * * ROTOR LOADS * * * * * *

	BEAM LOADS (IN-LBS)		CHORD LOADS (IN-LBS)			TORSION LOADS (IN-LBS)	
R/R	MEAN	OSC /MAX AZ/MIN AZ	MEAN	OSC /MAX AZ/MIN AZ	R/R	MEAN	OSC /MAX AZ/MIN AZ
.20	1.62	2.11 / 210. / 110.	2.03	1.96 / 70. / 240.	.20	1.55	1.35 / 170. / 250.
.35	0.52	1.78 / 220. / 110.	1.96	2.88 / 70. / 230.	.35	1.51	1.31 / 170. / 250.
.45	-0.09	2.14 / 250. / 100.	1.77	3.15 / 70. / 230.	.45	1.45	1.26 / 170. / 250.
.65	-1.23	2.72 / 260. / 100.	1.09	2.56 / 70. / 230.	.65	1.28	1.11 / 170. / 250.
.80	-1.45	2.17 / 260. / 100.	0.44	1.29 / 70. / 230.	.80	1.11	0.97 / 170. / 250.

Figure 8. Concluded: $\mu = 0.298$, $M_{1,90} = 0.408$, $C_L/\sigma = 0.049$.

BELL HELICOPTER COMPANY
ROTORCRAFT FLIGHT SIMULATION PROGRAM ANAL7213
COMPUTED 06/29/73

1 73062804*

MODEL ROTOR: FIBERGLASS WITH ZERO TWIST
NO CYCLIC DETUNING, CT/SIGMA = .027 AND .049 LOADS

ROTOR CONTROLS		ROTOR PARAMETERS		TUNNEL PARAMETERS		PROGRAM OPTIONS	
COLLECTIVE PITCH	4.930 DEG	ROTOR SPEED	734.00 RPM	FORWARD SPEED	82.90 KTS	NO INPUT MODES	6
F/A CYCLIC PITCH	3.738 DEG	SOLIDITY	0.0425	ADVANCE RATIO	0.3983	MAX YAW FLOW ANG	0.0 DEG
LAT CYCLIC PITCH	-1.214 DEG	BLADE RADIUS	4.67 FT	ADV TIP MACH NO	0.440	AERODYNAMICS	TABLE
TOT CYC FEATHER	3.930 DEG	CHORD	2.69 IN	SIGMA PRIME	1.000	TORSION	ON
DELTA 3	0.0 DEG	PRECONE	0.0 DEG	MAST TILT ANGLE	2.50 DEG	NON STEADY AERO	OFF
F/A FLAP ANGLE	-0.002 DEG	CONING	4.221 DEG	TPP ANG OF ATTACK	-2.50 DEG	FLAP ITERATION	ON
LAT FLAP ANGLE	0.057 DEG	TWIST	0.0 DEG	CNT PL ANG OF ATTACK	-6.24 DEG	FREQUENCY CHANGE	OFF
TOTAL FLAP ANGLE	0.057 DEG	TIP SWEEP	0.0 DEG	ROTOR TIP SPEED	351.3 FT/SEC	ELASTIC PYLON	OFF

* * * * * * FORCES AND MOMENTS * * * * * *

WIND AXIS SYSTEM	DIMENSIONLESS		DIMENSIONAL
	HELICOPTER	FIXED-WING	
LIFT FORCE	0.0273003	0.2702824	32.83 LBS
DRAG FORCE	-0.0003359	-0.0092660	-1.13 LBS
LAT FORCE	-0.0033373	-0.0033390	-0.41 LBS
ROLL MOMENT	-0.0001249	-0.0006183	-0.69 FT-LBS
PITCH MOMENT	0.0000363	0.0001796	6.20 FT-LBS
YAW MOMENT	0.0022357	0.0110673	12.29 FT-LBS

SHAFT AXIS SYSTEM	DIMENSIONLESS		DIMENSIONAL
	HELICOPTER	FIXED-WING	
THRUST	0.0273152	0.2704294	32.84 LBS
H FORCE	0.0002558	0.0025323	0.31 LBS
Y FORCE	-0.0033373	-0.0033390	-0.41 LBS
ROLL MOMENT	-0.0000273	-0.0001350	-0.15 FT-LBS
PITCH MOMENT	0.0000363	0.0001796	0.20 FT-LBS
YAW MOMENT	0.0022391	0.0110837	12.30 FT-LBS
POWER	0.0022391	0.0556522	1.72 HP

* * * * * * ROTOR LOADS * * * * * *

BEAM LOADS (IN-LBS)

R/R	MEAN	OSC /MAX AZ/MIN AZ
.20	2.17	1.20 / 10. / 60.
.35	1.54	0.96 / 10. / 60.
.45	1.36	0.91 / 10. / 70.
.65	0.68	0.89 / 260. / 180.
.80	0.02	0.95 / 260. / 180.

CHORD LOADS (IN-LBS)

MEAN	OSC /MAX AZ/MIN AZ
1.56	0.32 / 180. / 250.
1.11	1.28 / 50. / 10.
0.83	1.49 / 50. / 10.
0.31	1.39 / 60. / 10.
0.06	0.79 / 60. / 10.

TORSION LOADS (IN-LBS)

R/R	MEAN	OSC /MAX AZ/MIN AZ
.20	0.67	0.71 / 180. / 120.
.35	0.65	0.69 / 180. / 120.
.45	0.63	0.66 / 180. / 120.
.65	0.55	0.58 / 180. / 120.
.80	0.48	0.51 / 180. / 120.

Figure 9. Baseline Case Fiberglass Blade with 0° Twist, $\mu = 0.398$, $M_{1,90} = 0.440$, $C_L/\sigma = 0.027$.

BELL HELICOPTER COMPANY
ROTORCRAFT FLIGHT SIMULATION PROGRAM ANAL7213
COMPUTED 06/29/73

10 73062804

MODEL ROTOR: FIBERGLASS WITH ZERO TWIST
NO CYCLIC DETUNING, CT/SIGMA = .027 AND .049 LOADS

ROTOR CONTROLS		ROTOR PARAMETERS		TUNNEL PARAMETERS		PROGRAM OPTIONS	
COLLECTIVE PITCH	5.044 DEG	ROTOR SPEED	734.00 RPM	FORWARD SPEED	62.10 KTS	NO INPUT MODES	6
F/A CYCLIC PITCH	3.747 DEG	SOLIDITY	0.0625	ADVANCE RATIO	0.2984	MAX YAW FLOW ANG	0.0 DEG
LAT CYCLIC PITCH	-1.699 DEG	BLADE RADIUS	4.57 FT	ADV TIP MACH NO	0.408	AERODYNAMICS	TABLE
TOT CYC FEATHER	4.114 DEG	CHORD	2.69 IN	SIGMA PRIME	1.000	TORSION	ON
DELTA 3	0.0 DEG	PRECONE	0.0 DEG	MAST TILT ANGLE	0.0 DEG	NON STEADY AERO	OFF
F/A FLAP ANGLE	-0.035 DEG	CONING	5.717 DEG	TPP ANG OF ATTACK	-0.03 DEG	FLAP ITERATION	ON
LAT FLAP ANGLE	0.054 DEG	TWIST	0.0 DEG	CNT PL ANG OF ATTACK	-3.75 DEG	FREQUENCY CHANGE	OFF
TOTAL FLAP ANGLE	0.065 DEG	TIP SWEEP	0.0 DEG	ROTOR TIP SPEED	351.3 FT/SEC	ELASTIC PYLON	OFF

* * * * * * FORCES AND MOMENTS * * * * * *

	WIND AXIS SYSTEM DIMENSIONLESS		DIMENSIONAL		SHAFT AXIS SYSTEM DIMENSIONLESS		DIMENSIONAL
	HELICOPTER	FIXED-WING			HELICOPTER	FIXED-WING	
LIFT FORCE	0.0499983	0.9821298	60.12 LBS	THRUST	0.0499983	0.9821288	60.12 LBS
DRAG FORCE	-0.0002542	-0.0044857	-0.31 LBS	H FORCE	-0.0002542	-0.0044857	-0.31 LBS
LAT FORCE	-0.0008913	-0.0157262	-1.07 LBS	Y FORCE	-0.0008913	-0.0157262	-1.07 LBS
ROLL MOMENT	-0.0001158	-0.0010216	-0.64 FT-LBS	ROLL MOMENT	-0.0001158	-0.0010216	-0.64 FT-LBS
PITCH MOMENT	0.0000604	0.0005325	0.33 FT-LBS	PITCH MOMENT	0.0000604	0.0005325	0.33 FT-LBS
YAW MOMENT	0.0024776	0.0218566	13.61 FT-LBS	YAW MOMENT	0.0024776	0.0218566	13.61 FT-LBS
				POWER	0.0024776	0.1465010	1.90 HP

* * * * * * ROTOR LOADS * * * * * *

BEAM LOADS (IN-LBS)			CHORD LOADS (IN-LBS)			TORSION LOADS (IN-LBS)		
R/R	MEAN	OSC /MAX AZ/MIN AZ	MEAN	OSC /MAX AZ/MIN AZ	R/R	MEAN	OSC /MAX AZ/MIN AZ
.20	2.64	1.09 / 0. / 70.	1.69	1.41 / 70. / 250.	.20	1.00	0.82 / 180. / 260.
.35	1.69	0.93 / 0. / 70.	1.11	2.20 / 70. / 250.	.35	0.97	0.80 / 180. / 260.
.45	1.35	0.99 / 260. / 80.	0.79	2.48 / 70. / 250.	.45	0.93	0.77 / 180. / 260.
.65	0.60	1.29 / 270. / 180.	0.23	2.13 / 70. / 250.	.65	0.82	0.68 / 180. / 260.
.80	-0.20	1.25 / 270. / 180.	0.01	1.11 / 70. / 250.	.80	0.72	0.59 / 180. / 260.

Figure 9. Concluded: $\mu = 0.298$, $M_{1,90} = 0.408$, $C_L/\sigma = 0.049$.

BELL HELICOPTER COMPANY
ROTORCRAFT FLIGHT SIMULATION PROGRAM ANAL7213
COMPUTED 06/29/73

10 73062801 FIBERGLASS BLD,NO TWIST,TRAILING EDGE FLAP
FIBERGLASS BLADE WITH NO TWIST
NO CYCLIC DETUNING

ROTOR CONTROLS		ROTOR PARAMETERS		TUNNEL PARAMETERS		PROGRAM OPTIONS	
COLLECTIVE PITCH	3.230 DEG	ROTOR SPEED	734.00 RPM	FORWARD SPEED	92.90 KTS	NO INPUT MODES	6
F/A CYCLIC PITCH	2.620 DEG	SOLIDITY	0.0625	ADVANCE RATIO	0.3983	MAX YAW FLOW ANG	0.0 DEG
LAT CYCLIC PITCH	-1.087 DEG	BLADE RADIUS	4.67 FT	ADV TIP MACH NO	0.440	AERODYNAMICS	TABLE
TOT CYC FEATHER	2.837 DEG	CHORD	2.69 IN	SIGMA PRIME	1.000	TORSION	ON
DELTA 3	0.0 DEG	PRECONE	0.0 DEG	MAST TILT ANGLE	2.50 DEG	NON STEADY AERO	OFF
F/A FLAP ANGLE	-0.120 DEG	CONING	3.537 DEG	TPP ANG OF ATTACK	-2.62 DEG	FLAP ITERATION	ON
LAT FLAP ANGLE	0.089 DEG	TWIST	0.0 DEG	CNT PL ANG OF ATTACK	-5.12 DEG	FREQUENCY CHANGE	OFF
TOTAL FLAP ANGLE	0.149 DEG	TIP SWEEP	0.0 DEG	ROTOR TIP SPEED	351.3 FT/SEC	ELASTIC PYLON	OFF

* * * * * * FORCES AND MOMENTS * * * * * *

WIND AXIS SYSTEM	DIMENSIONLESS		DIMENSIONAL	SHAFT AXIS SYSTEM	DIMENSIONLESS		DIMENSIONAL
	HELICOPTER	FIXED-WING			HELICOPTER	FIXED-WING	
LIFT FORCE	0.0272550	0.2699340	32.77 LBS	THRUST	0.0272430	0.2699128	32.78 LBS
DRAG FORCE	-0.0007769	-0.0076914	-0.93 LBS	H FORCE	-0.0004127	0.0040859	0.50 LBS
LAT FORCE	-0.0002714	-0.0026874	-0.33 LBS	Y FORCE	-0.0002714	-0.0026874	-0.33 LBS
ROLL MOMENT	-0.0002113	-0.0010483	-1.16 FT-LBS	ROLL MOMENT	-0.0001288	-0.0006376	-0.71 FT-LBS
PITCH MOMENT	-0.0000006	-0.0000029	-0.00 FT-LBS	PITCH MOMENT	-0.0000006	-0.0000029	-0.00 FT-LBS
YAW MOMENT	0.0018975	0.0093931	10.43 FT-LBS	YAW MOMENT	0.0017050	0.0084299	10.47 FT-LBS
				POWER	0.0019050	0.0473479	1.46 HP

* * * * * * ROTOR LOADS * * * * * *

BEAM LOADS (IN-LBS)			CHORD LOADS (IN-LBS)			TORSION LOADS (IN-LBS)		
R/R	MEAN	OSC /MAX AZ/MIN AZ	MEAN	OSC /MAX AZ/MIN AZ	R/R	MEAN	OSC /MAX AZ/MIN AZ
.20	1.40	1.98 / 0. / 70.	1.52	1.06 / 70. / 350.	.20	-5.04	4.39 / 290. / 100.
.35	0.91	1.59 / 0. / 70.	1.19	1.35 / 70. / 0.	.35	-4.90	4.27 / 290. / 100.
.45	0.71	1.58 / 0. / 90.	0.98	2.15 / 70. / 0.	.45	-4.71	4.11 / 290. / 100.
.65	0.26	1.27 / 250. / 90.	0.48	1.99 / 70. / 0.	.65	-4.14	3.61 / 290. / 100.
.80	-0.15	1.18 / 250. / 130.	0.16	1.12 / 60. / 0.	.80	-3.62	3.15 / 290. / 100.

Figure 10. Baseline Case Fiberglass Blade with 0° Twist and Trailing Edge Flap, $\mu = 0.398$, $M_{1,90} = 0.440$, $C_L/\sigma = 0.027$.

BELL HELICOPTER COMPANY
ROTORCRAFT FLIGHT SIMULATION PROGRAM ANAL7213
COMPUTED 06/20/73

10 73062801 FIBERGLASS BLD,NO TWIST,TRAILING EDGE FLAP
FIBERGLASS BLADE WITH NO TWIST
NO CYCLIC DETUNING

ROTOR CONTROLS		ROTOR PARAMETERS		TUNNEL PARAMETERS		PROGRAM OPTIONS	
COLLECTIVE PITCH	3.200 DEG	ROTOR SPEED	734.00 RPM	FORWARD SPEED	62.10 KTS	NO INPUT MODES	6
F/A CYCLIC PITCH	2.332 DEG	SOLIDITY	0.0625	ADVANCE RATIO	0.2984	MAX YAW FLOW ANG	0.0 DEG
LAT CYCLIC PITCH	-1.597 DEG	BLADE RADIUS	4.57 FT	ADV TIP MACH NO	0.408	AERODYNAMICS	TABLE
TOT CYC FEATHER	3.251 DEG	CHORD	2.69 IN	SIGMA PRIME	1.000	TORSION	ON
DELTA 3	0.0 DEG	PRECONE	0.0 DEG	MAST TILT ANGLE	0.0 DEG	NON STEADY AERO	OFF
F/A FLAP ANGLE	-0.067 DEG	CONING	4.502 DEG	TPP ANG OF ATTACK	-0.07 DEG	FLAP ITERATION	ON
LAT FLAP ANGLE	0.043 DEG	TWIST	0.0 DEG	CNT PL ANG OF ATTACK	-2.83 DEG	FREQUENCY CHANGE	OFF
TOTAL FLAP ANGLE	0.092 DEG	TIP SWEEP	0.0 DEG	ROTOR TIP SPEED	351.3 FT/SEC	ELASTIC PYLON	OFF

* * * * * * FORCES AND MOMENTS * * * * * *

	WIND AXIS SYSTEM DIMENSIONLESS HELICOPTER	WIND AXIS SYSTEM DIMENSIONLESS FIXED-WING	WIND AXIS SYSTEM DIMENSIONAL		SHAFT AXIS SYSTEM DIMENSIONLESS HELICOPTER	SHAFT AXIS SYSTEM DIMENSIONLESS FIXED-WING	SHAFT AXIS SYSTEM DIMENSIONAL
LIFT FORCE	0.0493310	0.8650625	58.95 LBS	THRUST	0.0493310	0.8650625	58.95 LBS
DRAG FORCE	0.0002136	0.0037693	0.26 LBS	H FORCE	0.0002136	0.0037693	0.26 LBS
LAT FORCE	-0.0008298	-0.0146394	-1.00 LBS	Y FORCE	-0.0008298	-0.0146394	-1.00 LBS
ROLL MOMENT	-0.0001933	-0.0017048	-1.06 FT-LBS	ROLL MOMENT	-0.0001933	-0.0017048	-1.06 FT-LBS
PITCH MOMENT	0.0000530	0.0004678	0.29 FT-LBS	PITCH MOMENT	0.0000530	0.0004678	0.29 FT-LBS
YAW MOMENT	0.0016399	0.0144661	9.01 FT-LBS	YAW MOMENT	0.0016399	0.0144661	9.01 FT-LBS
				POWER	0.0016399	0.0969641	1.26 HP

* * * * * * ROTOR LOADS * * * * * *

BEAM LOADS (IN-LBS) R/R	MEAN	OSC /MAX AZ/MIN AZ	CHORD LOADS (IN-LBS) MEAN	OSC /MAX AZ/MIN AZ	TORSION LOADS (IN-LBS) R/R	MEAN	OSC /MAX AZ/MIN AZ
.20	1.85	1.67 / 0. / 90.	1.35	1.41 / 70. / 250.	.20	-4.07	3.13 / 300. / 90.
.35	1.08	1.45 / 0. / 90.	1.05	2.30 / 70. / 250.	.35	-3.96	3.05 / 300. / 90.
.45	0.71	1.53 / 250. / 90.	0.36	2.61 / 70. / 250.	.45	-3.81	2.93 / 300. / 90.
.65	0.14	1.55 / 260. / 90.	0.41	2.26 / 70. / 250.	.65	-3.35	2.58 / 300. / 90.
.80	-0.52	1.37 / 270. / 170.	0.12	1.18 / 70. / 250.	.80	-2.93	2.25 / 300. / 90.

Figure 10. Concluded: $\mu = 0.298$, $M_{1,90} = 0.408$, $C_L/\sigma = 0.049$.

BELL HELICOPTER TEXTRON
ROTORCRAFT FLIGHT SIMULATION PROGRAM ANAL7213
COMPUTED 04/29/73

1 73062803 ALUMINUM BLD , COLLECTIVE SWEEP=.027 1ST-FOLLOWED BY .049
ALUMINUM BLADE WITH ZERO TWIST
NO CYCLIC DETUNING

ROTOR CONTROLS		ROTOR PARAMETERS		TUNNEL PARAMETERS		PROGRAM OPTIONS	
COLLECTIVE PITCH	4.933 DEG	ROTOR SPEED	734.00 RPM	FORWARD SPEED	82.90 KTS	NO INPUT MODES	6
F/A CYCLIC PITCH	3.690 DEG	SOLIDITY	0.0625	ADVANCE RATIO	0.3983	MAX YAW FLOW ANG	0.0 DEG
LAT CYCLIC PITCH	-1.176 DEG	BLADE RADIUS	4.57 FT	ADV TIP MACH NO	0.440	AERODYNAMICS	TABLE
TOT CYC FEATHER	3.873 DEG	CHORD	2.69 IN	SIGMA PRIME	1.000	TORSION	ON
DELTA 3	0.0 DEG	PRECONE	0.0 DEG	MAST TILT ANGLE	2.50 DEG	NON STEADY AERO	OFF
F/A FLAP ANGLE	-0.705 DEG	CONING	4.106 DEG	TPP ANG OF ATTACK	-3.20 DEG	FLAP ITERATION	ON
LAT FLAP ANGLE	0.0 DEG	TWIST	0.0 DEG	CNT PL ANG OF ATTACK	-6.19 DEG	FREQUENCY CHANGE	OFF
TOTAL FLAP ANGLE	0.705 DEG	TIP SWEEP	0.0 DEG	ROTOR TIP SPEED	351.3 FT/SEC	ELASTIC PYLON	OFF

* * * * * * FORCES AND MOMENTS * * * * * *

WIND AXIS SYSTEM

	DIMENSIONLESS		DIMENSIONAL
	HELICOPTER	FIXED-WING	
LIFT FORCE	0.0263826	0.2661472	32.32 LBS
DRAG FORCE	-0.0001738	-0.0046509	-1.05 LBS
LAT FORCE	-0.0003281	-0.0032480	-0.39 LBS
ROLL MOMENT	-0.0001352	-0.0006199	-0.69 FT-LBS
PITCH MOMENT	0.0000561	0.0002775	0.31 FT-LBS
YAW MOMENT	0.0021913	0.0108475	12.04 FT-LBS

SHAFT AXIS SYSTEM

	DIMENSIONLESS		DIMENSIONAL
	HELICOPTER	FIXED-WING	
THRUST	0.0268952	0.2662714	32.34 LBS
H FORCE	0.0002996	0.0029666	0.36 LBS
Y FORCE	-0.0003281	-0.0032480	-0.39 LBS
ROLL MOMENT	-0.0000295	-0.0001451	-0.16 FT-LBS
PITCH MOMENT	0.0000561	0.0002775	0.31 FT-LBS
YAW MOMENT	0.0021947	0.0108642	12.06 FT-LBS
POWER	0.0021947	0.0545500	1.69 HP

* * * * * * BEAM LOADS (IN-LBS)

R/R	MEAN	OSC /MAX AZ/MIN AZ
.20	4.76	2.10 / 0. / 80.
.35	4.03	2.20 / 0. / 70.
.45	3.39	2.16 / 0. / 70.
.65	1.87	2.47 / 250. / 190.
.80	0.58	1.82 / 260. / 190.

* * * * * * ROTOR LOADS * * * * * *

CHORD LOADS (IN-LBS)

MEAN	OSC /MAX AZ/MIN AZ
2.11	1.31 / 40. / 340.
1.60	2.11 / 40. / 350.
1.22	2.34 / 40. / 350.
0.39	1.90 / 40. / 350.
0.06	0.95 / 40. / 350.

TORSION LOADS (IN-LBS)

R/R	MEAN	OSC /MAX AZ/MIN AZ
.20	0.44	0.72 / 180. / 250.
.35	0.43	0.70 / 180. / 250.
.45	0.42	0.67 / 180. / 250.
.65	0.37	0.59 / 180. / 250.
.80	0.32	0.51 / 180. / 250.

Figure 11. Baseline Case Aluminum Blade with 0° Twist, $\mu = 0.398$, $M_{1,90} = 0.440$, $C_L/\sigma = 0.027$.

BELL HELICOPTER COMPANY
ROTORCRAFT FLIGHT SIMULATION PROGRAM ANAL7213
COMPUTED 06/29/73

1 73062901 ALUMINUM BLD , COLLECTIVE SWEEP:.027 1ST-FOLLOWED BY .049
ALUMINUM BLADE WITH ZERO TWIST
NO CYCLIC DETUNING

ROTOR CONTROLS		ROTOR PARAMETERS		TUNNEL PARAMETERS		PROGRAM OPTIONS	
COLLECTIVE PITCH	5.044 DEG	ROTOR SPEED	734.00 RPM	FORWARD SPEED	62.10 KTS	NO INPUT MODES	6
F/A CYCLIC PITCH	3.620 DEG	SOLIDITY	0.0625	ADVANCE RATIO	0.2984	MAX YAW FLOW ANG	0.0 DEG
LAT CYCLIC PITCH	-1.663 DEG	BLADE RADIUS	4.57 FT	ADV TIP MACH NO	0.408	AERODYNAMICS	TABLE
TOT CYC FEATHER	3.784 DEG	CHORD	2.69 IN	SIGMA PRIME	1.000	TORSION	ON
DELTA 3	0.0 DEG	PRECONE	0.0 DEG	MAST TILT ANGLE	0.0 DEG	NON STEADY AERO	OFF
F/A FLAP ANGLE	-1.358 DEG	CONING	5.452 DEG	TPP ANG OF ATTACK	-1.36 DEG	FLAP ITERATION	ON
LAT FLAP ANGLE	0.0 DEG	TWIST	0.0 DEG	CNT PL ANG OF ATTACK	-3.62 DEG	FREQUENCY CHANGE	OFF
TOTAL FLAP ANGLE	1.358 DEG	TIP SWEEP	0.0 DEG	ROTOR TIP SPEED	351.3 FT/SEC	ELASTIC PYLON	OFF

* * * * * * FORCES AND MOMENTS * * * * * *

	WIND AXIS SYSTEM DIMENSIONLESS HELICOPTER	WIND AXIS SYSTEM DIMENSIONLESS FIXED-WING	WIND AXIS SYSTEM DIMENSIONAL		SHAFT AXIS SYSTEM DIMENSIONLESS HELICOPTER	SHAFT AXIS SYSTEM DIMENSIONLESS FIXED-WING	SHAFT AXIS SYSTEM DIMENSIONAL
LIFT FORCE	0.0489261	0.8632109	58.83 LBS	THRUST	0.0489261	0.8632109	58.83 LBS
DRAG FORCE	-0.0001360	-0.0023989	-0.16 LBS	H FORCE	-0.0001360	-0.0023989	-0.16 LBS
LAT FORCE	-0.0008652	-0.0152640	-1.04 LBS	Y FORCE	-0.0008652	-0.0152640	-1.04 LBS
ROLL MOMENT	-0.0001263	-0.0011144	-0.69 FT-LBS	ROLL MOMENT	-0.0001263	-0.0011144	-0.69 FT-LBS
PITCH MOMENT	0.0000757	0.0006682	0.42 FT-LBS	PITCH MOMENT	0.0000757	0.0006682	0.42 FT-LBS
YAW MOMENT	0.0023546	0.0207716	12.94 FT-LBS	YAW MOMENT	0.0023546	0.0207716	12.94 FT-LBS
				POWER	0.0023546	0.1392282	1.91 HP

* * * * * * ROTOR LOADS * * * * * *

BEAM LOADS (IN-LBS)			CHORD LOADS (IN-LBS)			TORSION LOADS (IN-LBS)		
R/R	MEAN	OSC /MAX AZ/MIN AZ	MEAN	OSC /MAX AZ/MIN AZ	R/R	MEAN	OSC /MAX AZ/MIN AZ
.20	5.19	2.68 / 0. / 90.	2.33	1.91 / 40. / 240.	.20	0.87	0.93 / 130. / 260.
.35	3.87	2.79 / 0. / 90.	1.72	3.04 / 40. / 240.	.35	0.95	0.91 / 130. / 260.
.45	3.25	3.17 / 260. / 90.	1.30	3.31 / 40. / 240.	.45	0.82	0.87 / 180. / 260.
.65	1.39	3.32 / 270. / 180.	0.41	2.56 / 40. / 240.	.65	0.72	0.77 / 180. / 260.
.80	-0.01	2.34 / 270. / 180.	0.03	1.25 / 40. / 230.	.80	0.62	0.67 / 180. / 260.

Figure 11. Concluded: $\mu = 0.298$, $M_{1,90} = 0.408$, $C_L/\sigma = 0.049$.

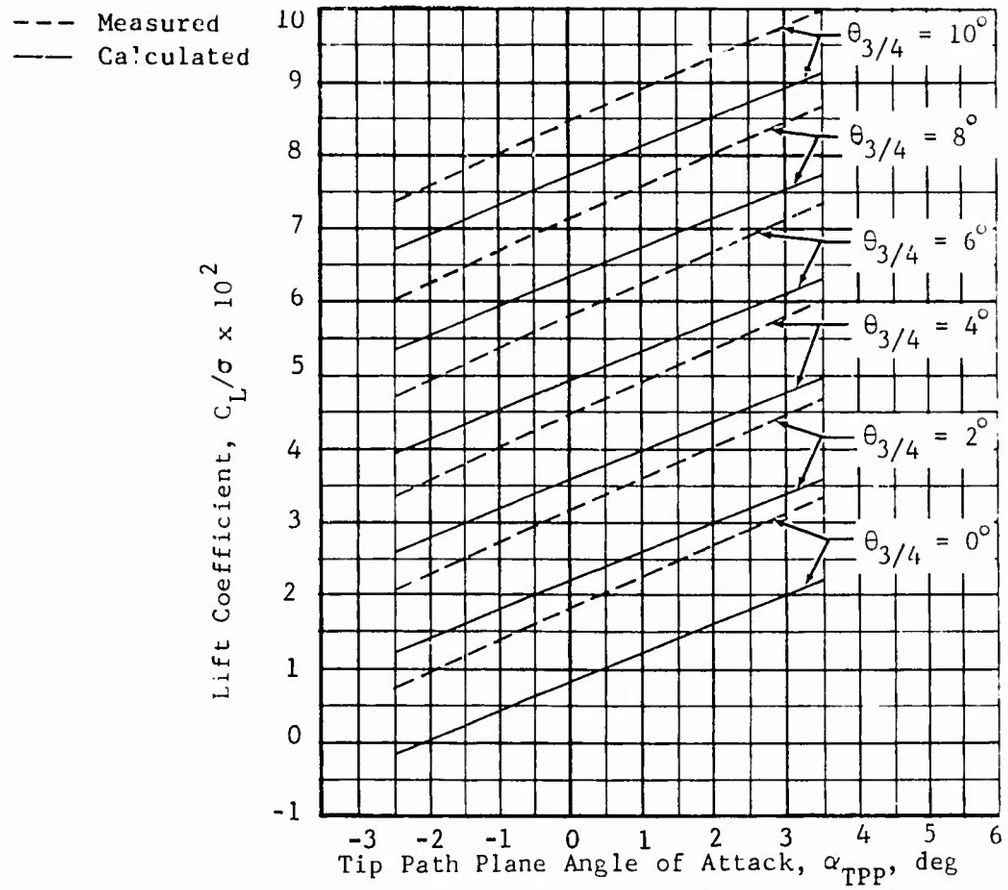

Figure 12. Comparison of Regression Analysis Results for Measured and Calculated Lift.

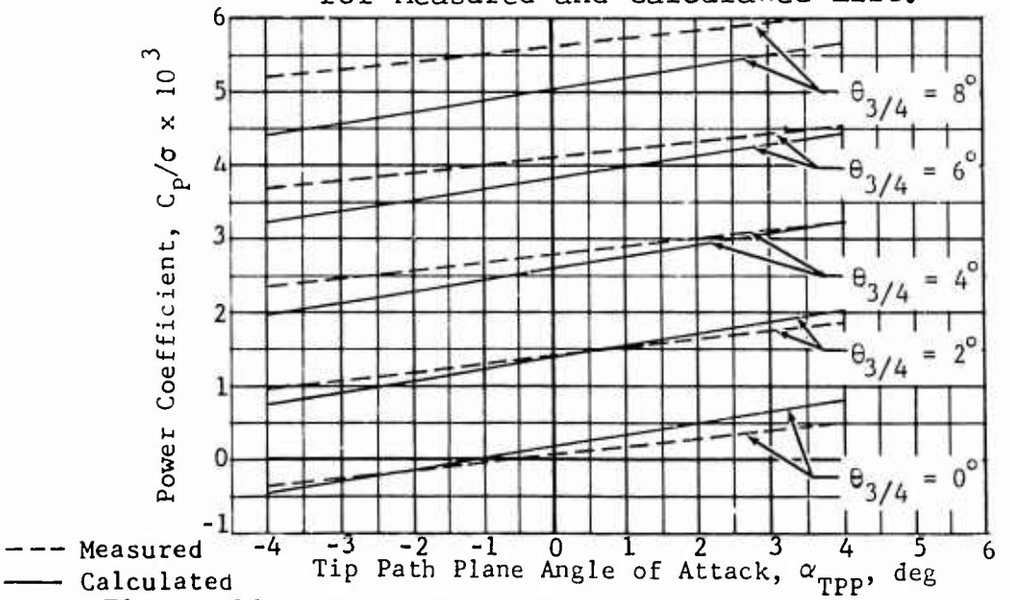

Figure 13. Comparison of Regression Analysis Results for Measured and Calculated Power.

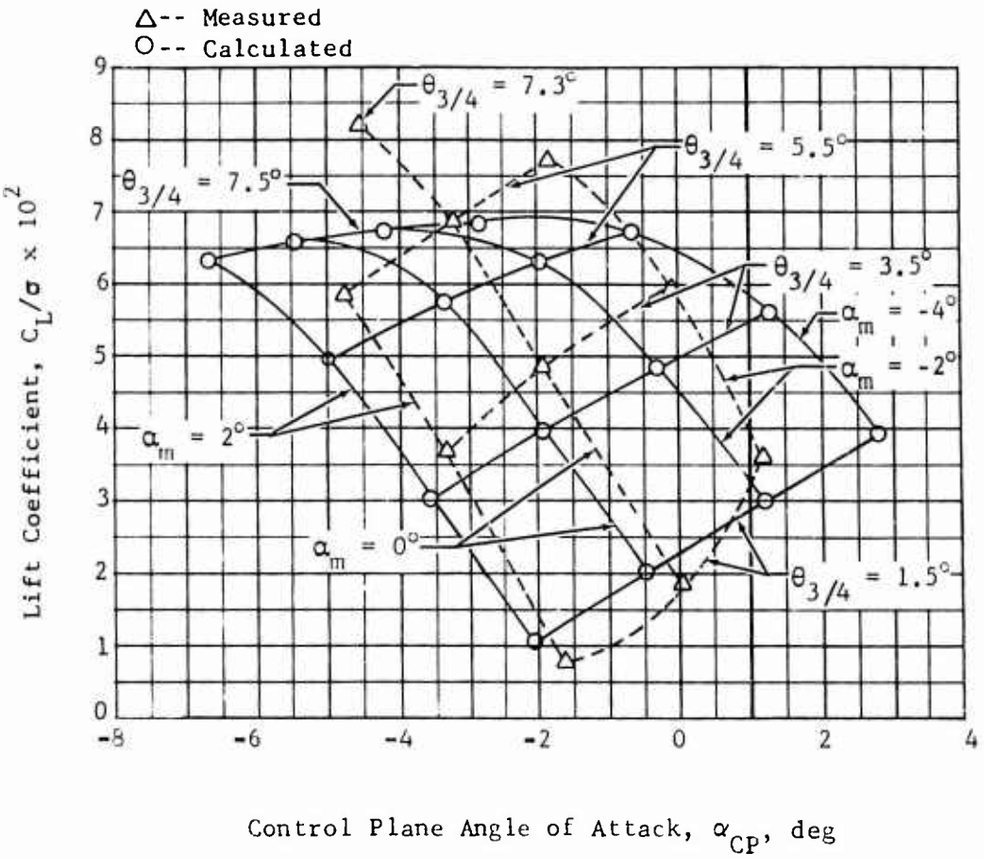

Figure 14. Lift Coefficient vs. Control Plane Angle of Attack, Fiberglass Blade, -8^o Twist, μ=0.299, $M_{1.90}$=0.408 Model Aerodynamic Data Without Unsteady Terms.

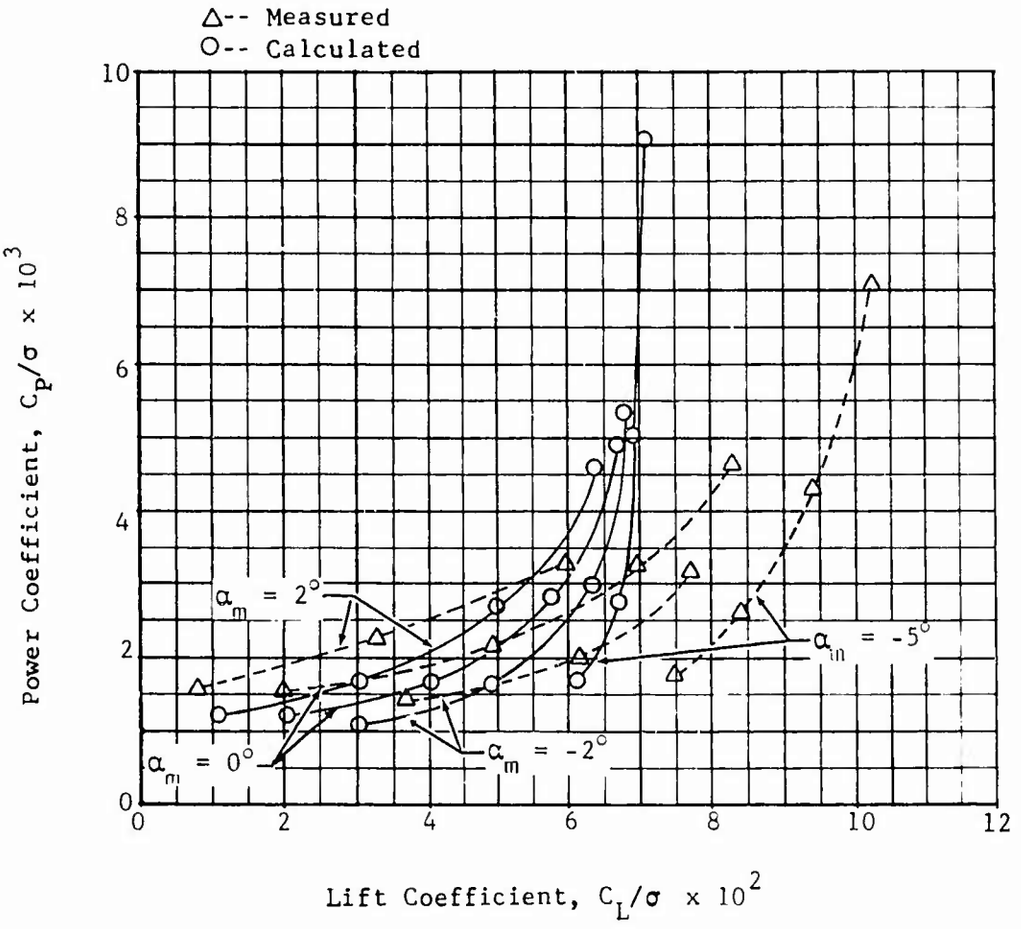

Figure 15. Power Coefficient vs. Lift Coefficient, Fiberglass Blade, -8° Twist, μ=0.299, $M_{L,90}$=0.408 Model Aerodynamic Data Without Unsteady Terms.

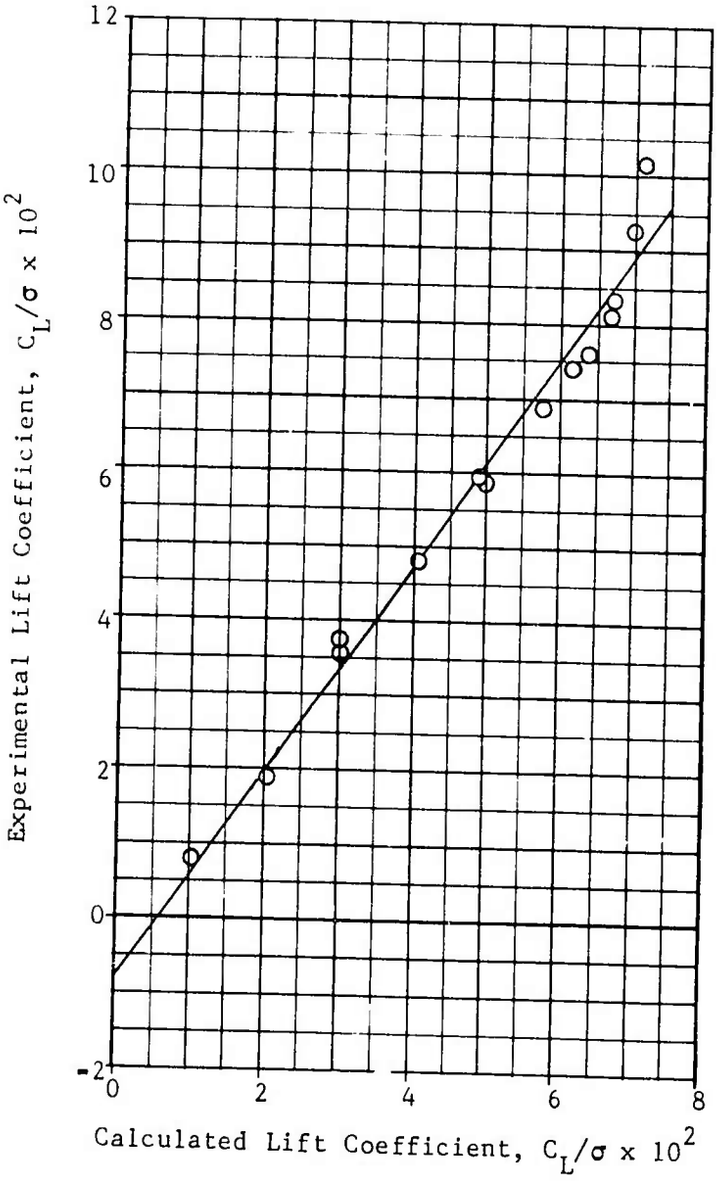

Figure 16. Experimental Lift Coefficient vs. Calculated Lift Coefficient, Fiberglass Blade, -8^o Twist, μ=0.299, $M_{1,90}$=0.408 Model Aerodynamic Data Without Unsteady Terms.

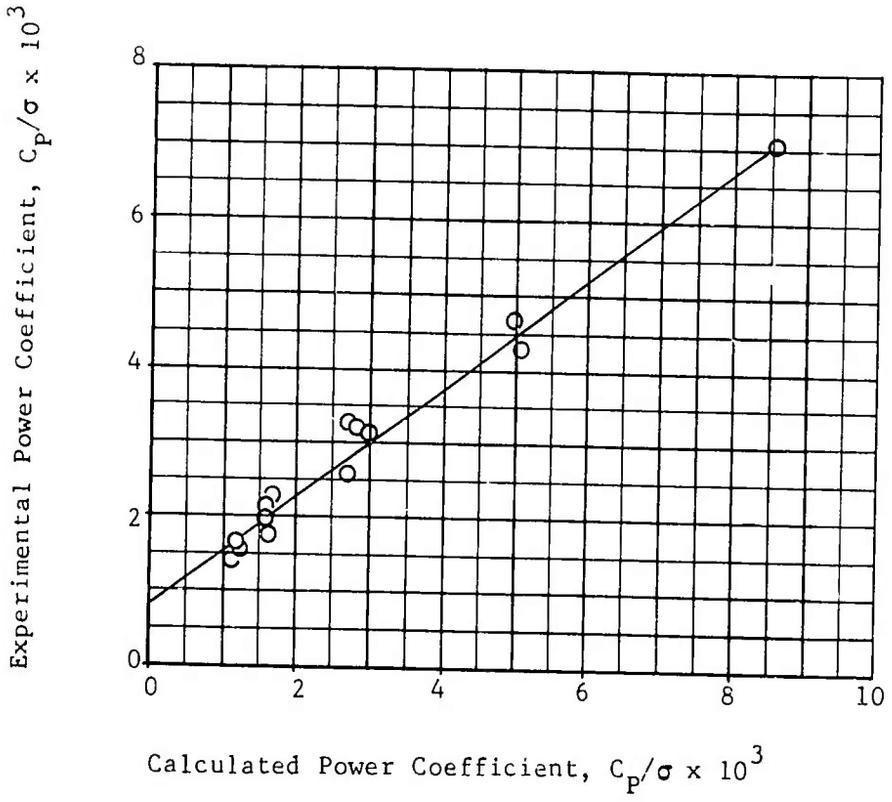

Figure 17. Experimental Power Coefficient vs. Calculated Power Coefficient, Fiberglass Blade, -8° Twist, μ=0.299, $M_{1,90}$=0.408 Model Aerodynamic Data Without Unsteady Terms.

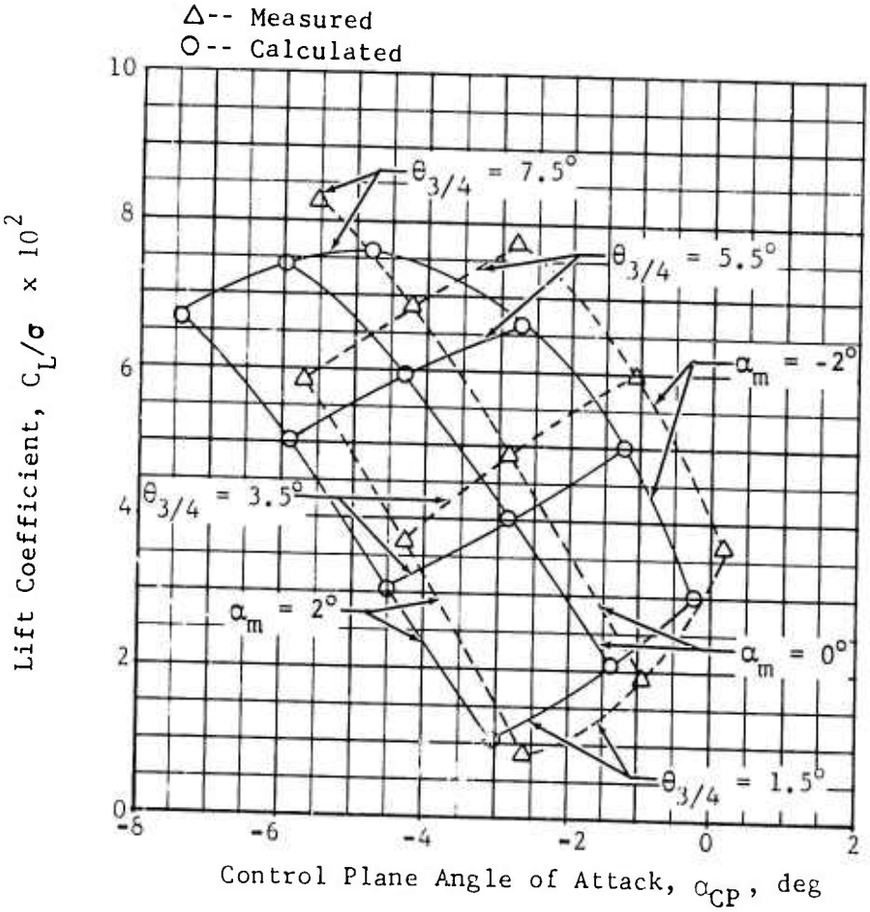

Figure 18. Lift Coefficient vs. Control Plane Angle of Attack, Fiberglass Blade, -8^o Twist, μ=0.299, $M_{1,90}$=0.408 Model Aerodynamic Data With Unsteady Terms.

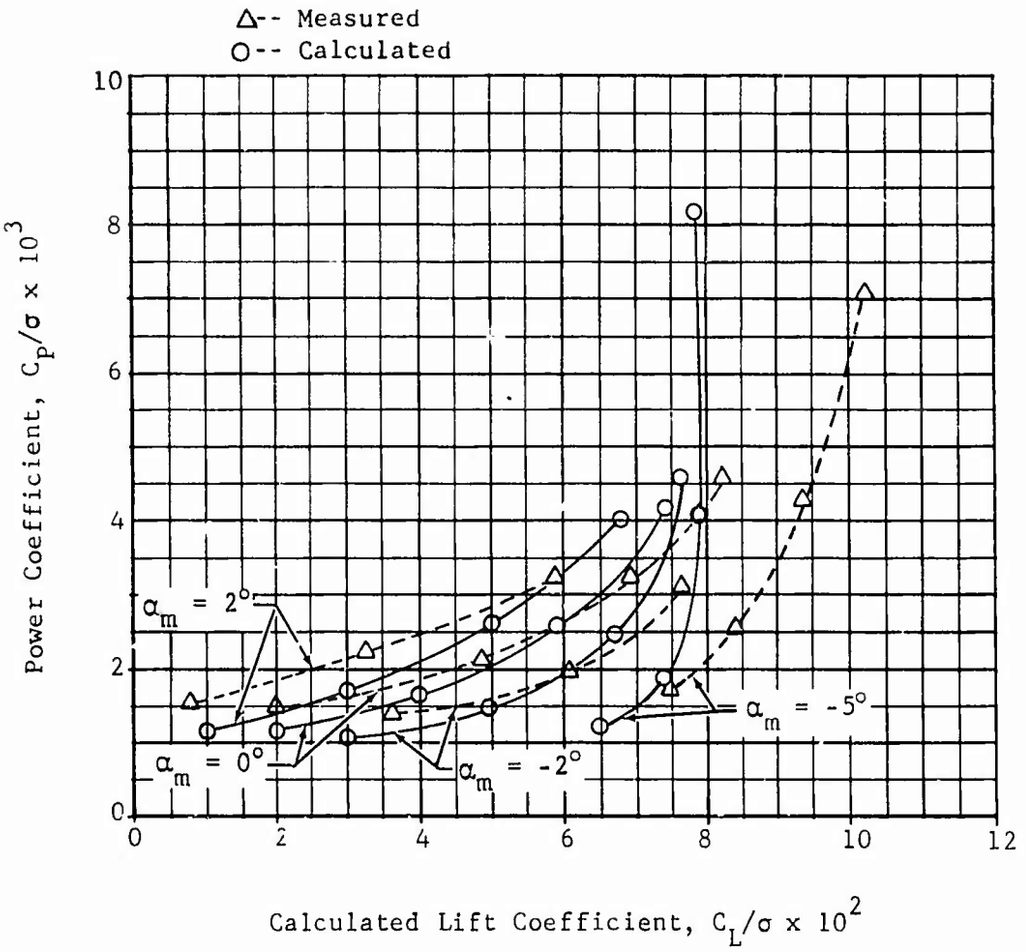

Figure 19. Power Coefficient vs. Lift Coefficient, Fiberglass Blade, -8^o Twist, μ=0.299, $M_{1,90}$=0.408 Model Aerodynamic Data With Unsteady Terms.

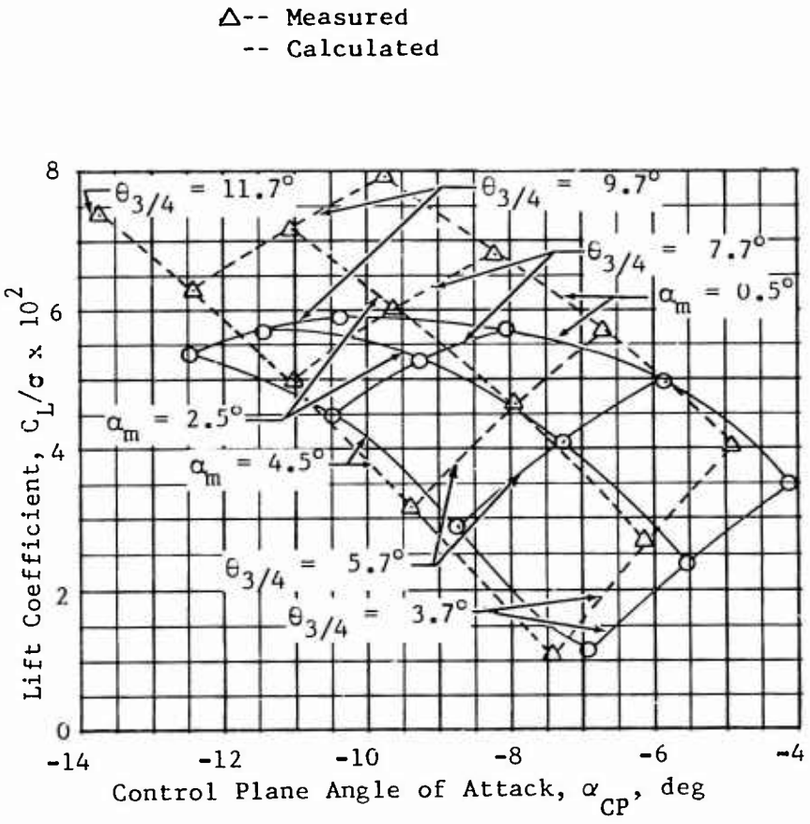

Figure 20. Lift Coefficient vs. Control Plane Angle-of-Attack, Fiberglass Blade, -8° Twist, $\mu = 0.400$, $M_{1,90} = 0.435$

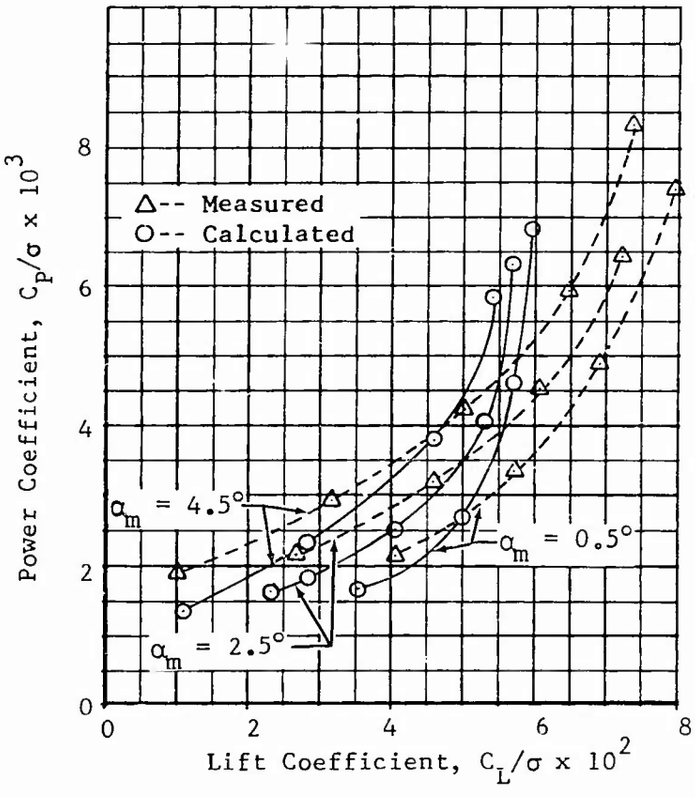

Figure 21. Power Coefficient vs. Lift Coefficient, Fiberglass Blade, -8° Twist, $\mu = 0.400$, $M_{1,90} = 0.435$

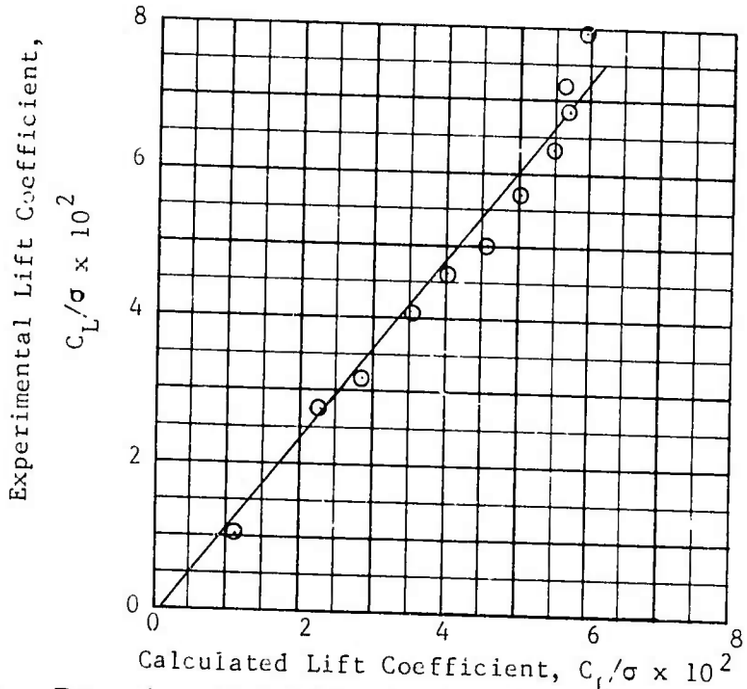

Figure 22. Experimental Lift Coefficient vs. Calculated Lift Coefficient, Fiberglass Blade, -8° Twist, $\mu = 0.400$, $M_{1,90} = 0.435$.

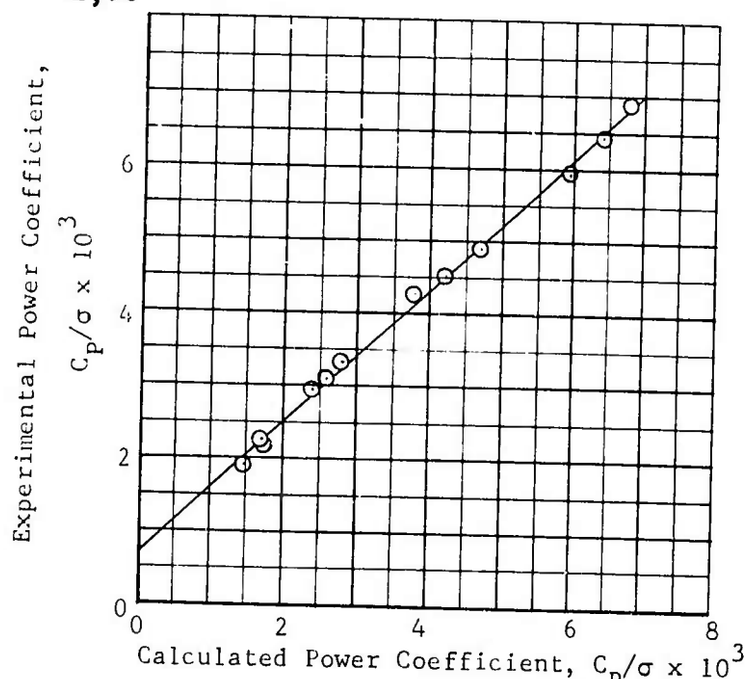

Figure 23. Experimental Power Coefficient vs. Calculated Power Coefficient, Fiberglass Blade, -8° Twist, $\mu = 0.400$, $M_{1,90} = 0.435$

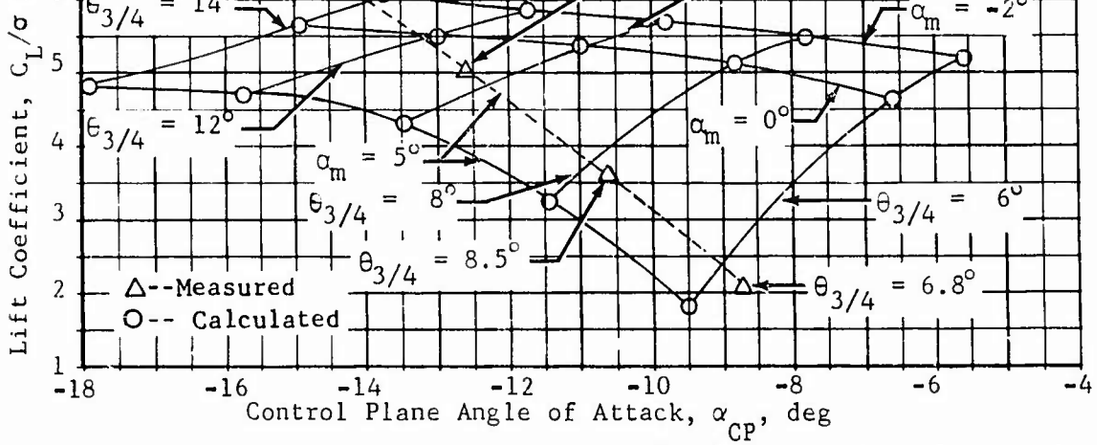

Figure 24. Lift Coefficient vs. Control Plane Angle of Attack, Fiberglass Blade, -8° Twist, μ = 0.502, $M_{1,90}$ = 0.467.

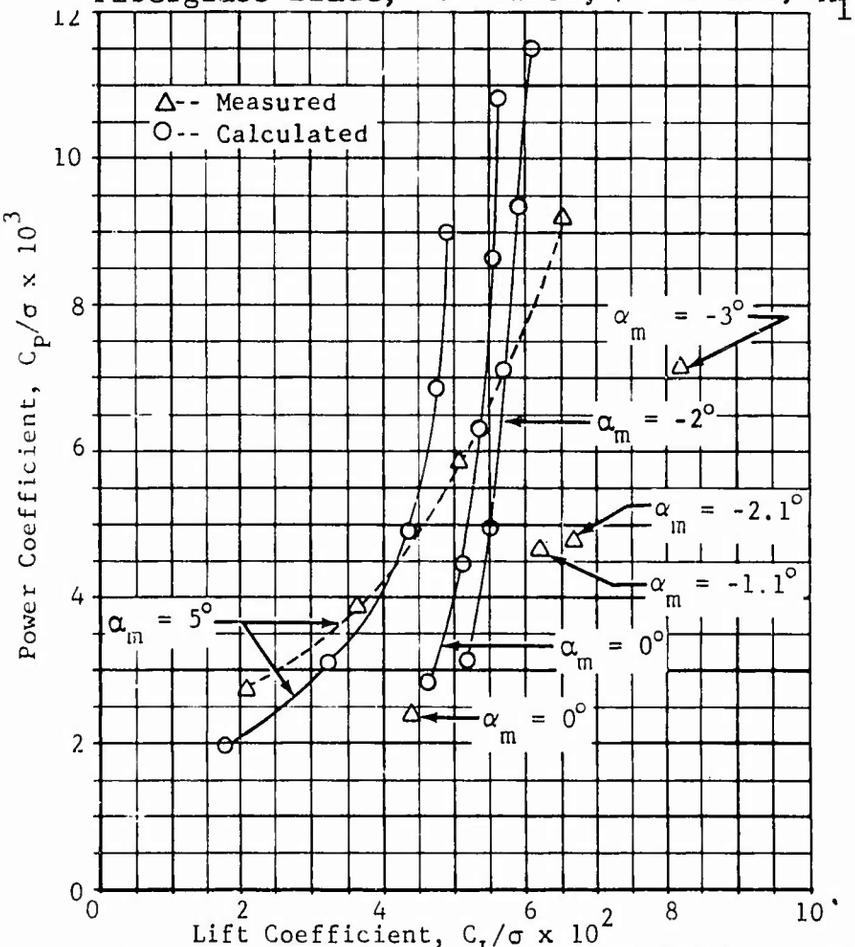

Figure 25. Power Coefficient vs. Lift Coefficient, Fiberglass Blade, -8° Twist, μ = 0.502, $M_{1,90}$ = 0.467.

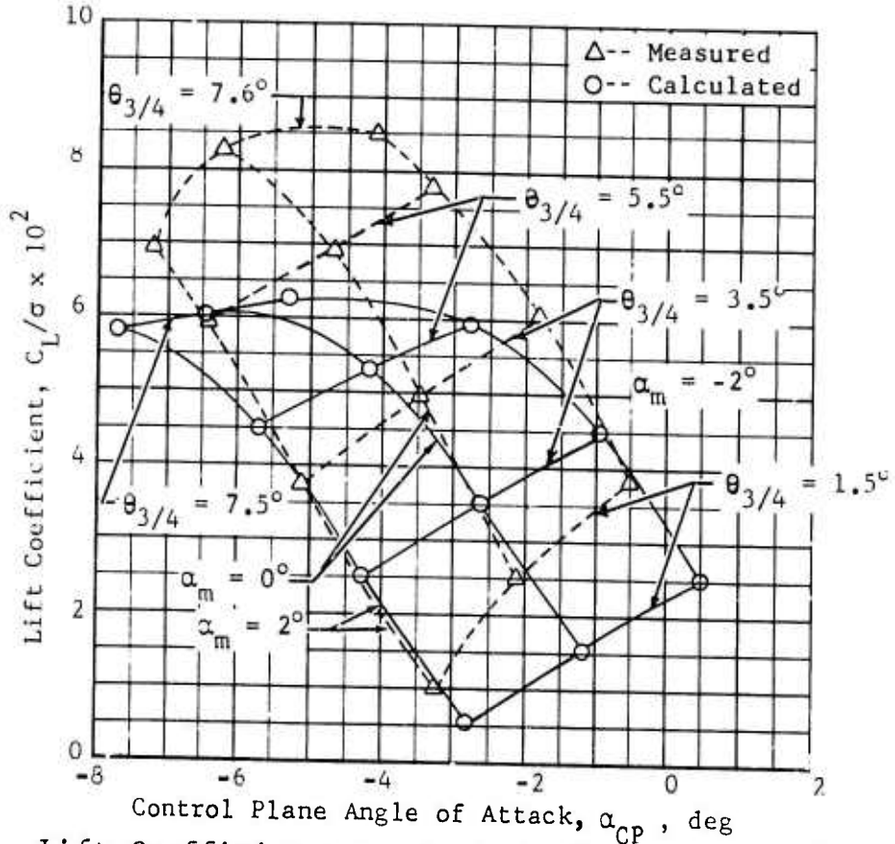

Figure 26. Lift Coefficient vs. Control Plane Angle of Attack, Fiberglass Blade, 0° Twist, $\mu = 0.299$, $M_{1,90} = 0.408$.

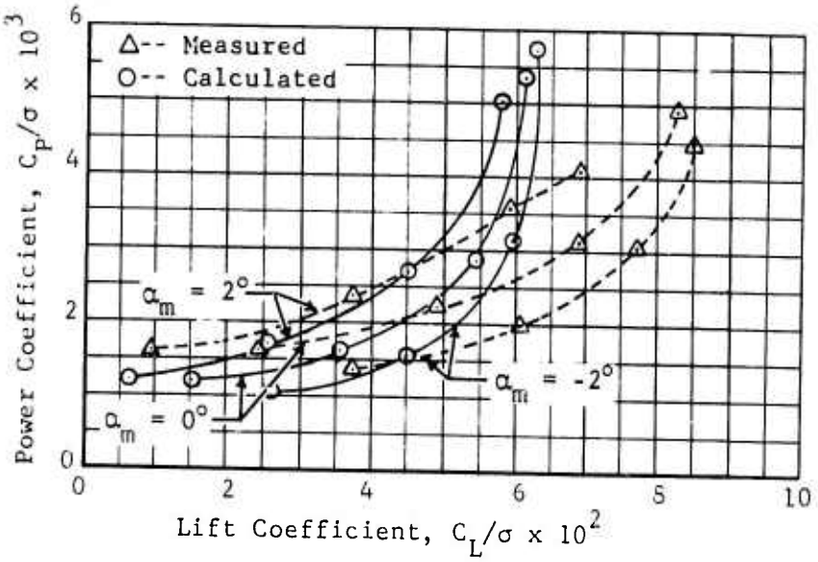

Figure 27. Power Coefficient vs. Lift Coefficient, Fiberglass Blade, 0° Twist, $\mu = 0.299$, $M_{1,90} = 0.408$.

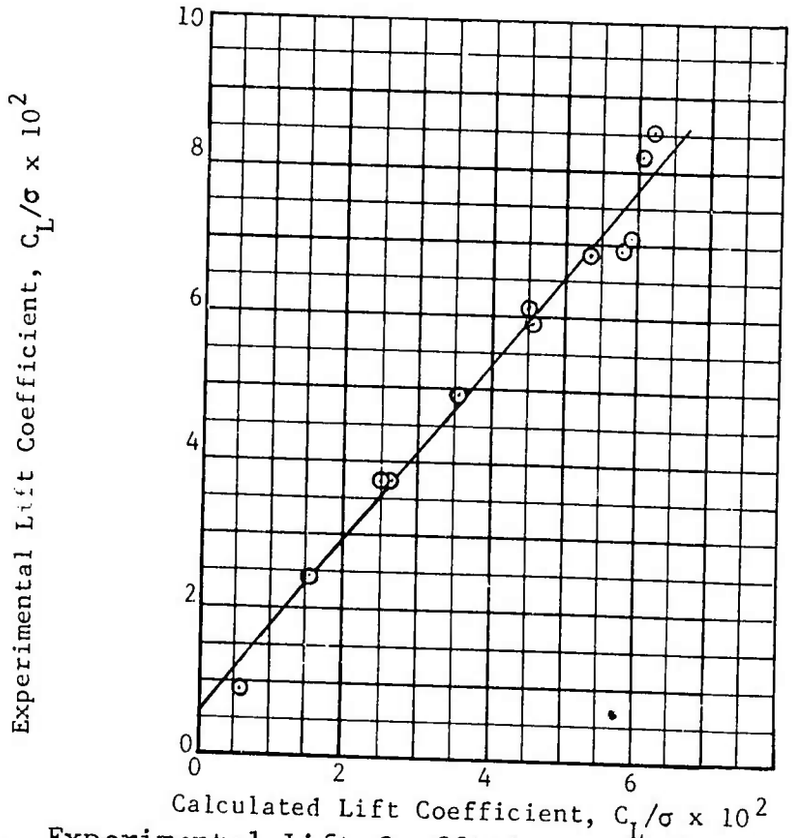

Figure 28. Experimental Lift Coefficient vs. Calculated Lift Coefficient, Fiberglass Blade, 0° Twist, $\mu = 0.299$, $M_{1,90} = 0.408$.

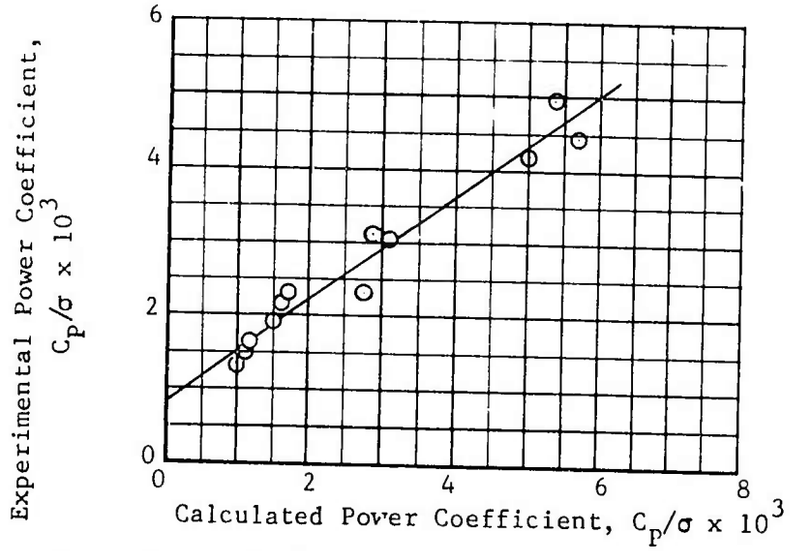

Figure 29. Experimental Power Coefficient vs. Calculated Power Coefficient, Fiberglass Blade, 0° Twist, $\mu = 0.299$, $M_{1,90} = 0.408$.

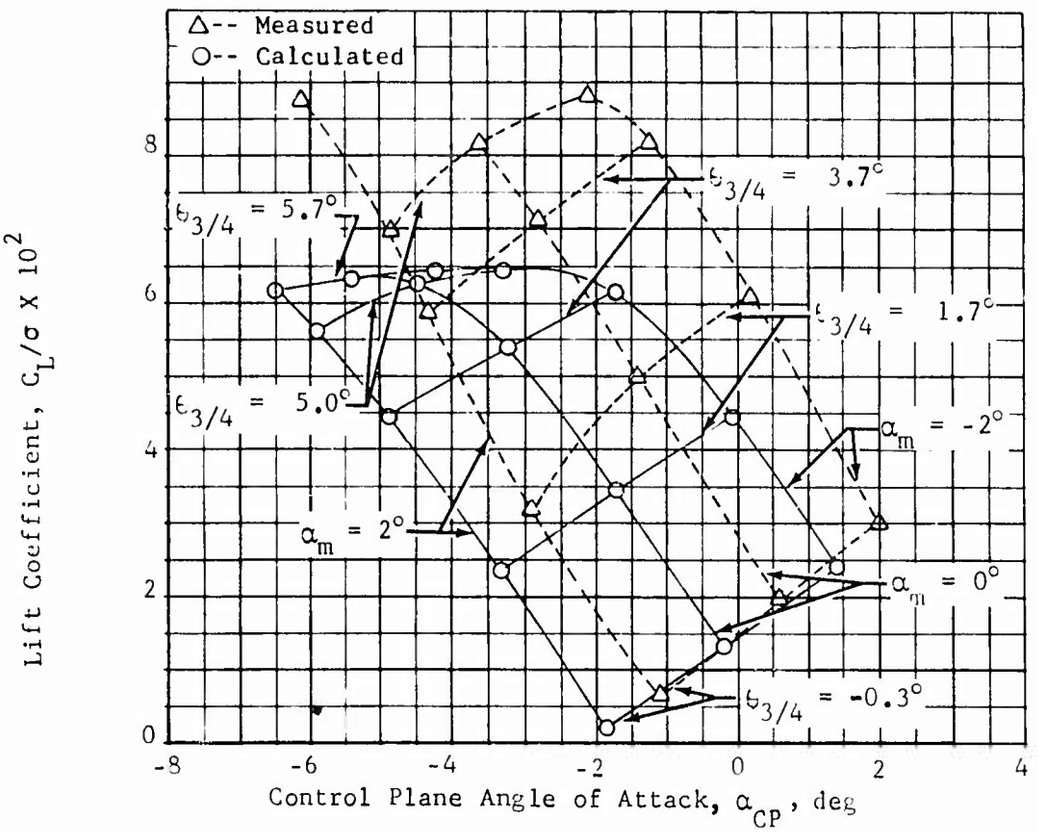

Figure 30. Lift Coefficient vs. Control Plane Angle of Attack, Fiberglass Blade, 0° Twist, δ_F = 5°, μ = 0.299, $M_{1,90}$ = 0.408.

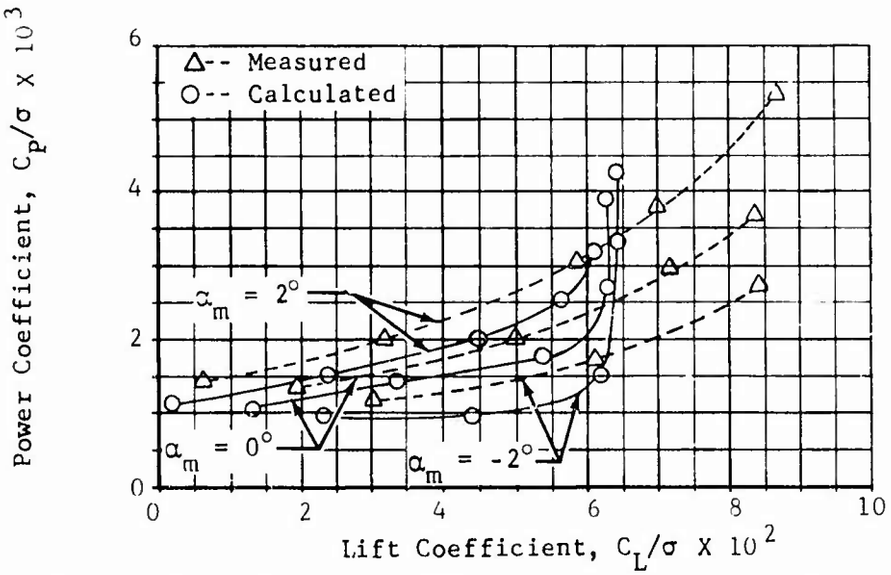

Figure 31. Power Coefficient vs. Lift Coefficient for Collective Pitch Sweep, Fiberglass Blade, 0° Twist, δ_F = 5°, μ = 0.299, $M_{1,90}$ = 0.408.

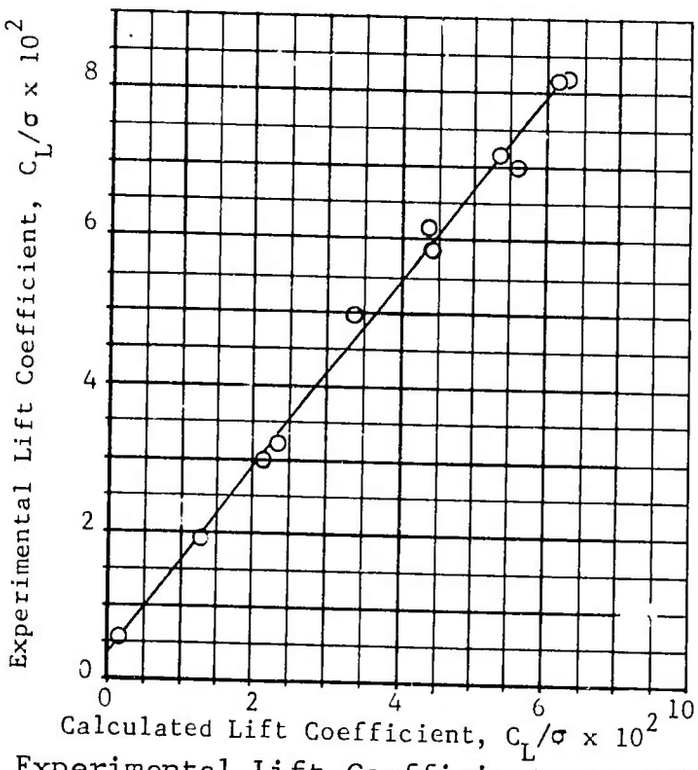

Figure 32. Experimental Lift Coefficient vs. Calculated Lift Coefficient, Fiberglass Blade, 0° Twist, $\delta_F = 5°$, $\mu = 0.299$, $M_{1,90} = 0.408$.

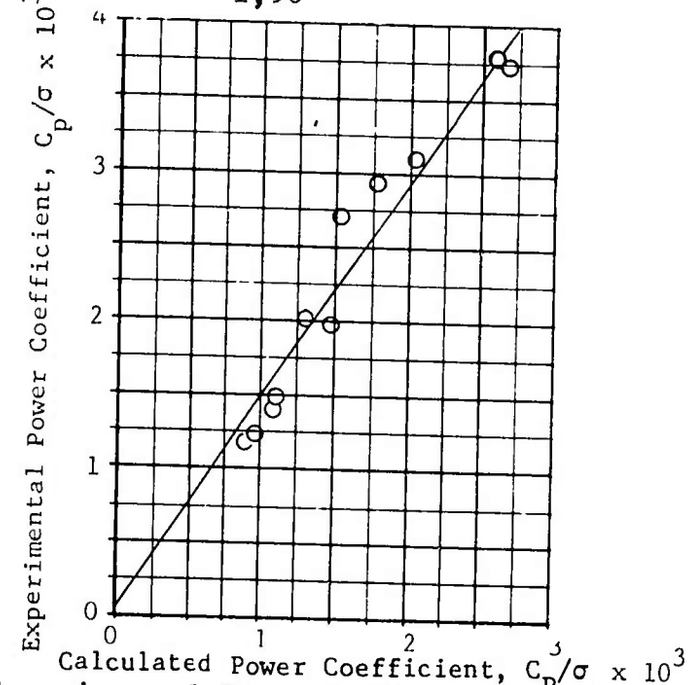

Figure 33. Experimental Power Coefficient vs. Calculated Power Coefficient, Fiberglass Blade, 0° Twist, $\delta_F = 5°$ $\mu = 0.299$, $M_{1,90} = 0.408$.

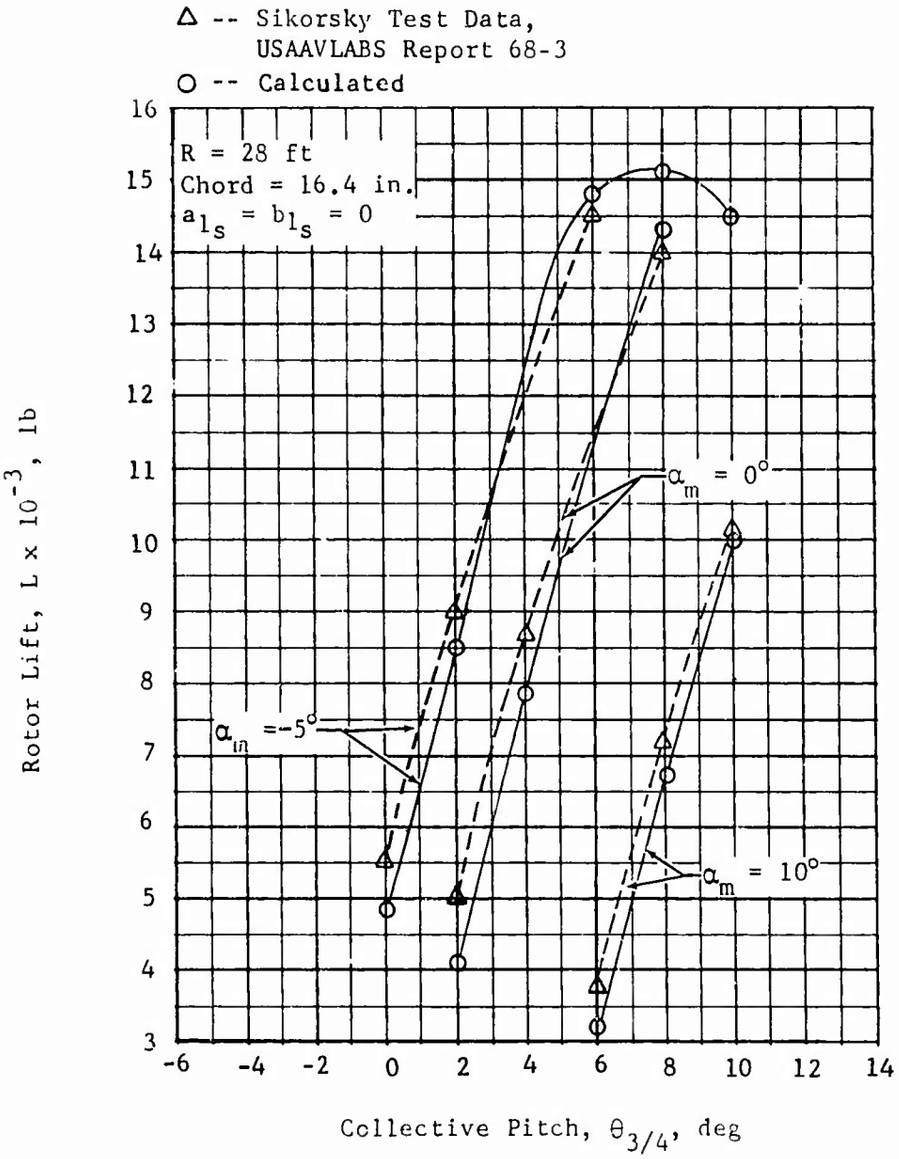

Figure 34. Rotor Lift vs. Collective Pitch for Full-Scale Rotor, -8° Twist, $\mu = 0.300$, $M_{1,90} = 0.740$.

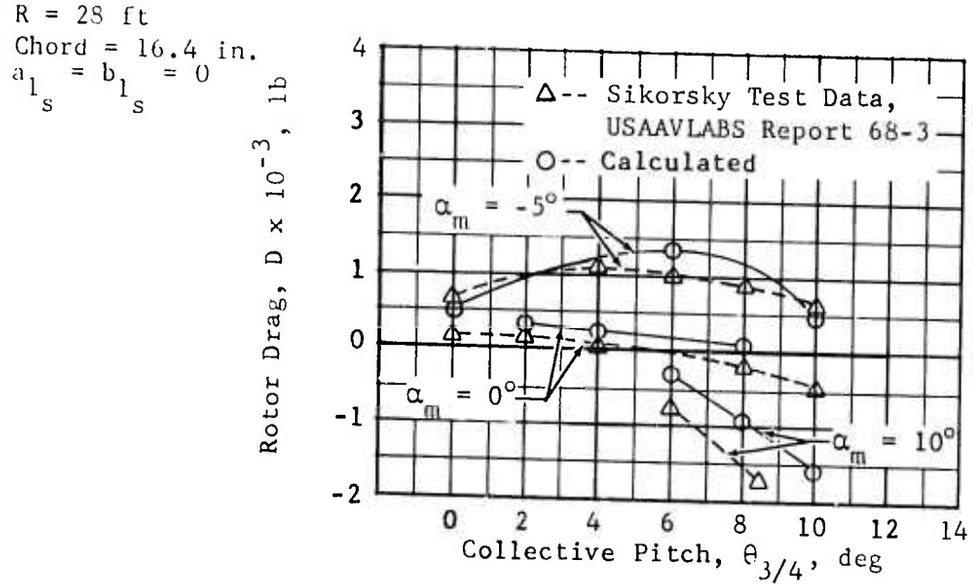

Figure 35. Rotor Drag vs. Collective Pitch for Full-Scale Rotor, -8° Twist, μ = 0.300, $M_{1,90}$ = 0.740.

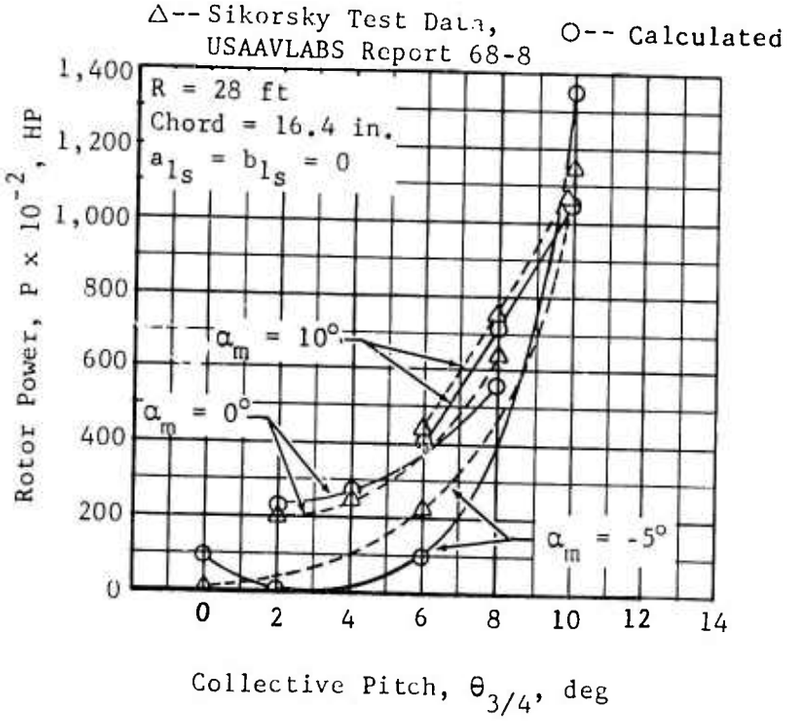

Figure 36. Rotor Power vs. Collective Pitch for Full-Scale Rotor, -8° Twist, μ = 0.300, $M_{1,90}$ = 0.740.

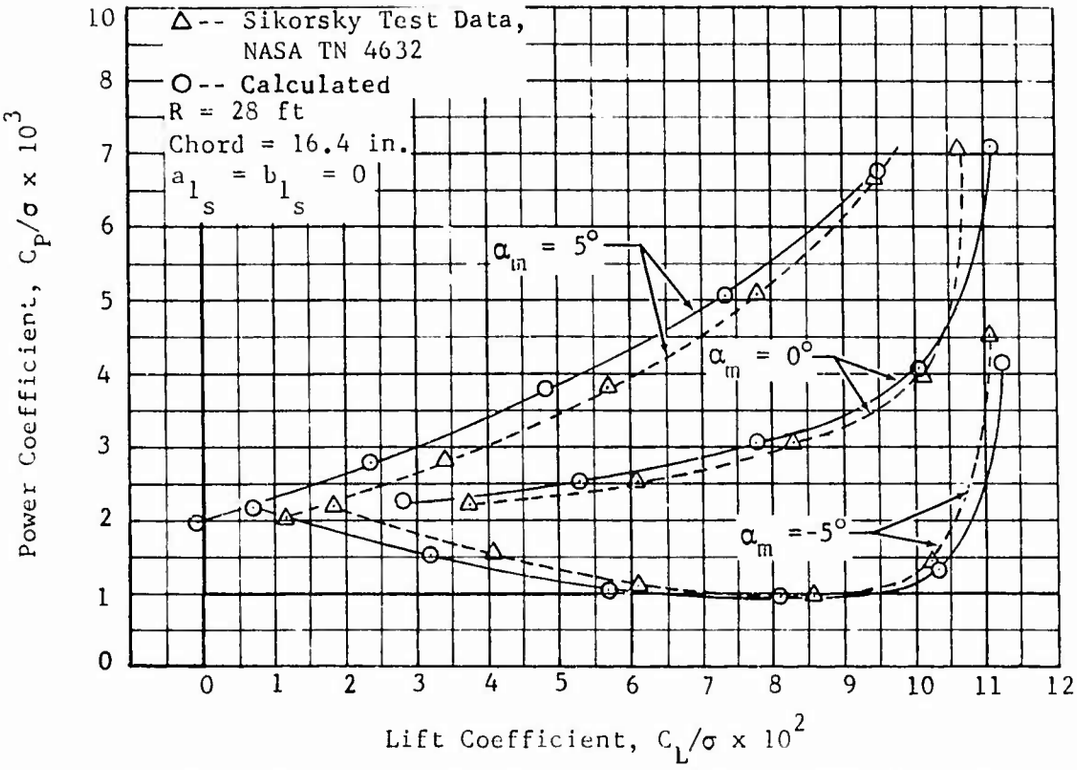

Figure 37. Power Coefficient vs. Lift Coefficient for Full-Scale Rotor, -8° Twist, $\mu = 0.300$, $M_{1,90} = 0.740$.

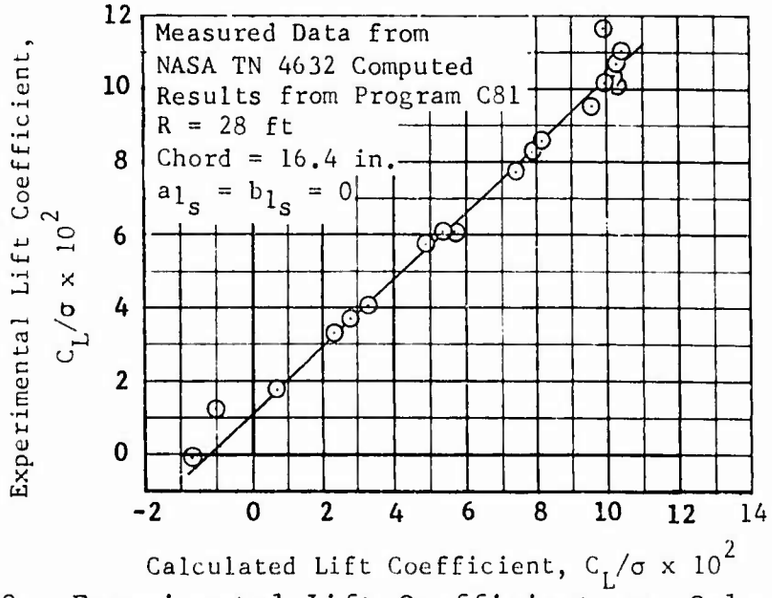

Figure 38. Experimental Lift Coefficient vs. Calculated Coefficient for Full-Scale Rotor, -8° Twist, $\mu = 0.300$, $M_{1,90} = 0.740$.

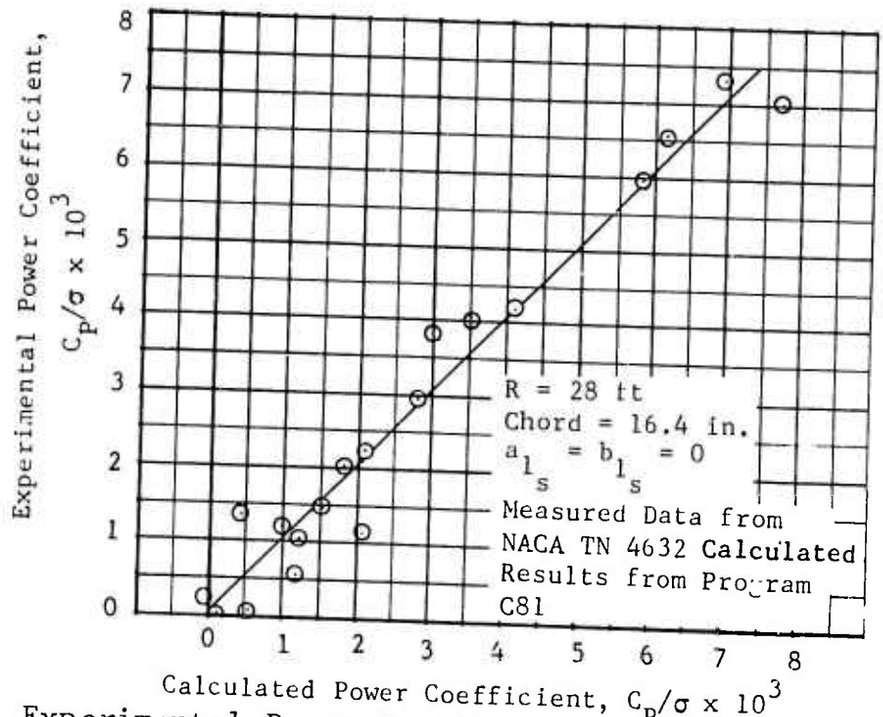

Figure 39. Experimental Power Coefficient vs. Calculated Power Coefficient for Full-Scale Rotor, -8° Twist, $\mu = 0.300$, $M_{1,90} = 0.740$.

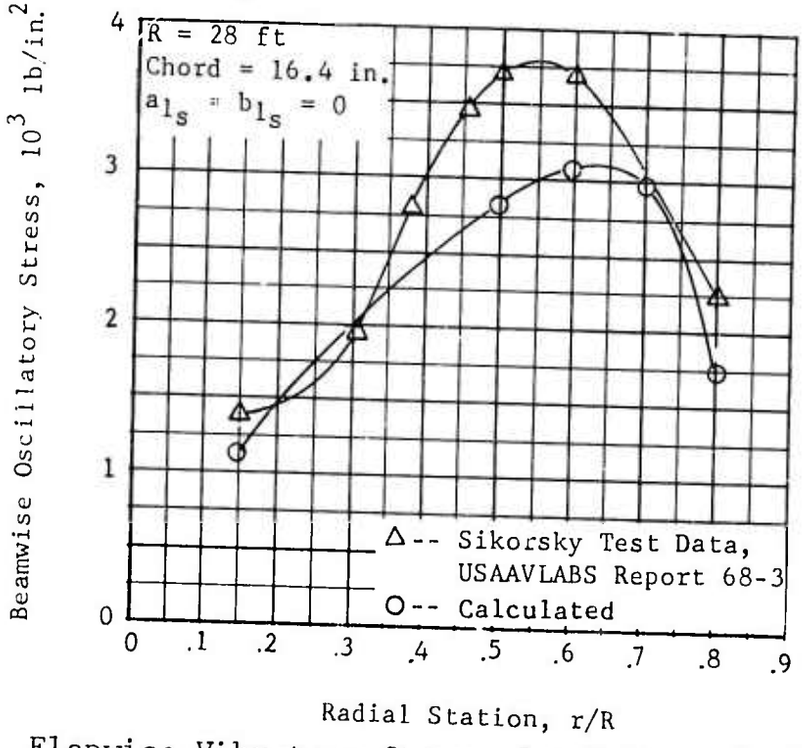

Figure 40. Flapwise Vibratory Stress for Full-Scale Rotor, -8° Twist, $\mu = 0.300$, $M_{1,90} = 0.740$.

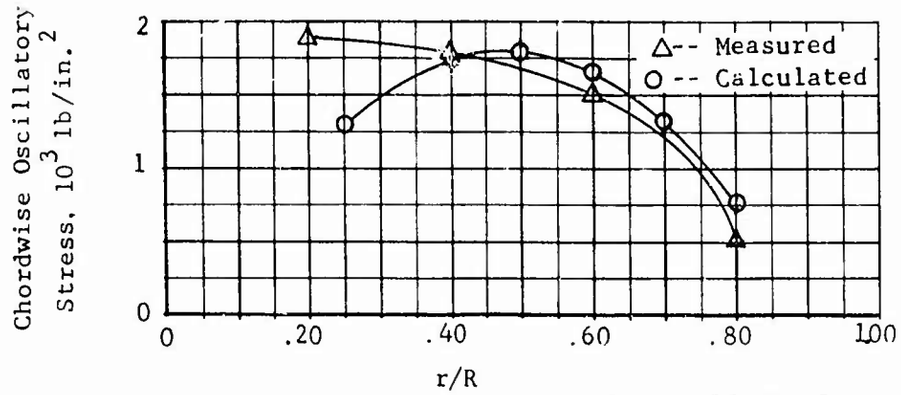

Figure 41. Chordwise Vibrator Stress for Full-Scale Rotor, -8° Twist, $\mu = 0.300$, $M_{1,90} = 0.740$.

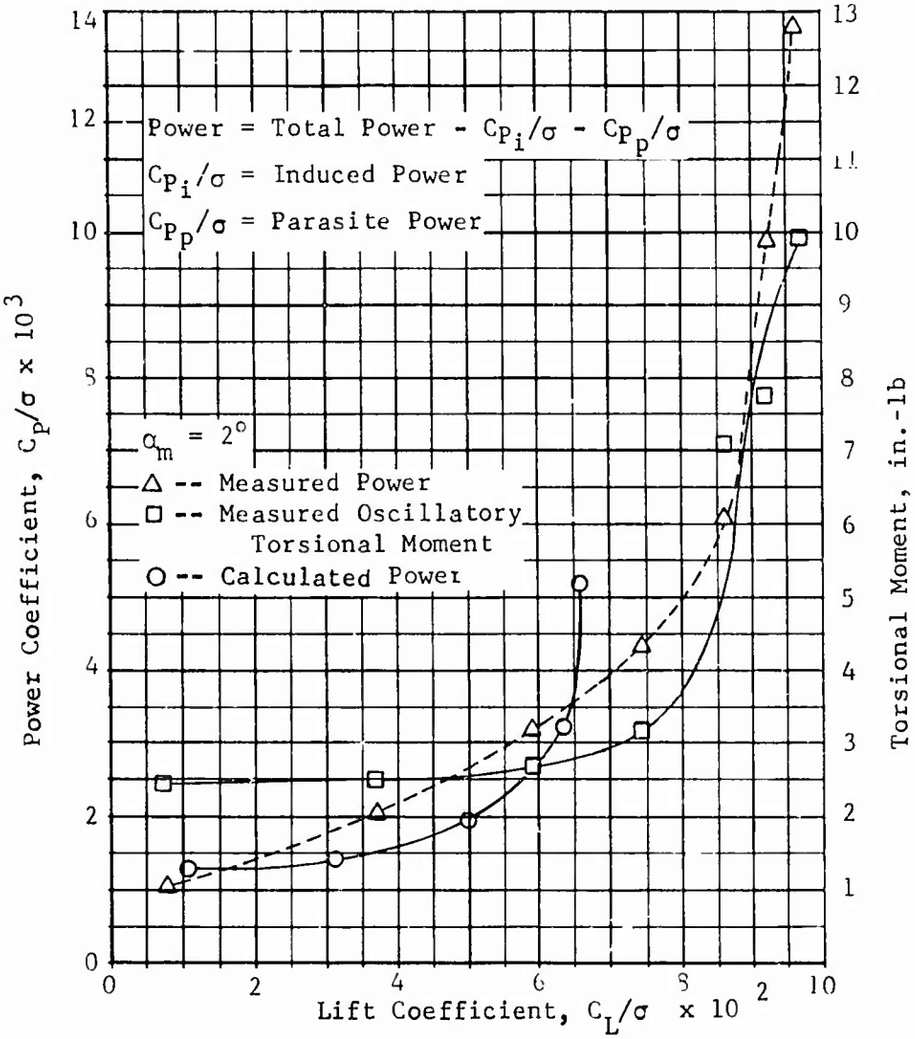

Figure 42. Stall Characteristics of Model Rotor, Fiberglass Blade, -8° Twist, $\mu = 0.299$, $M_{1,90} = 0.408$.

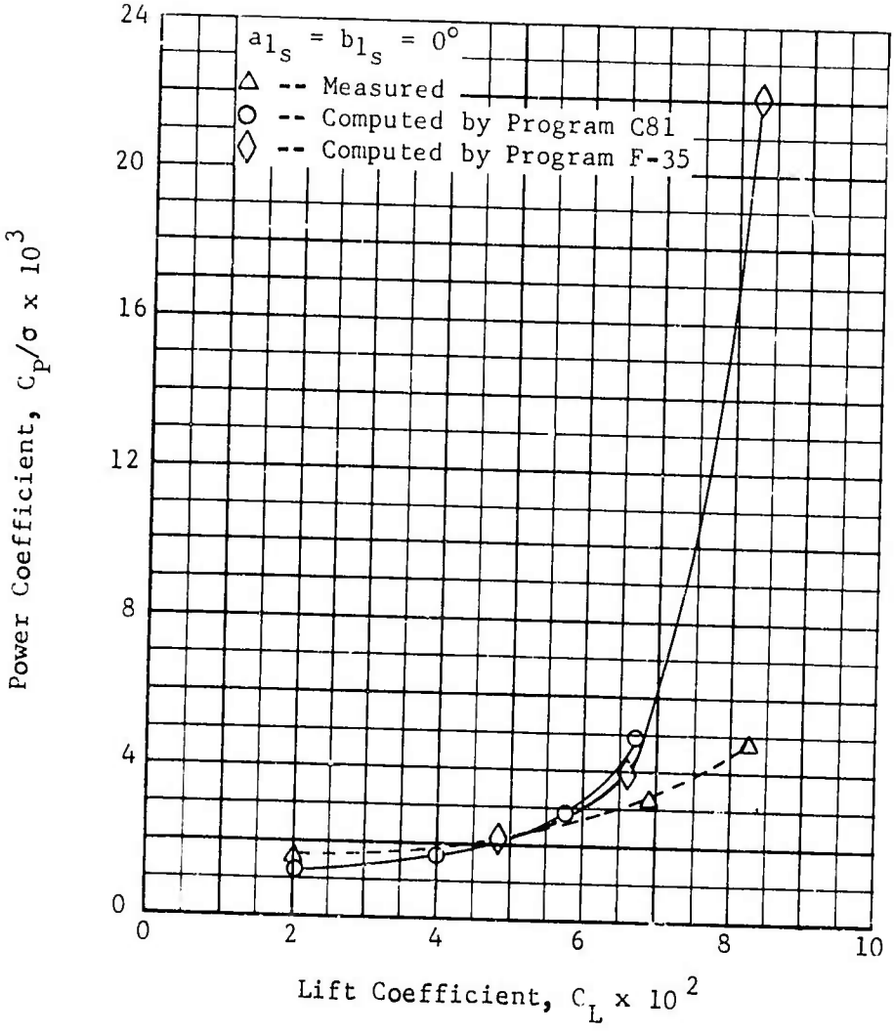

Figure 43. Rotor Power Coefficient vs. Rotor Lift Coefficient, Fiberglass Blade, -8° Twist, $\mu = 0.299$, $M_{1,90} = 0.408$.

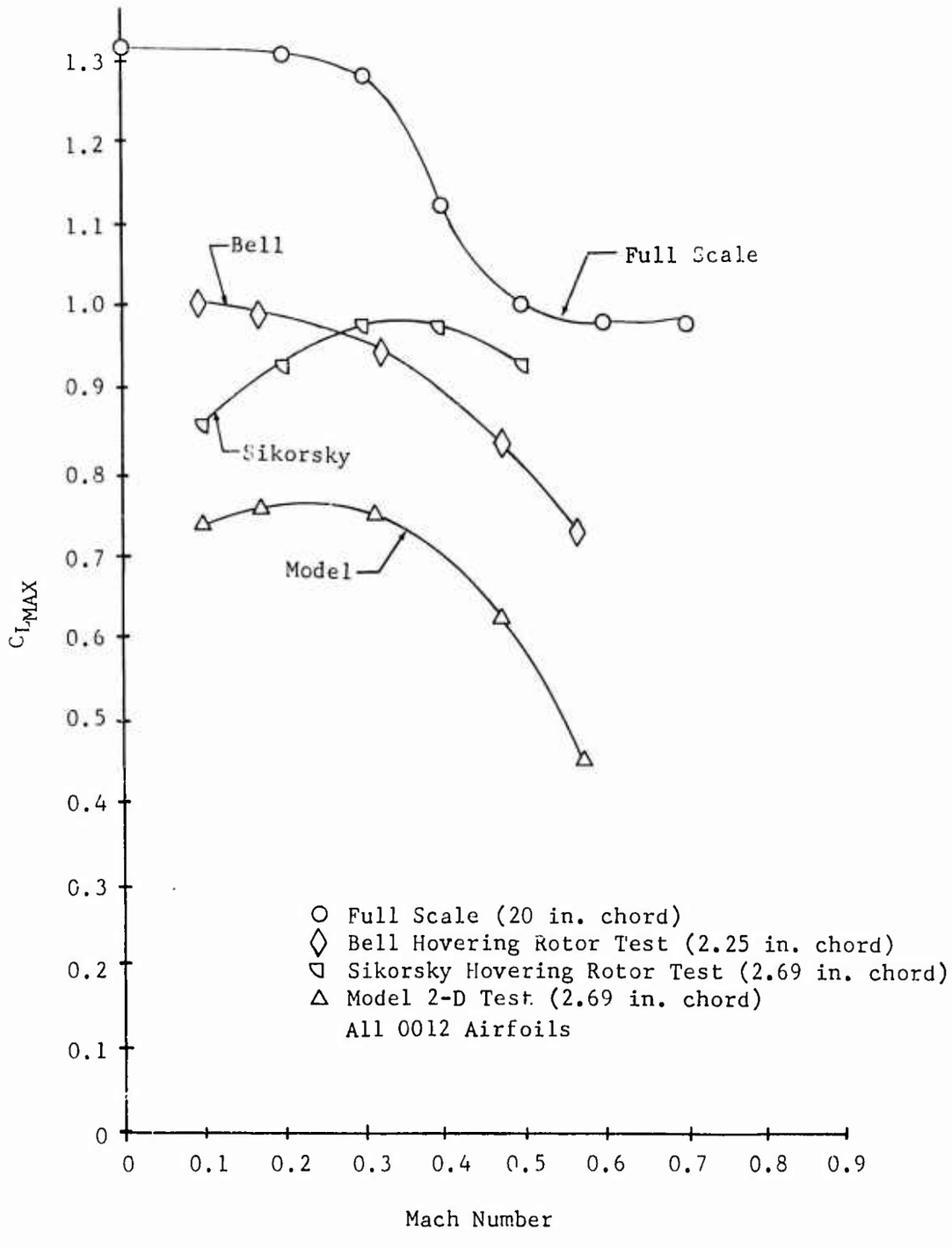

Figure 44. Effect of Mach Number on $C_{L_{MAX}}$ for a 0012 Airfoil.

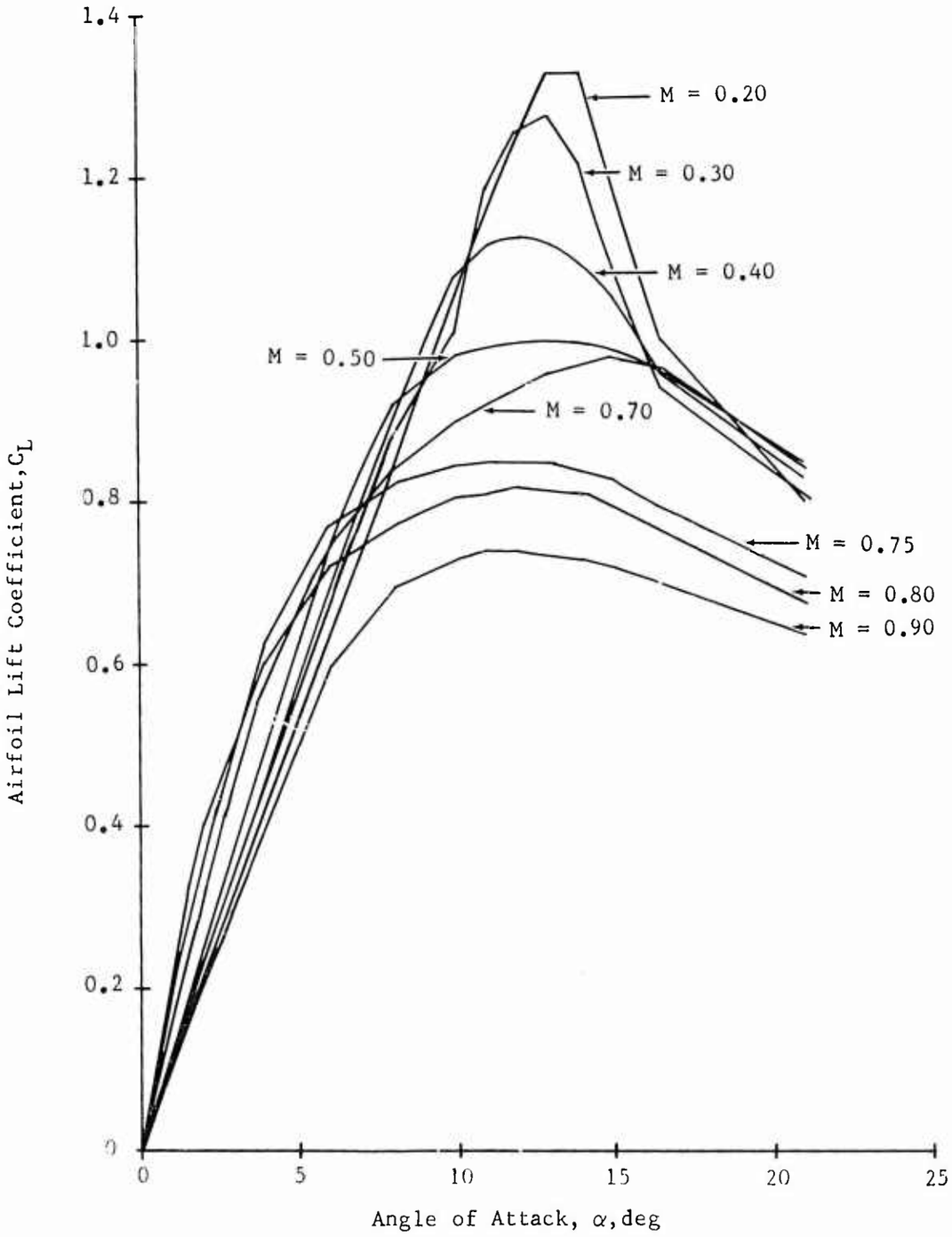

Figure 45. Full-Scale 0012 Airfoil Lift Coefficient vs. Angle of Attack.

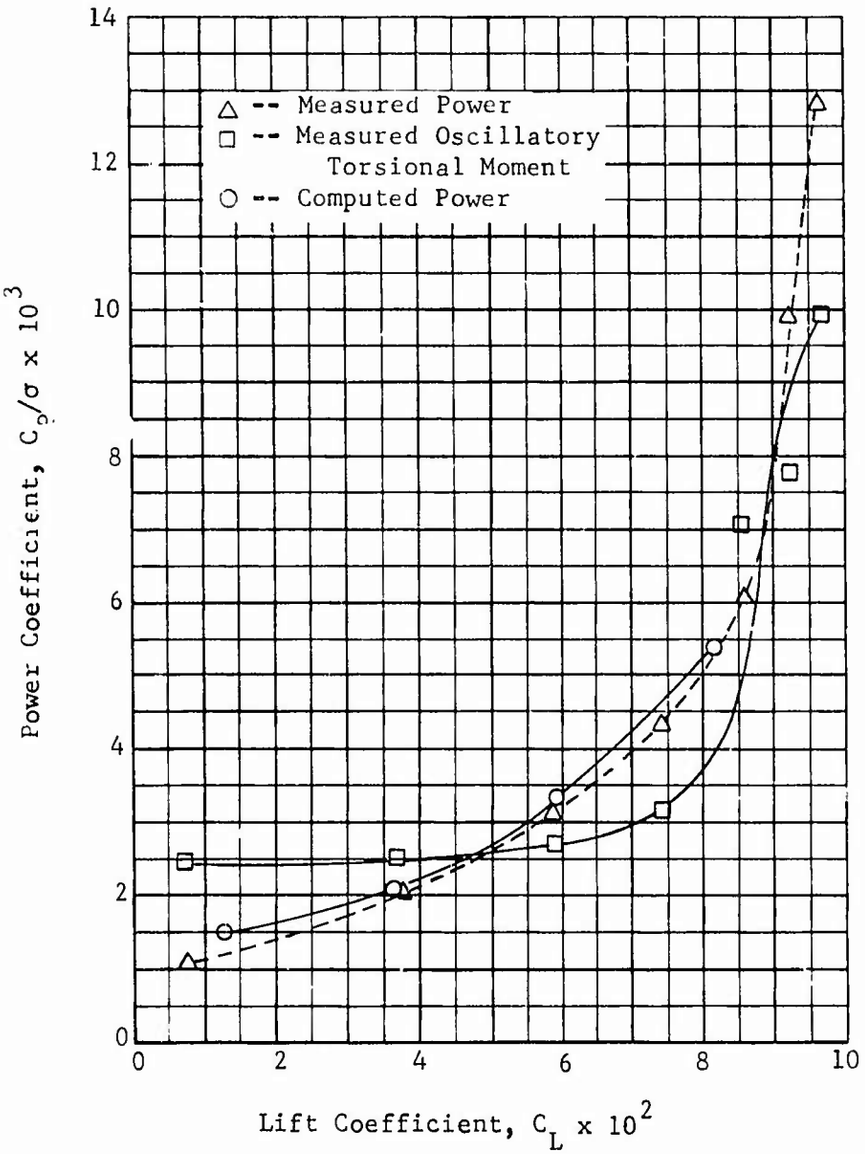

Figure 46. Stall Characteristics of Model Rotor Using Modified Airfoil Data Tables, -8^0 Twist, $\mu = 0.299$, $M_{1,90} = 0.408$.

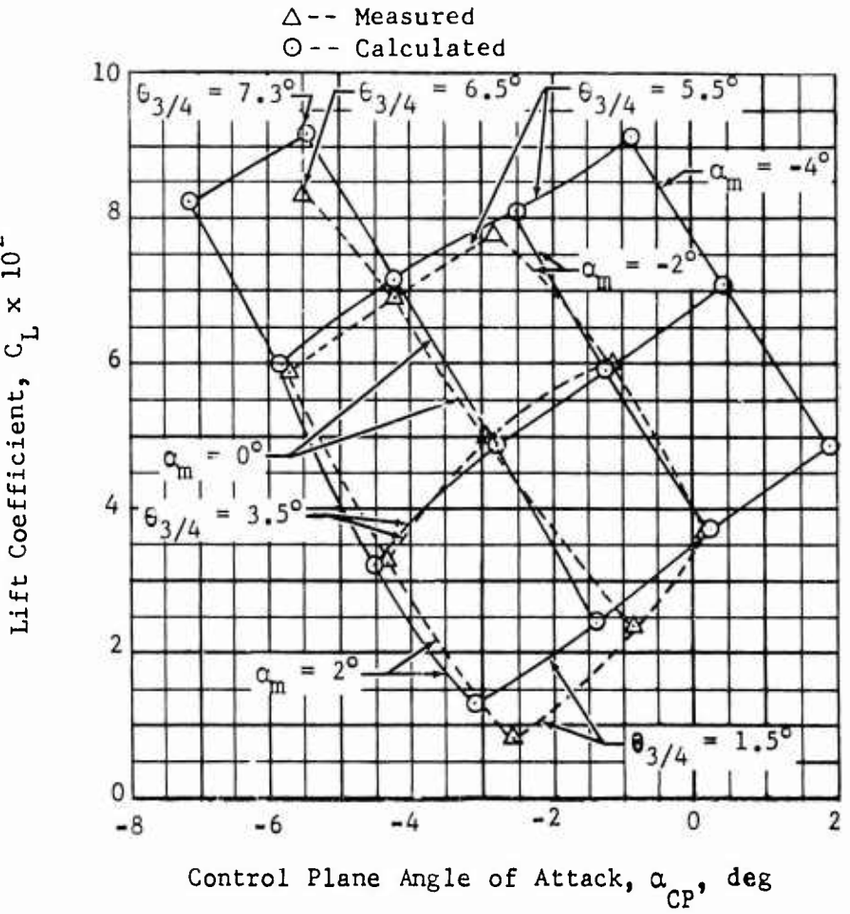

Figure 47. Rotor Lift Coefficient vs. Control Plane Angle of Attack Using Modified Airfoil Data Tables, -8° Twist, $\mu = 0.299$, $M_{1.90} = 0.408$.

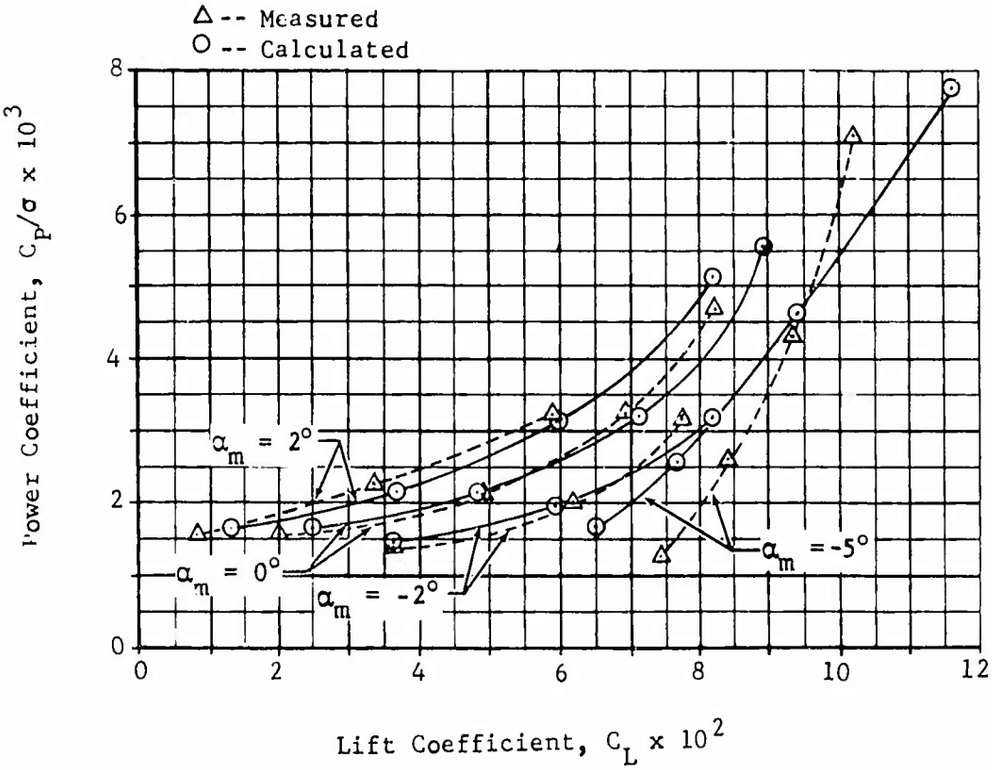

Figure 48. Rotor Power Coefficient vs. Rotor Lift Coefficient, Modified Airfoil Data Tables, Fiberglass Blade, -8° Twist, $\mu = 0.299$, $M_{1,90} = 0.408$.

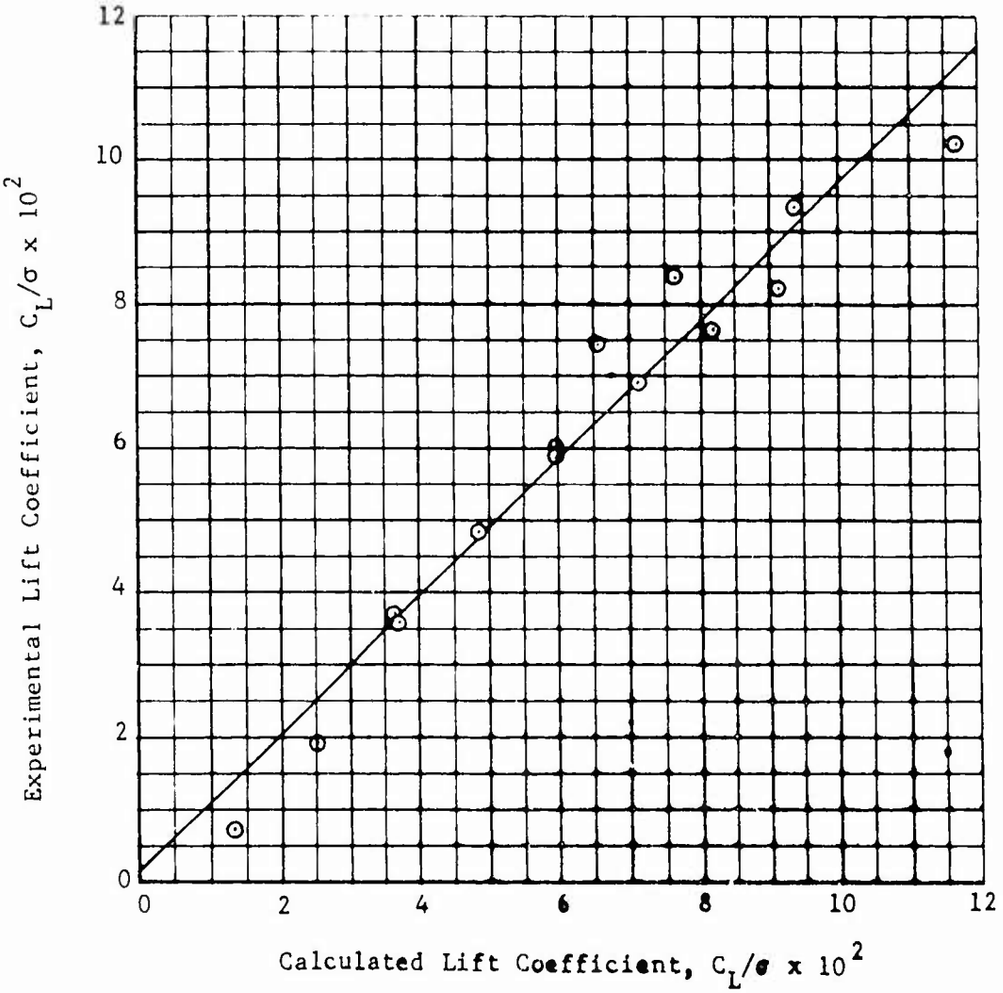

Figure 49. Experimental Lift Coefficient vs. Calculated Lift Coefficient Using Modified Airfoil Data Tables, Fiberglass Blade, -8° Twist, μ = 0.299, $M_{1,90}$ = 0.408.

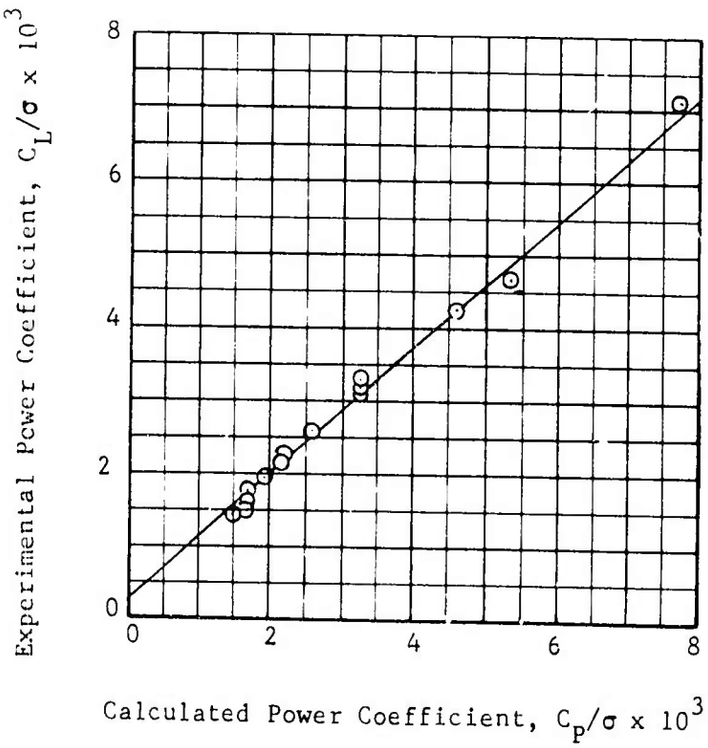

Figure 50. Experimental Power Coefficient vs. Calculated Power Coefficient Using Modified Airfoil Tables, Fiberglass Blade, -8° Twist, $\mu = 0.299$, $M_{1,90} = 0.408$.

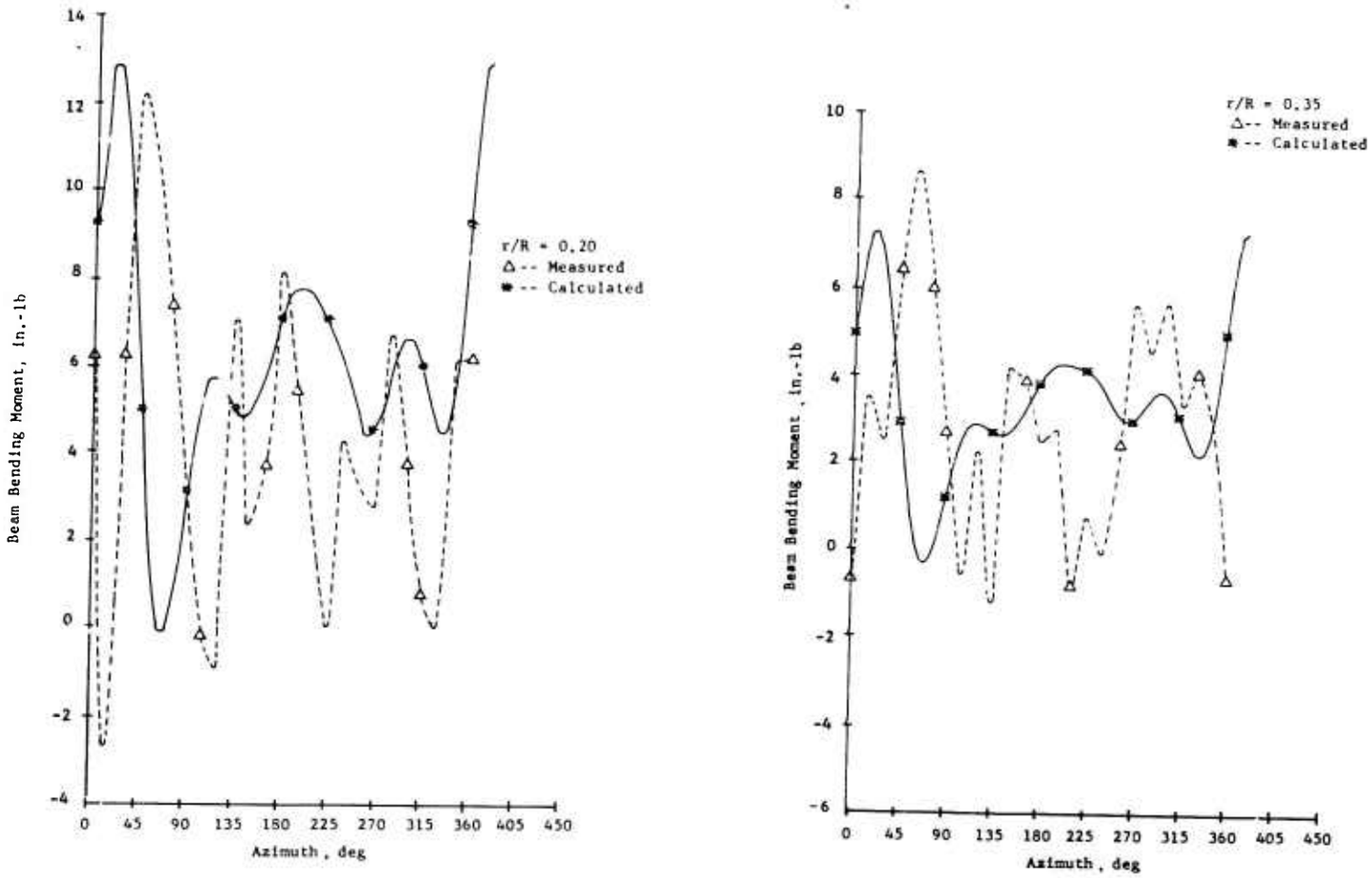

Figure 51. Measured and Calculated Beam Bending Moment Time Histories, Fiberglass Blade, 0° Twist $\mu = 0.399$, $M_{1,\ 90} = 0.434$, $\alpha_m = 0.5°$ (Cond. 25).

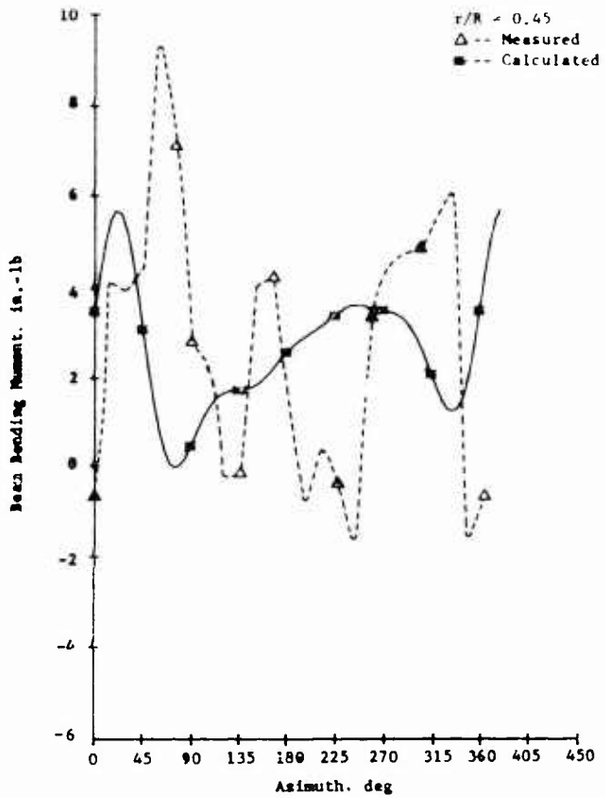

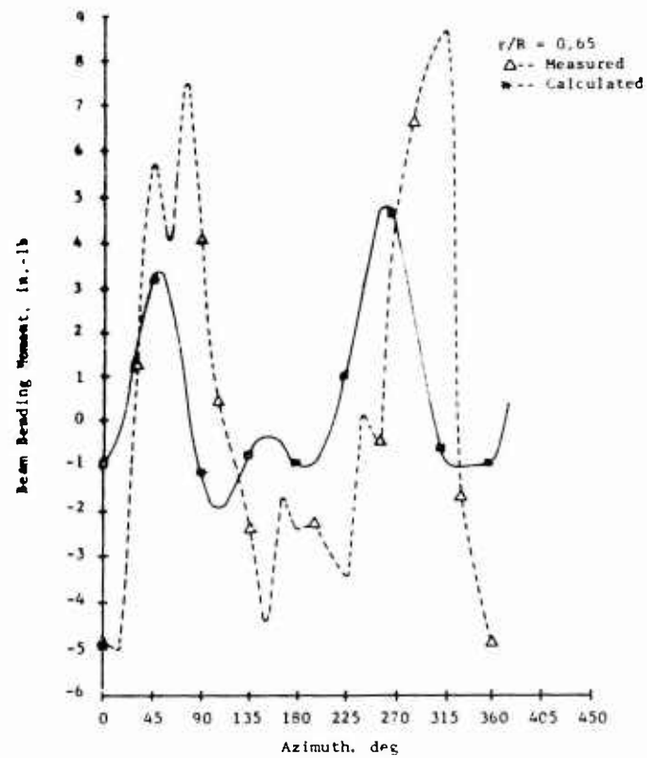

Figure 51. Continued.

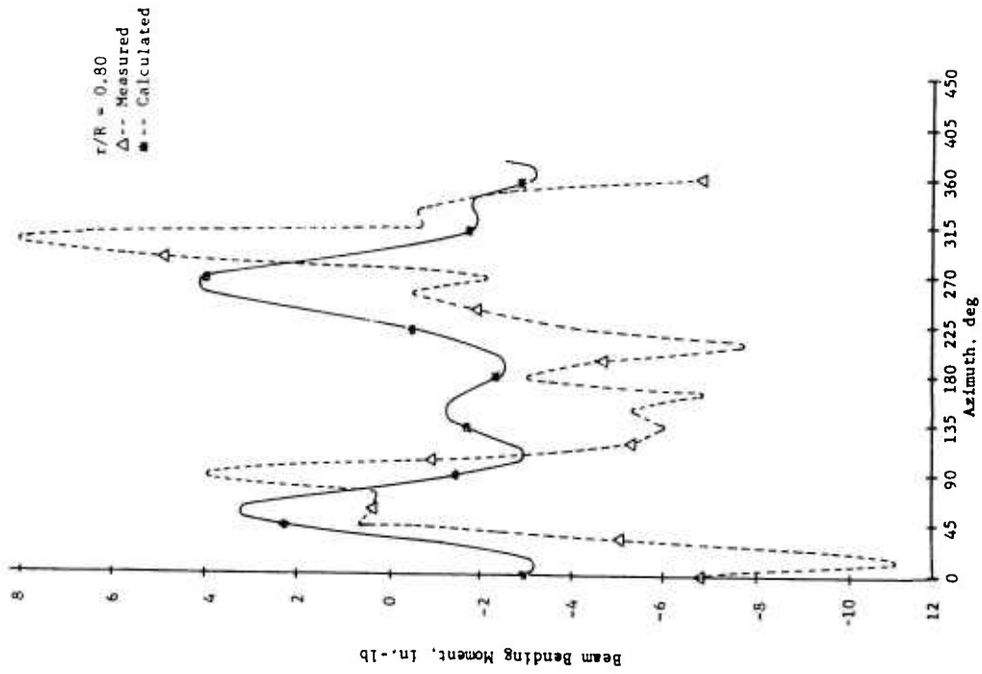

Figure 51. Concluded.

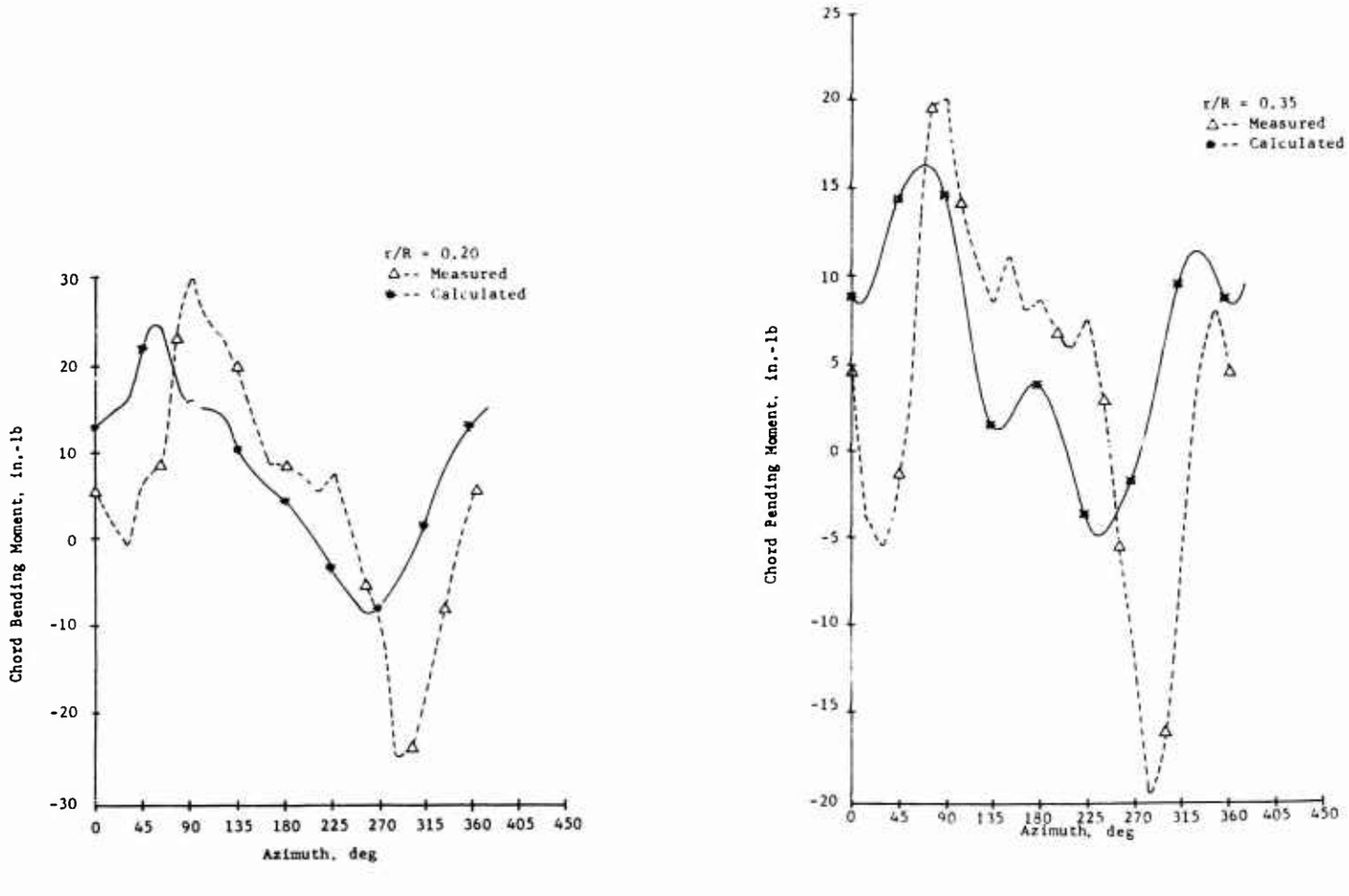

Figure 52. Measured and Calculated Chord Bending Moment Time Histories, Fiberglass Blade, 0° Twist $\mu = 0.399$, $M_{1,\,90} = 0.434$, $\alpha_m = 0.5^\circ$ (Cond. 25).

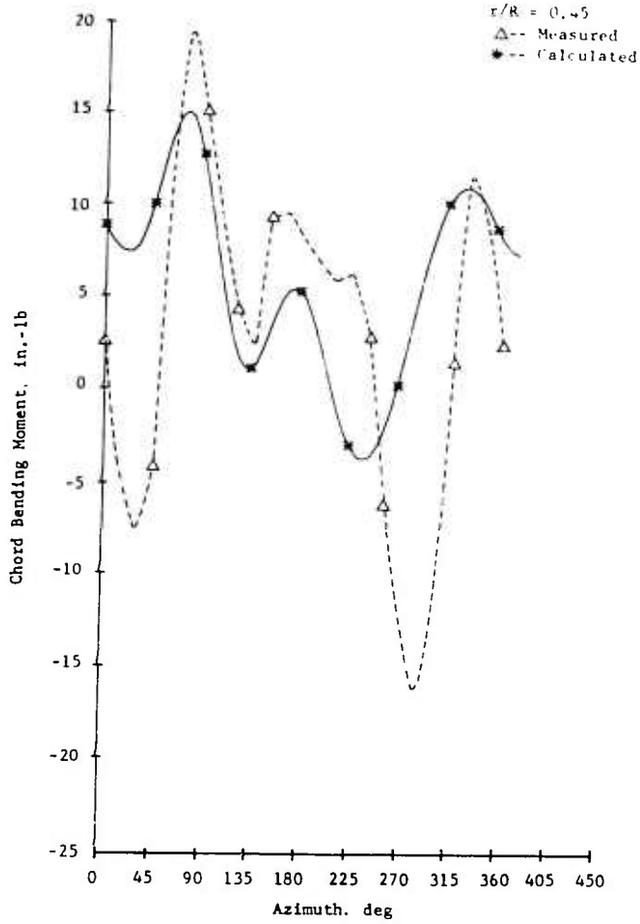

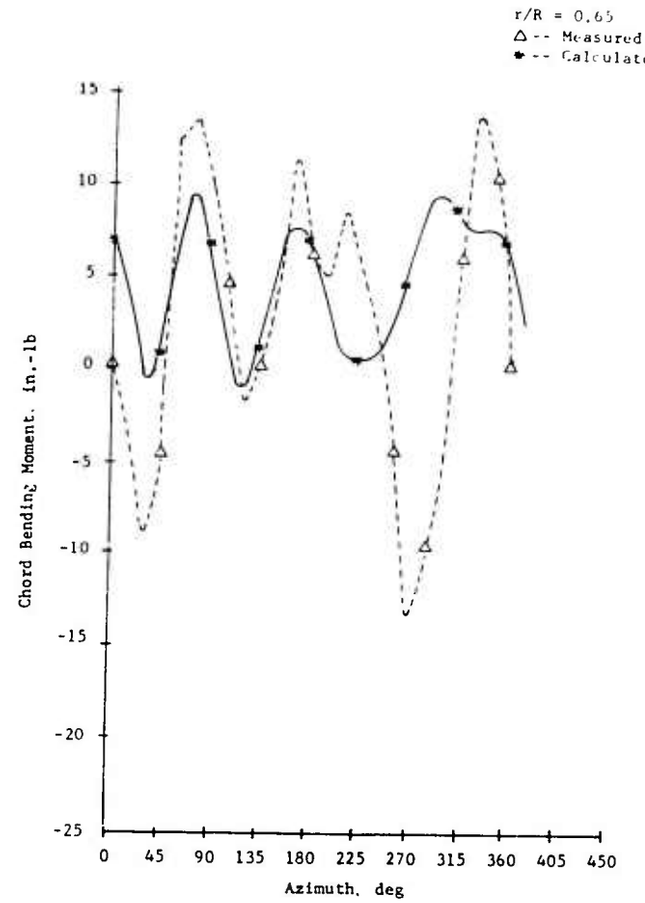

Figure 52. Continued.

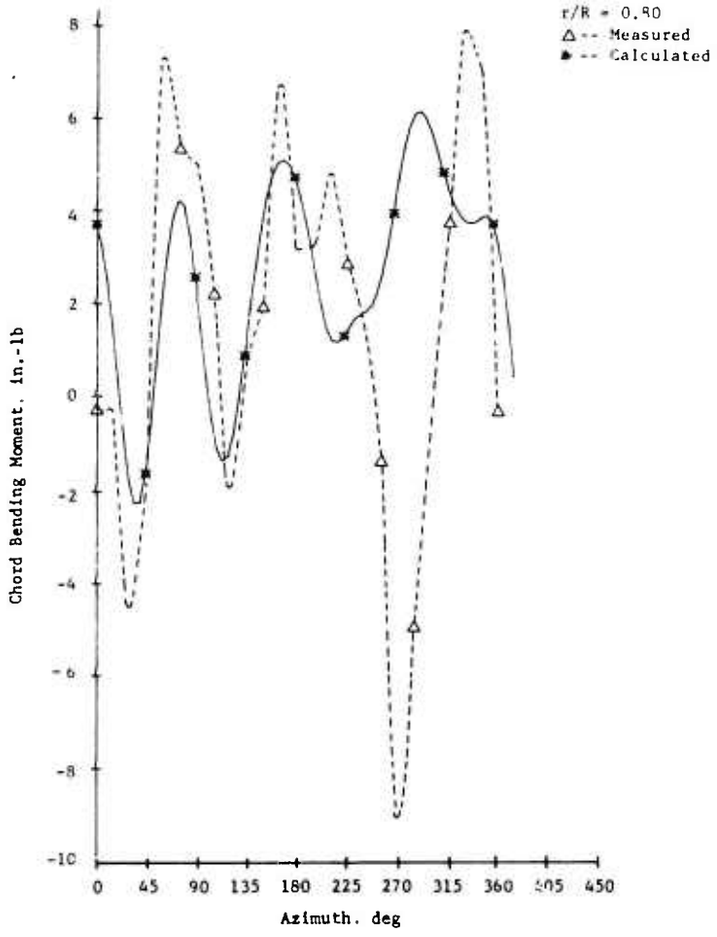

Figure 52. Concluded.

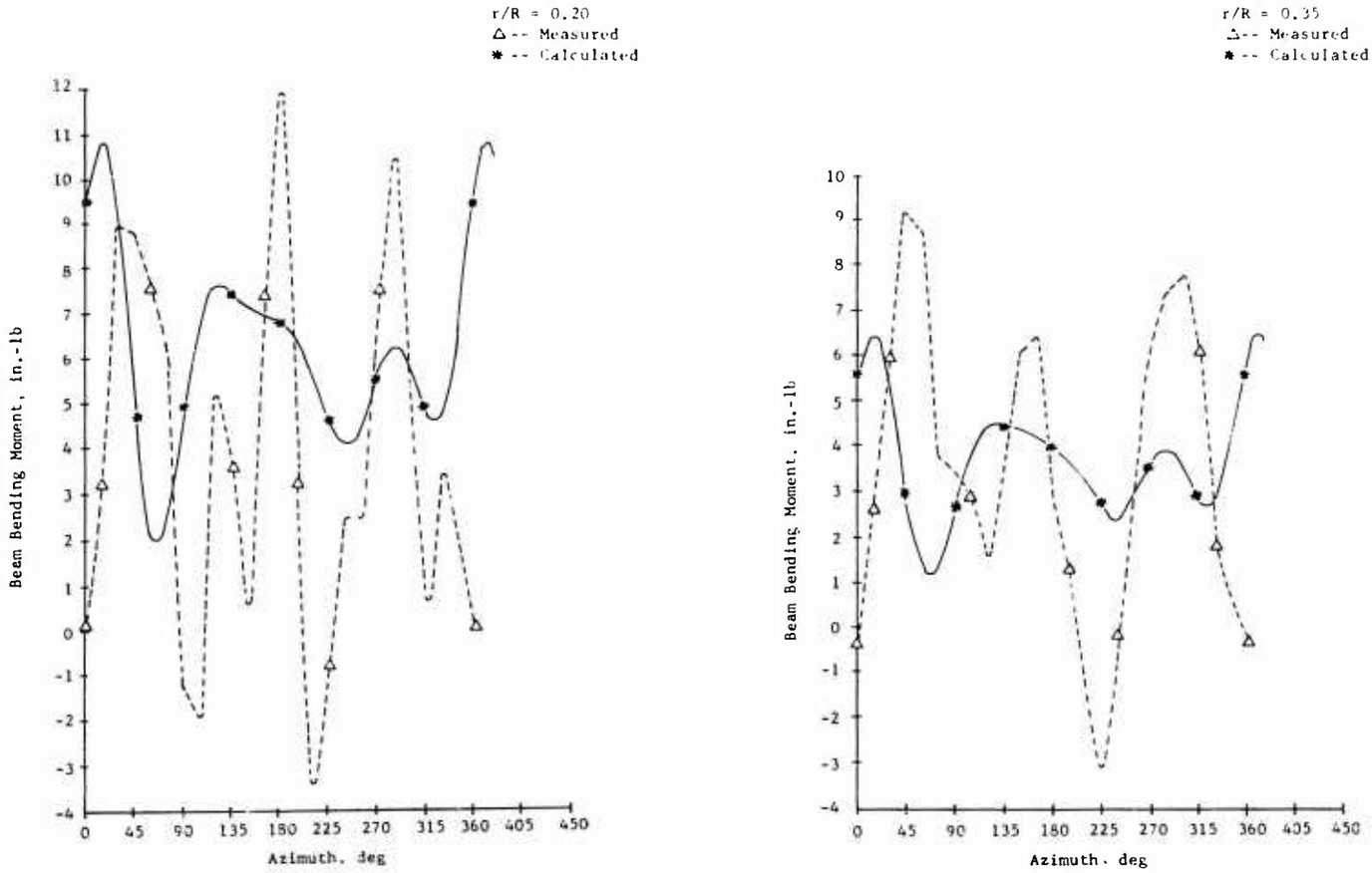

Figure 53. Measured and Calculated Beam Bending Moment Time Histories, Fiberglass Blade, 0° Twist $\mu = 0.502$, $M_{1,90} = 0.467$, $\alpha_m = 5^{\circ}$ (Cond. 44).

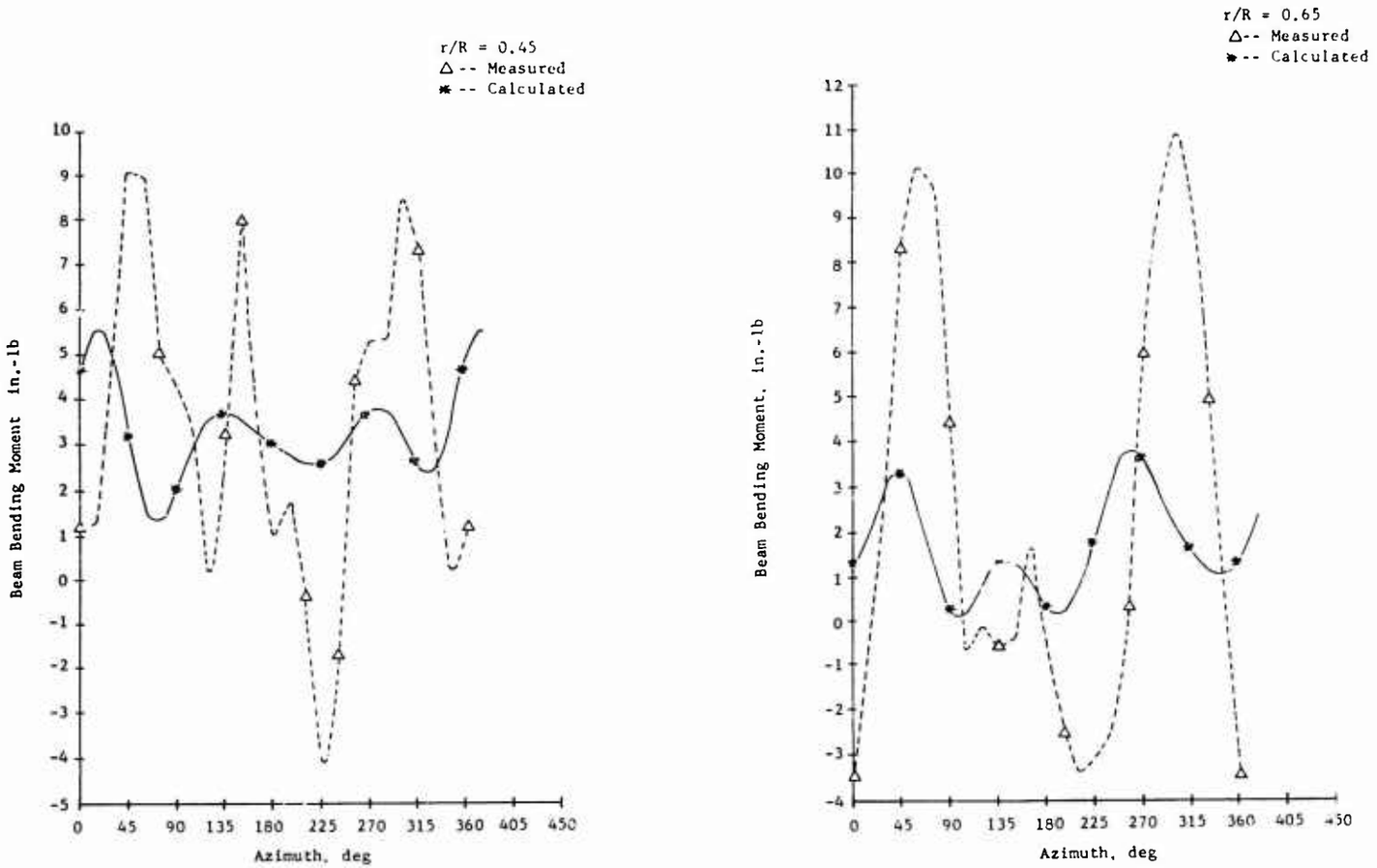

Figure 53. Continued.

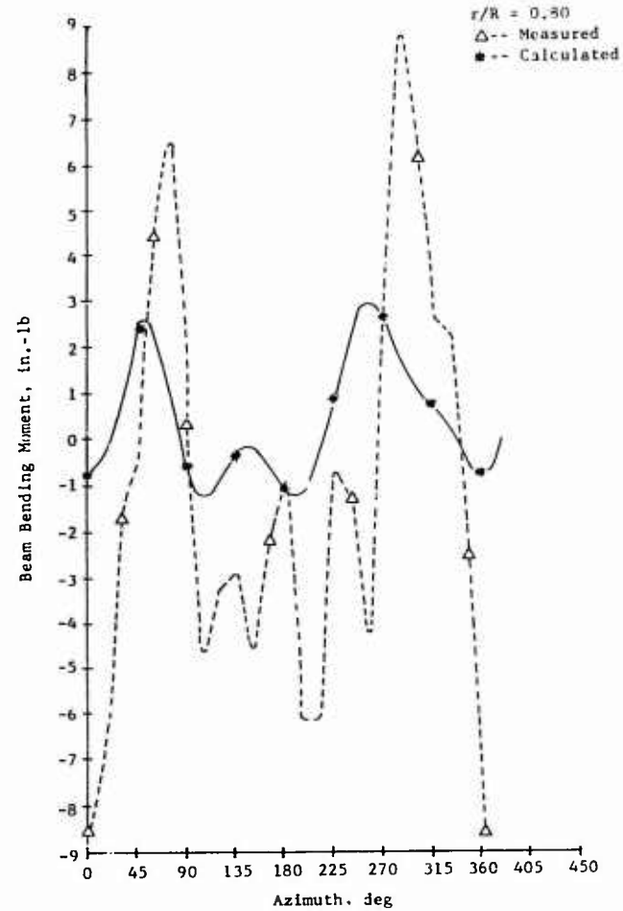

Figure 53. Concluded.

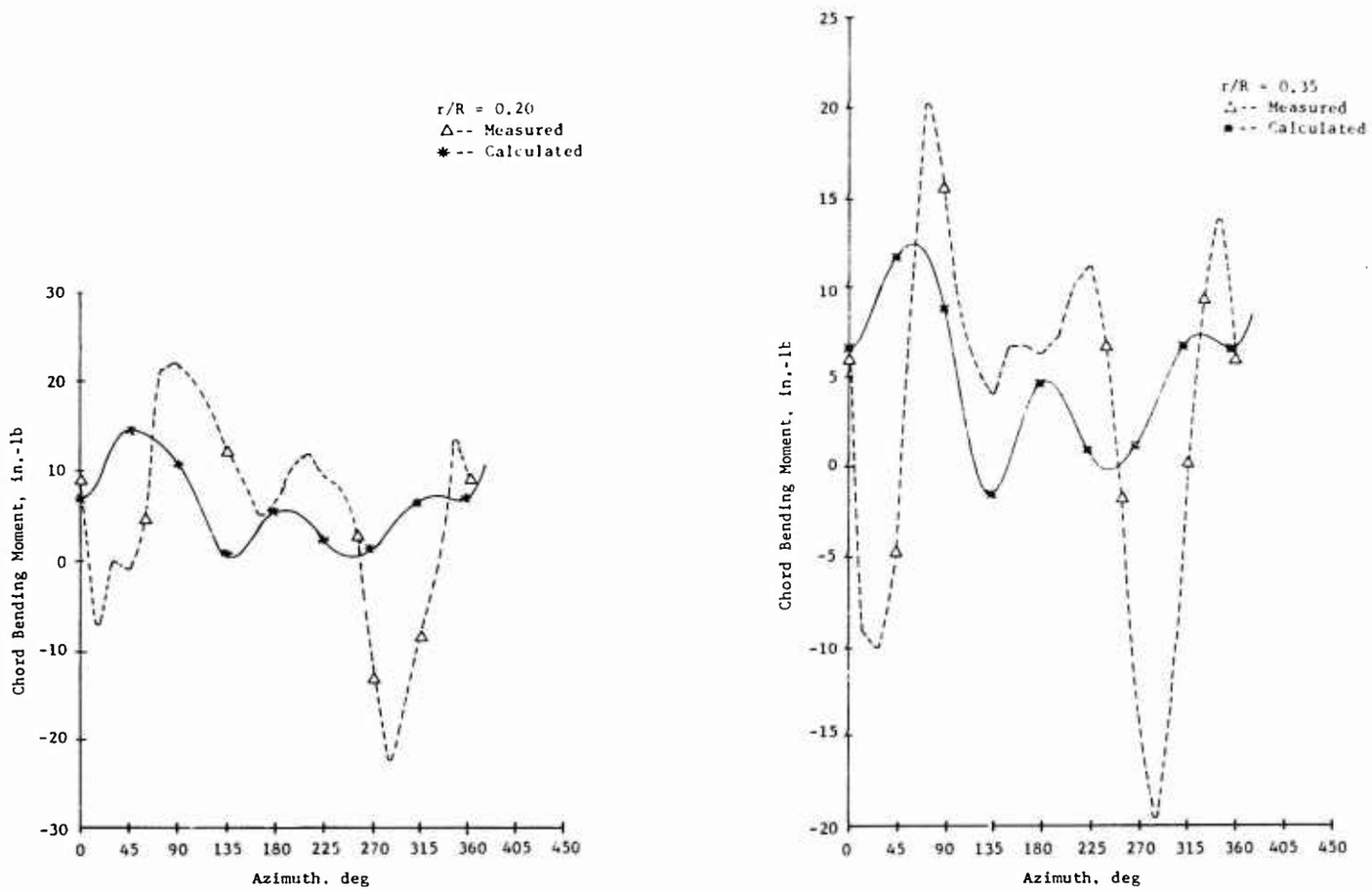

Figure 54. Measured and Calculated Chord Bending Moment Time Histories, Fiberglass Blade, 0° Twist, $\mu = 0.502$, $M_{1,90} = 0.467$, $\alpha_m = 5°$ (Cond. 44).

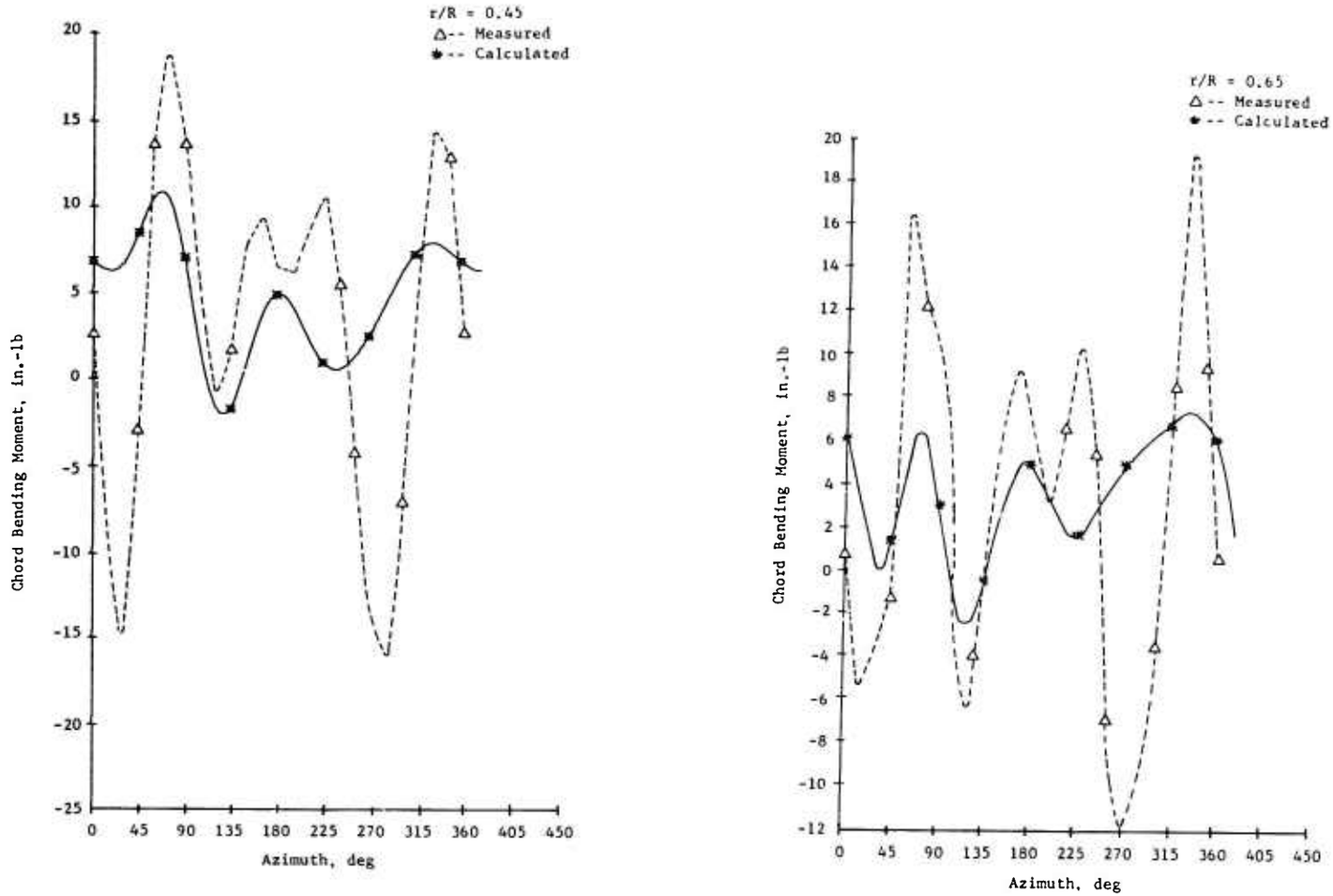

Figure 54. Continued.

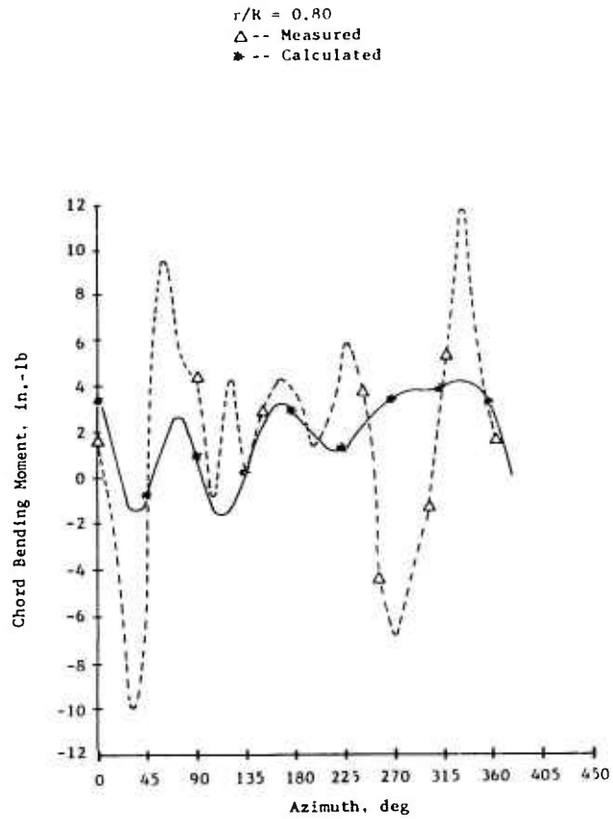

Figure 54. Concluded

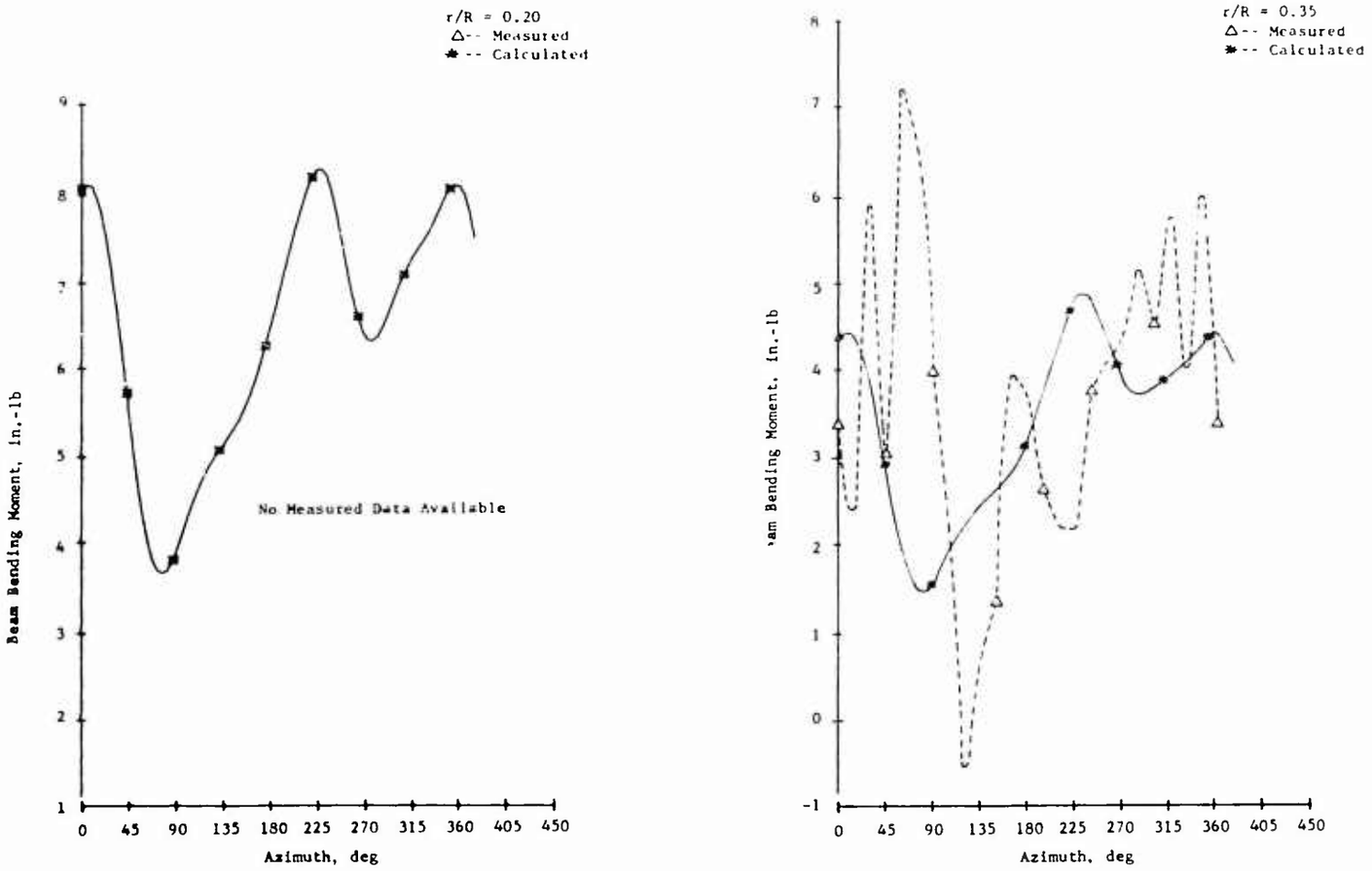

Figure 55. Measured and Calculated Beam Bending Moment Time Histories, Fiberglass Blade, 0° Twist, $\mu = 0.299$, $M_{1,90} = 0.408$, $\alpha_m = 0°$ (Cond. 68).

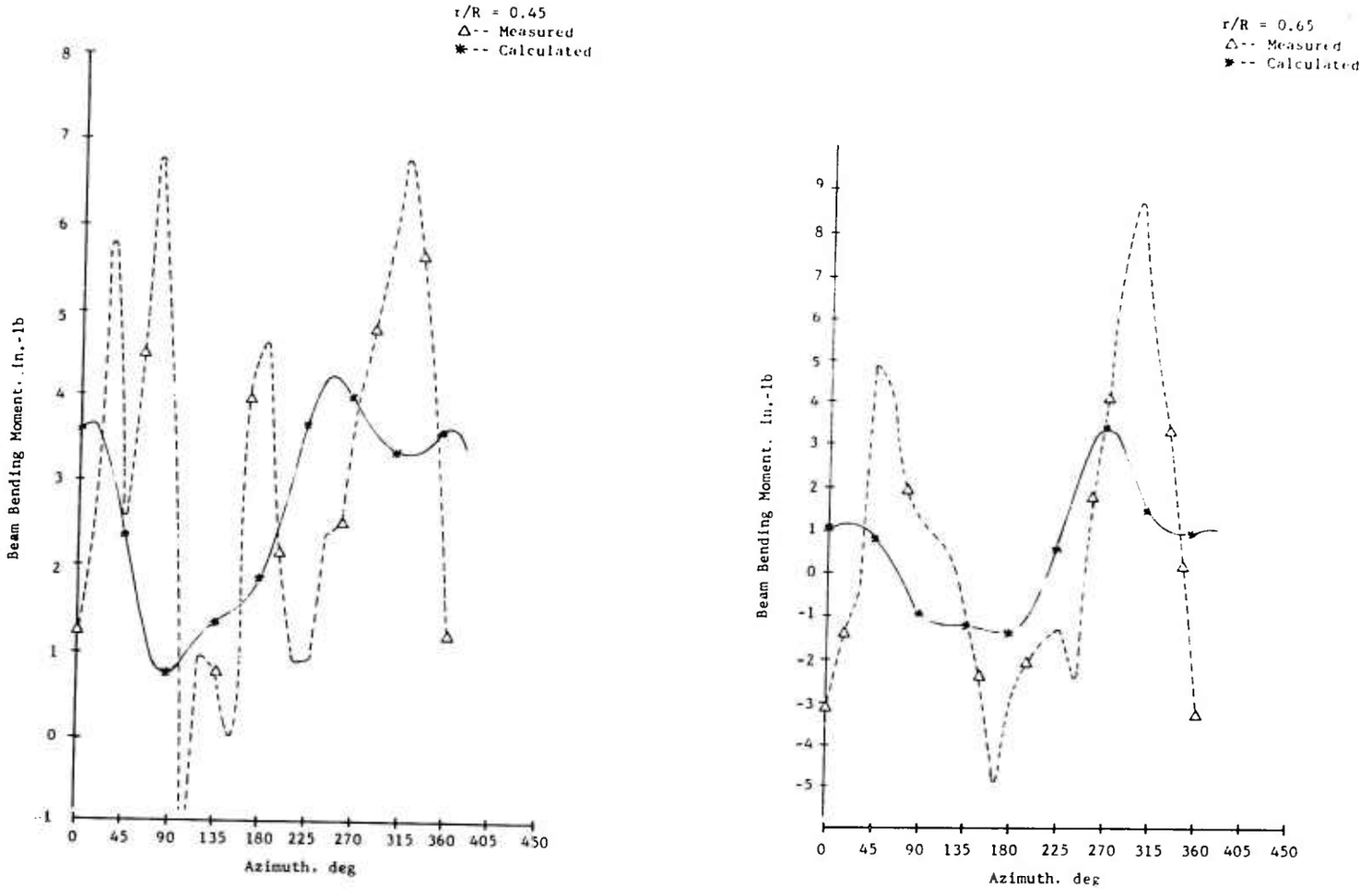

Figure 55. Continued.

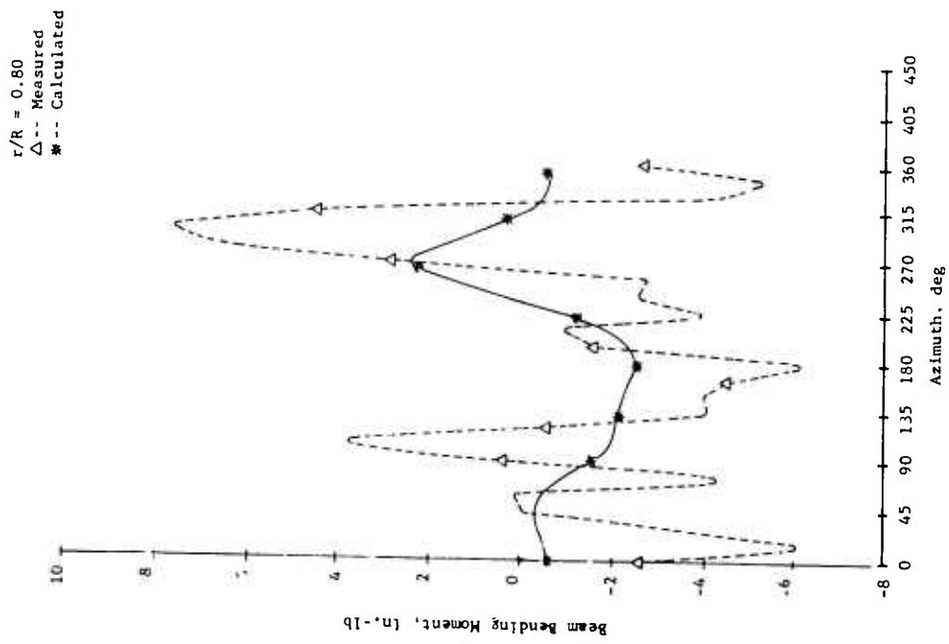

Figure 55. Concluded

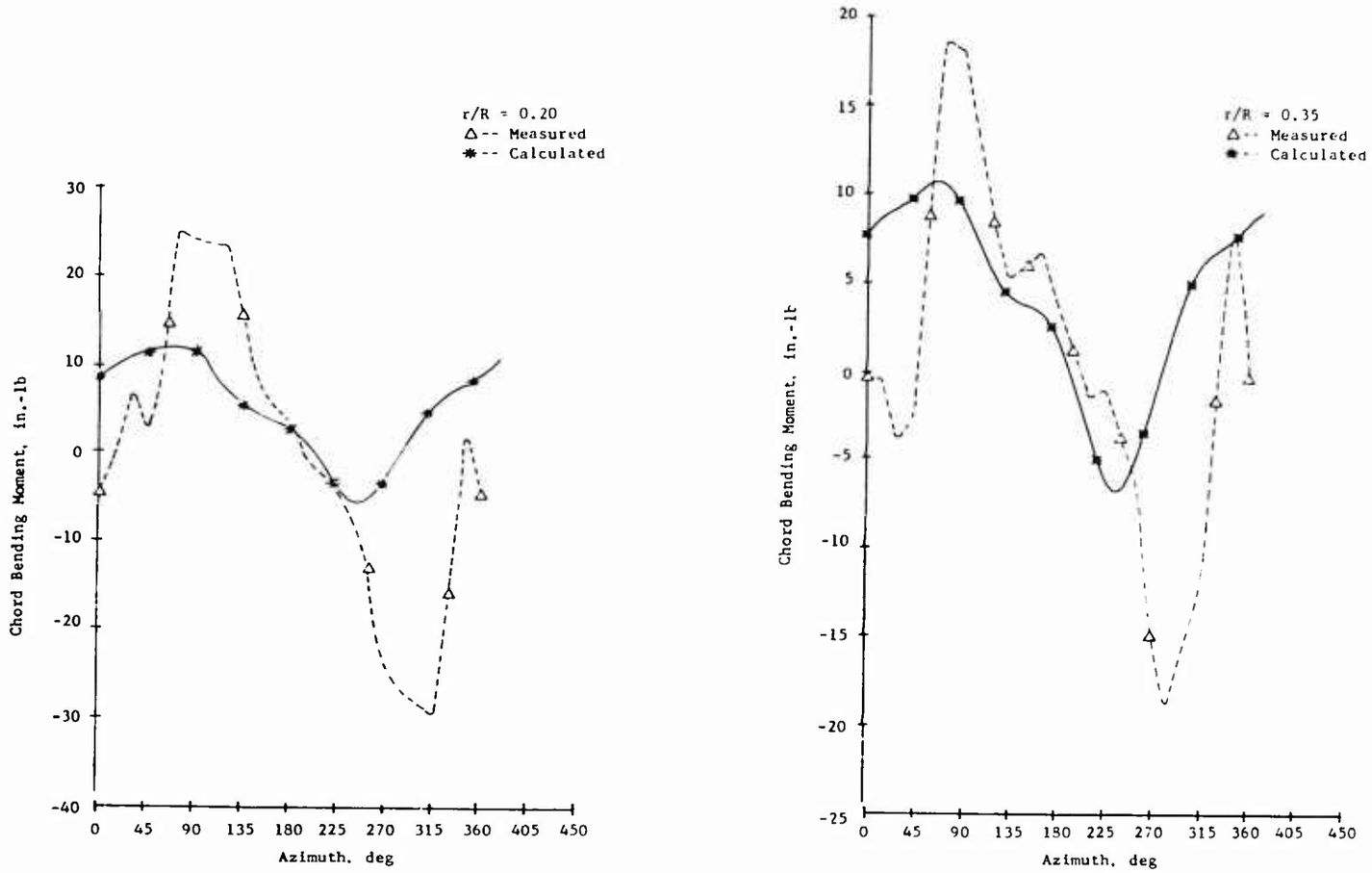

Figure 56. Measured and Calculated Chord Bending Moment Time Histories, Fiberglass Blade, 0° Twist, $\mu = 0.299$, $M_{1,90} = 0.408$, $\alpha_m = 0^\circ$ (Cond. 68).

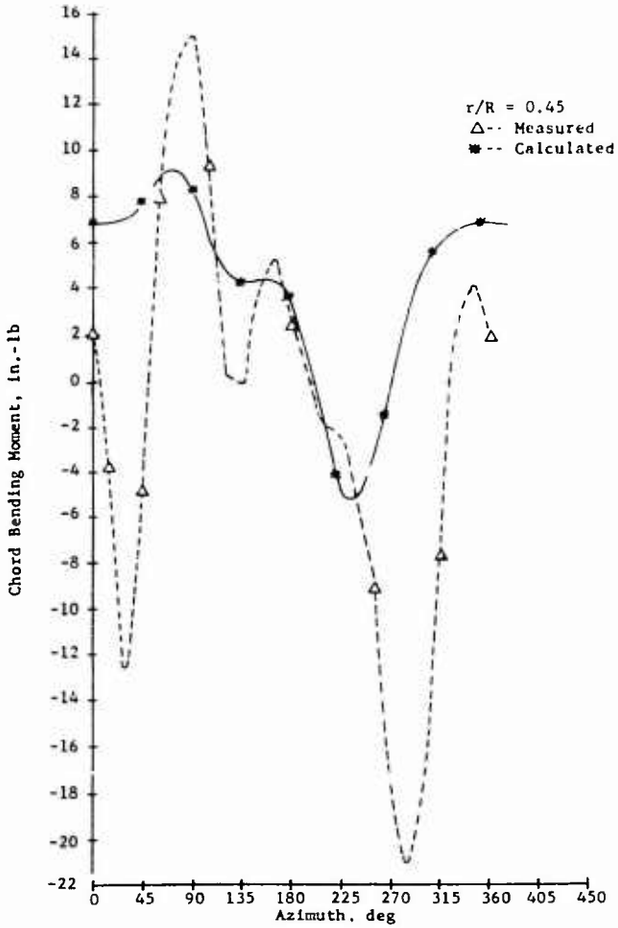

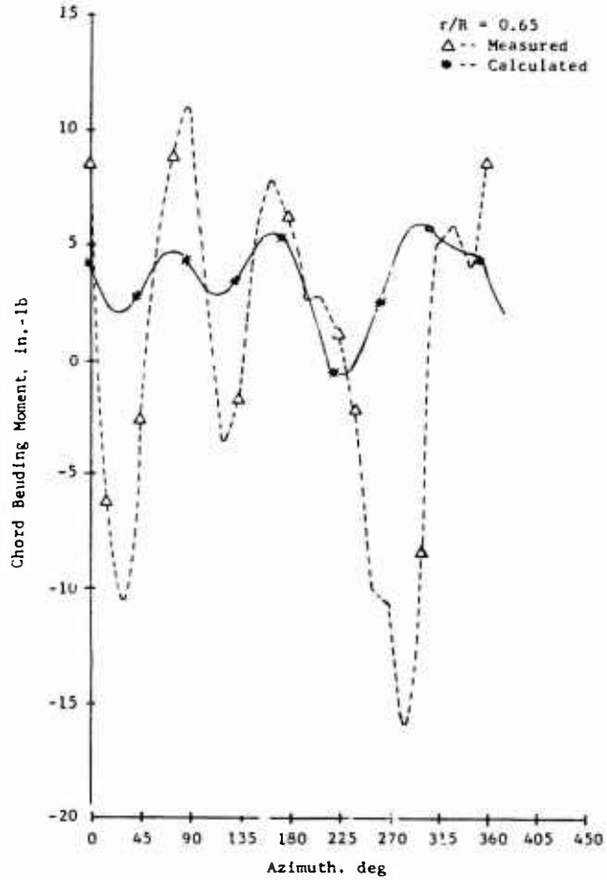

Figure 56. Continued.

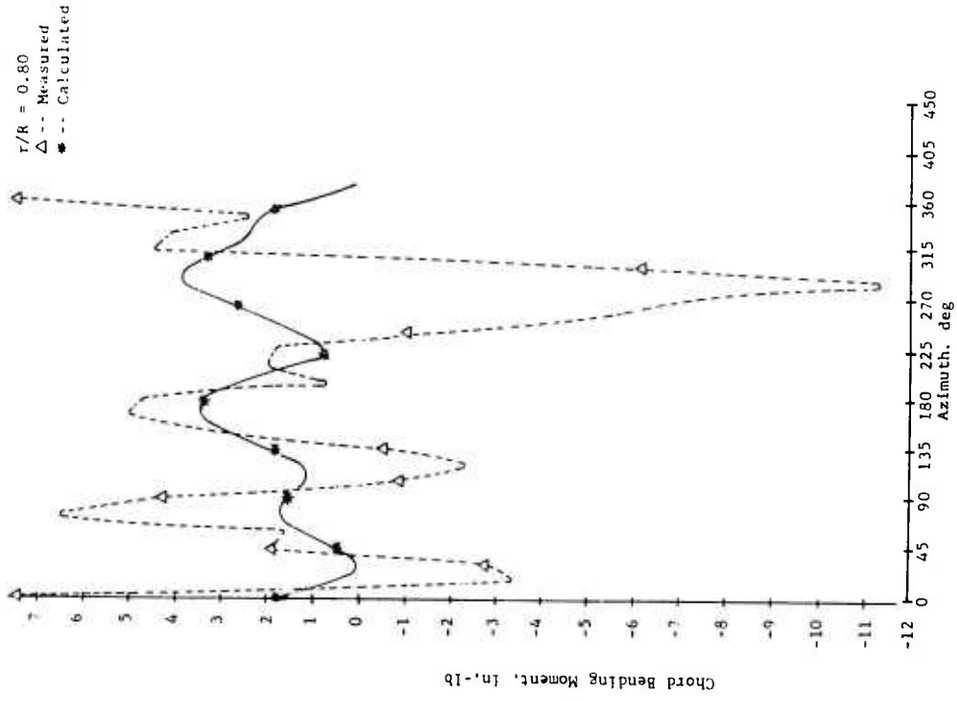

Figure 56. Concluded.

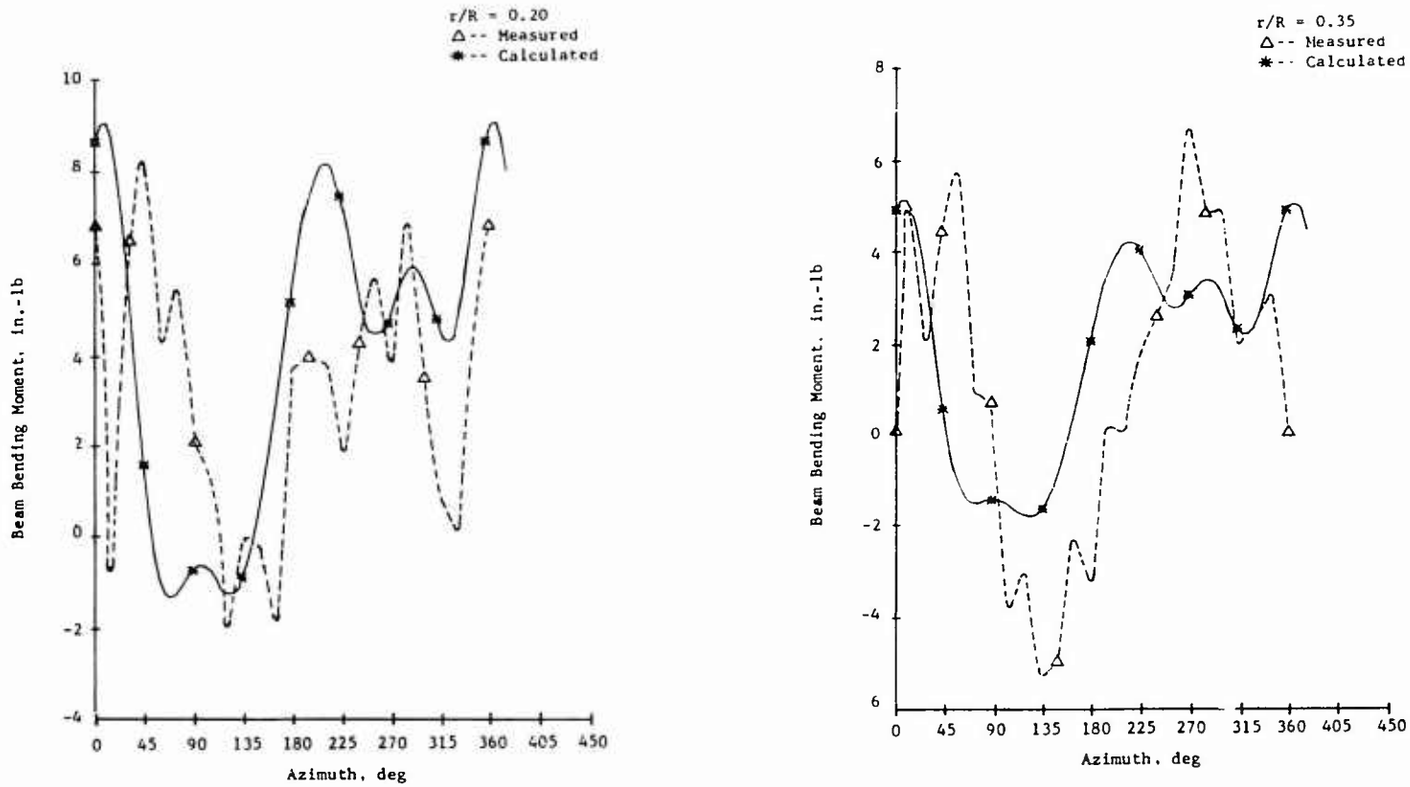

Figure 57. Measured and Calculated Beam Bending Moment Time Histories, Fiberglass Blade, -8° Twist, $\mu = 0.399$, $M_{1,90} = 0.434$, $\alpha_m = 0.5°$ (Cond. 25).

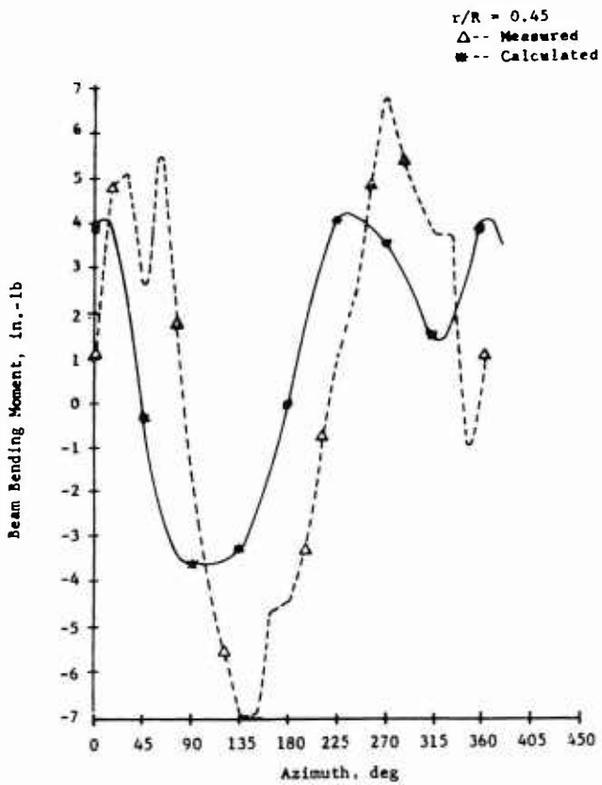

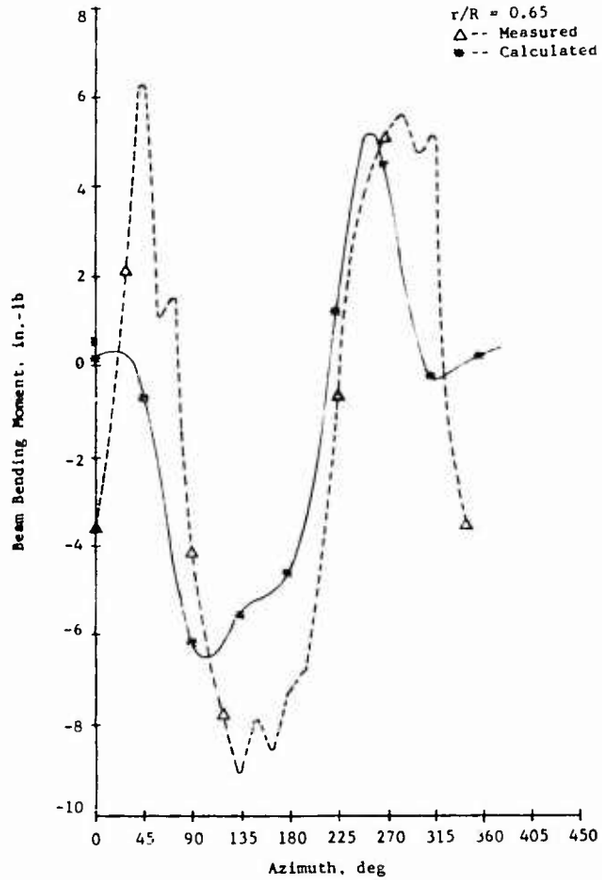

Figure 57. Continued.

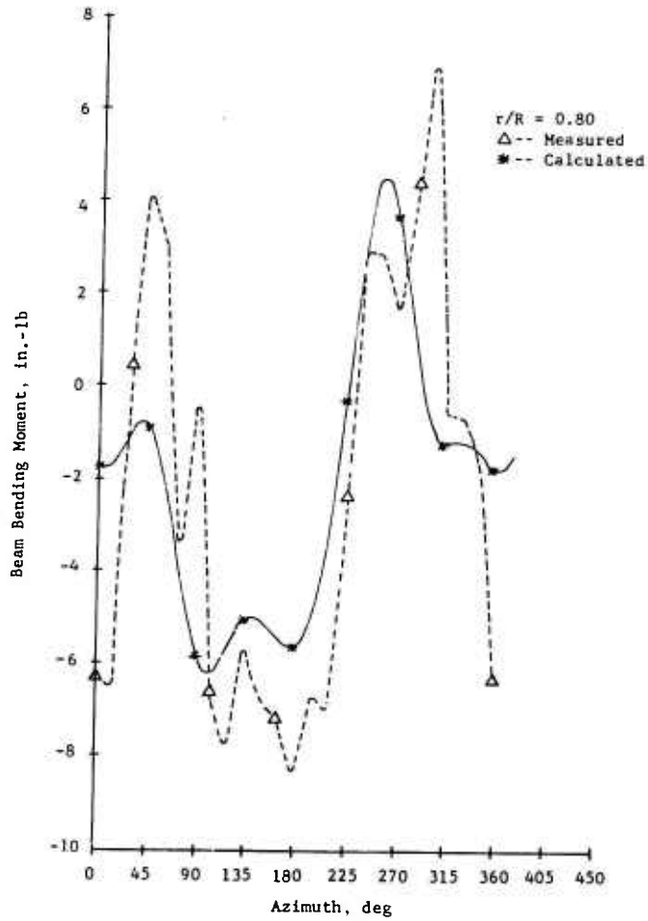

Figure 57. Concluded.

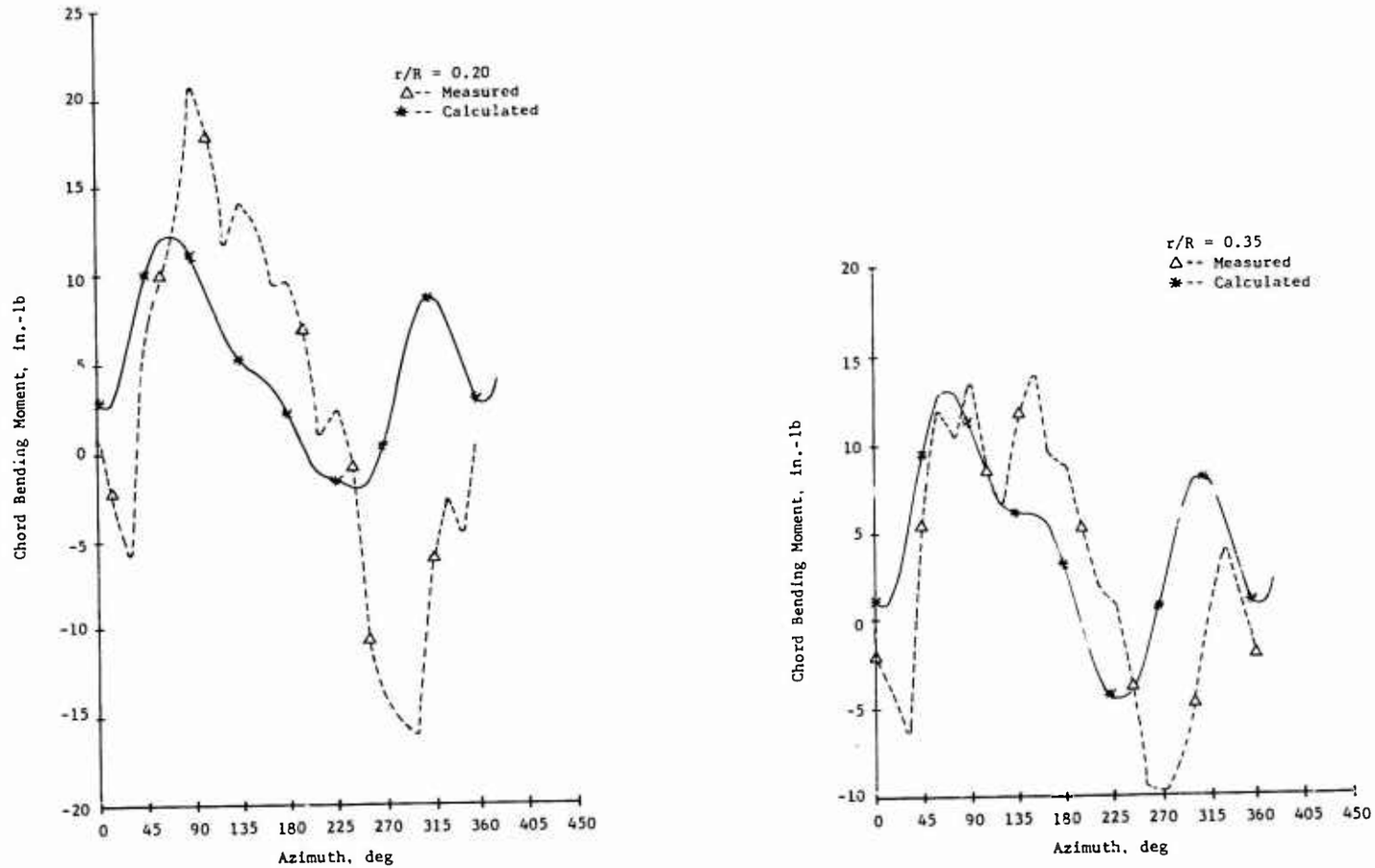

Figure 58. Measured and Calculated Chord Bending Moment Time Histories, Fiberglass Blade, -8° Twist, $\mu = 0.399$, $M_{1,90} = 0.434$, $\alpha_m = 0.5°$ (Cond. 25).

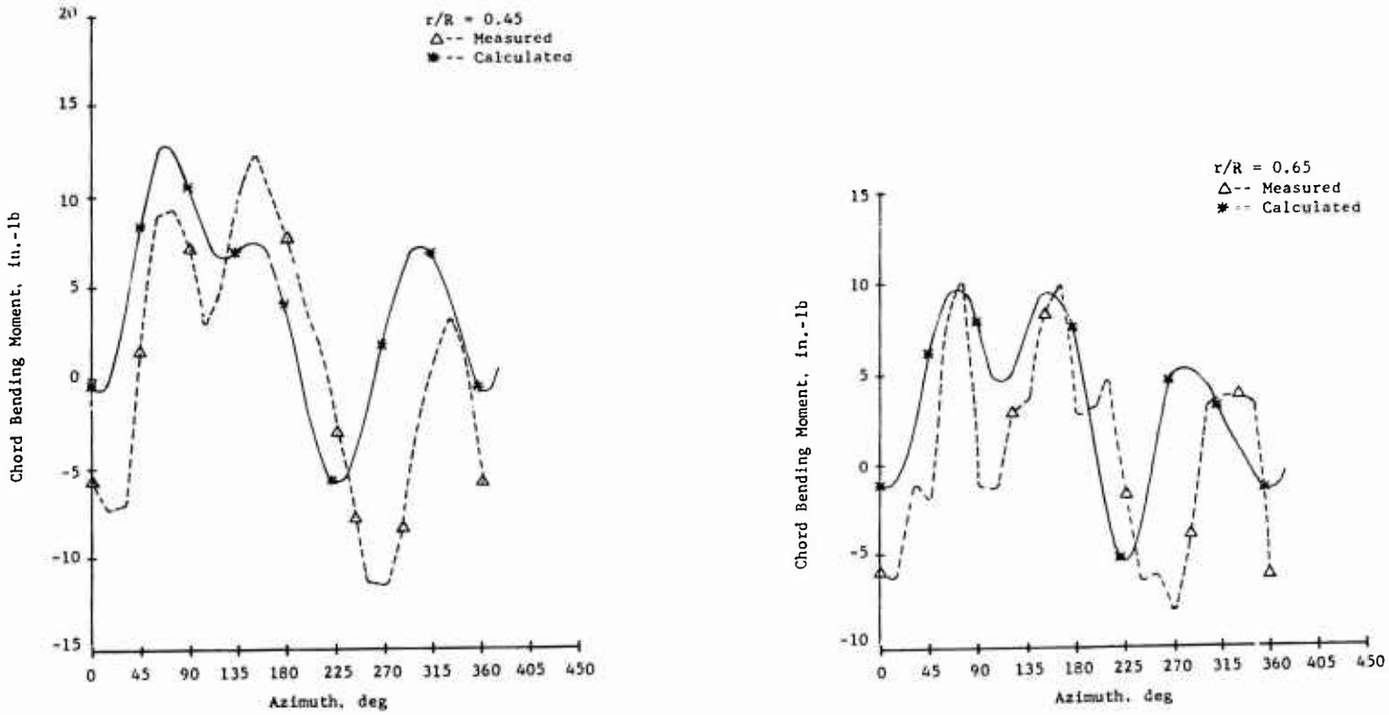

Figure 58. Continued.

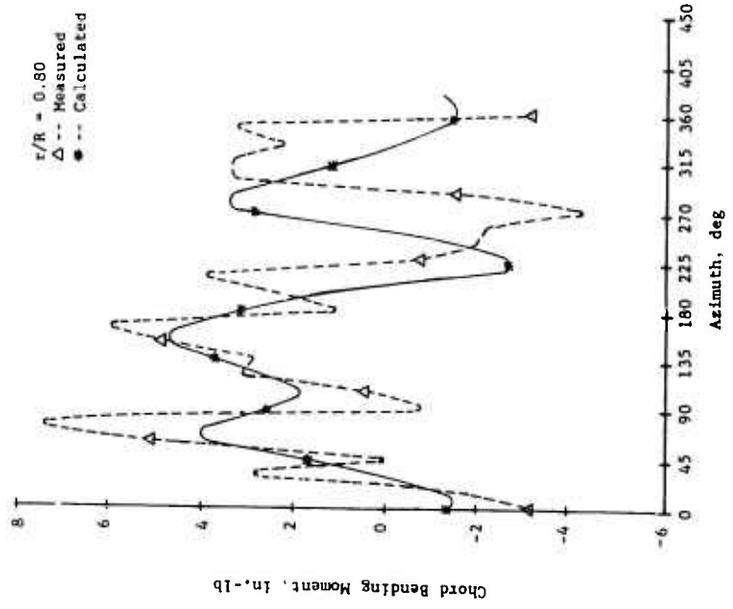

Figure 58. Concluded.

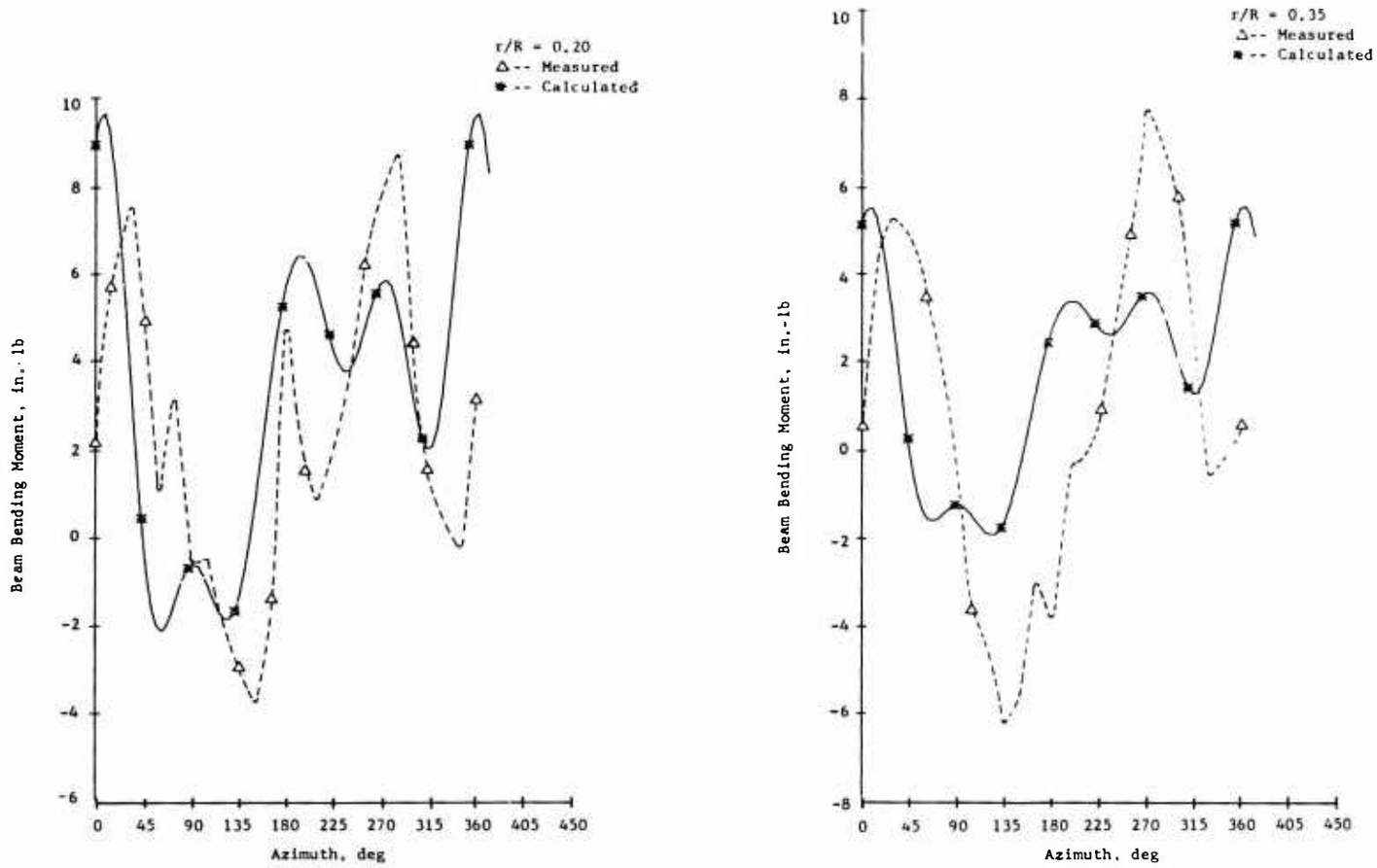

Figure 59. Measured and Calculated Beam Bending Moment Time Histories, Fiberglass Blade, -8° Twist, $\mu = 0.502$, $M_{1,90} = 0.467$, $\alpha_m = 5^{\circ}$ (Cond. 44).

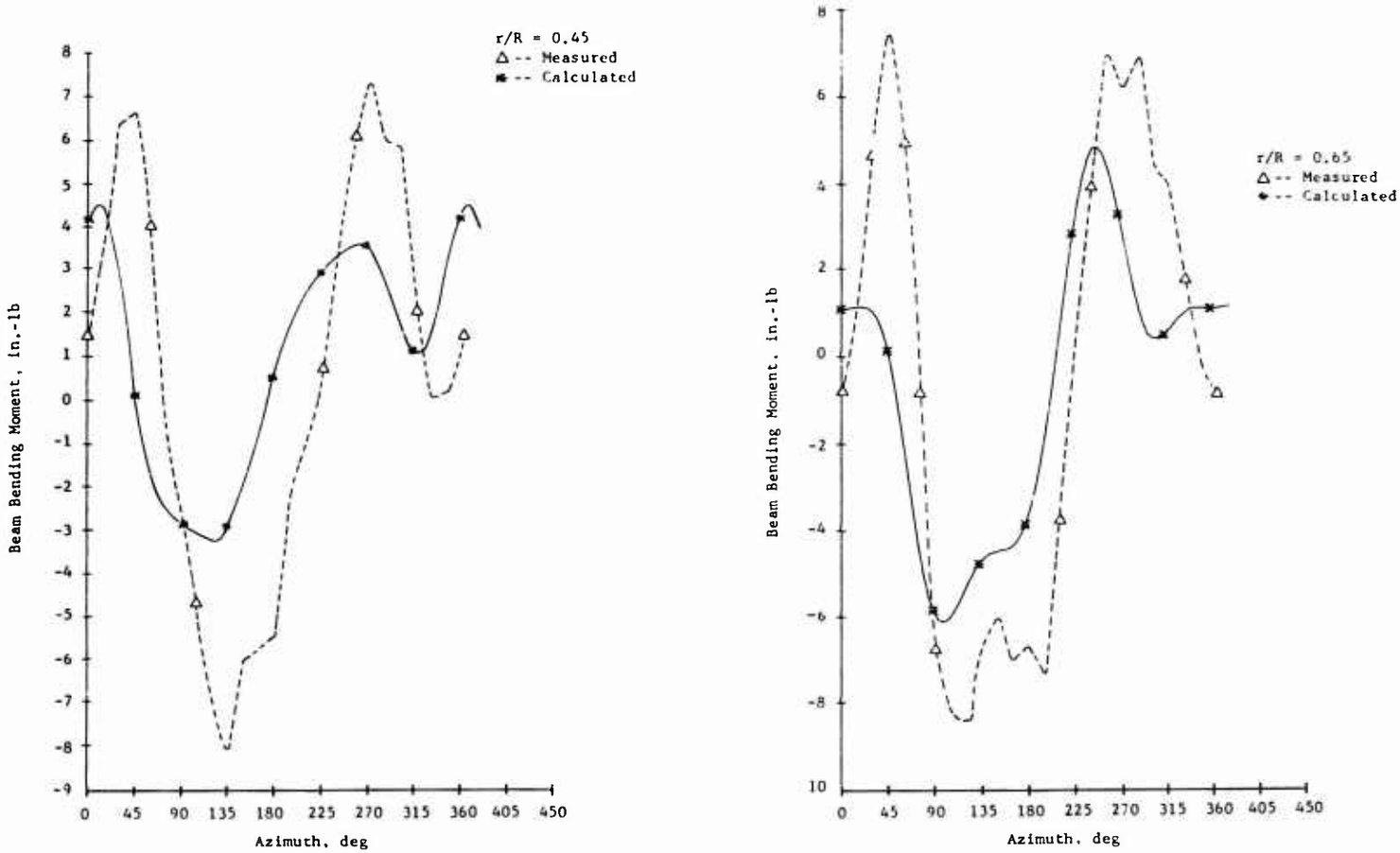

Figure 59. Continued.

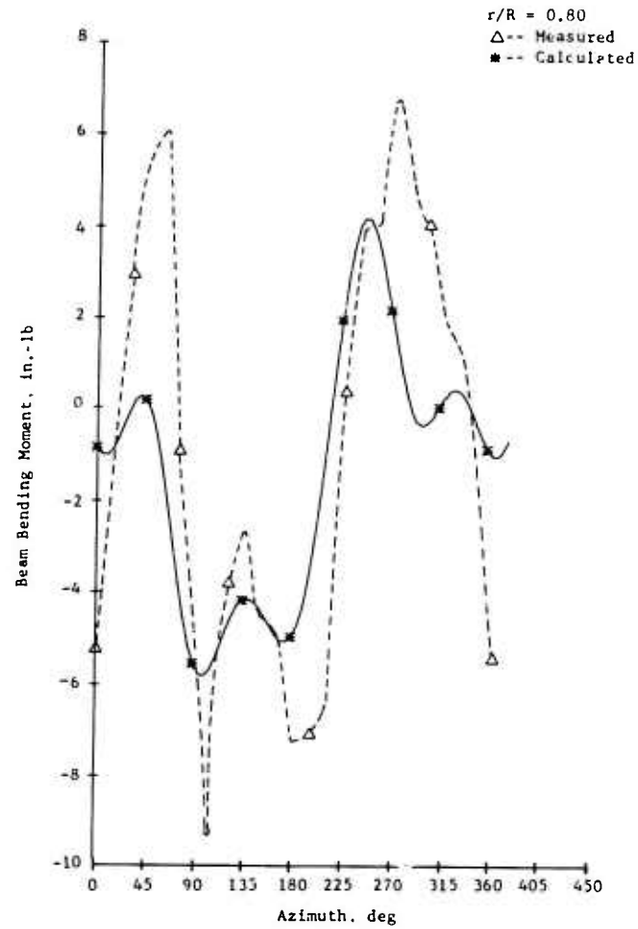

Figure 59. Concluded.

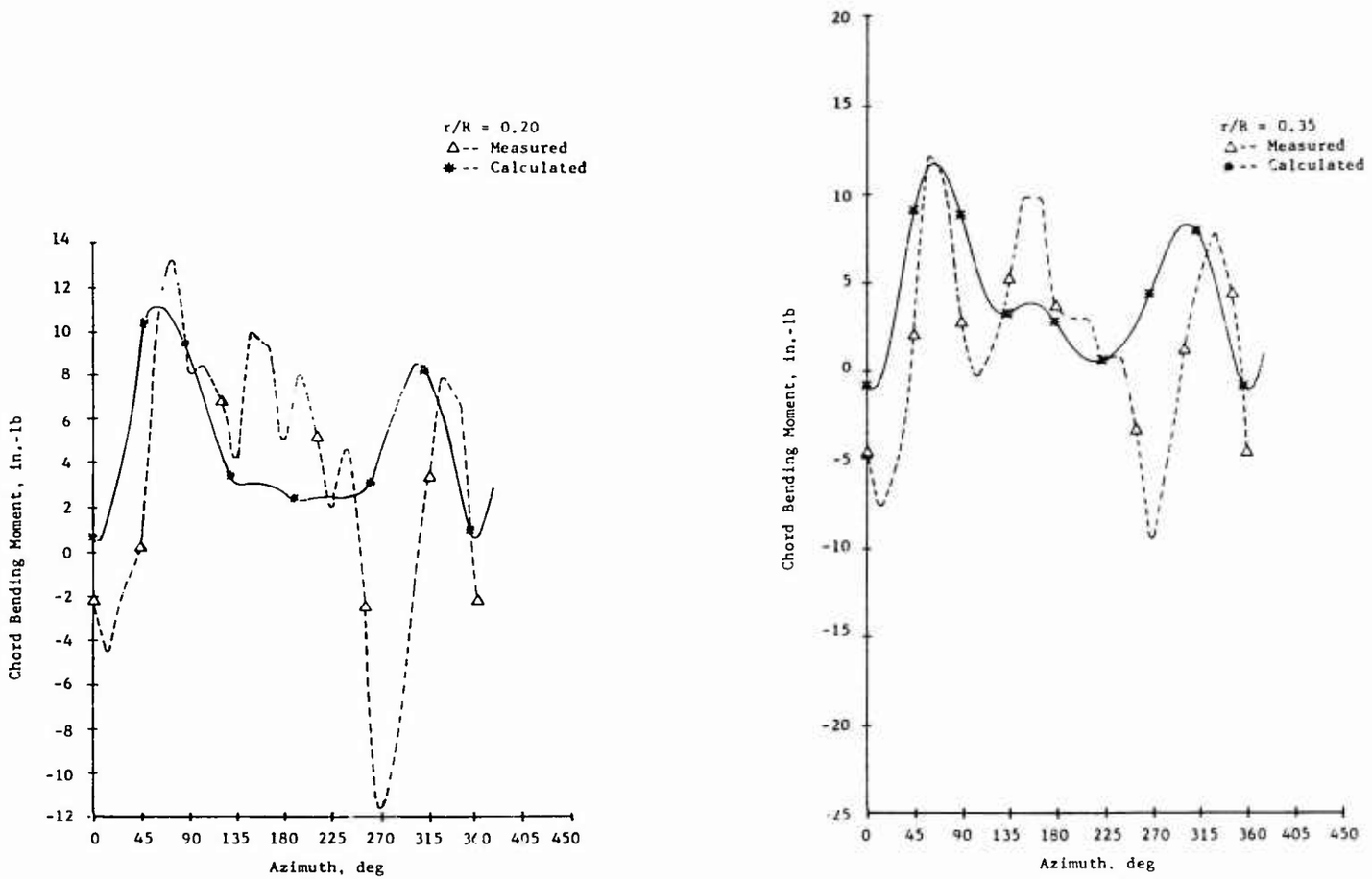

Figure 60. Measured and Calculated Chord Bending Moment Time Histories, Fiberglass Blade, -8° Twist, $\mu = 0.502$, $M_{1,90} = 0.467$, $\alpha_m = 5°$(Cond. 14).

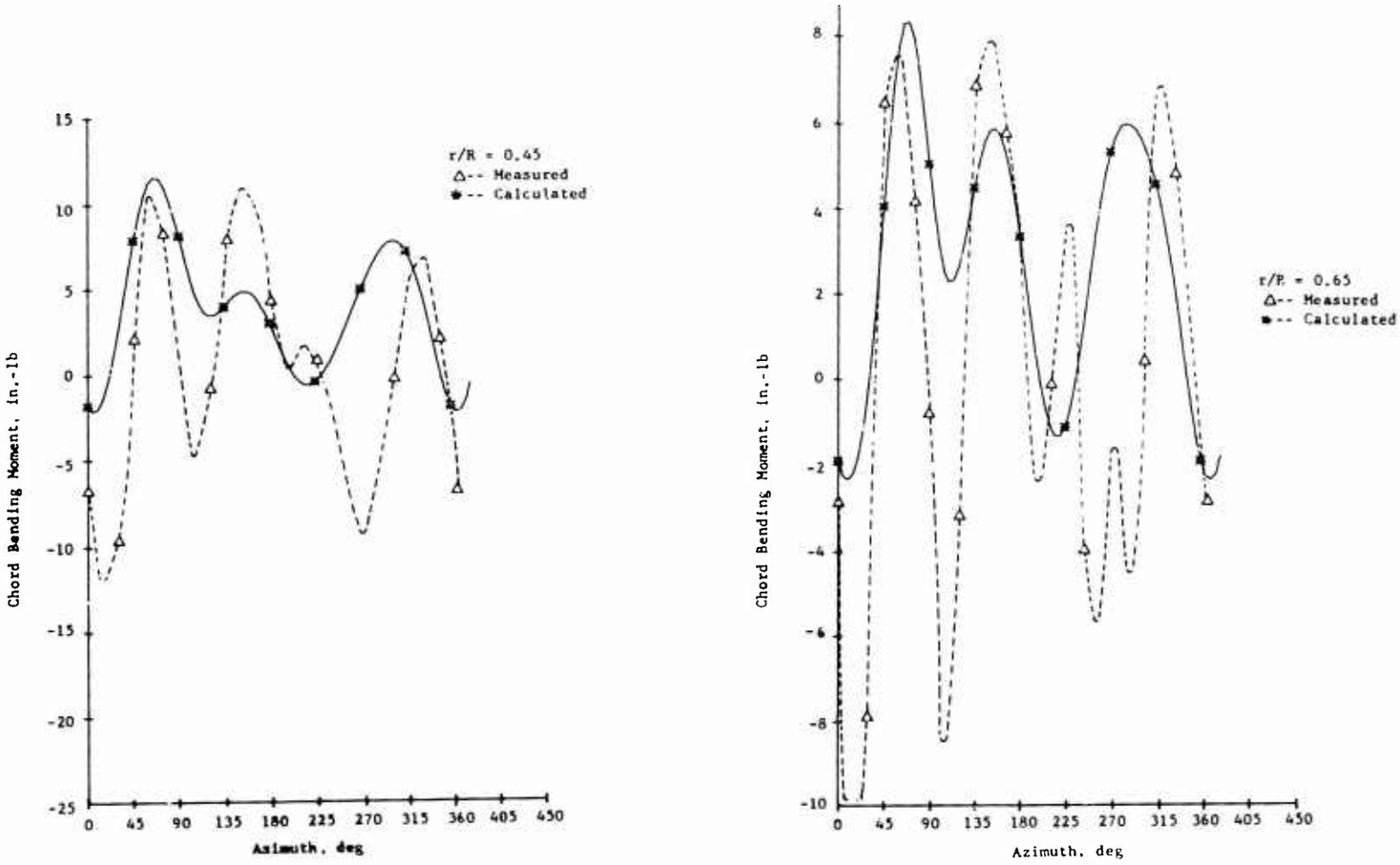

Figure 60. Continued.

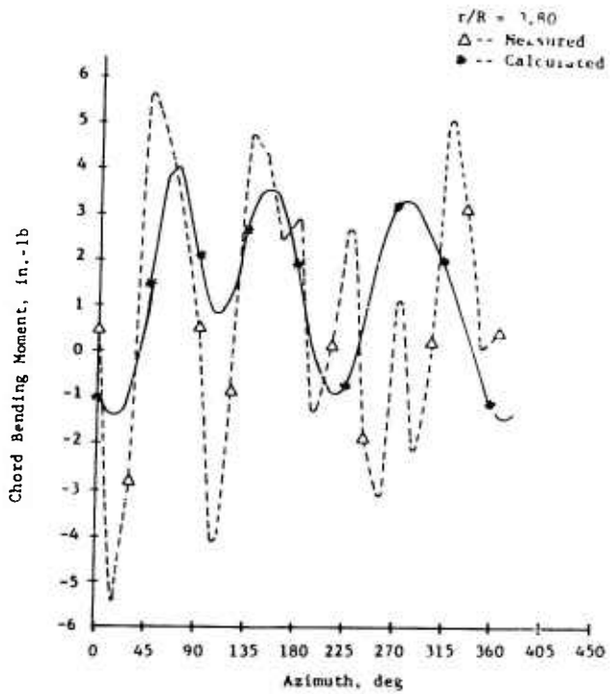

Figure 60. Concluded.

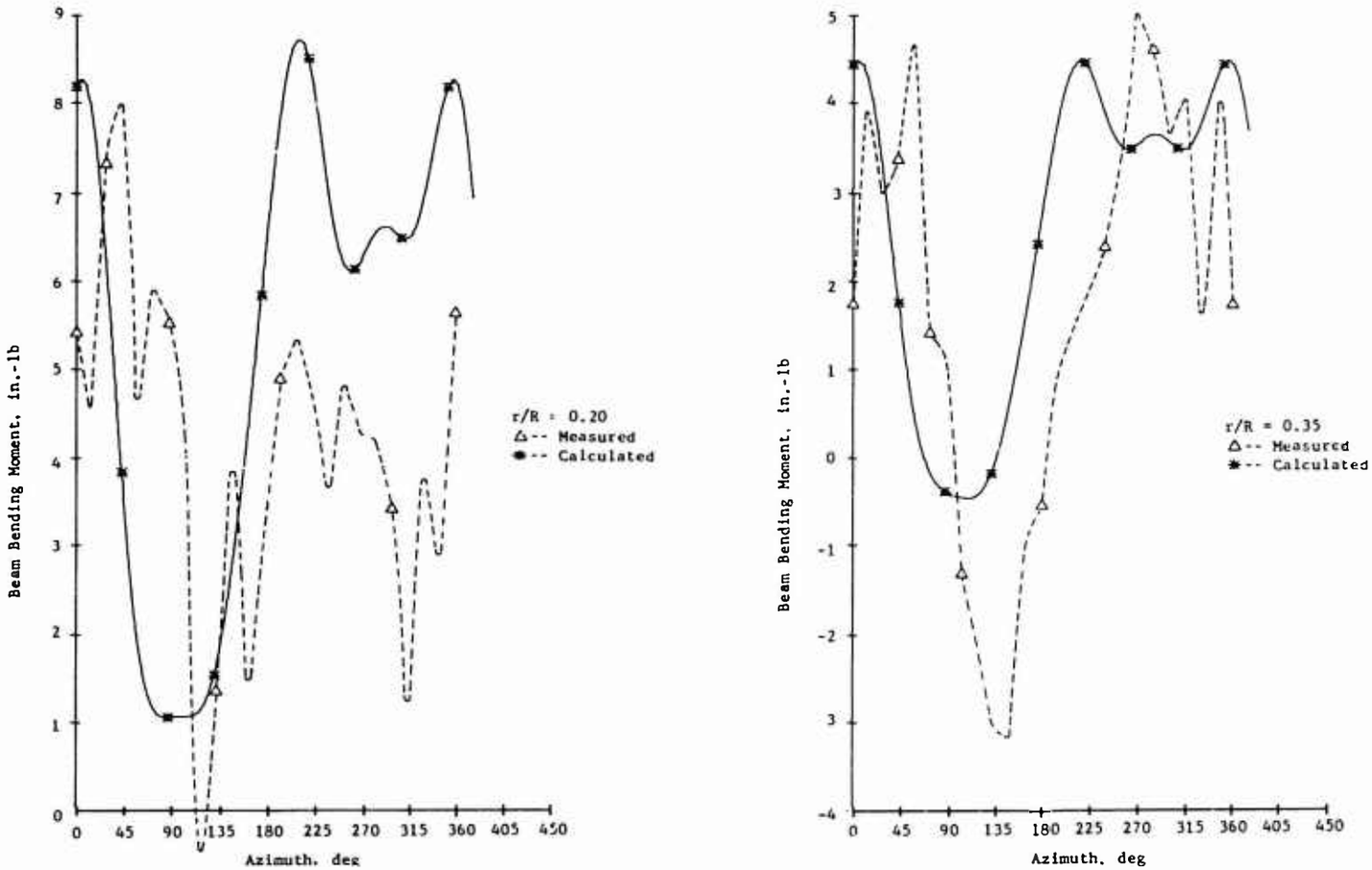

Figure 61. Measured and Calculated Beam Bending Moment Time Histories, Fiberglass Blade, -8° Twist, $\mu = 0.299$, $M_{1,90} = 0.408$, $\alpha_m = 0°$ (Cond. 68).

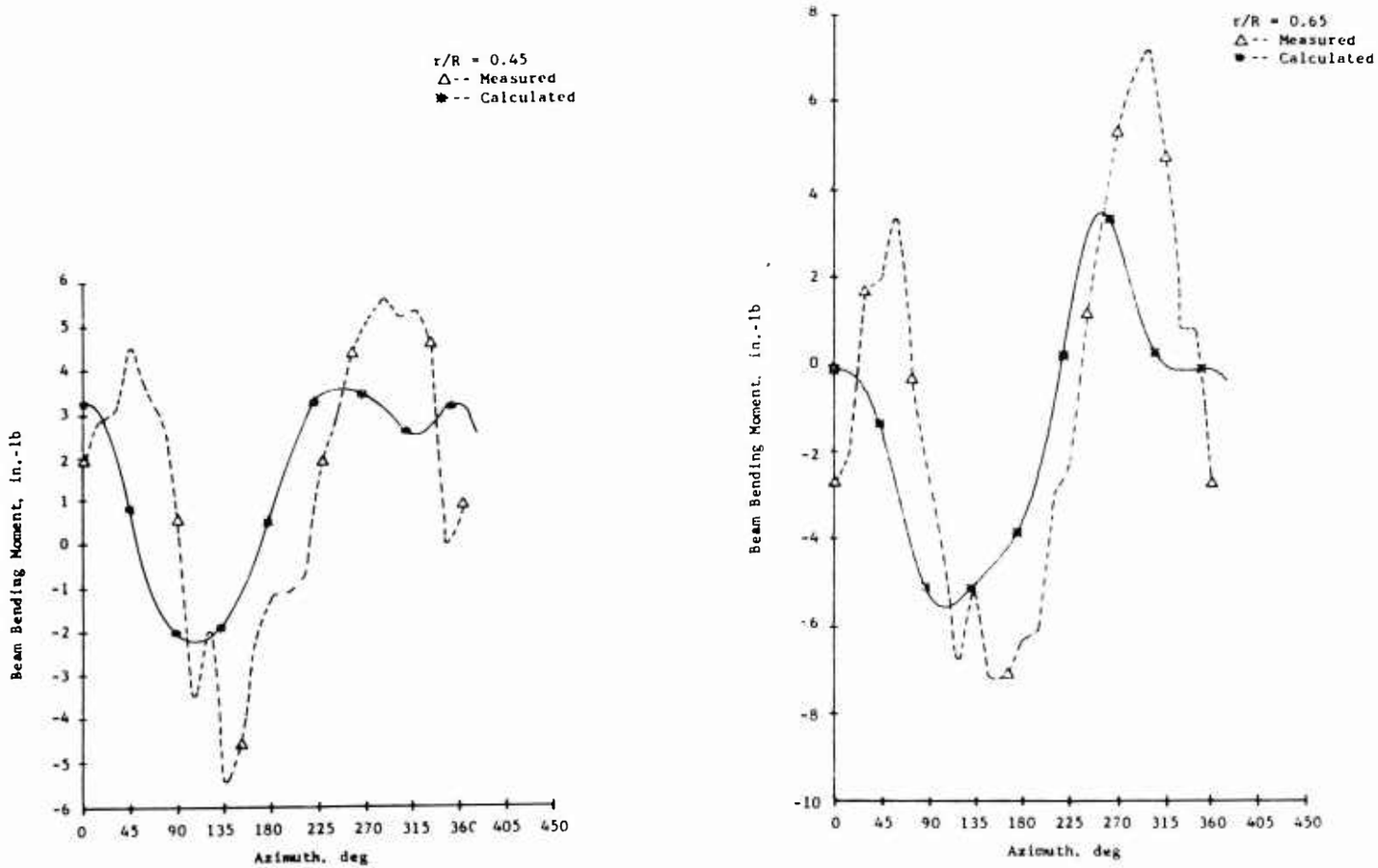

Figure 61. Continued.

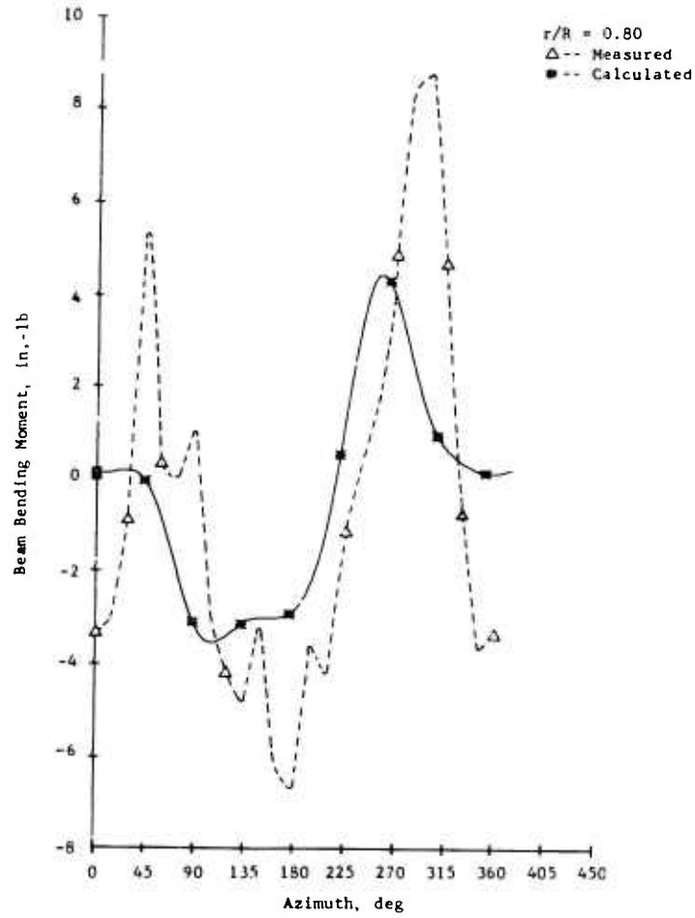

Figure 61. Concluded.

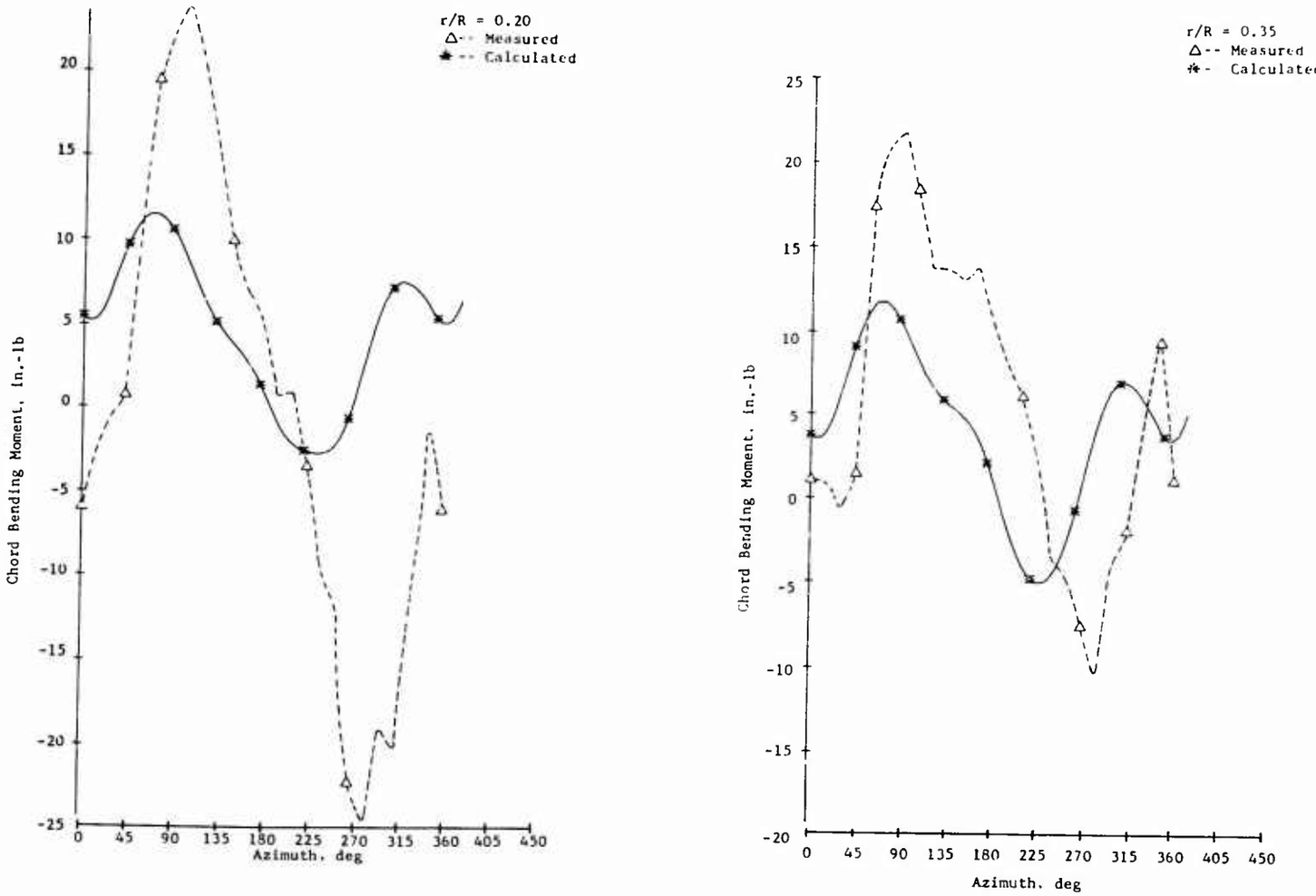

Figure 62. Measured and Calculated Chord Bending Moment Time Histories, Fiberglass Blade, -8° Twist, $\mu = 0.299$, $M_{1,90} = 0.408$, $\alpha_m = 0°$(Cond. 68).

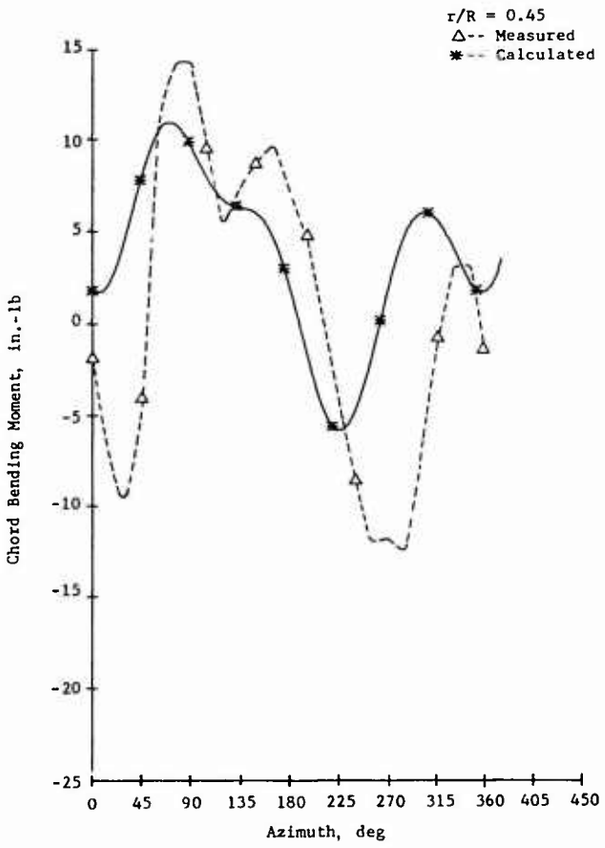

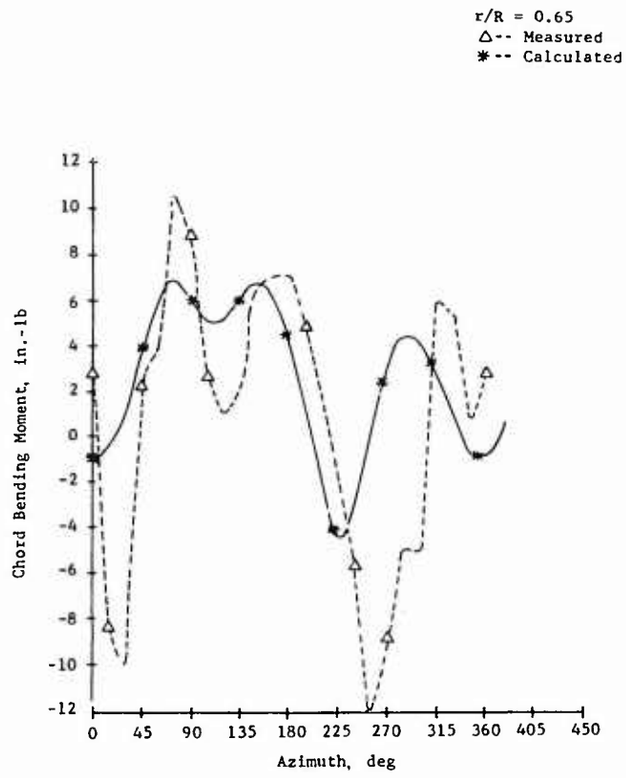

Figure 62. Continued.

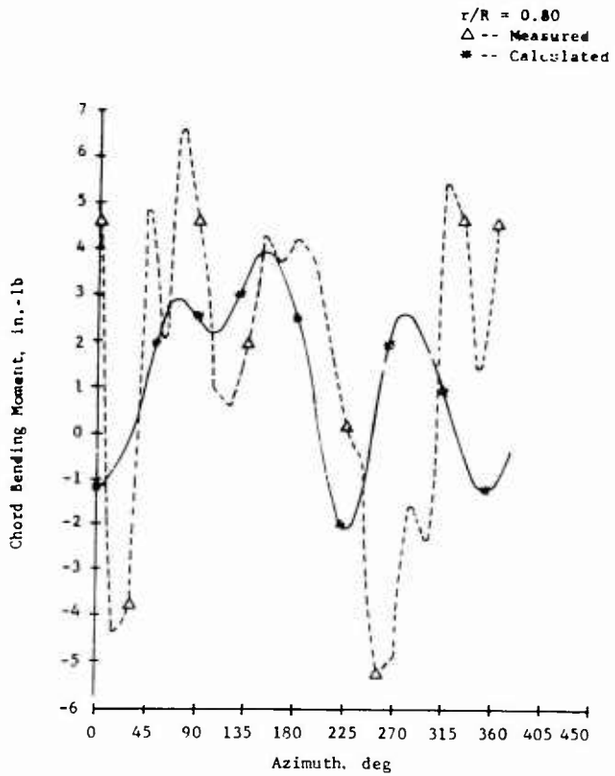

Figure 62. Concluded.

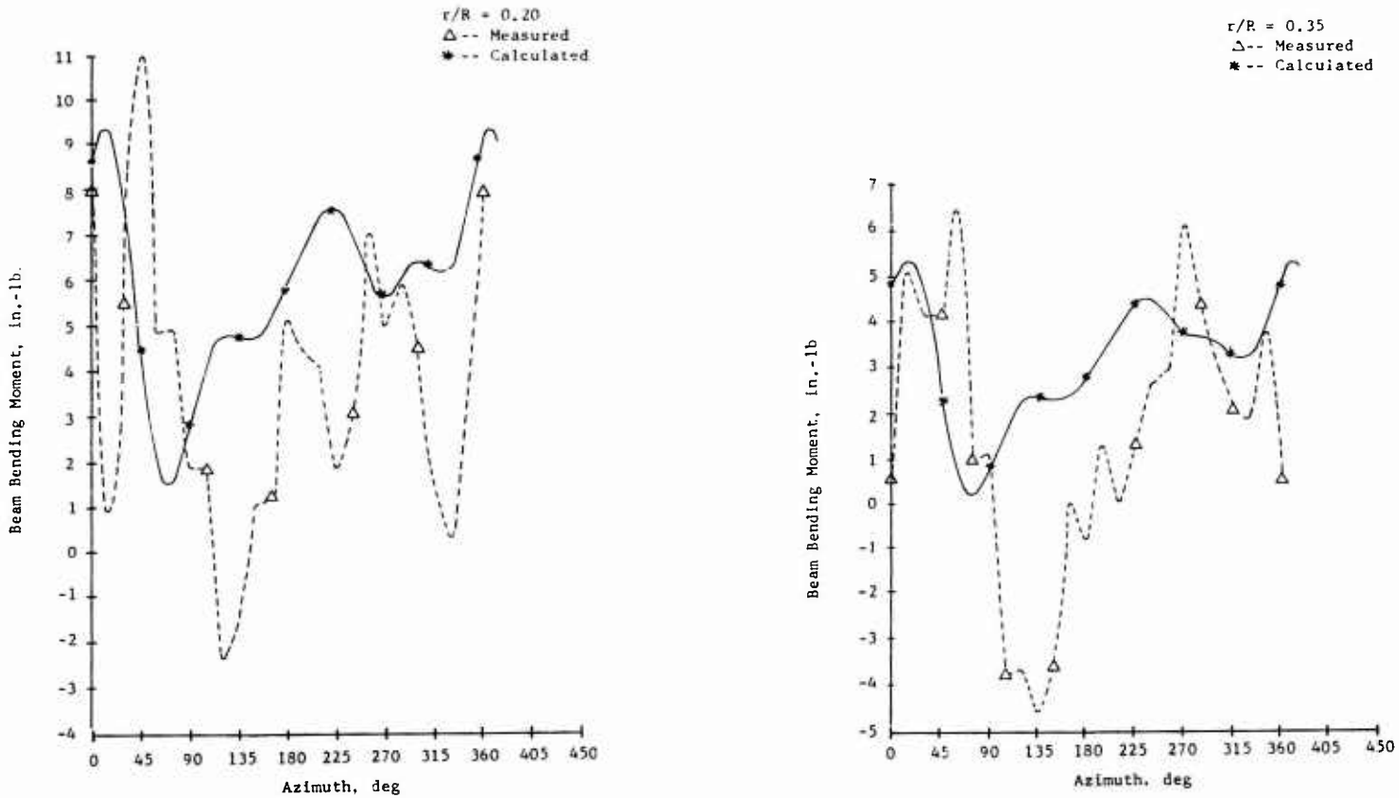

Figure 63. Measured and Calculated Beam Bending Moment Time Histories, Fiberglass Blade, 0° Twist, $\delta_F = 5°$ $\mu = 0.399$, $M_{1,90} = 0.434$, $\alpha_m = 0.5°$ (Cond. 25).

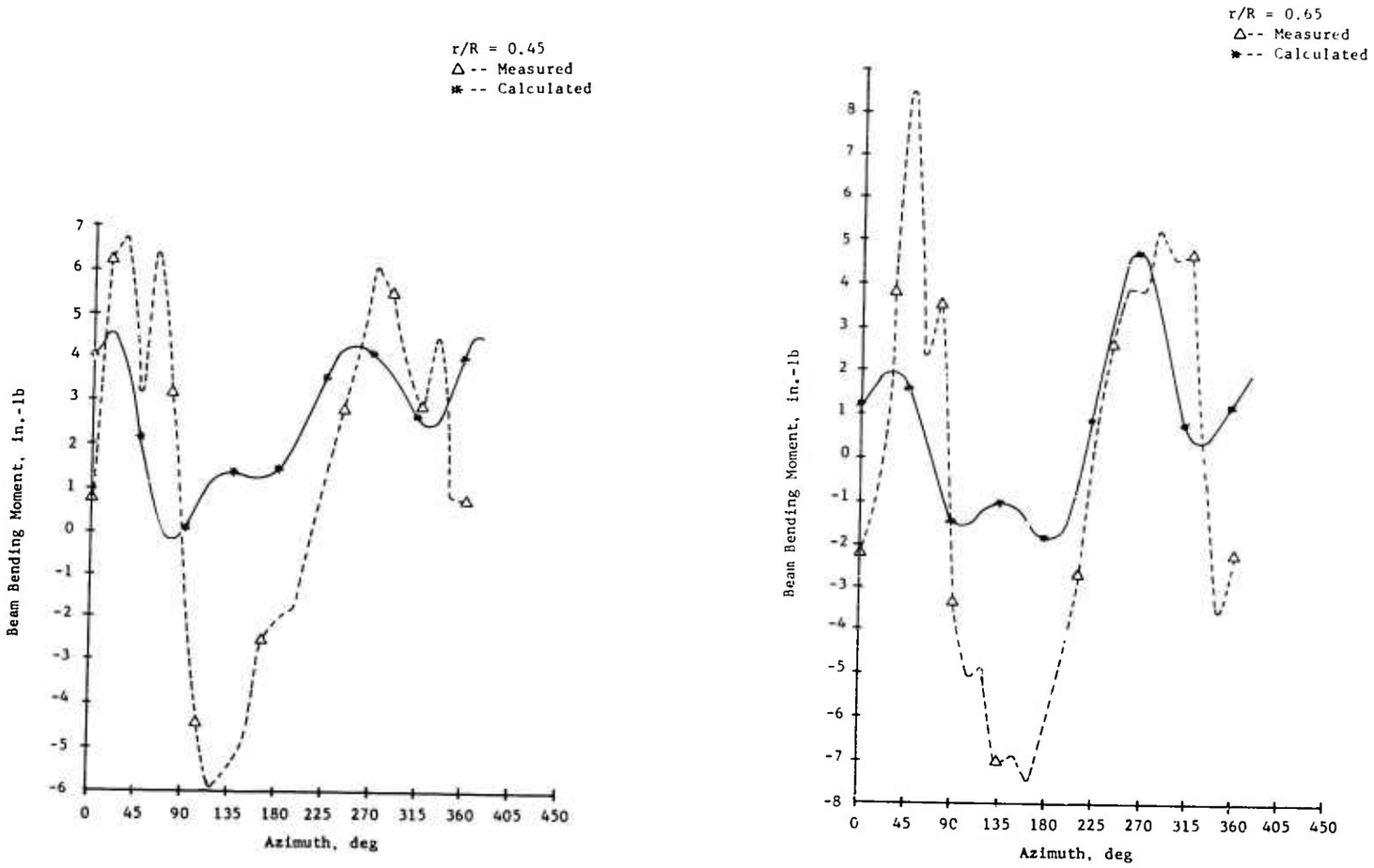

Figure 63. Continued.

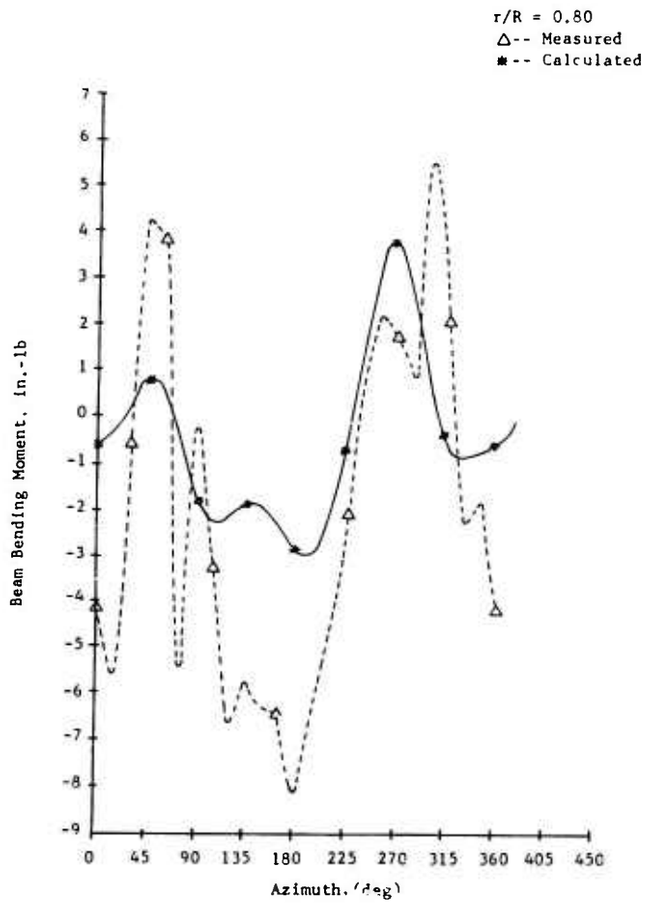

Figure 63. Concluded.

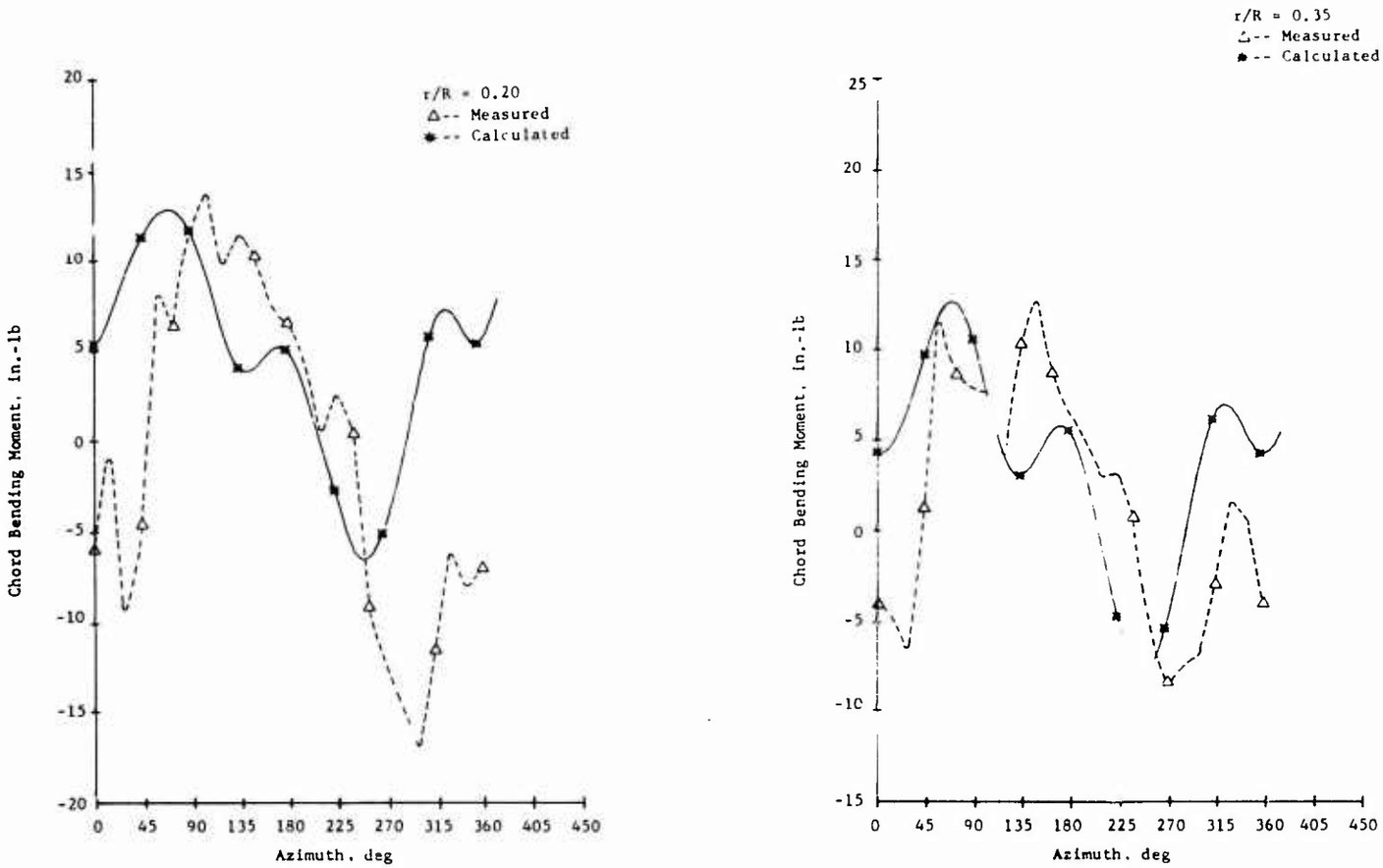

Figure 64. Measured and Calculated Chord Bending Moment Time Histories, Fiberglass Blade, 0° Twist, $\delta_5 = 5°$ $\mu = 0.399$, $M_{1,90} = 0.434$, $\alpha_m = 0.5°$ (Cond. 25).

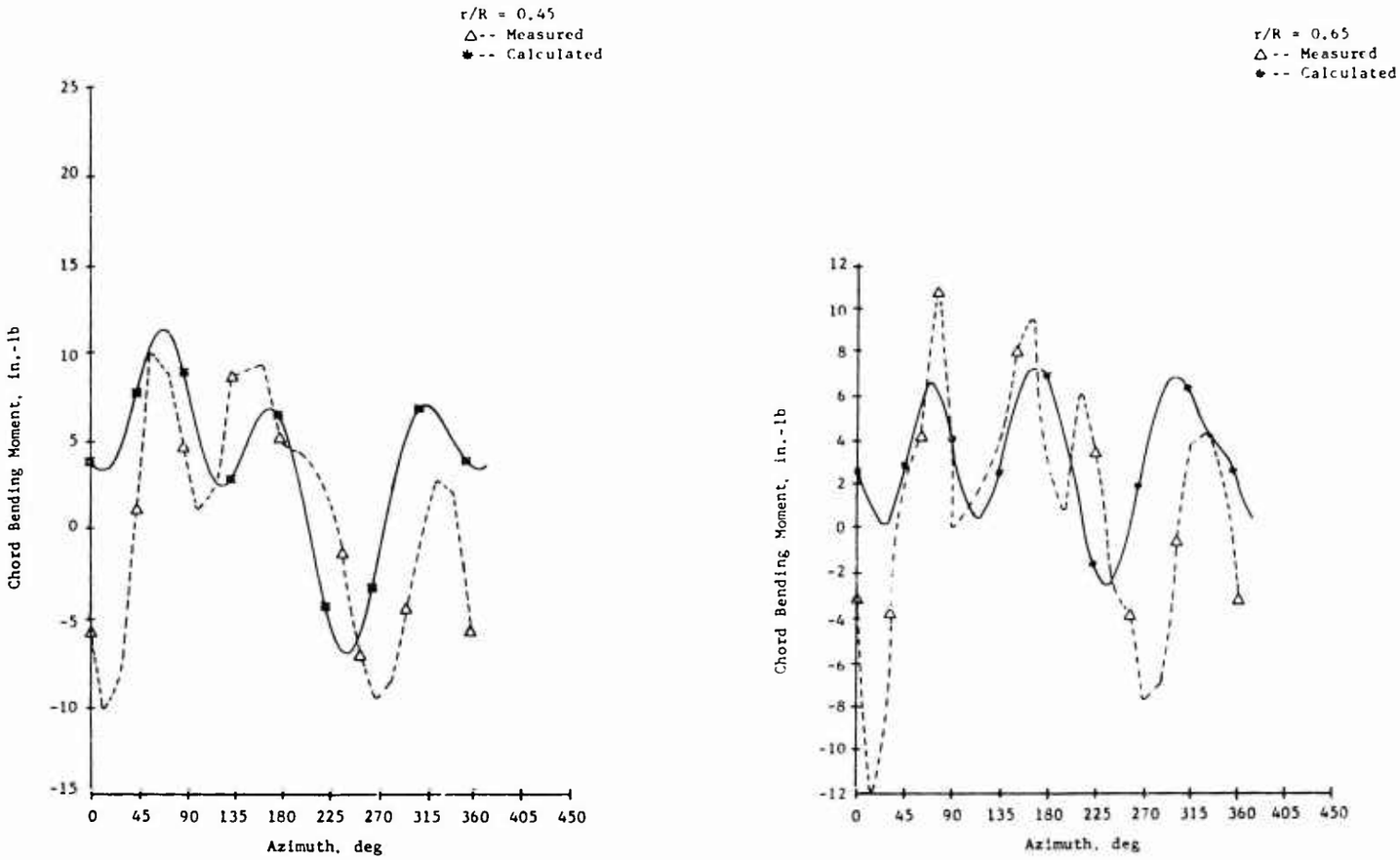

Figure 64. Continued.

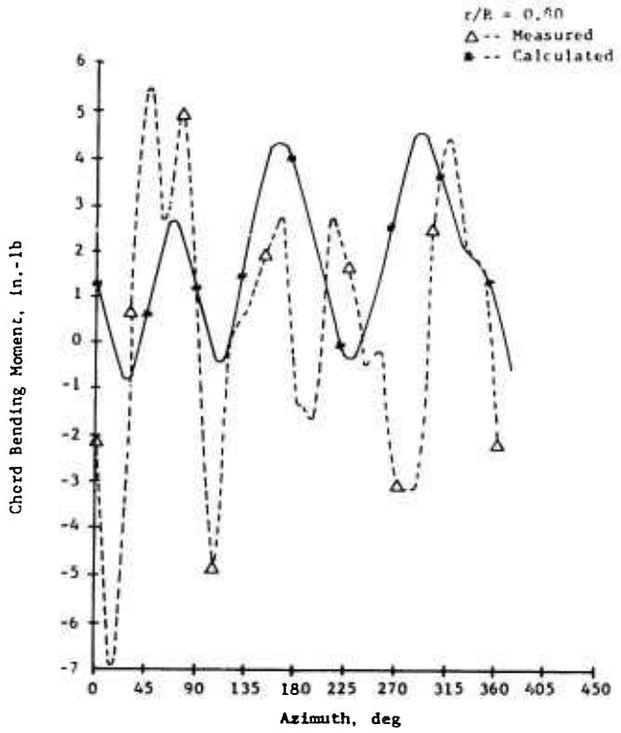

Figure 64. Concluded.

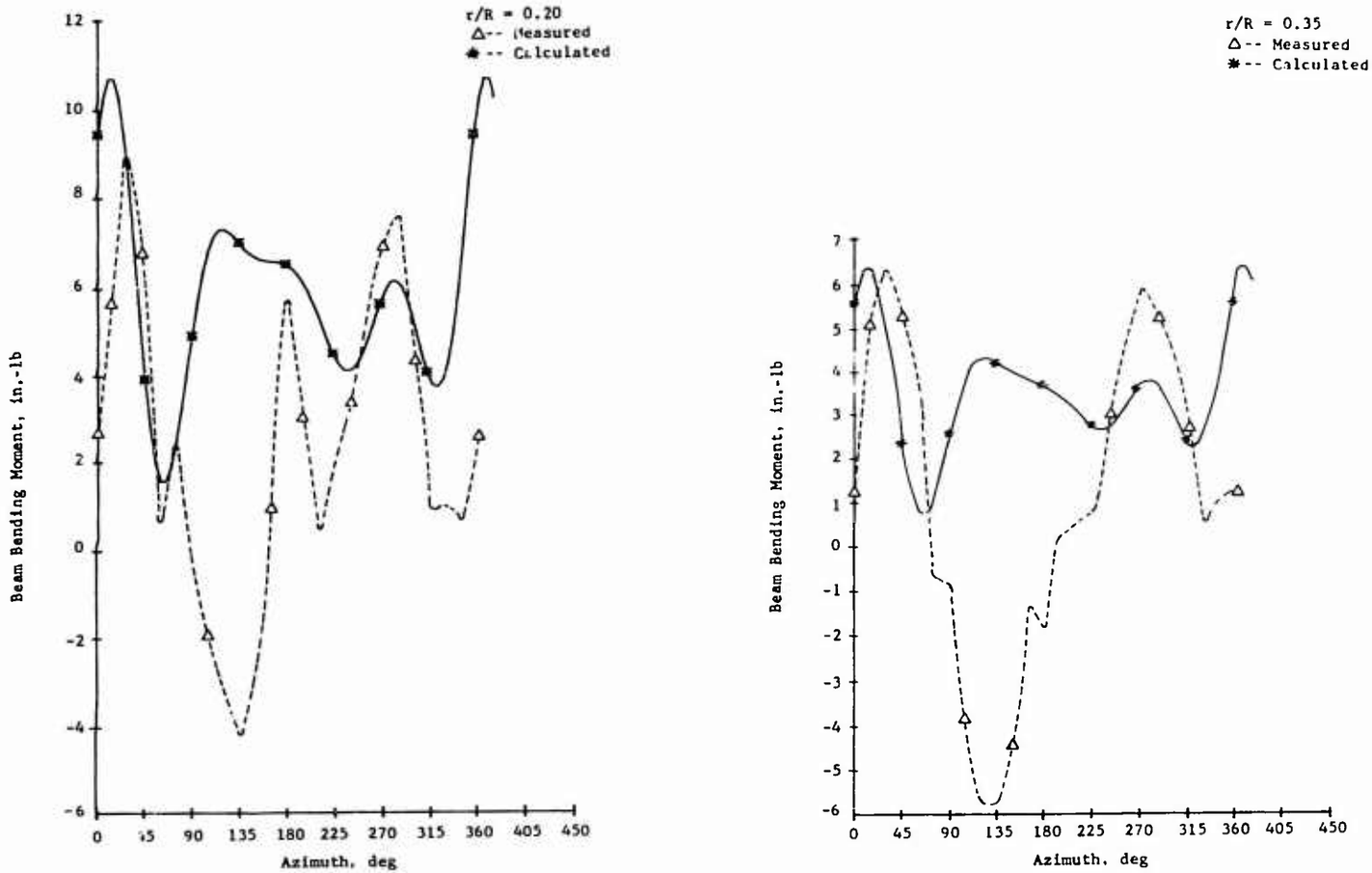

Figure 65. Measured and Calculated Beam Bending Moment Time Histories, Fiberglass Blade, 0° Twist, $\delta_F = 5°$ $\mu = 0.502$, $M_{1,90} = 0.467$, $\alpha_m = 5°$ (Cond. 44).

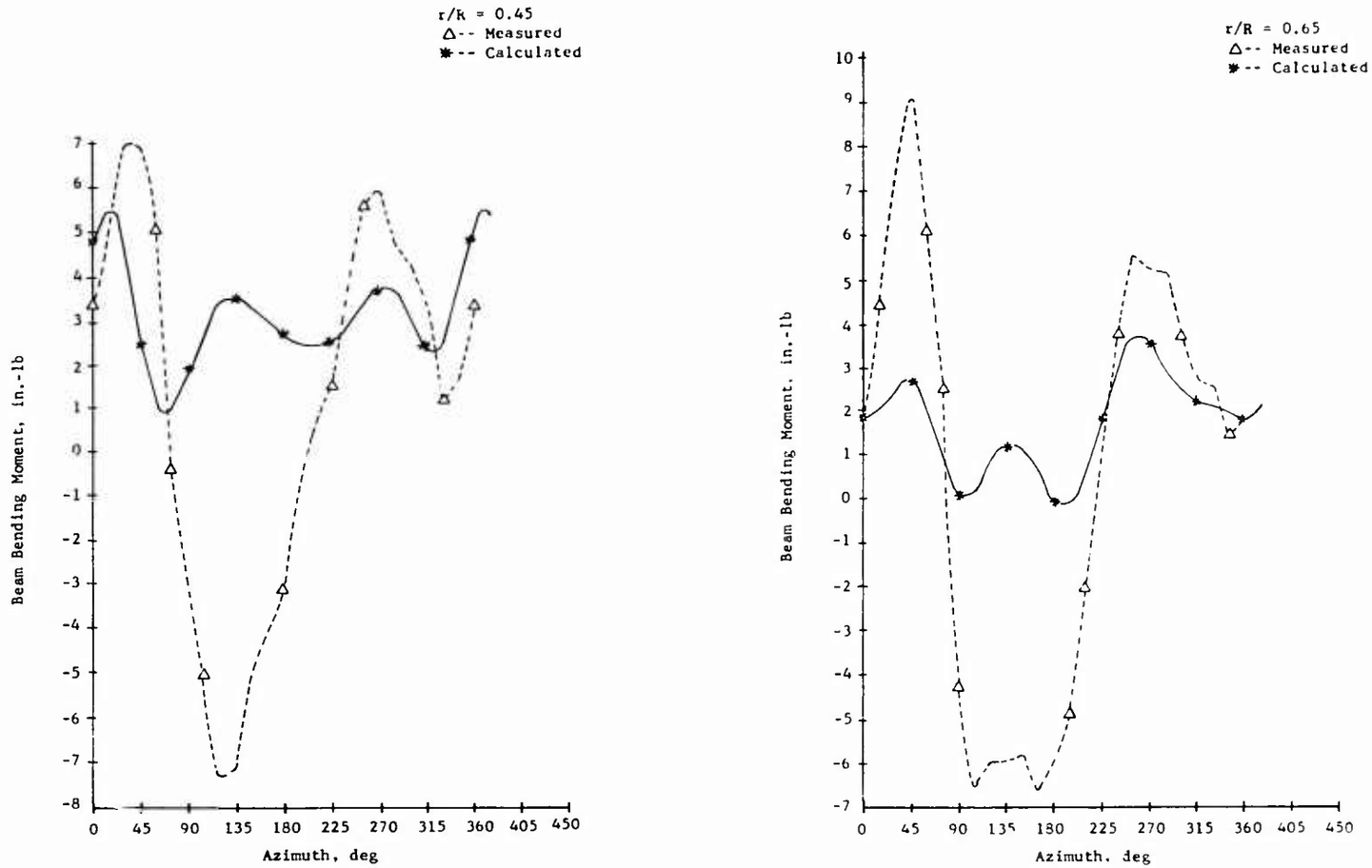

Figure 65. Continued.

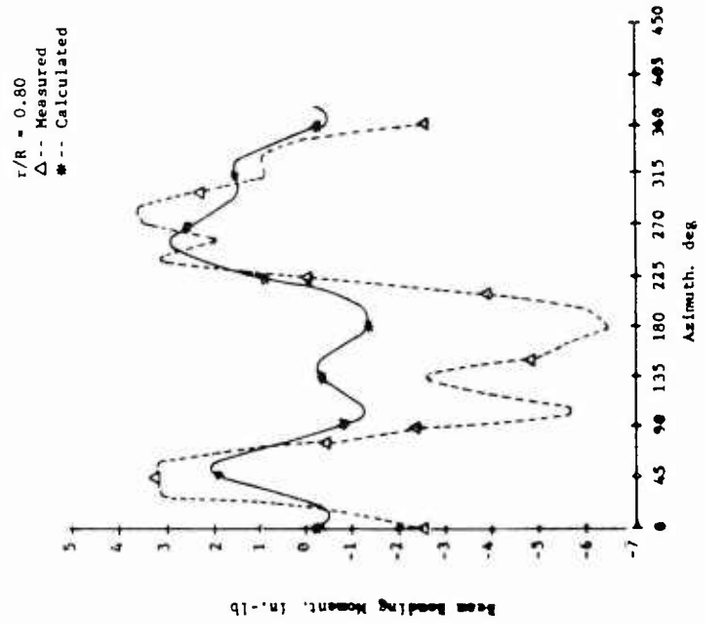

Figure 65. Concluded.

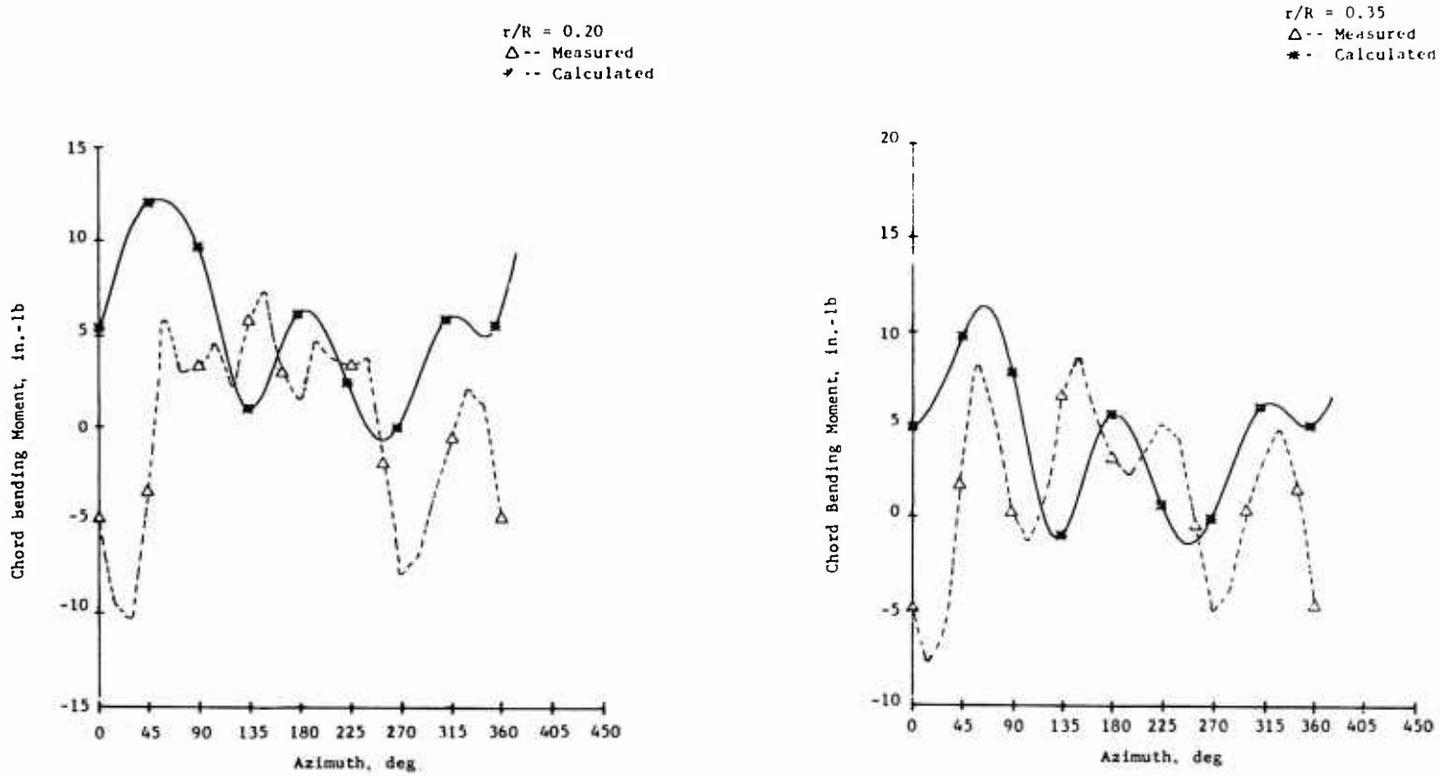

Figure 66. Measured and Calculated Chord Bending Moment Time Histories, Fiberglass Blade, 0° Twist, $\delta_F = 5°$ $\mu = 0.502$, $M_{1,90} = 0.467$, $\alpha_m = 5°$ (Cond. 44).

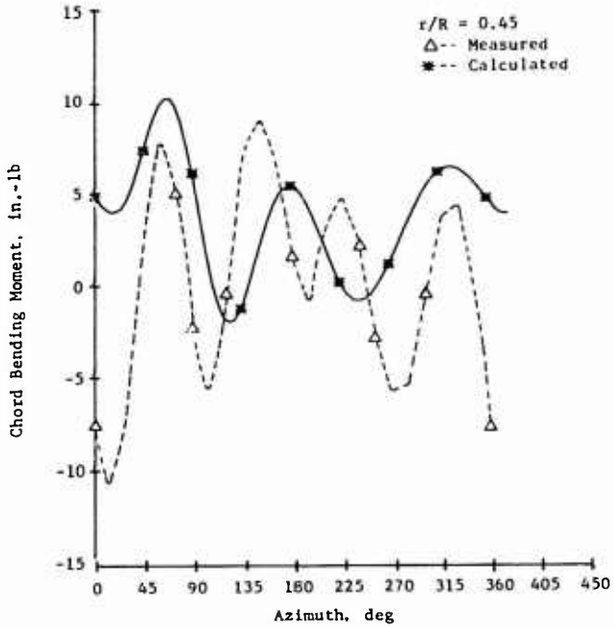

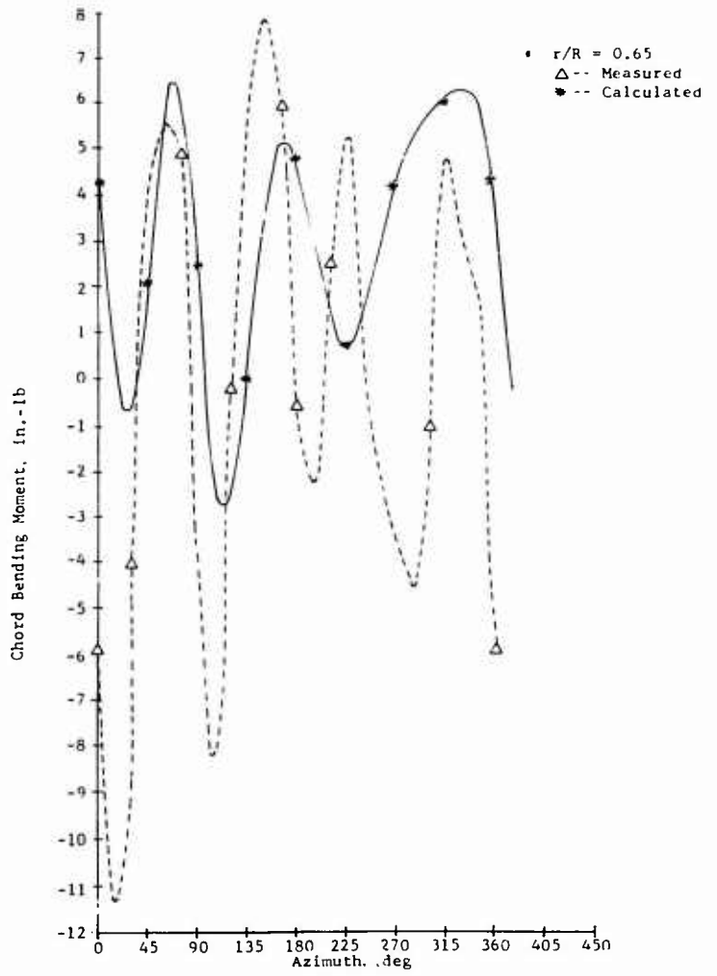

Figure 66. Continued.

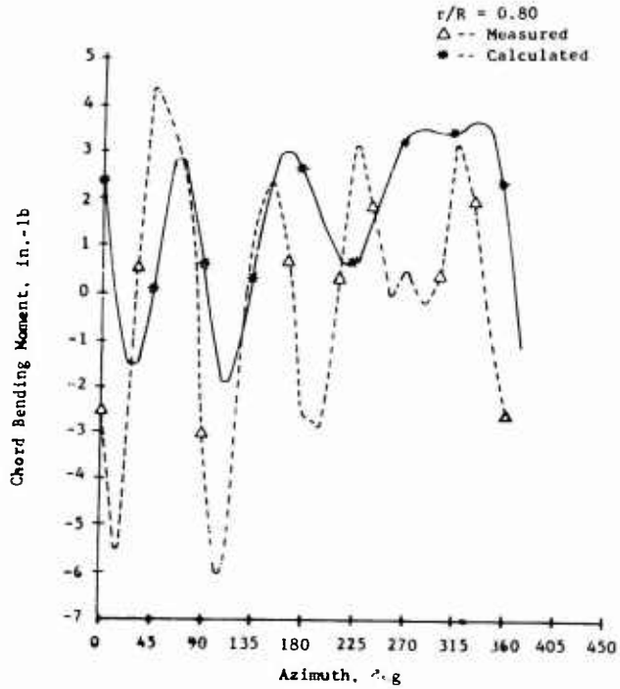

Figure 66. Concluded.

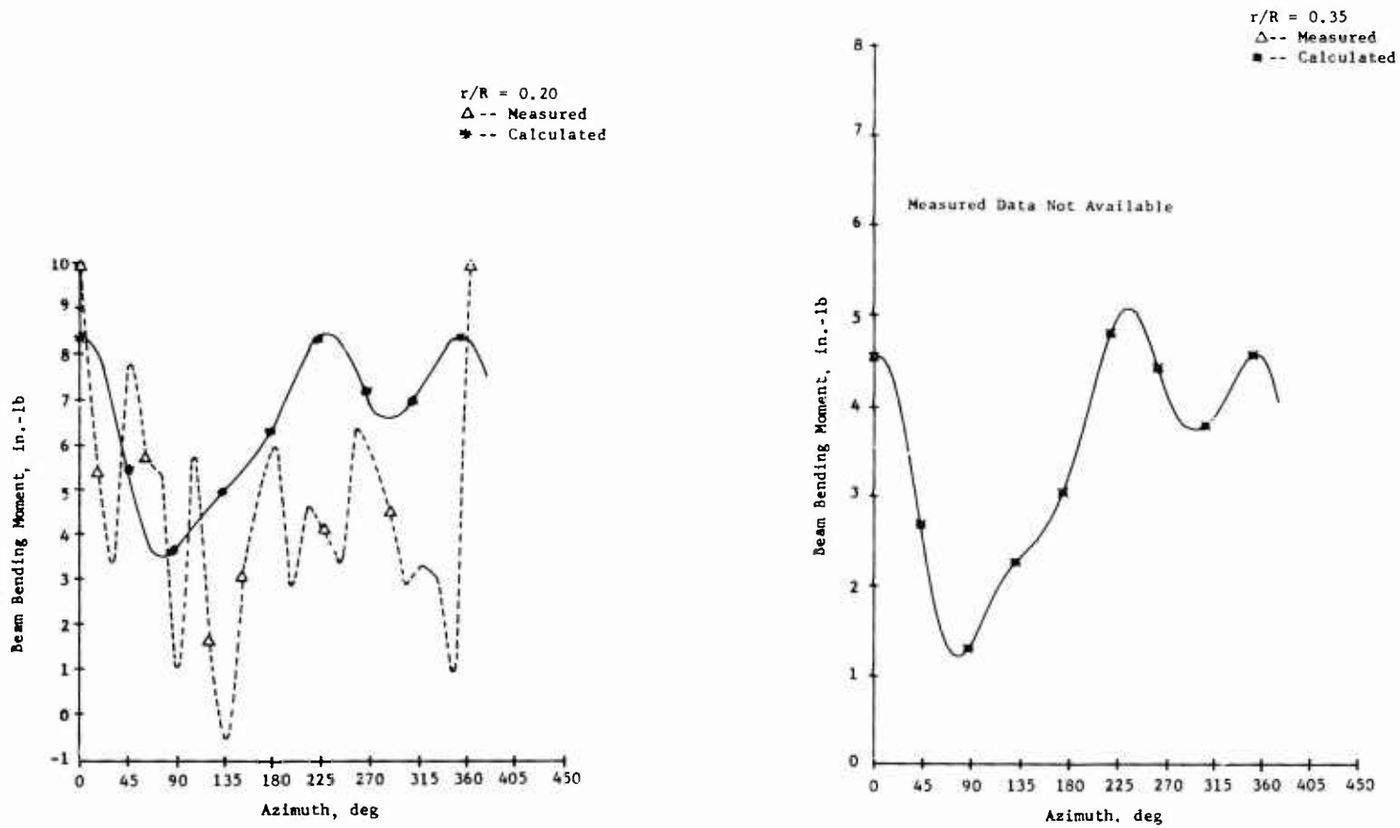

Figure 67. Measured and Calculated Beam Bending Moment Time Histories, Fiberglass Blade, 0° Twist, $\delta_F = 5°$ $\mu = 0.299$, $M_{1,90} = 0.408$, $\alpha_m = 0°$ (Cond. 68).

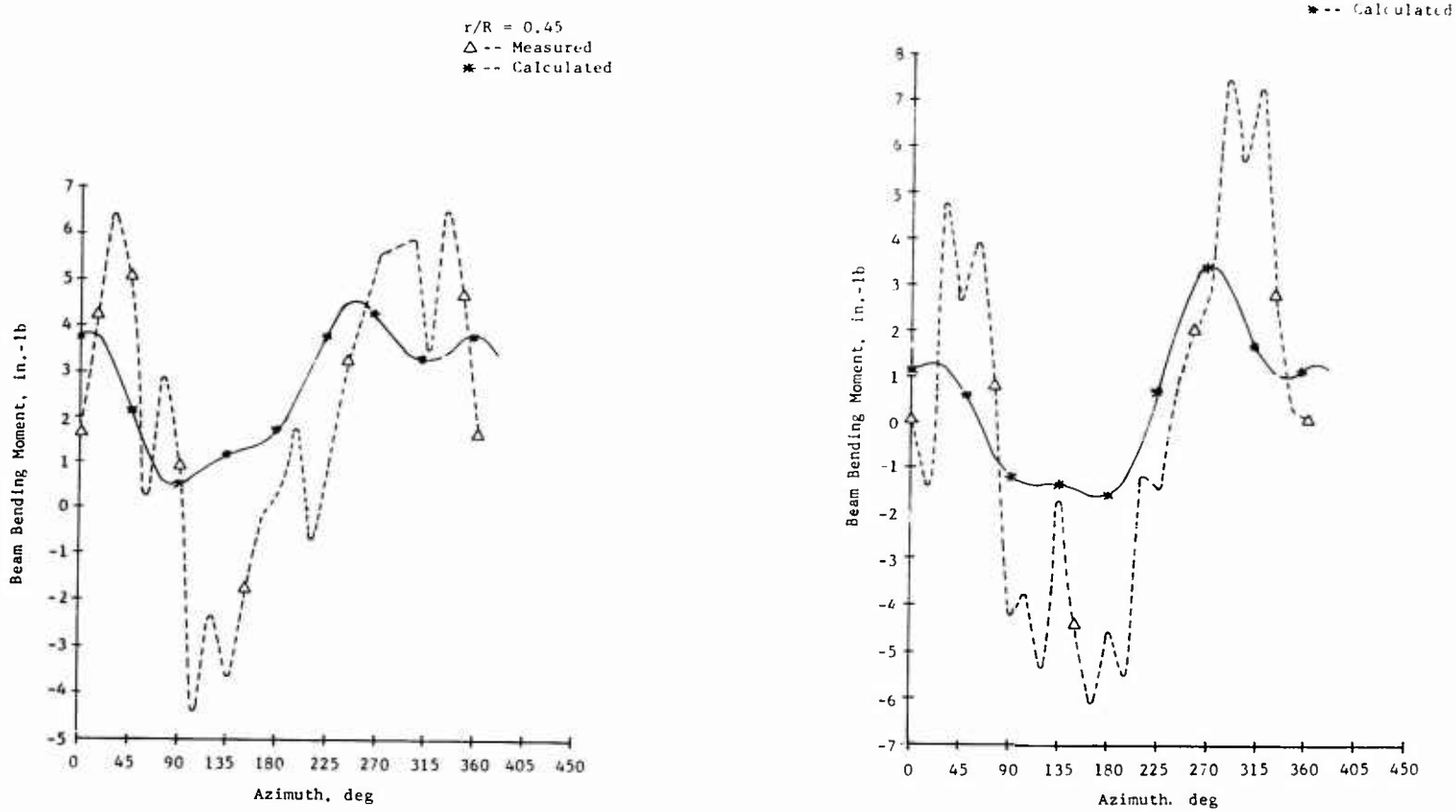

Figure 67. Continued.

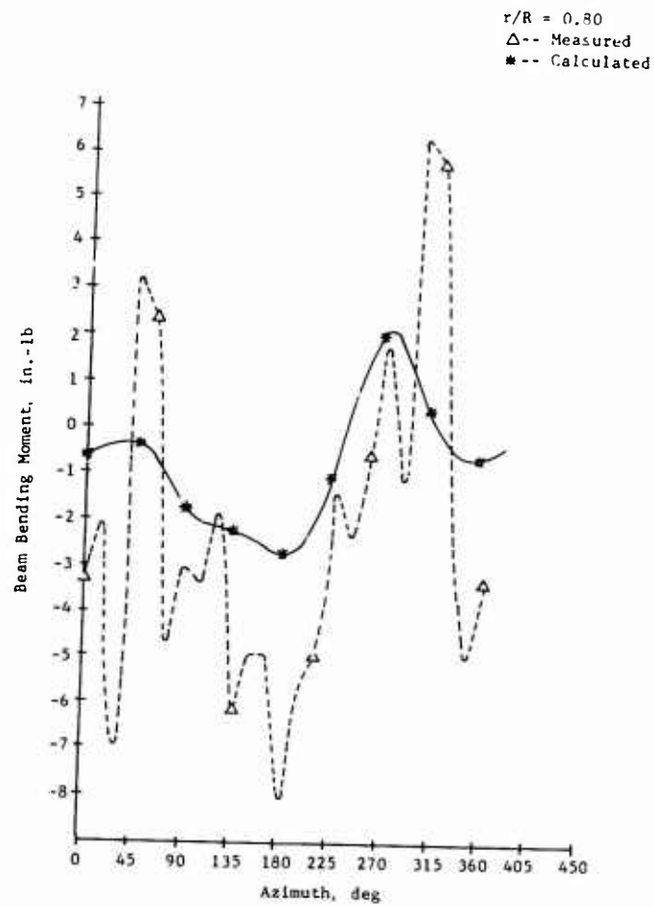

Figure 67. Concluded.

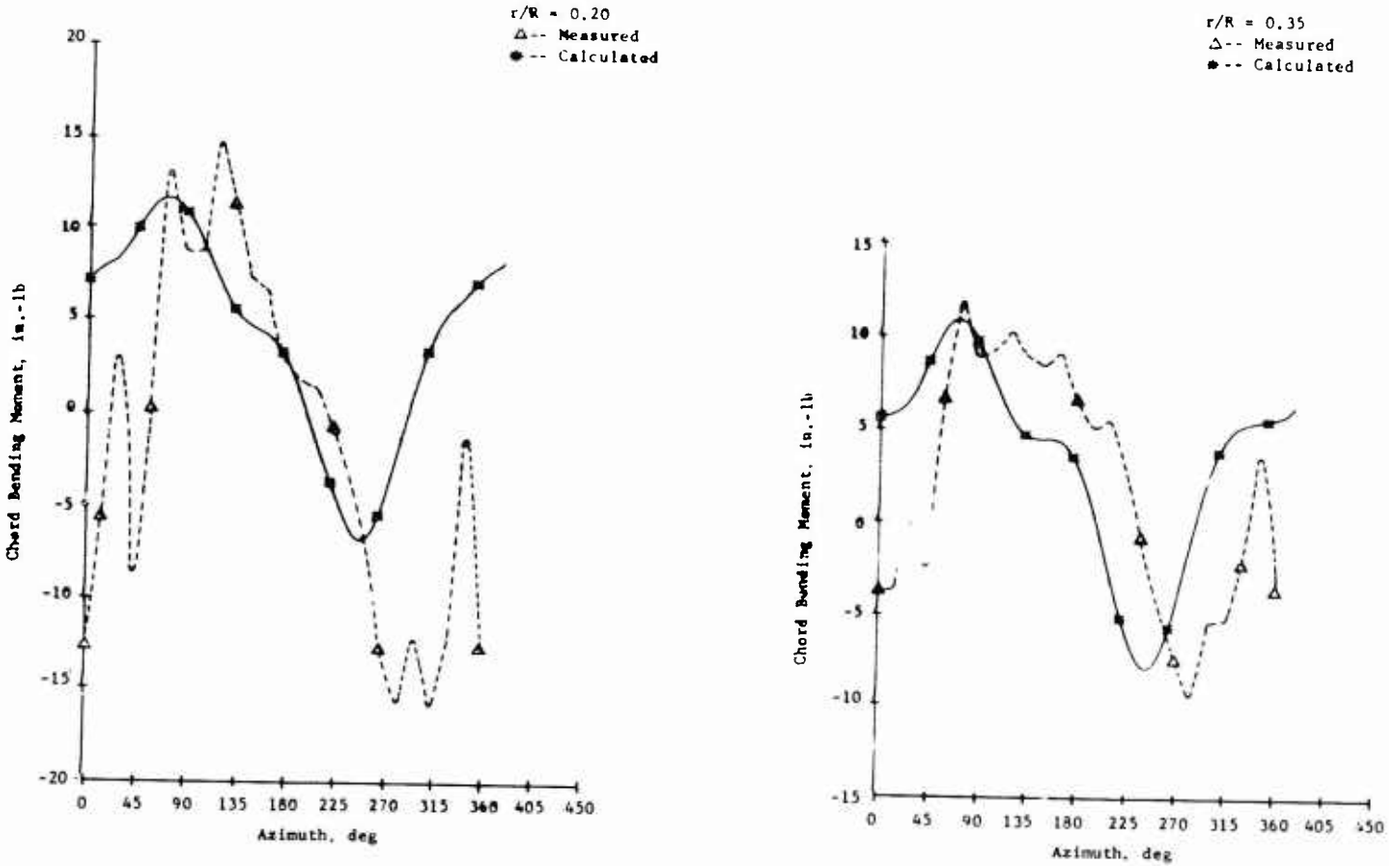

Figure 68. Measured and Calculated Chord Bending Moment Time Histories, Fiberglass Blade, 0° Twist, $\delta_F = 5°$ $\mu = 0.299$, $M_{1,90} = 0.408$, $\alpha_m = 0°$(Cond. 68).

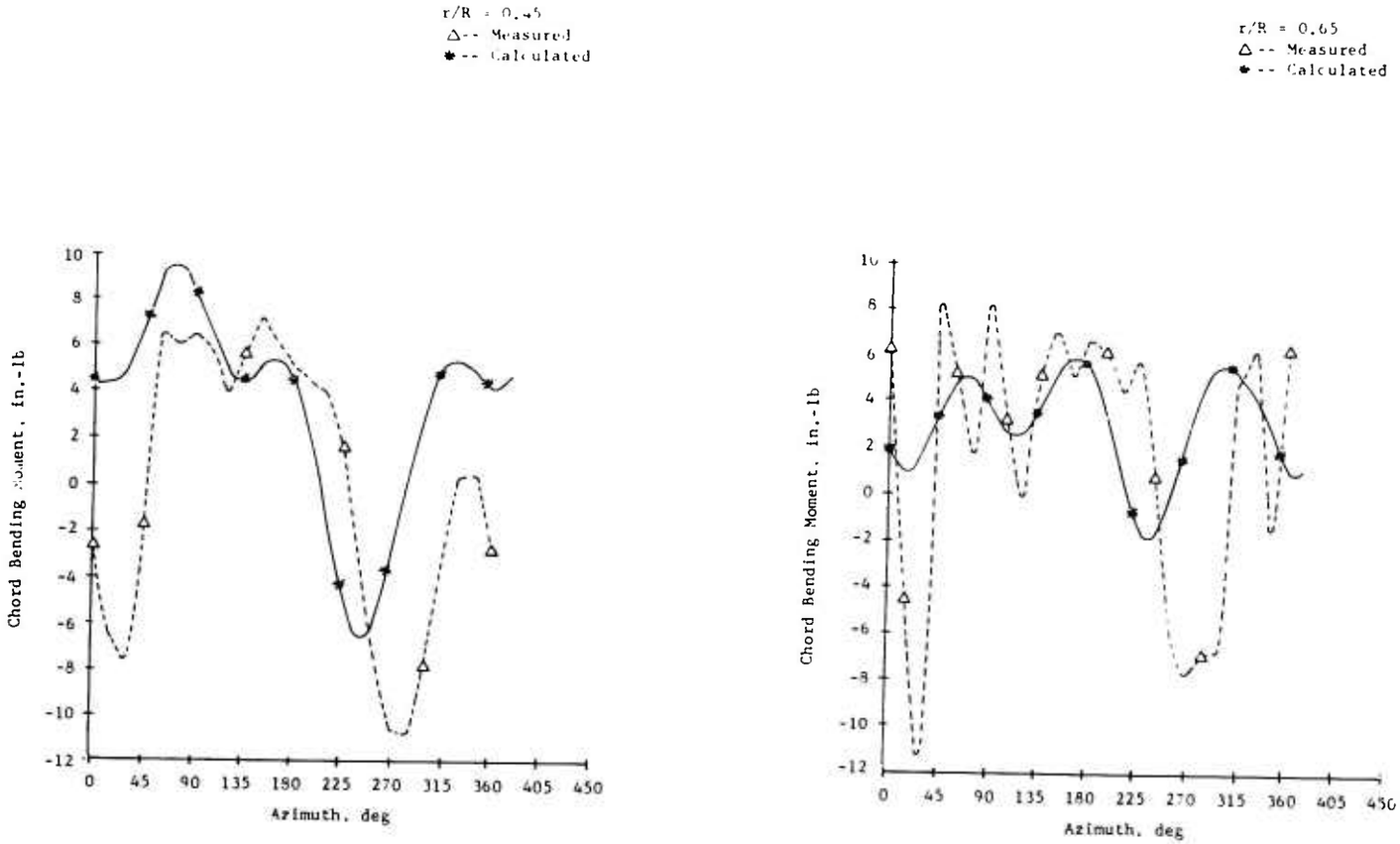

Figure 68. Continued.

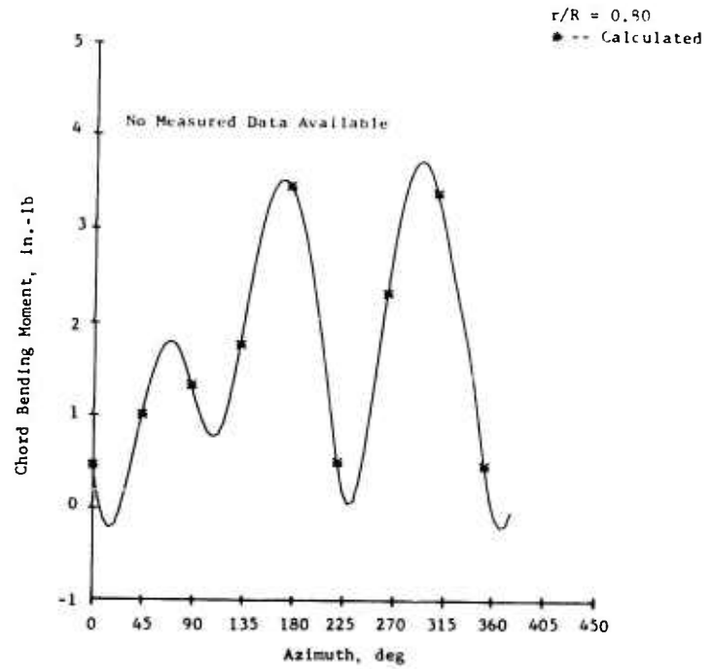

Figure 68. Concluded.

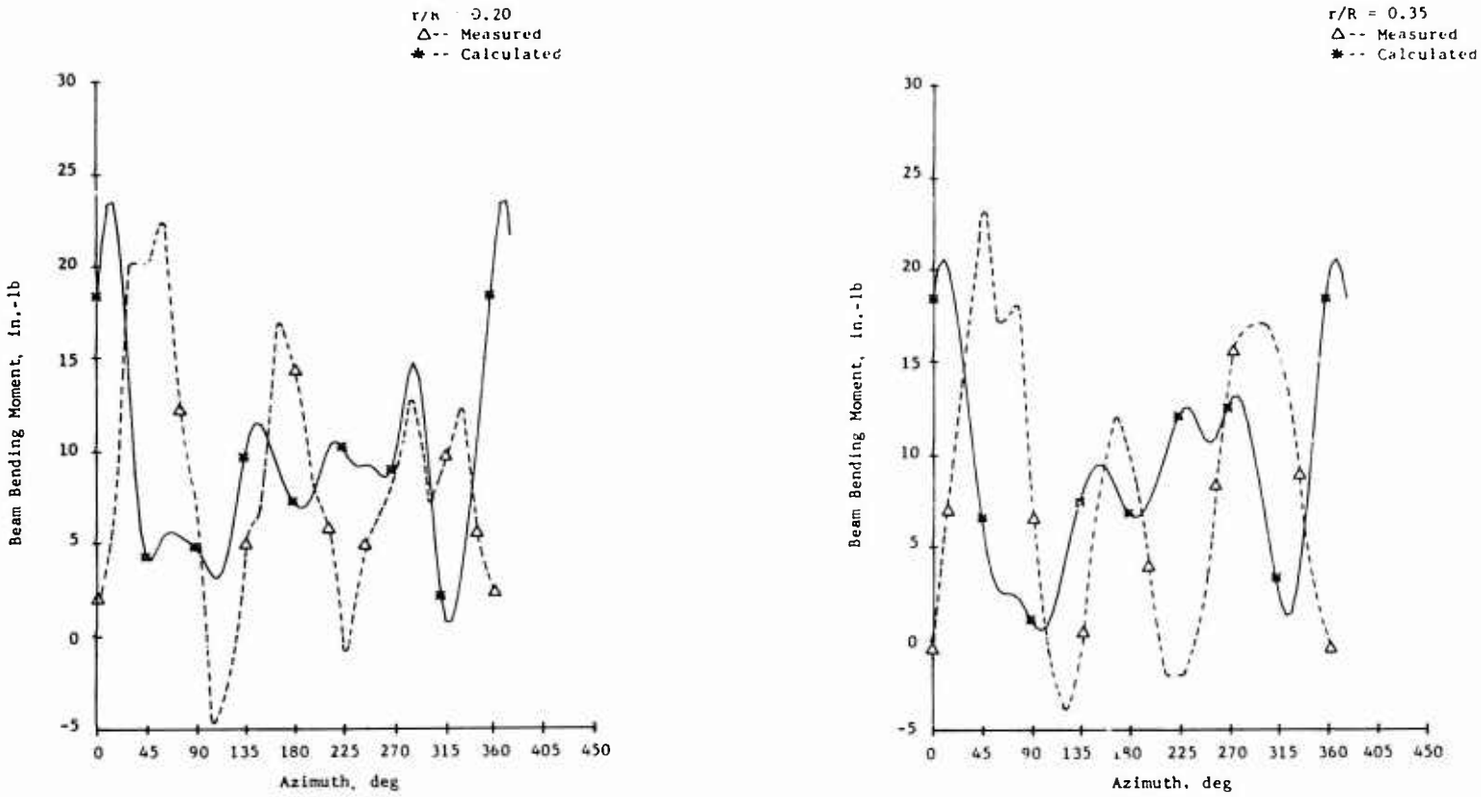

Figure 69. Measured and Calculated Beam Bending Moment Time Histories, Aluminum Blade, 0° Twist, $\mu = 0.399$, $M_{1,90} = 0.434$, $\alpha_m = 0.5°$ (Cond. 25).

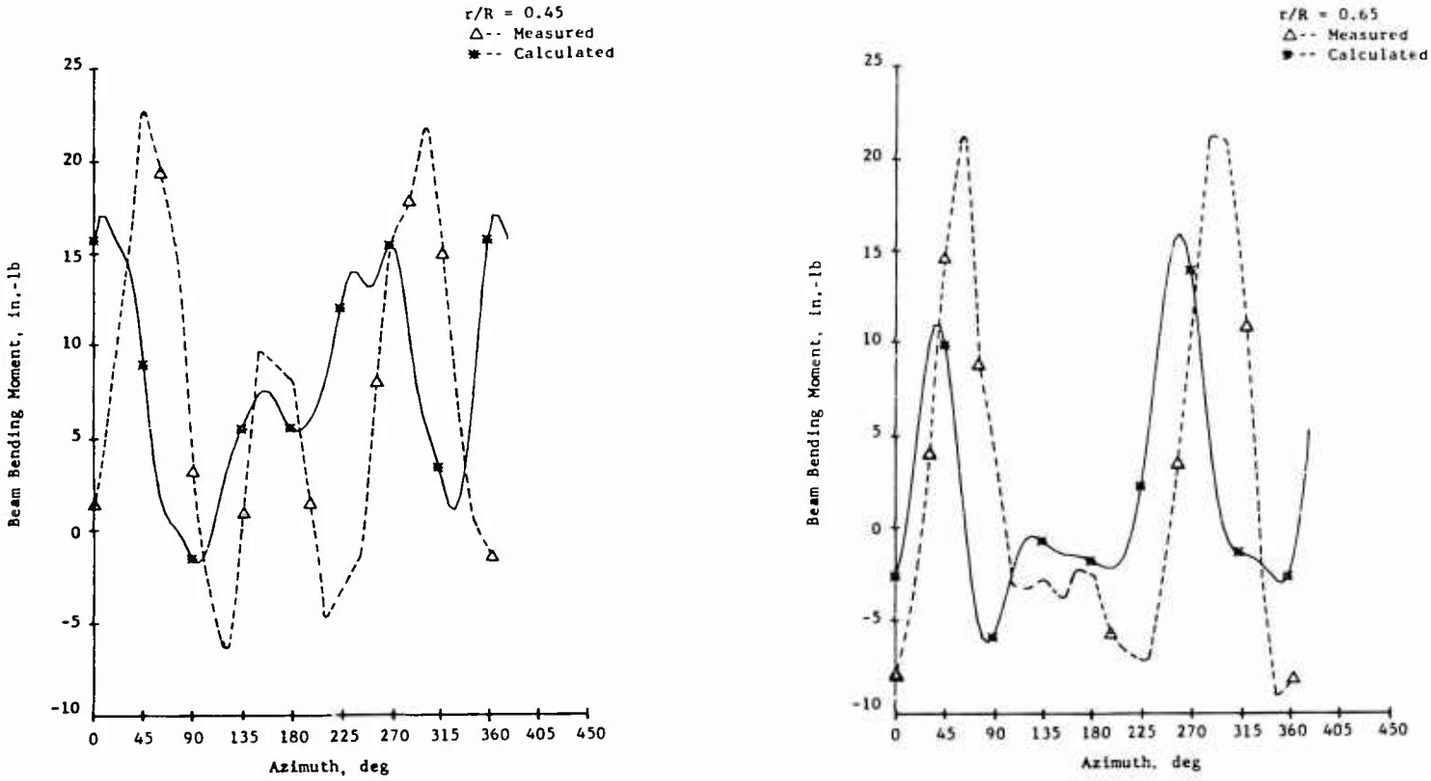

Figure 69. Continued.

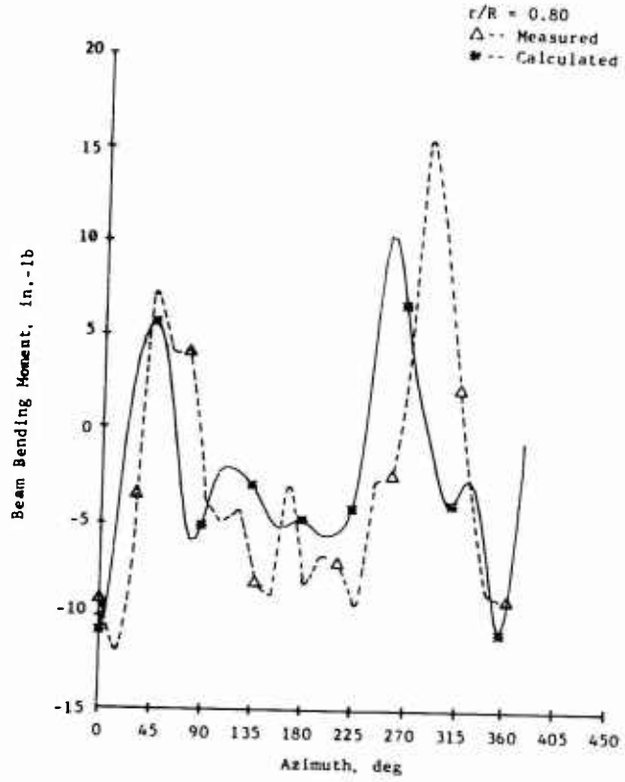

Figure 69. Concluded.

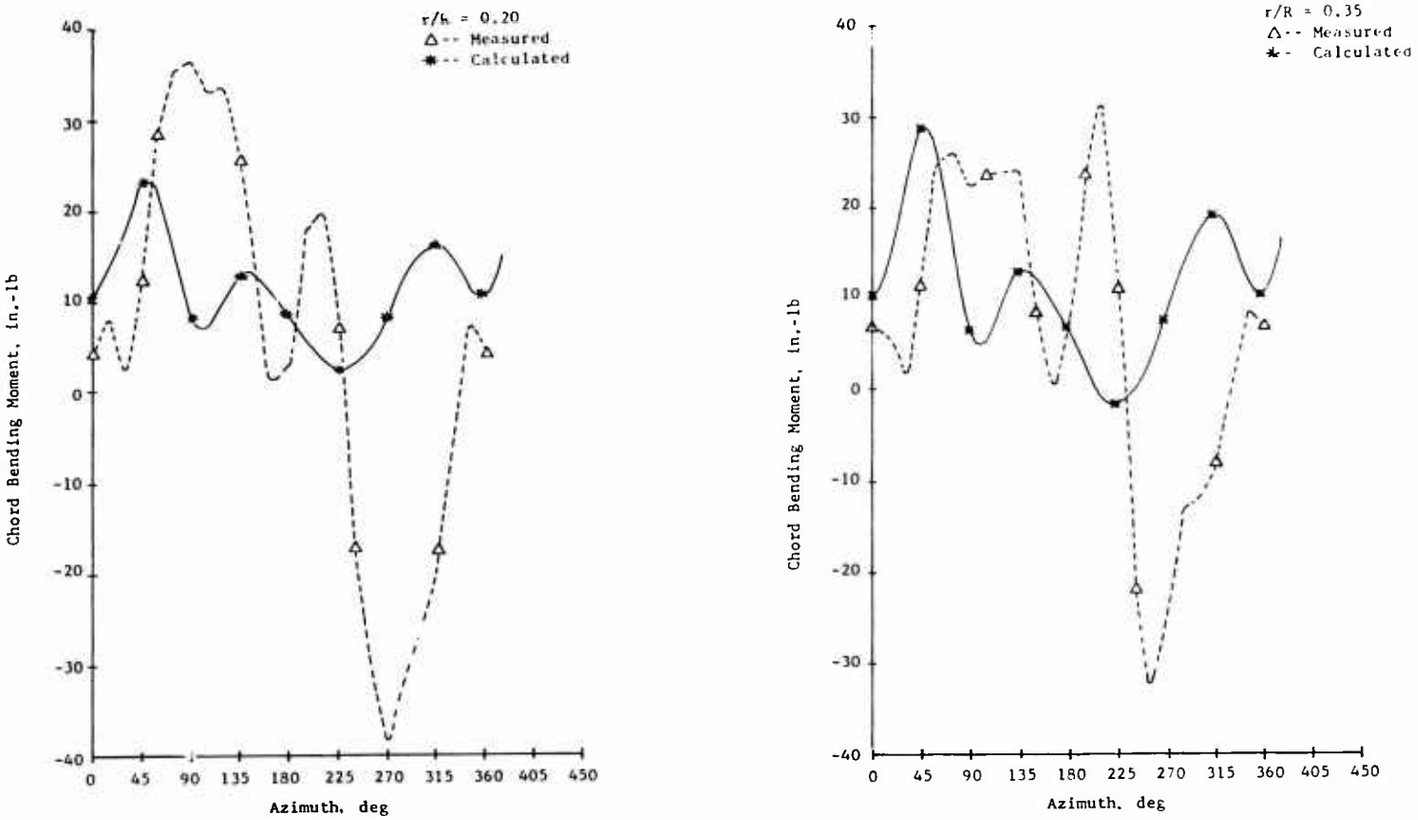

Figure 70. Measured and Calculated Chord Bending Moment Time Histories, Aluminum Blade, 0° Twist, $\mu = 0.399$, $M_{1,90} = 0.434$, $\alpha_m = 0.5°$ (Cond. 25).

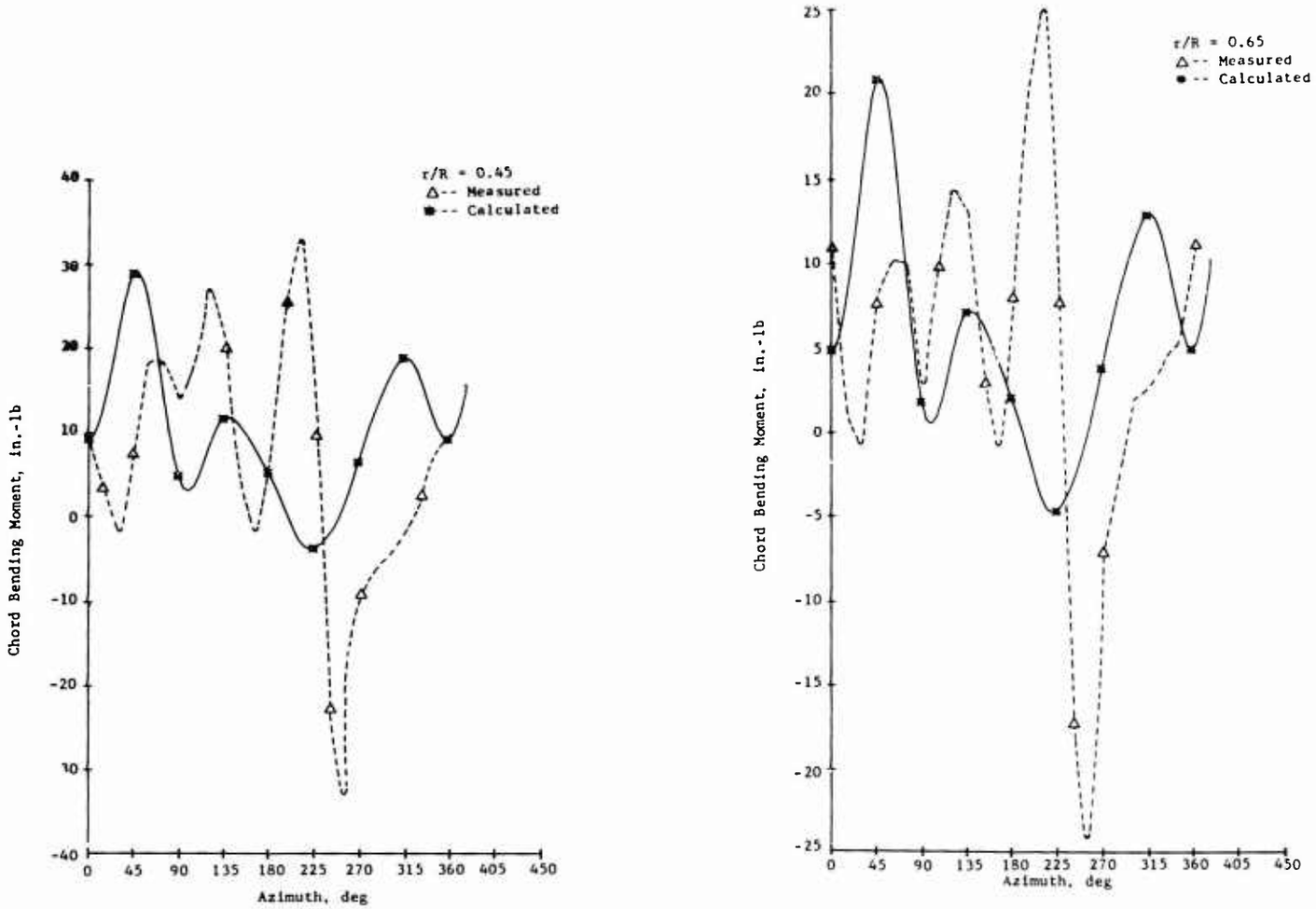

Figure 70. Continued.

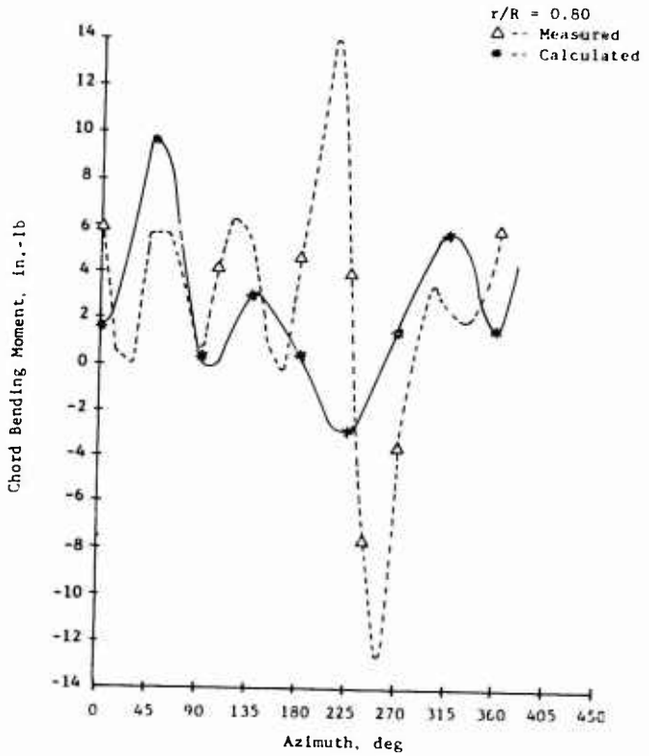

Figure 70. Concluded.

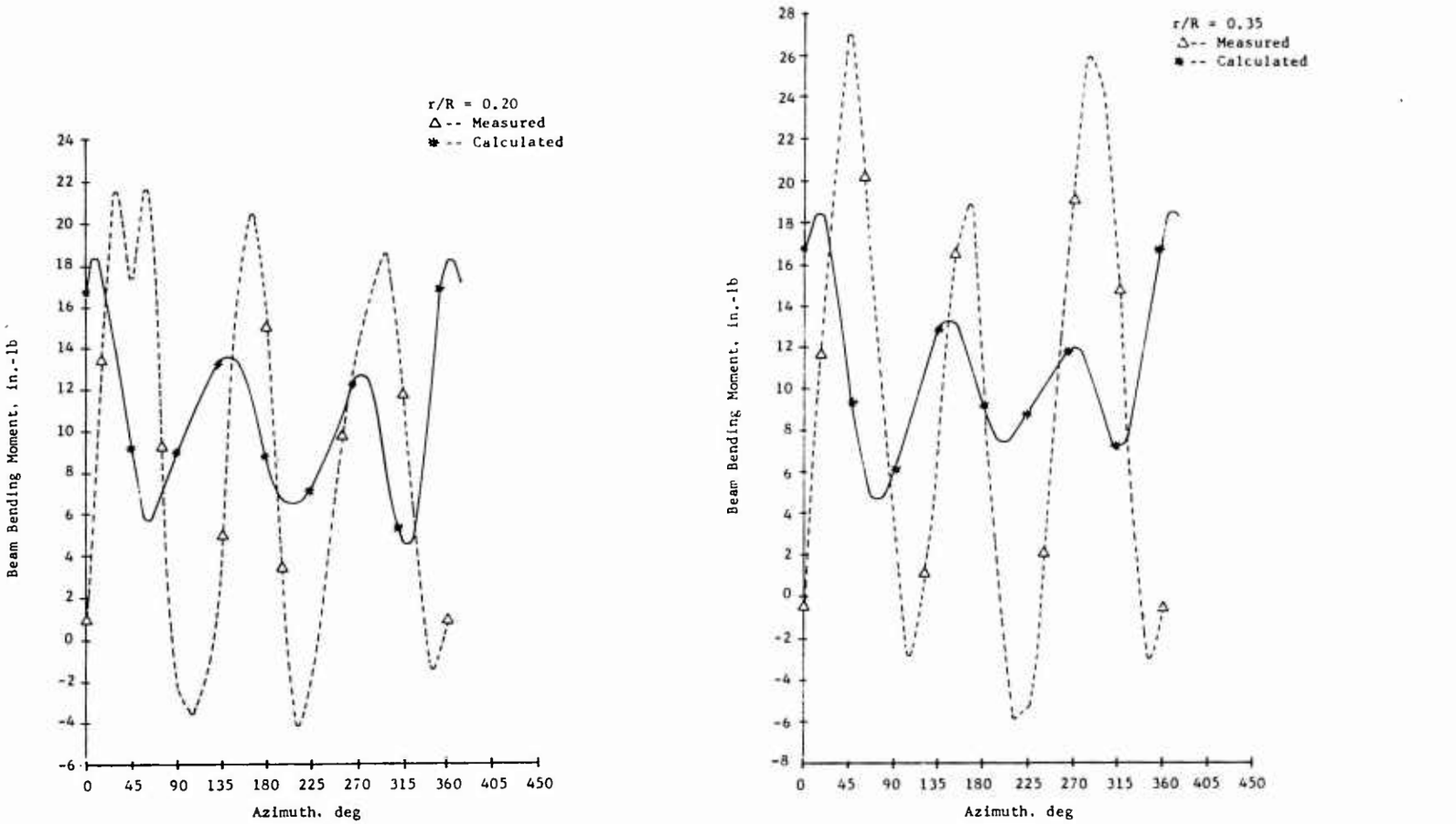

Figure 71. Measured and Calculated Beam Bending Moment Time Histories, Aluminum Blade, 0° Twist, $\mu = 0.502$, $M_{1,90} = 0.467$, $\alpha_m = 5°$ (Cond. 44).

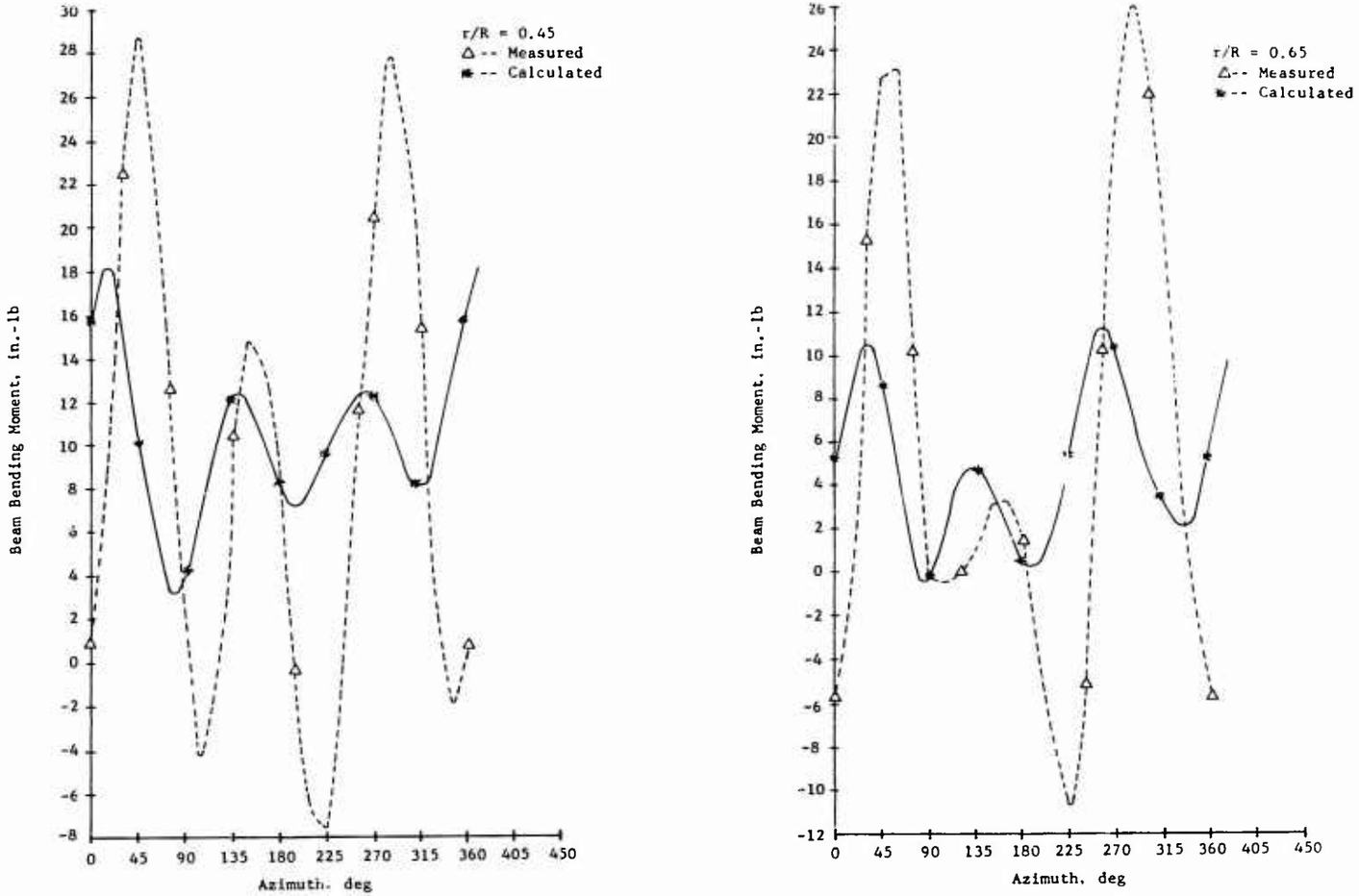

Figure 71. Continued.

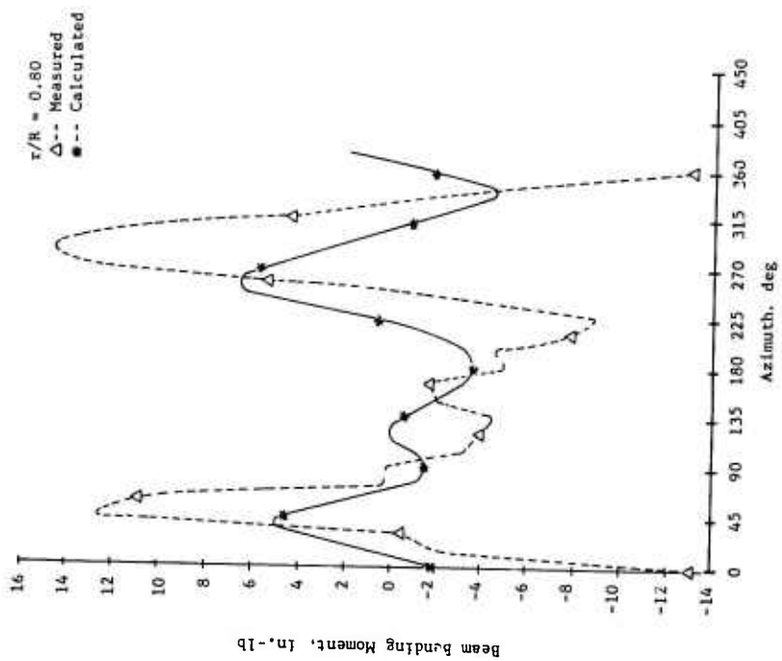

Figure 71. Concluded.

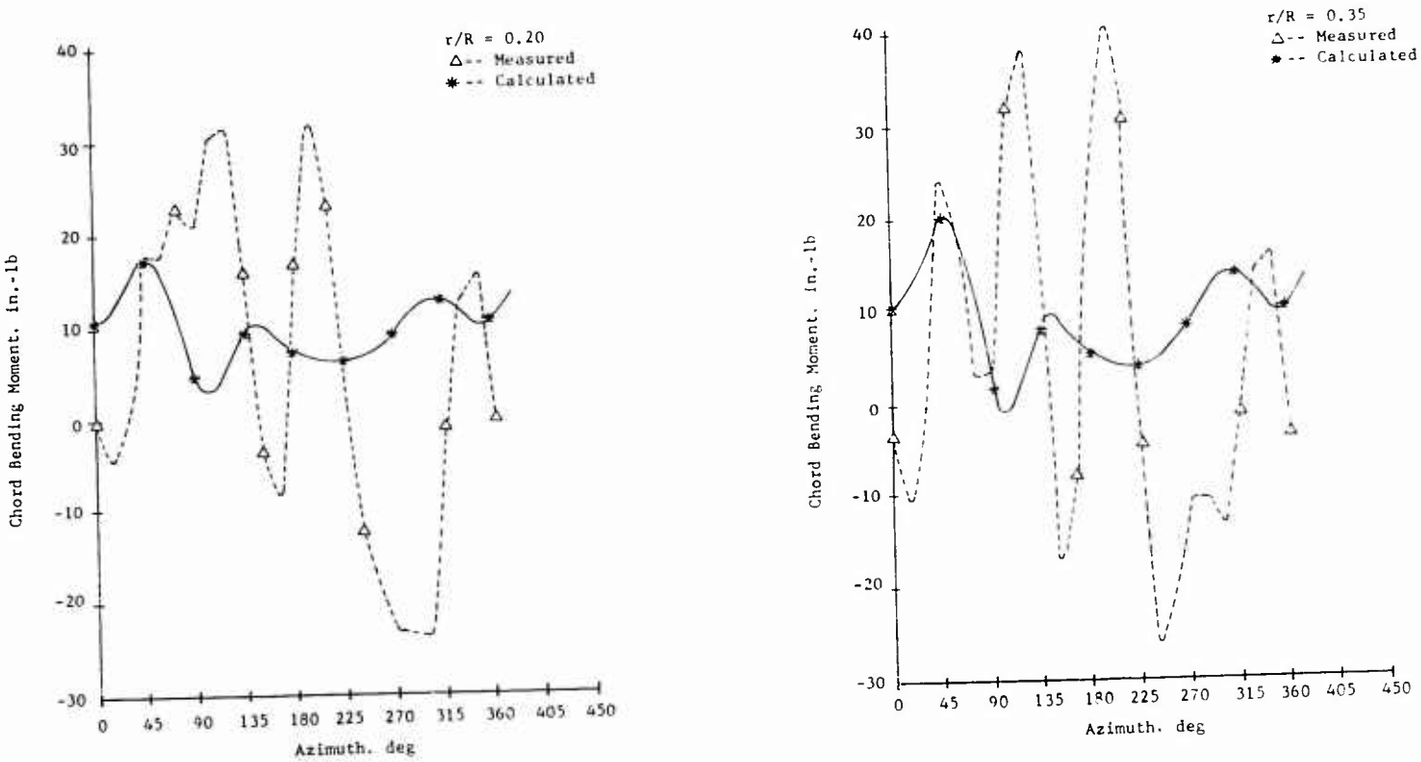

Figure 72. Measured and Calculated Chord Bending Moment Time Histories, Aluminum Blade, 0° Twist, $\mu = 0.502$, $M_{1,90} = 0.467$, $\alpha_m = 5^{\circ}$ (Cond. 44).

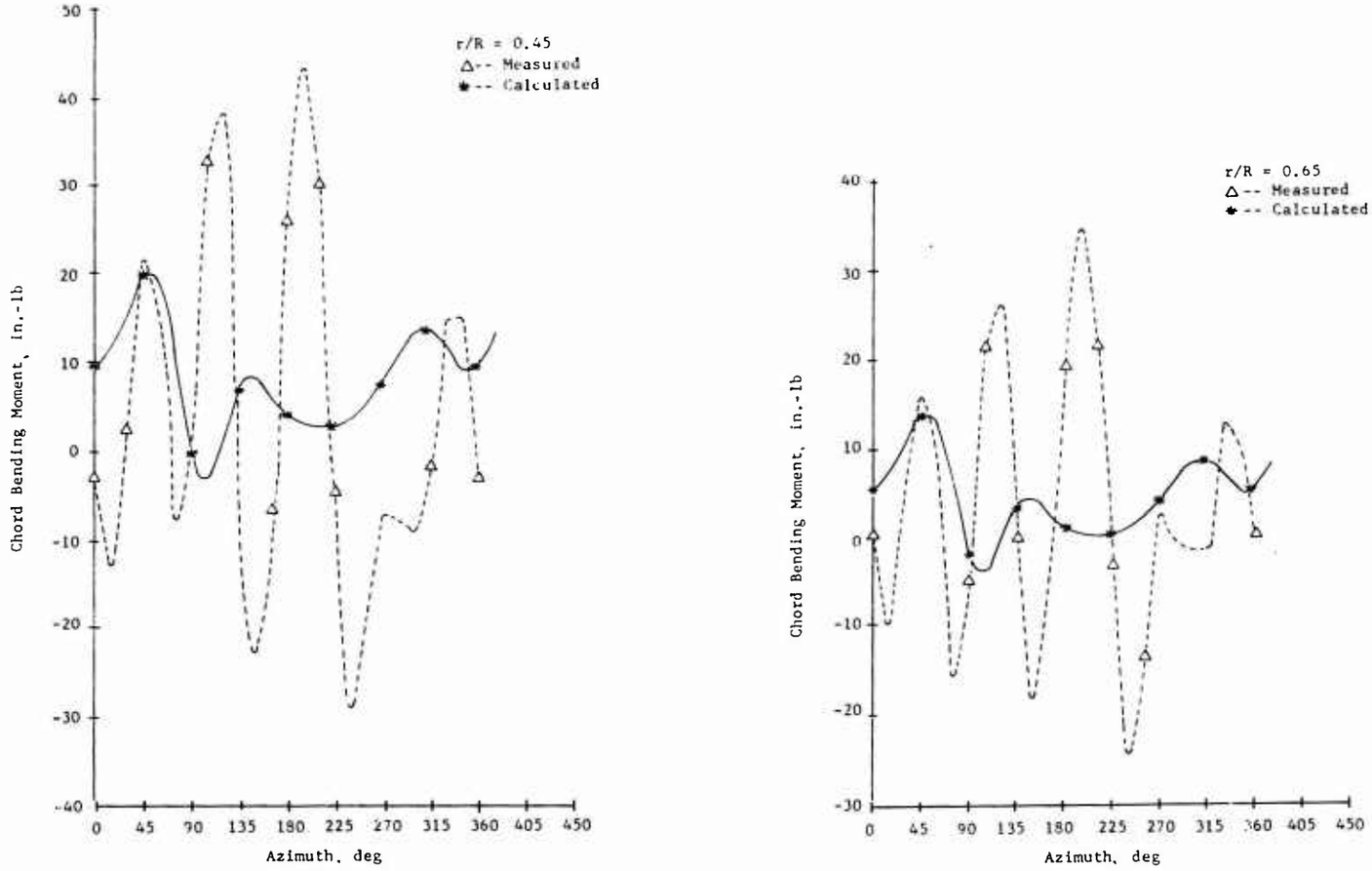

Figure 72. Continued.

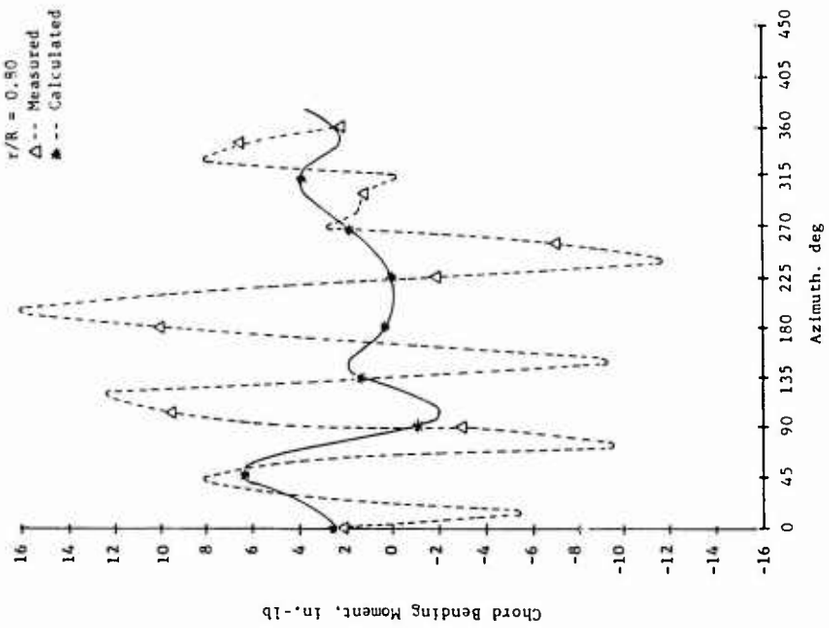

Figure 72. Concluded.

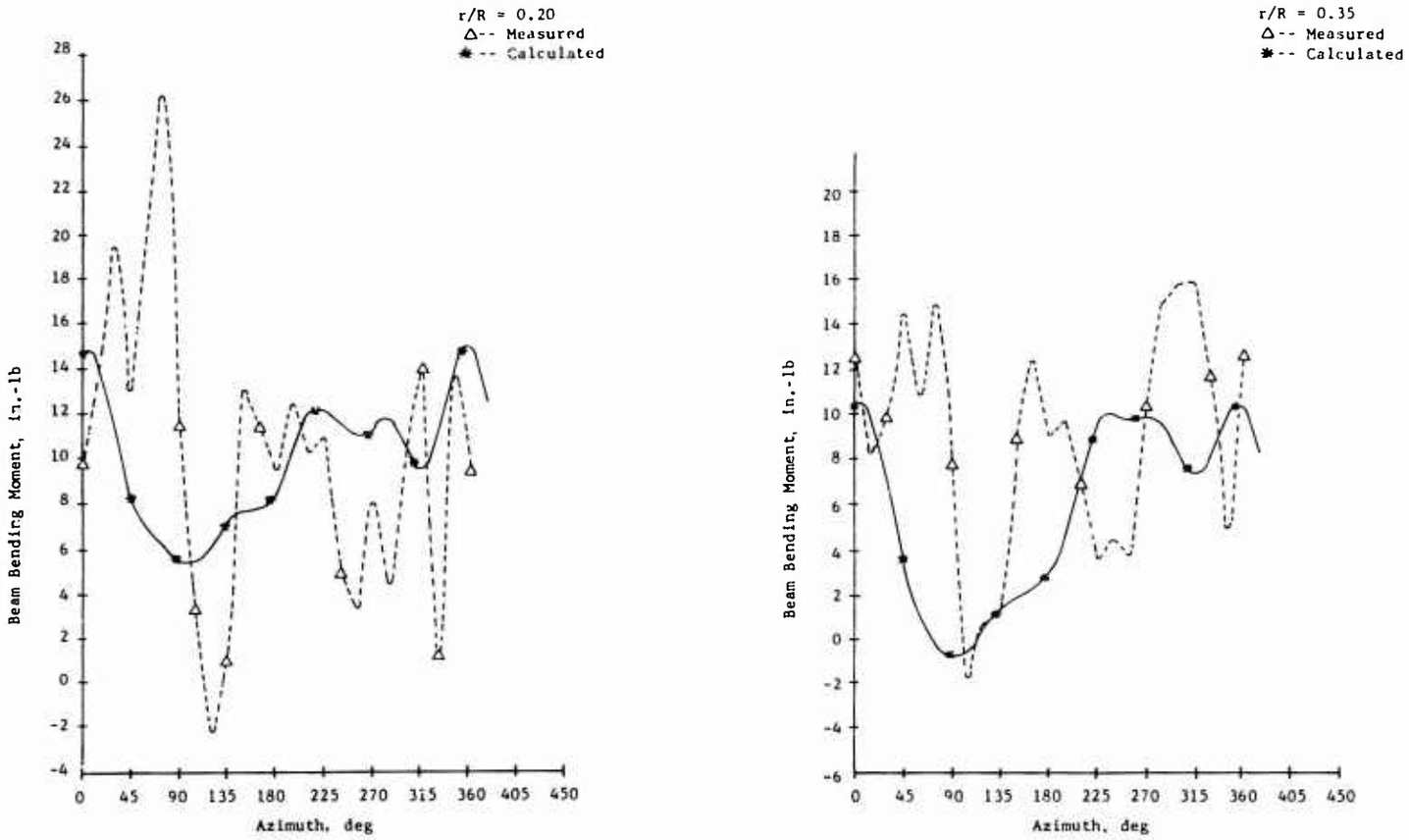

Figure 73. Measured and Calculated Beam Bending Moment Time Histories, Aluminum Blade, 0° Twist, $\mu = 0.299$, $M_{1,90} = 0.408$, $\alpha_m = 0°$ (Cond. 68).

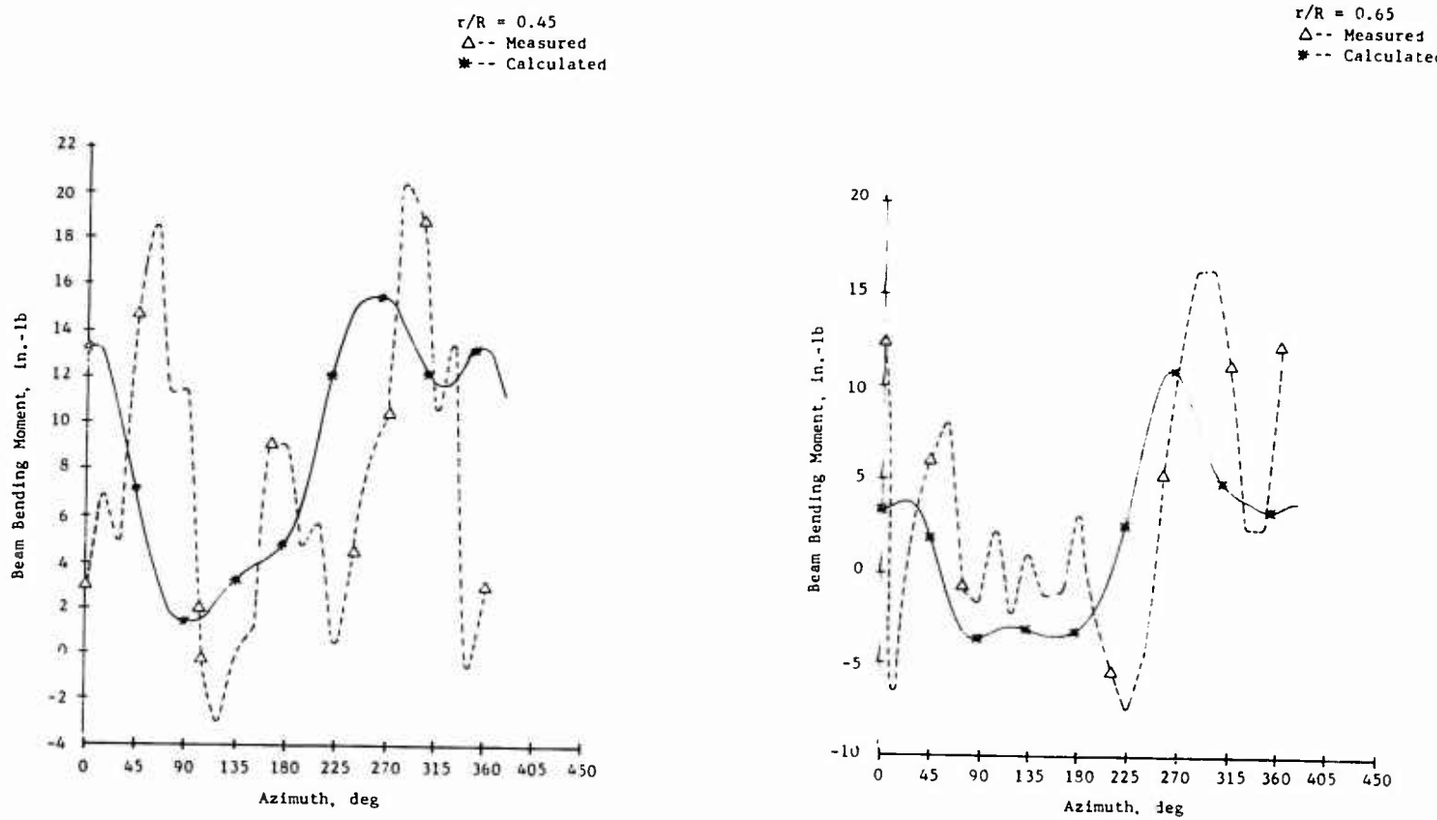

Figure 73. Continued.

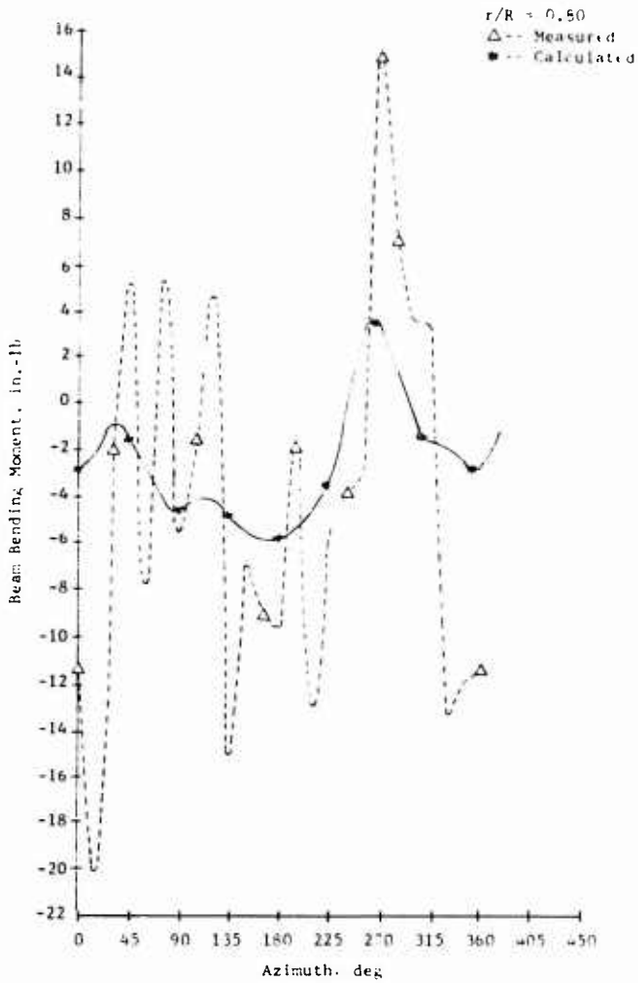

Figure 73. Concluded.

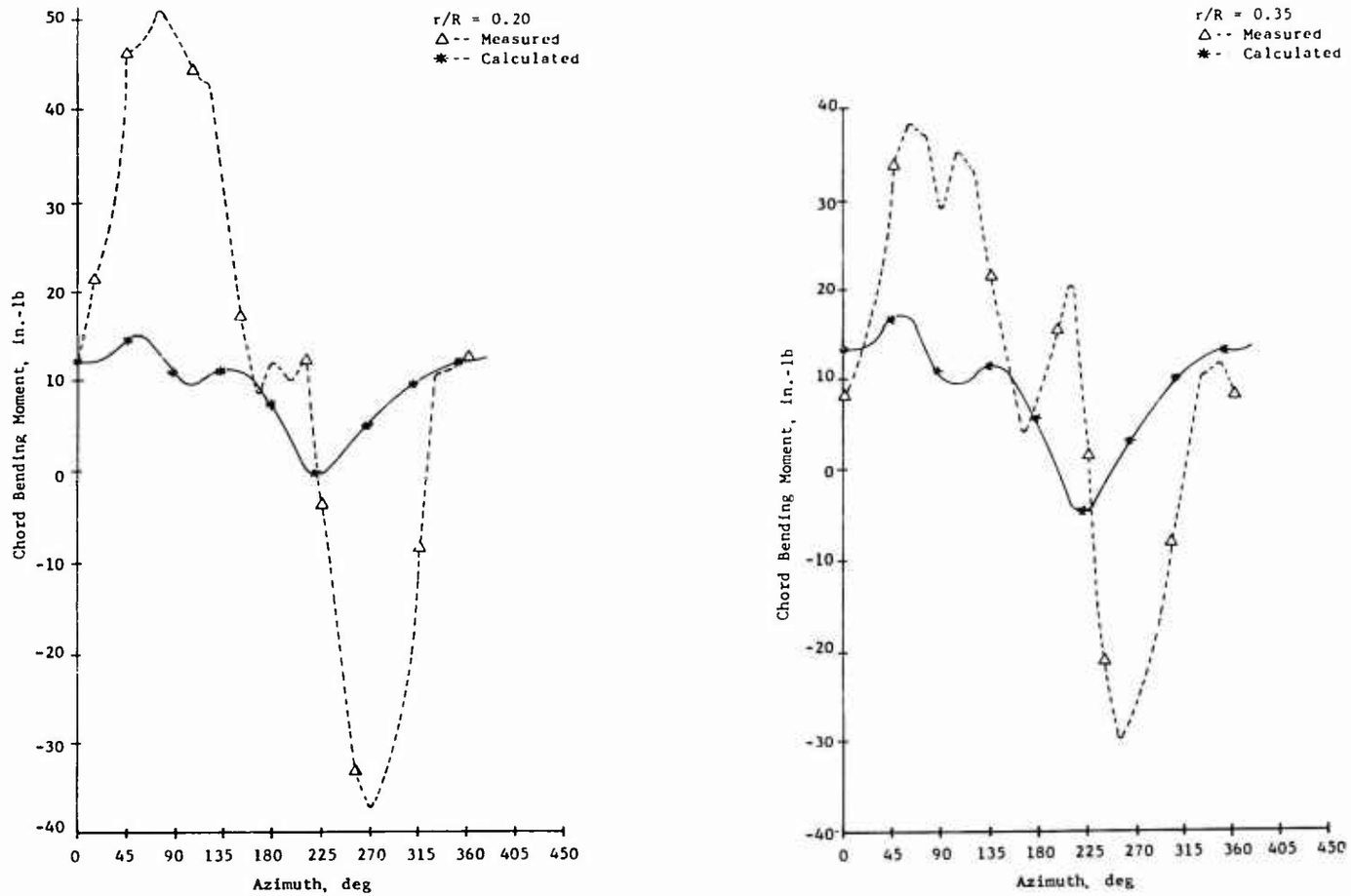

Figure 74. Measured and Calculated Chord Bending Moment Time Histories, Aluminum Blade, 0° Twist, $\mu = 0.299$, $M_{1,90} = 0.408$, $\alpha_m = 0°$ (Cond. 68).

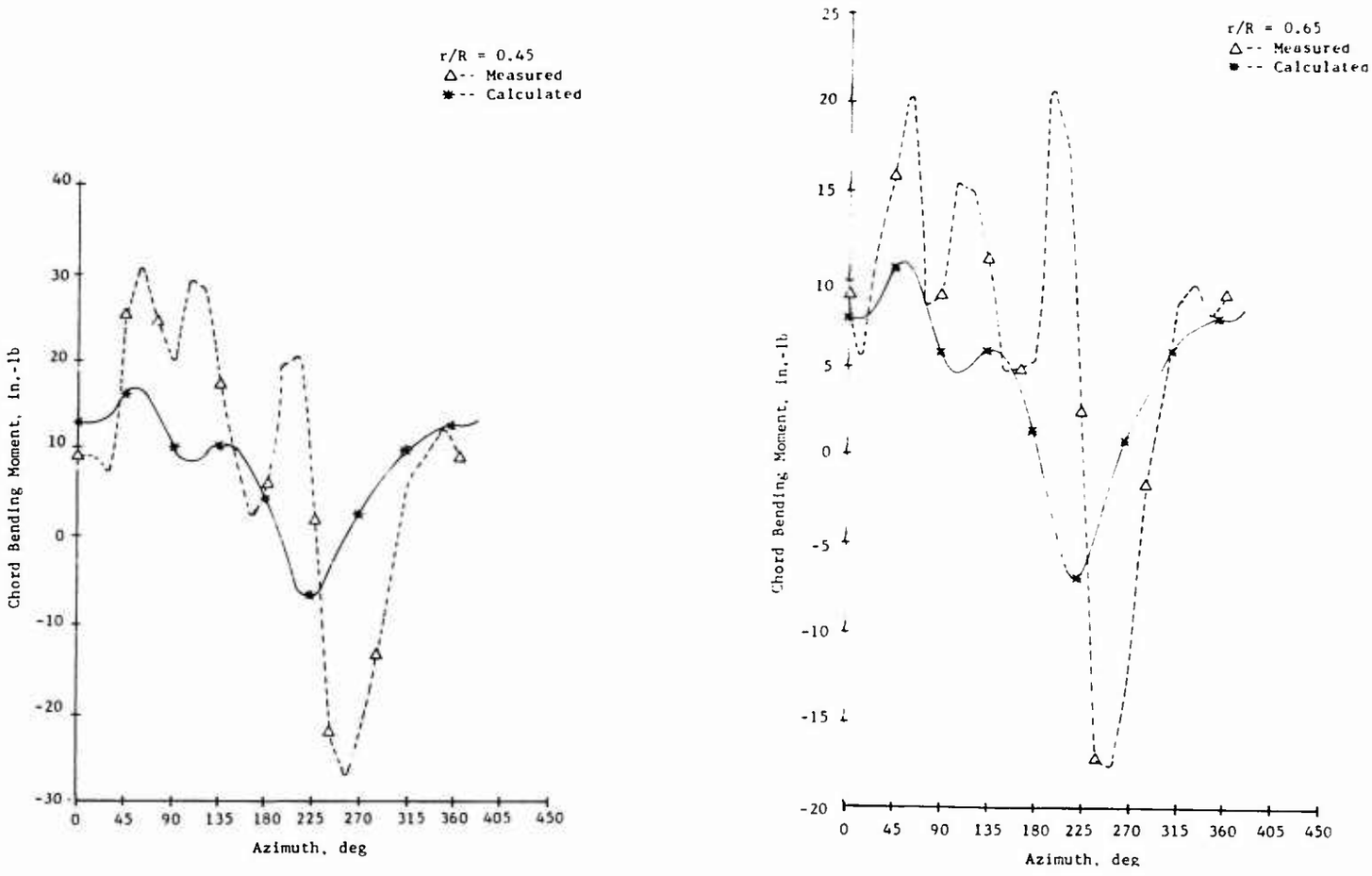

Figure 74. Continued.

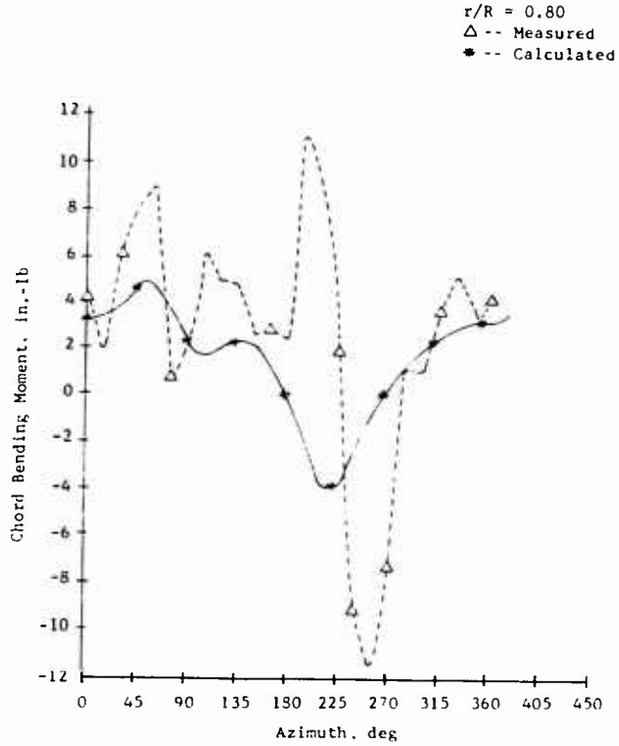

Figure 74. Concluded.

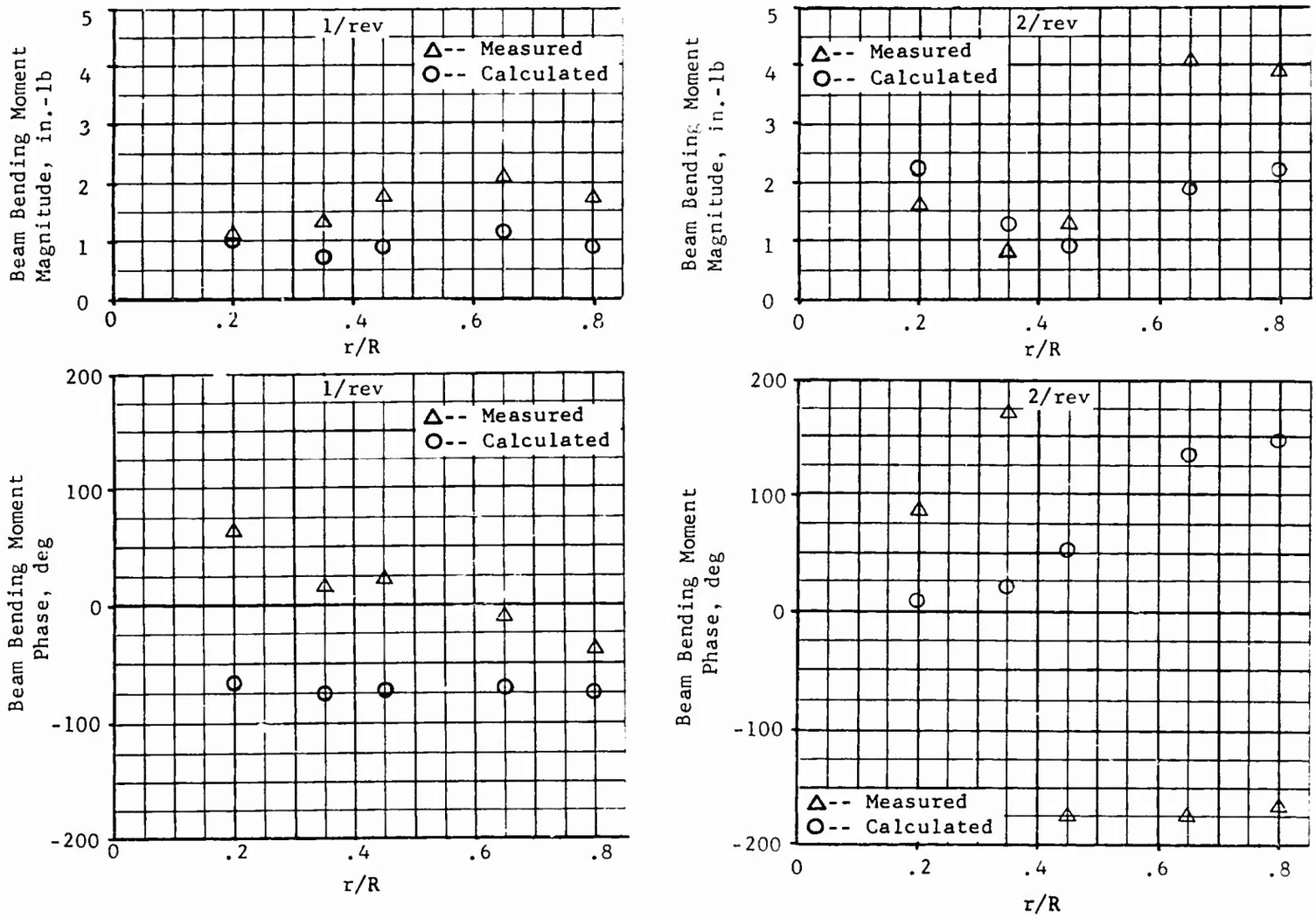

Figure 75. Measured and Calculated Beam Bending Moment Harmonics, Fiberglass Blade, 0° Twist, $\mu = 0.399$, $M_{1,90} = 0.434$, $\alpha_m = 0.5°$ (Cond. 25).

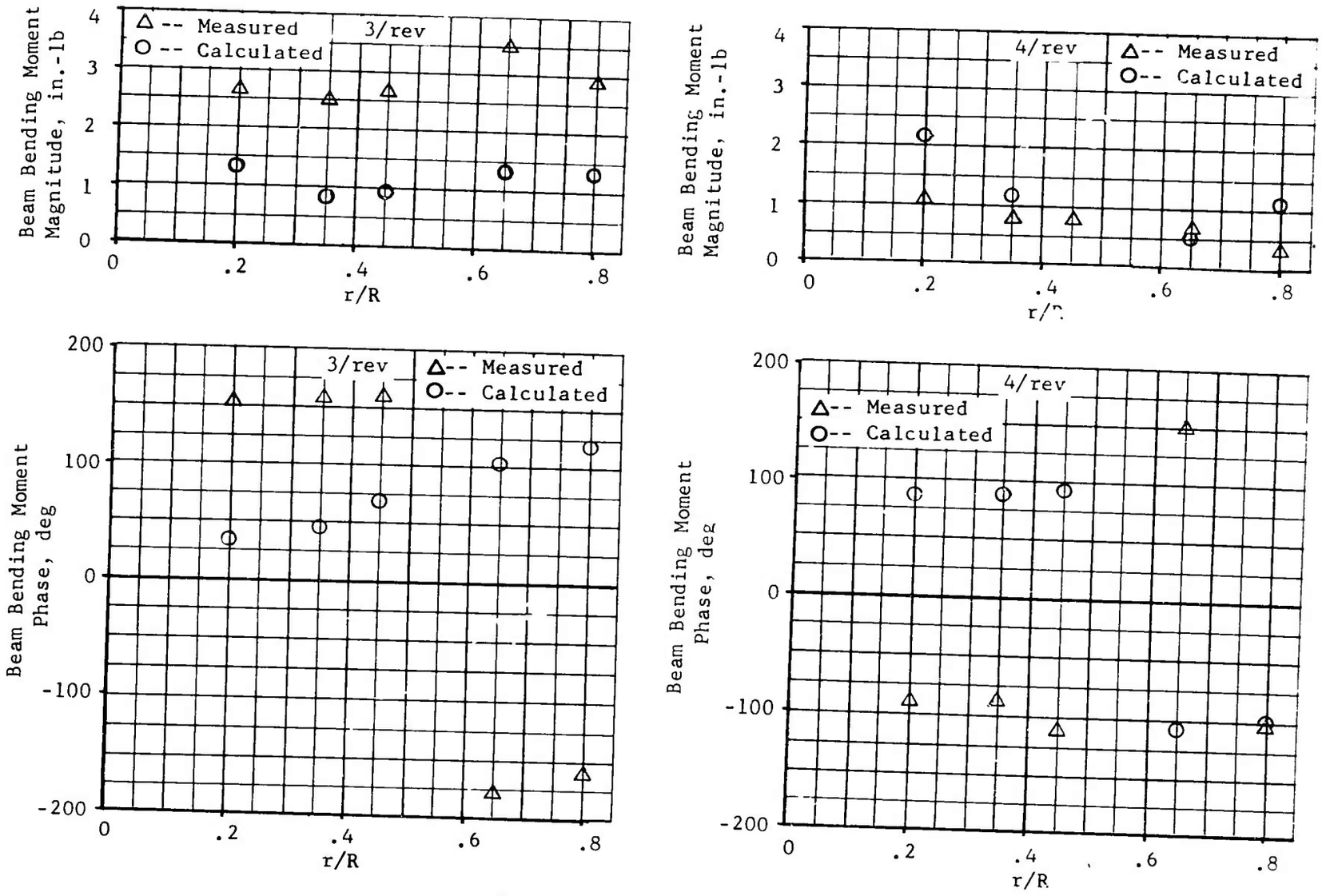

Figure 75. Concluded.

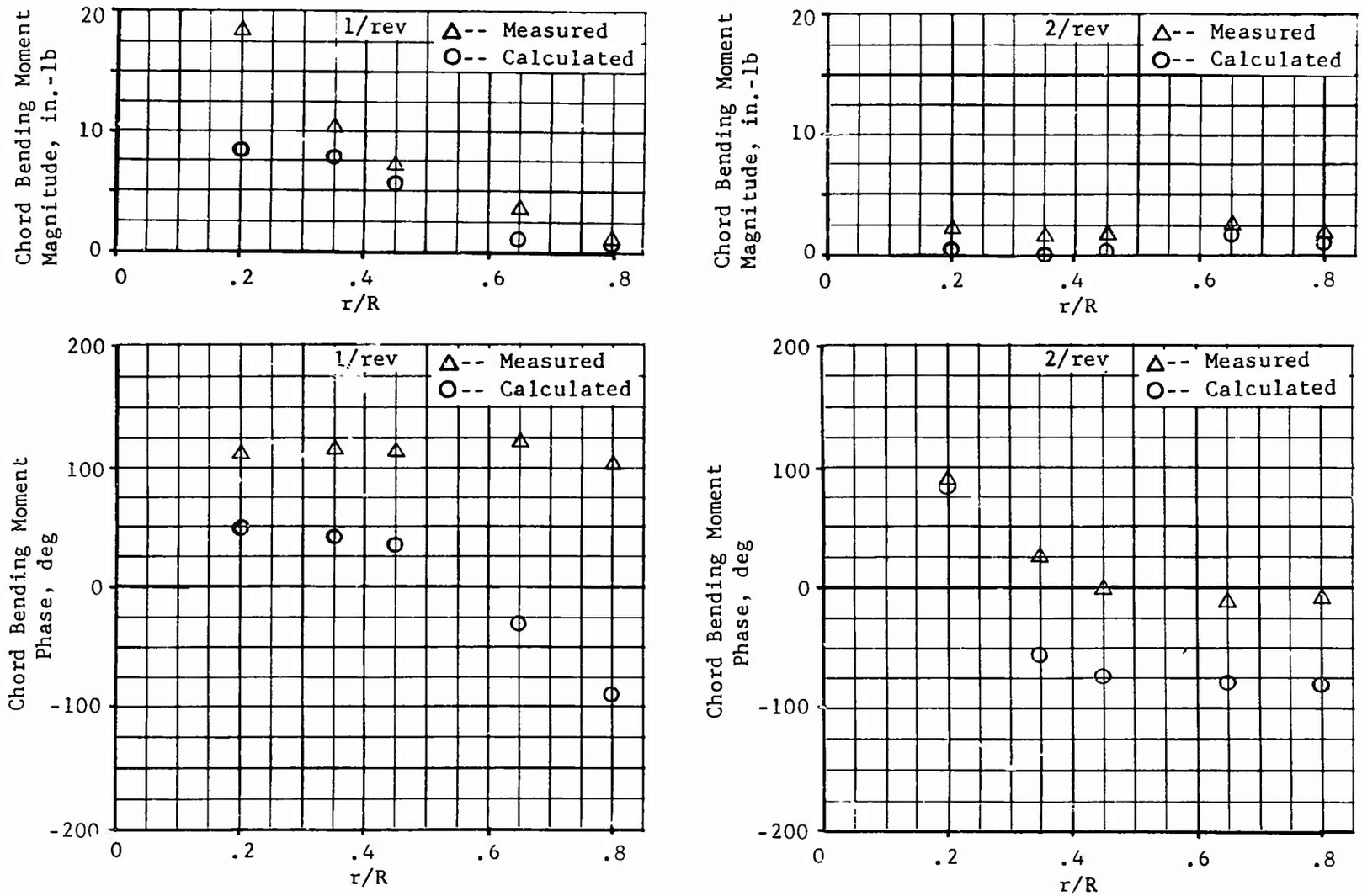

Figure 76. Measured and Calculated Chord Bending Moment Harmonics, Fiberglass Blade, 0° Twist, $\mu = 0.399$, $M_{1,90} = 0.434$, $\alpha_m = 0.5°$ (Cond. 25).

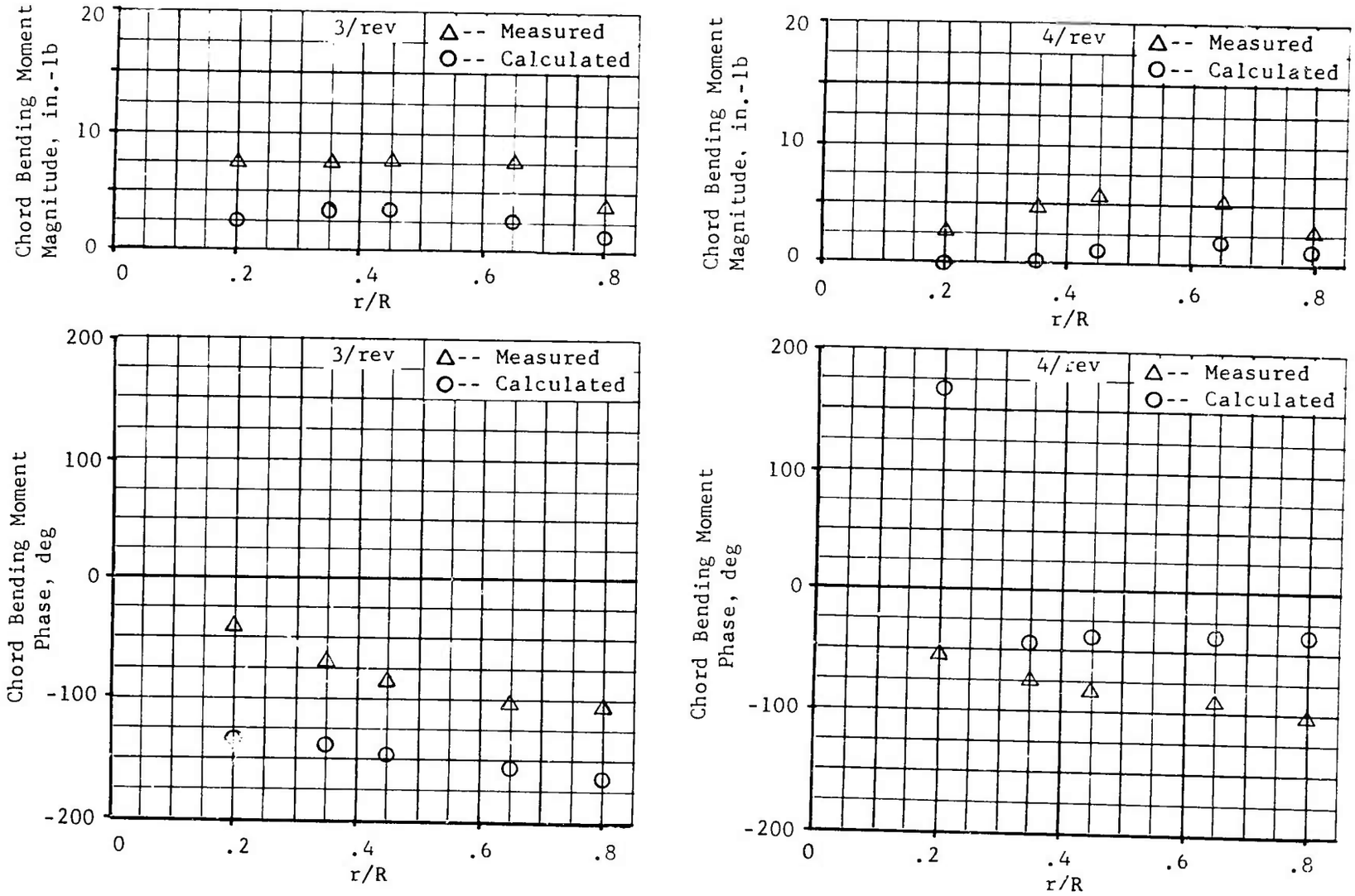

Figure 76. Concluded.

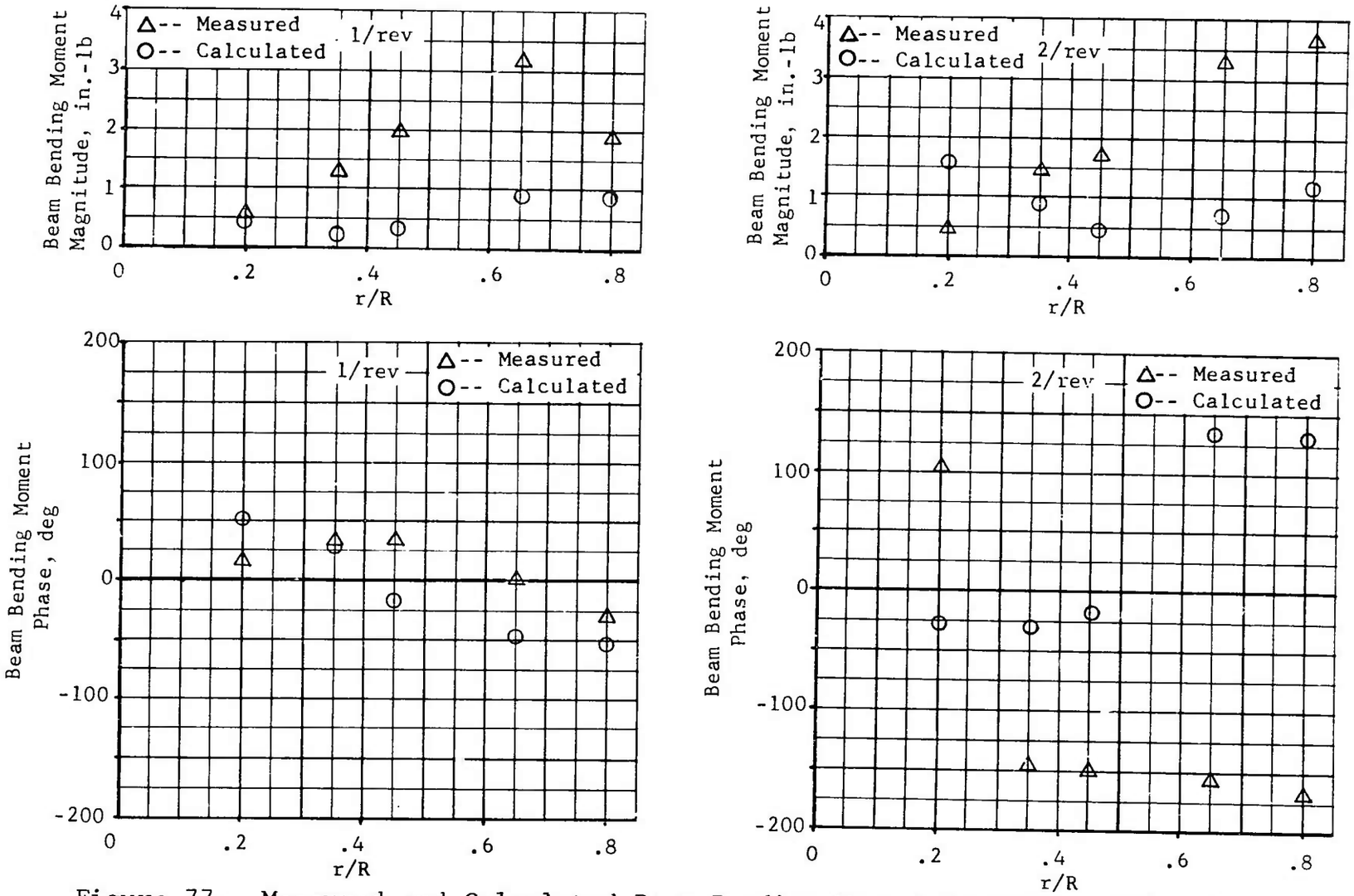

Figure 77. Measured and Calculated Beam Bending Moment Harmonics, Fiberglass Blade, 0° Twist, $\mu = 0.502$, $M_{1,90} = 0.467$, $\alpha_m = 5°$ (Cond. 44).

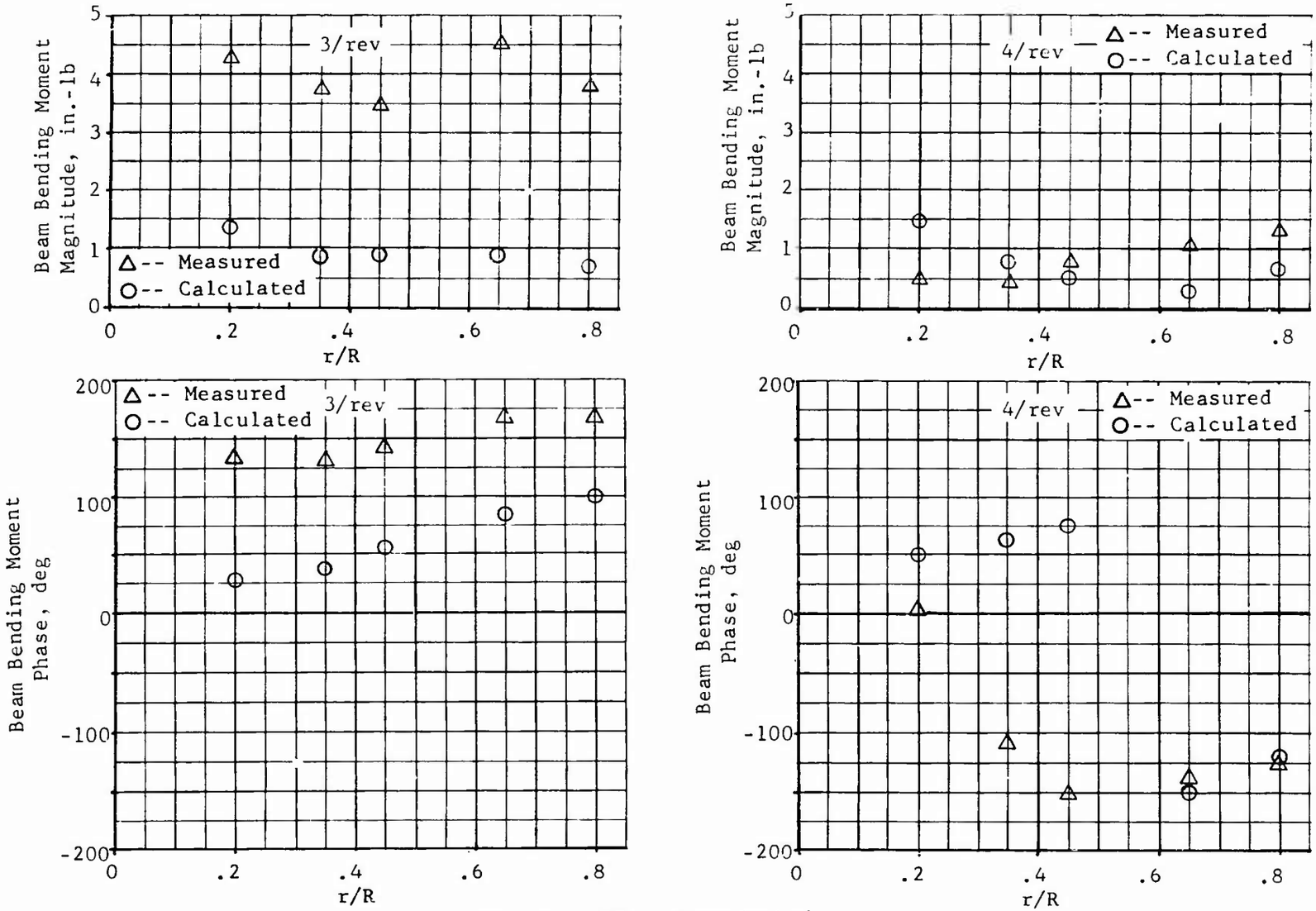

Figure 77. Concluded.

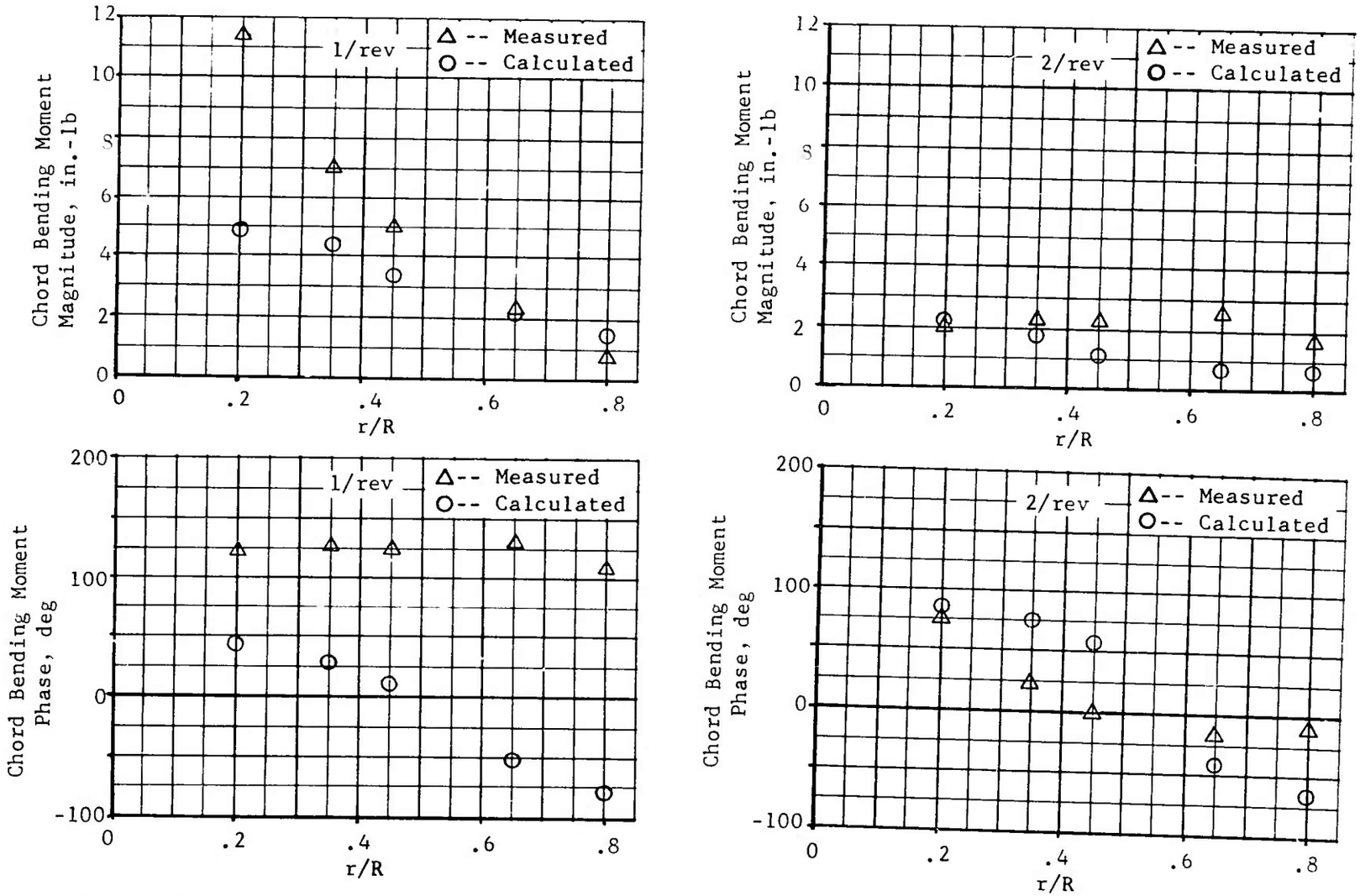

Figure 78. Measured and Calculated Chord Bending Moment Harmonics, Fiberglass Blade, 0° Twist, $\mu = 0.502$, $M_{1,90} = 0.467$, $\alpha_m = 5°$ (Cond. 44).

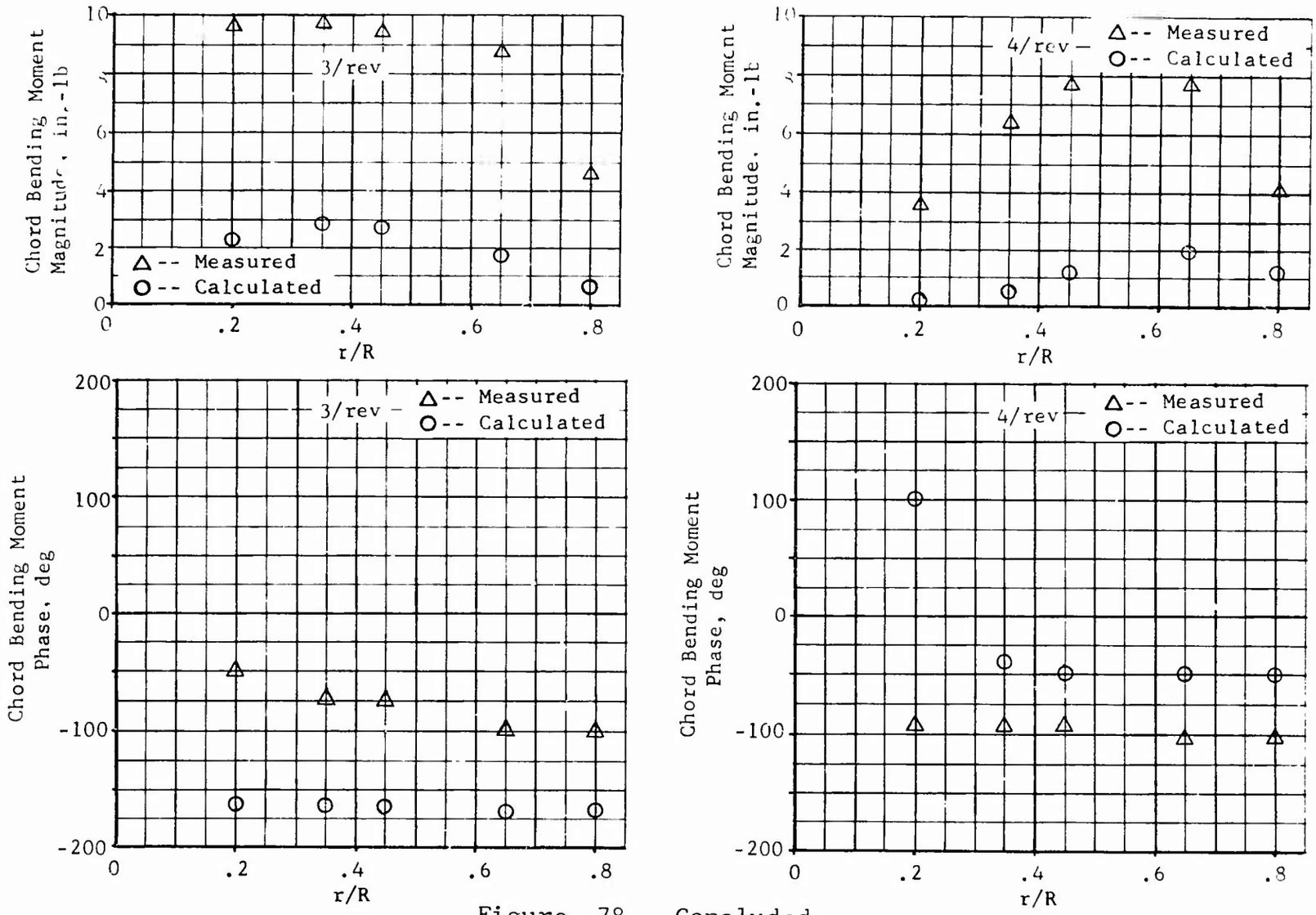

Figure 78. Concluded.

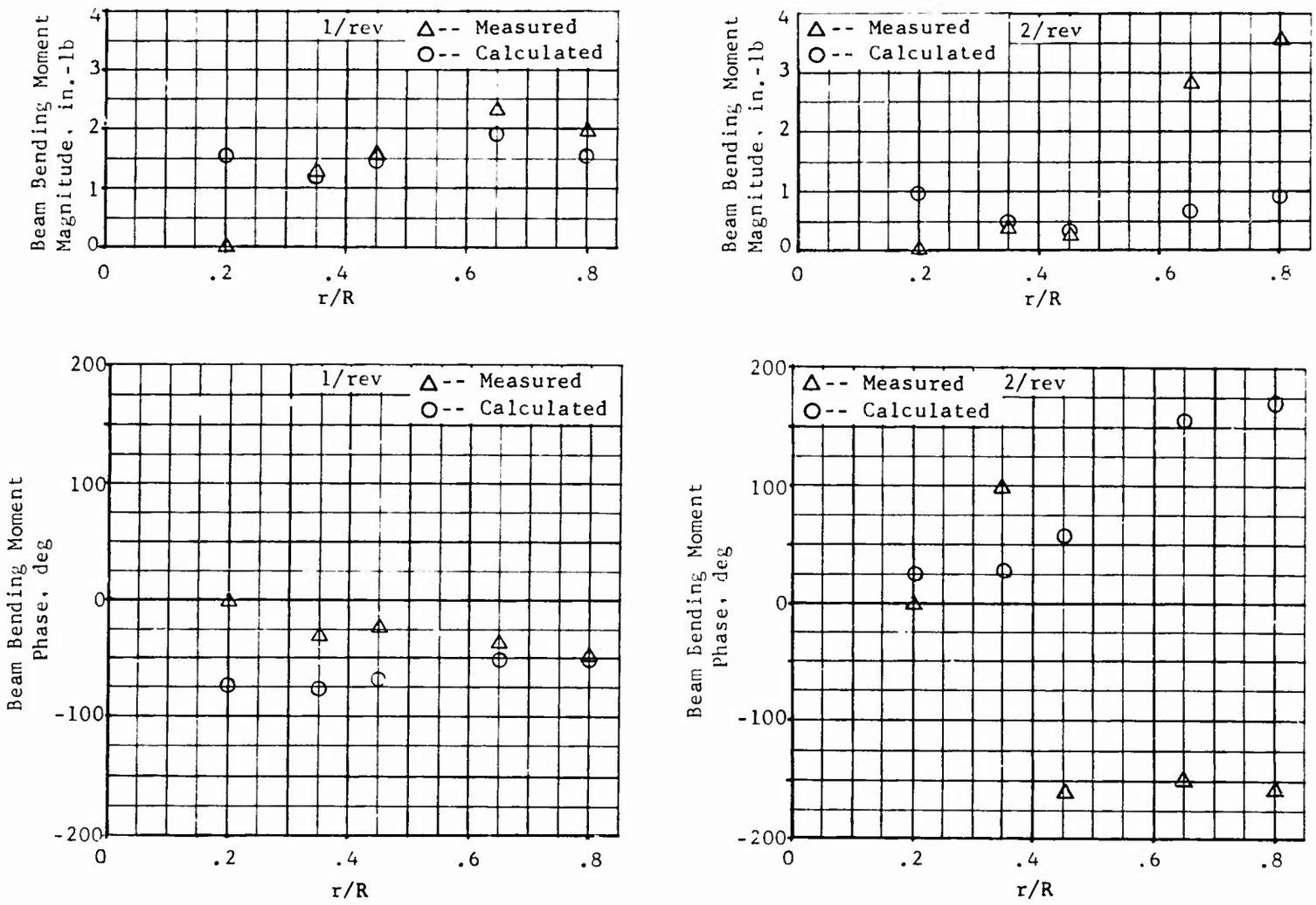

Figure 79. Measured and Calculated Beam Bending Moment Harmonics, Fiberglass Blade, 0° Twist, $\mu = 0.299$, $M_{1,90} = 0.408$, $\alpha_m = 0°$ (Cond. 68).

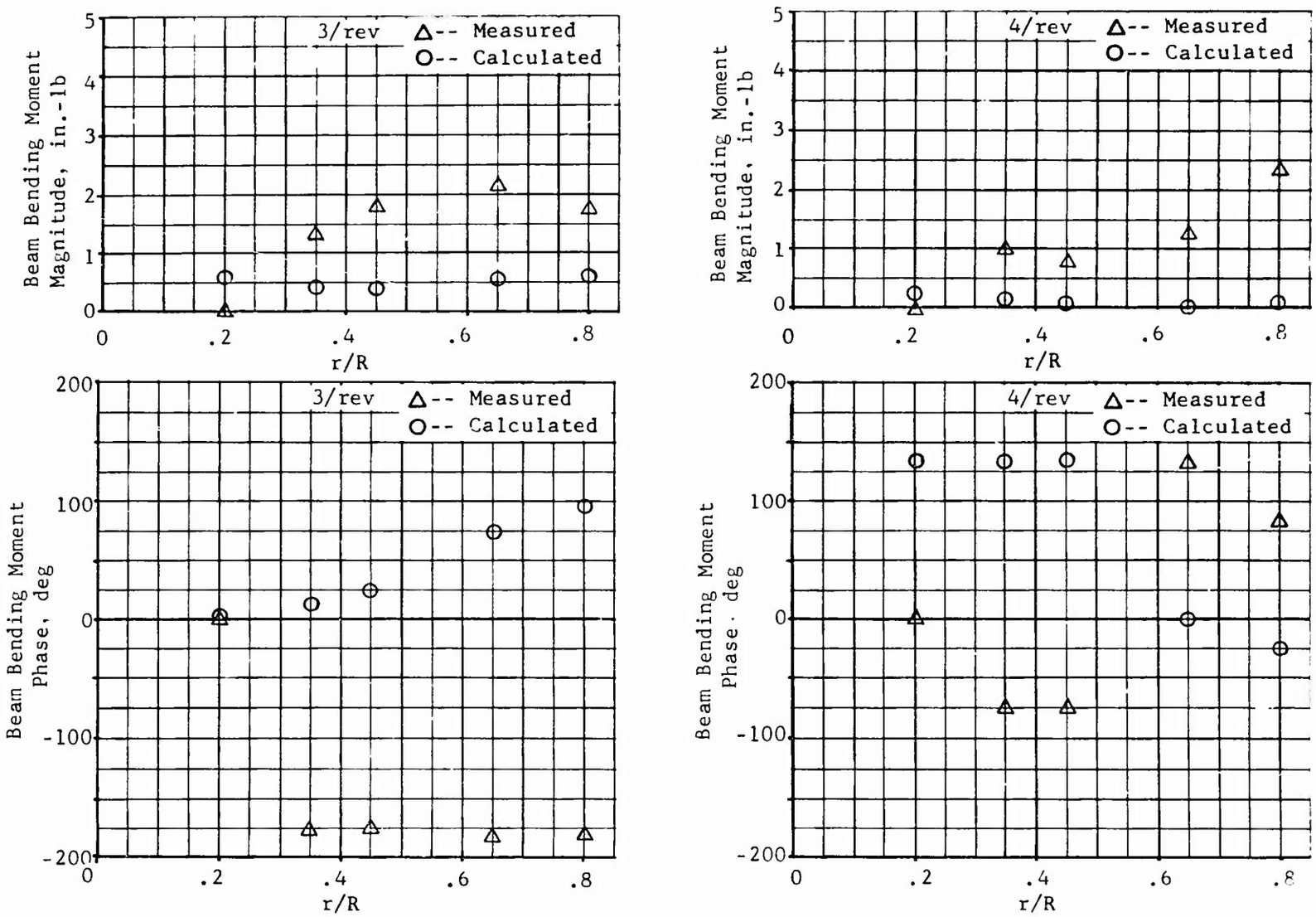

Figure 79. Concluded.

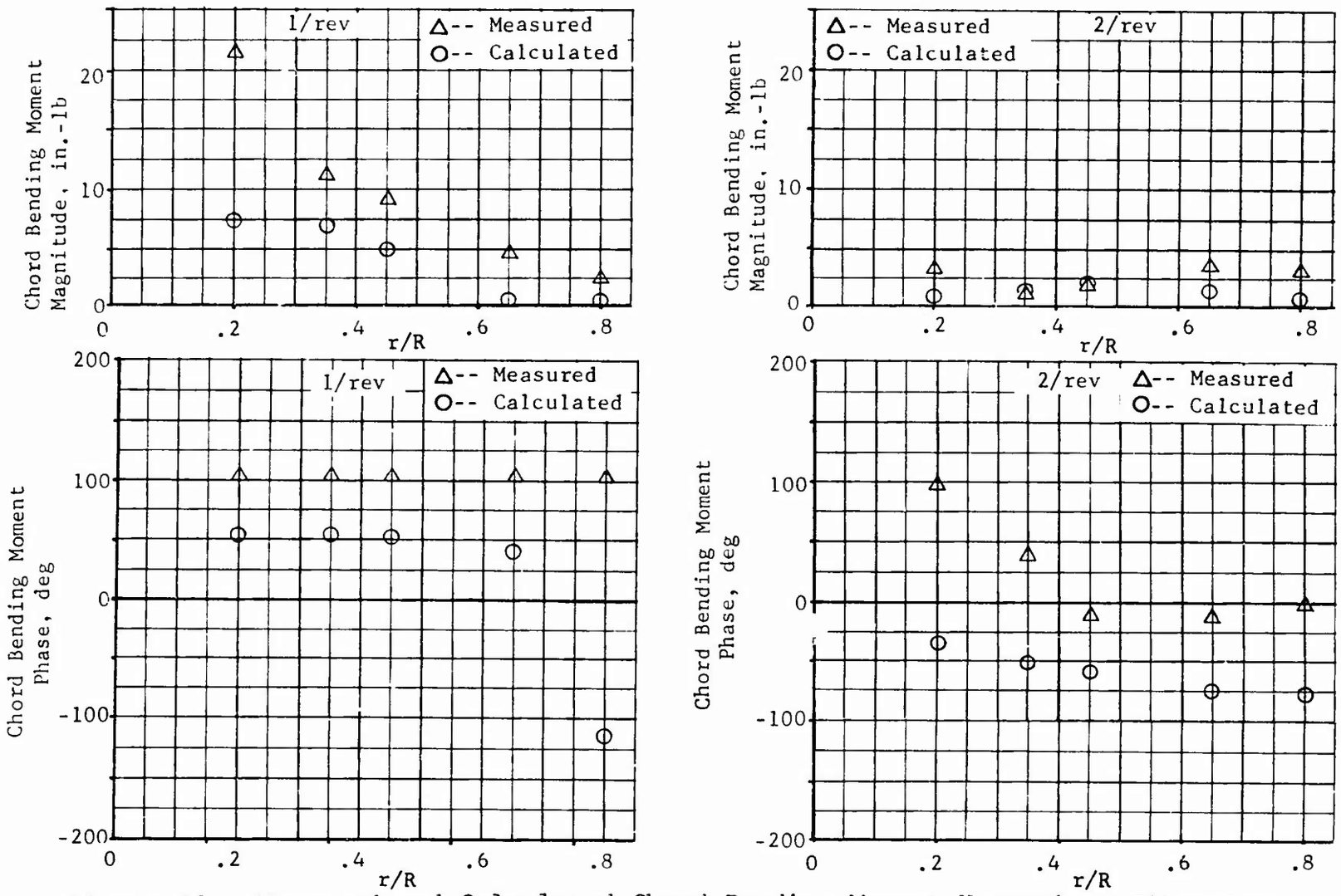

Figure 80. Measured and Calculated Chord Bending Moment Harmonics, Fiberglass Blade, 0° Twist, $\mu = 0.299$, $M_{1,90} = 0.408$, $\alpha_m = 0°$ (Cond. 68).

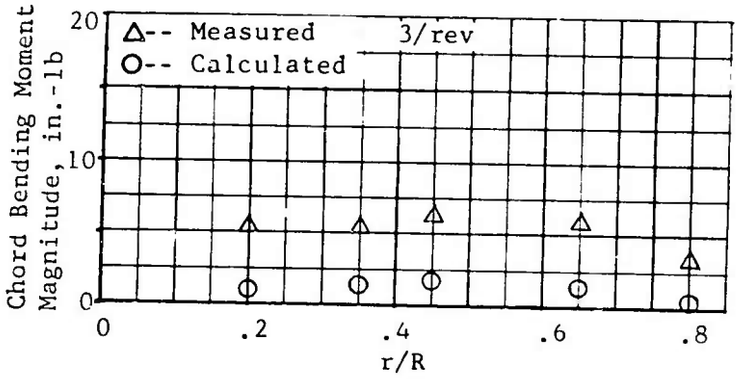

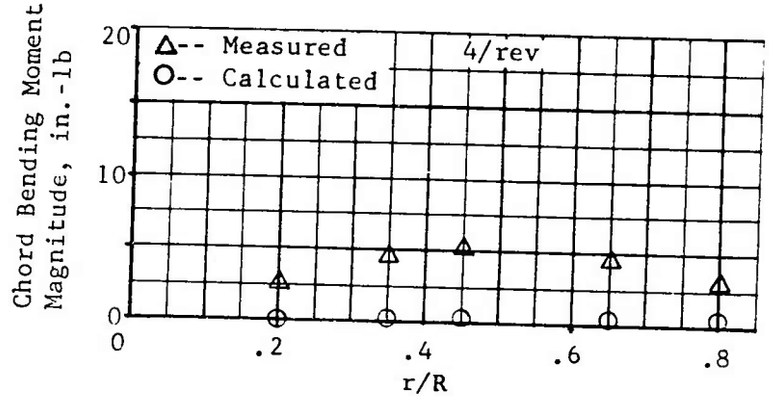

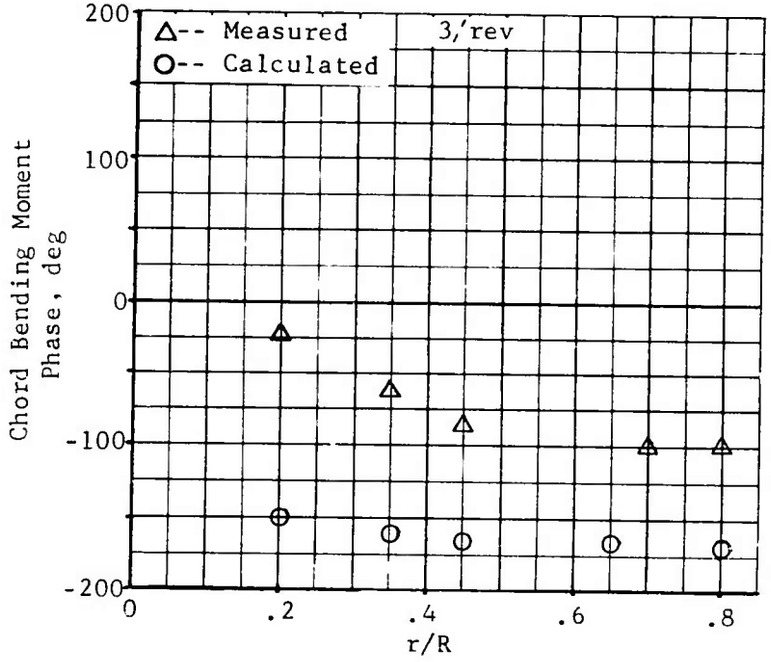

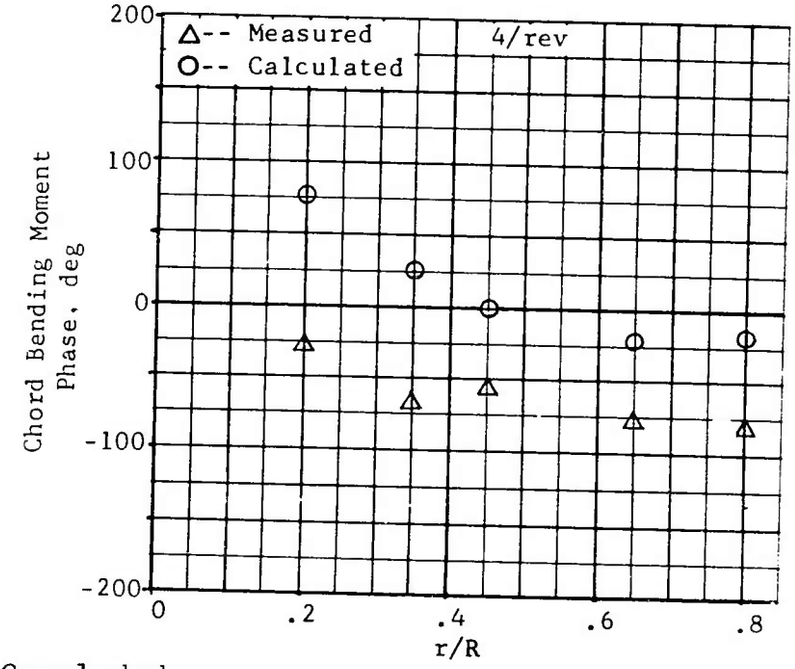

Figure 80. Concluded.

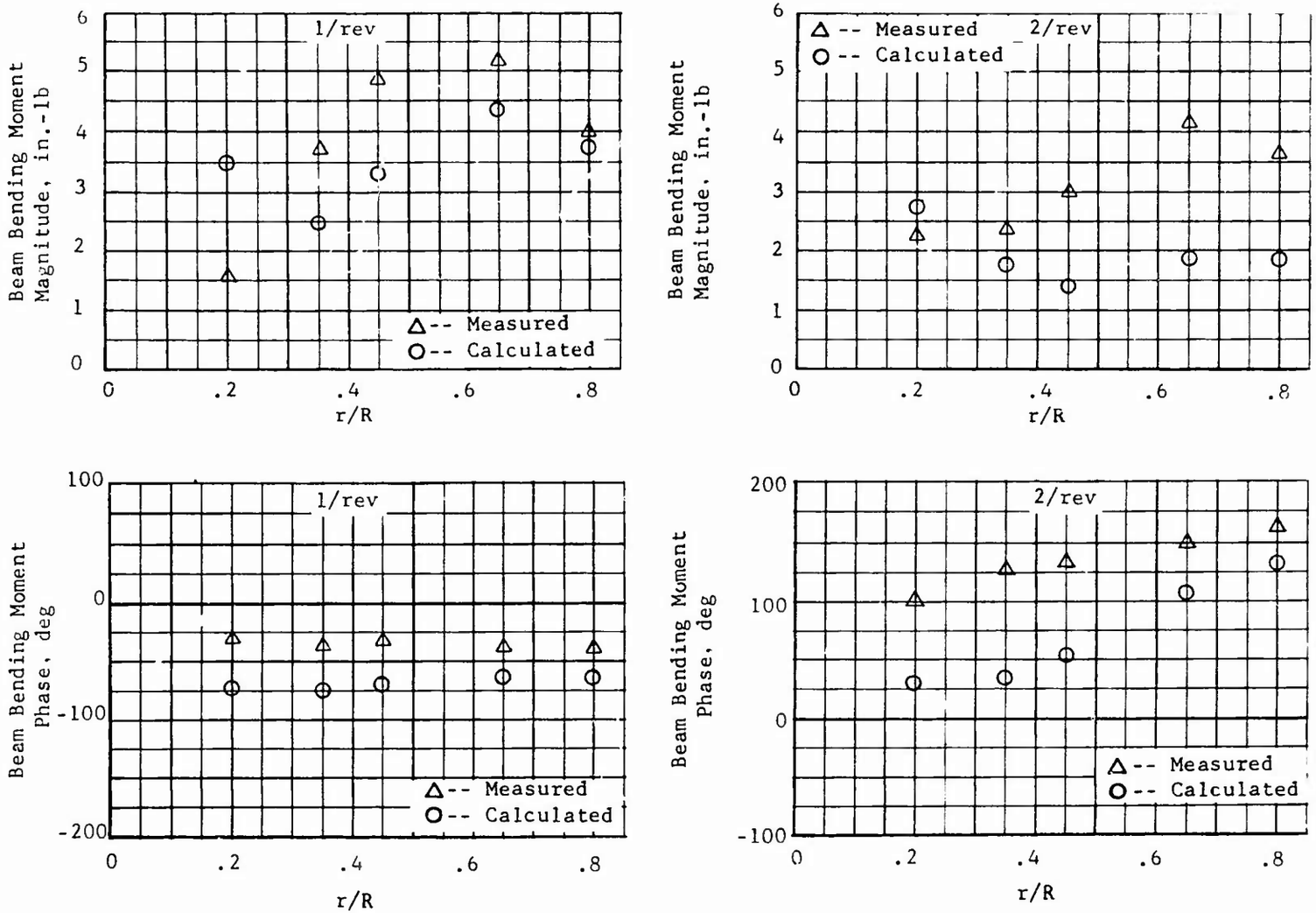

Figure 81. Measured and Calculated Beam Bending Moment Harmonics, Fiberglass Blade, -8° Twist, $\mu = 0.399$, $M_{1,90} = 0.434$, $\alpha_m = 0.5°$ (Cond. 25).

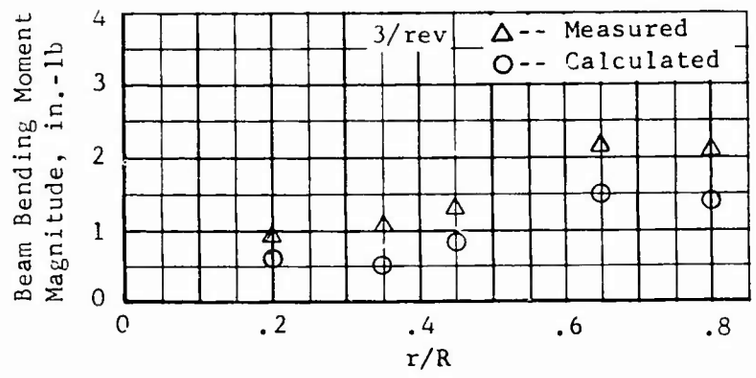

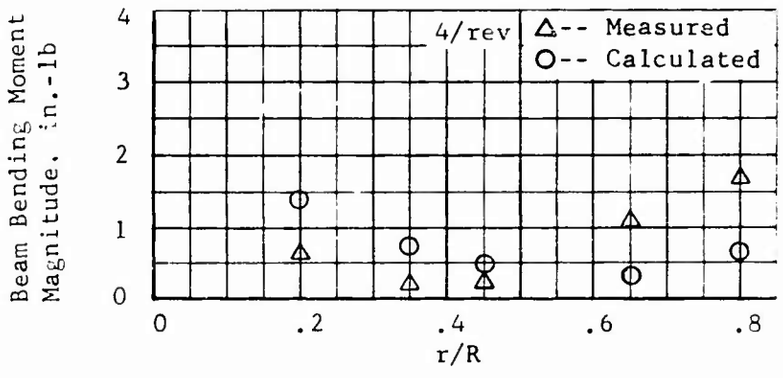

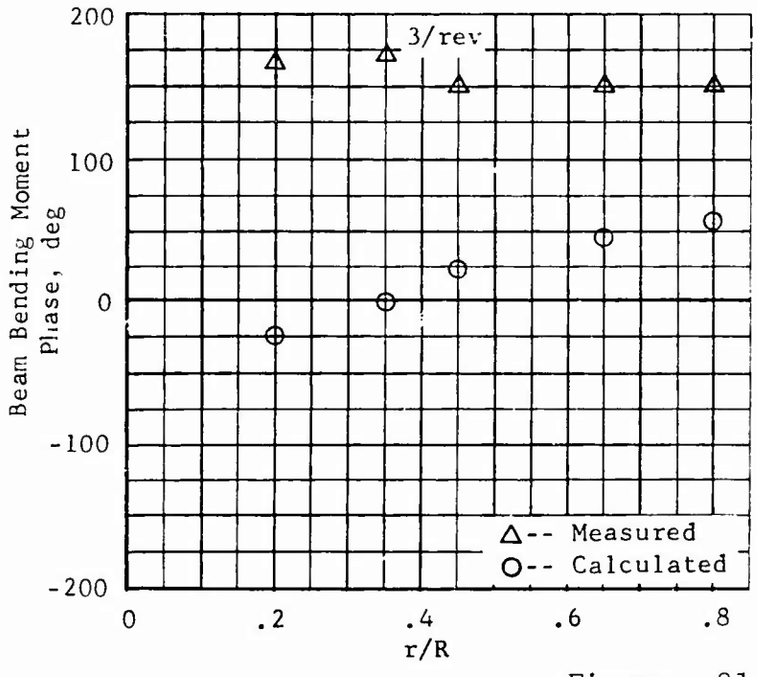

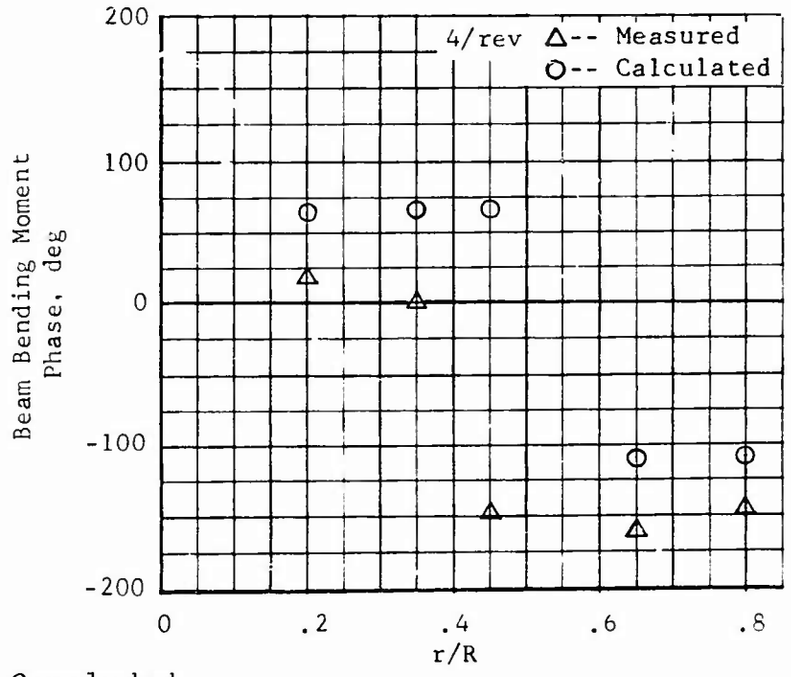

Figure 81. Concluded.

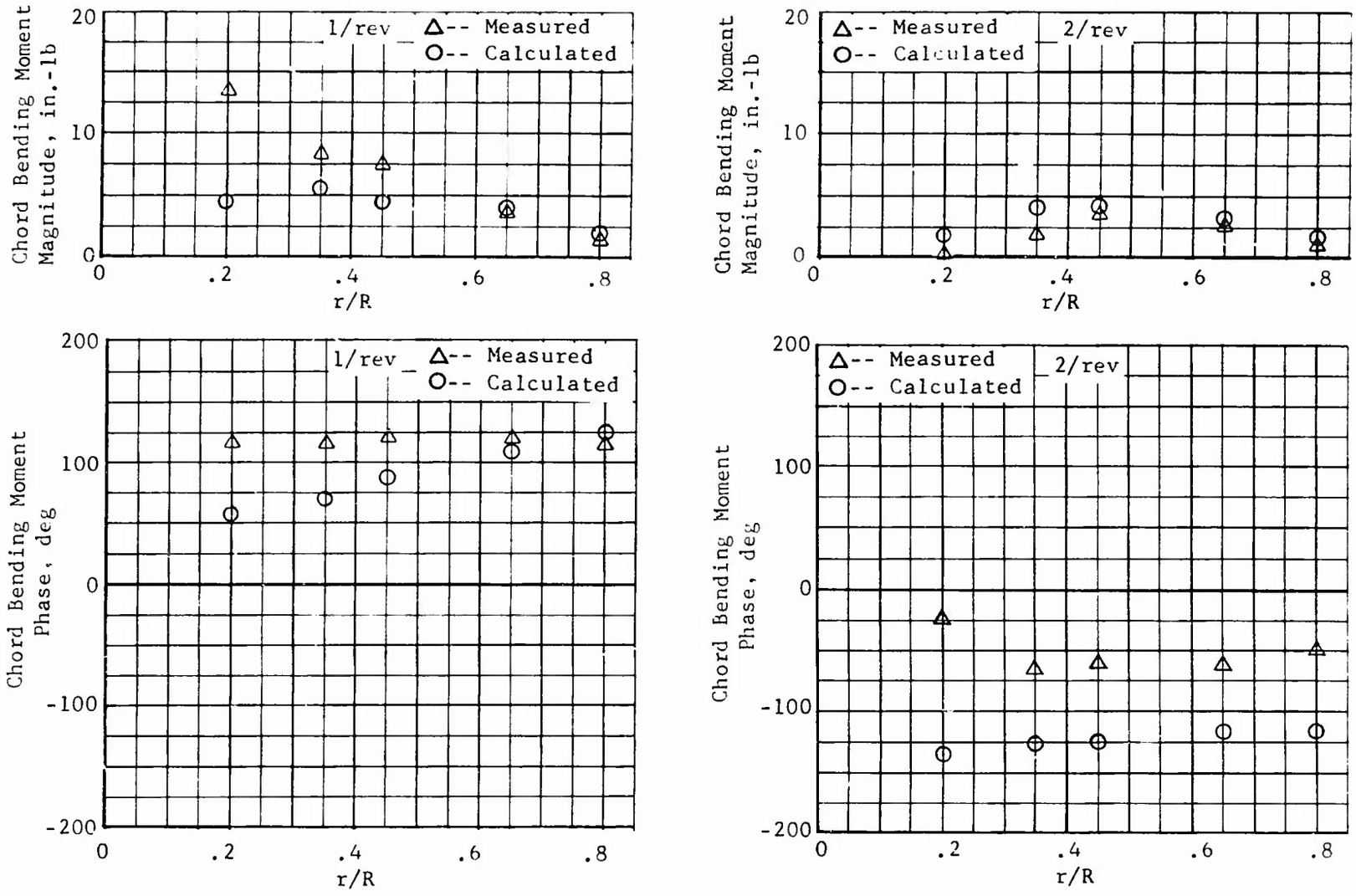

Figure 82. Measured and Calculated Chord Bending Moment Harmonics, Fiberglass Blade, -8° Twist, $\mu = 0.399$, $M_{1,90} = 0.434$, $\alpha_m = 0.5°$ (Cond. 25).

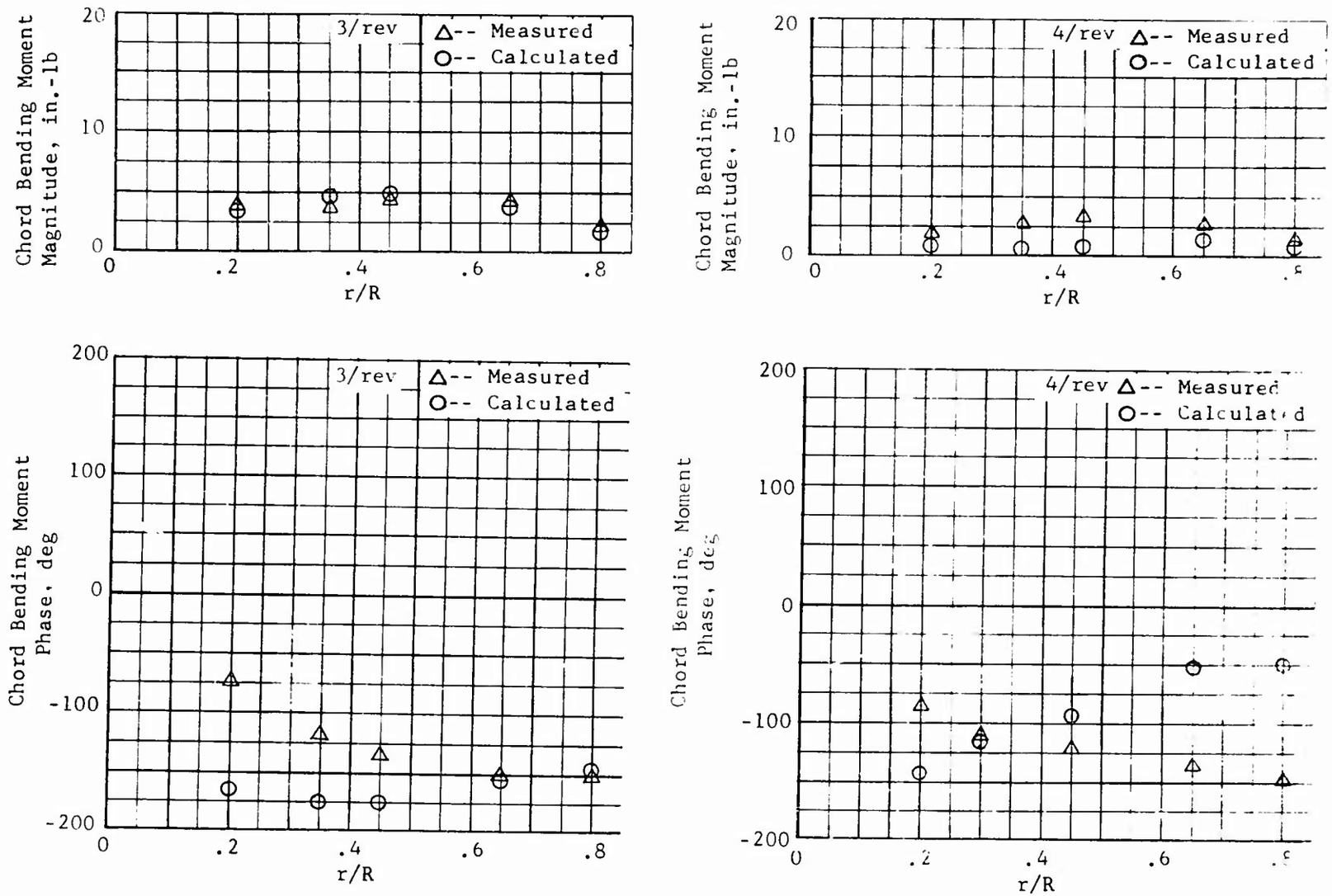

Figure 82. Concluded.

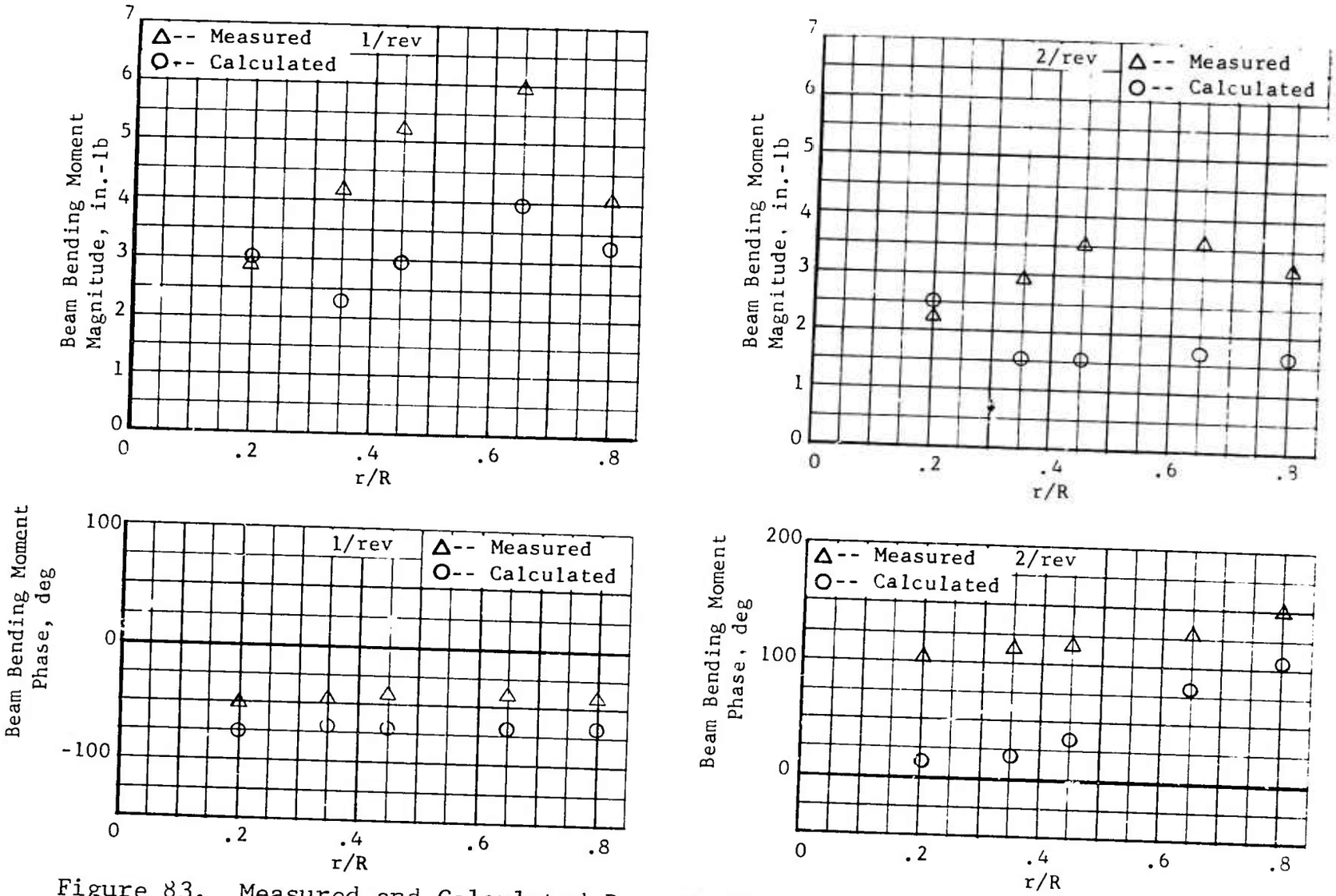

Figure 83. Measured and Calculated Beam Bending Moment Harmonics, Fiberglass Blade, -8° Twist, $\mu = 0.502$, $M_{1,90} = 0.467$, $\alpha_m = 5°$ (Cond. 44).

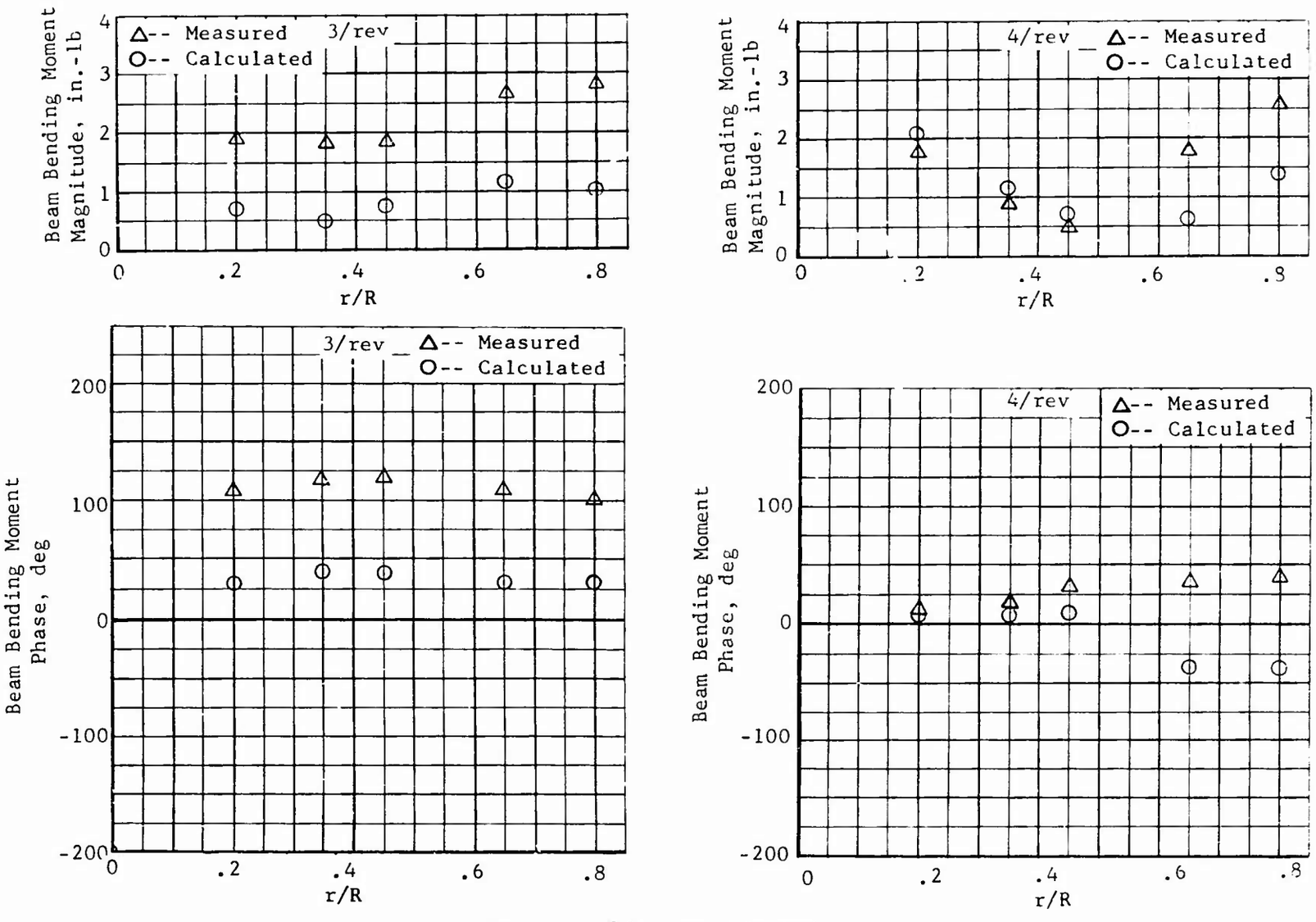

Figure 83. Concluded.

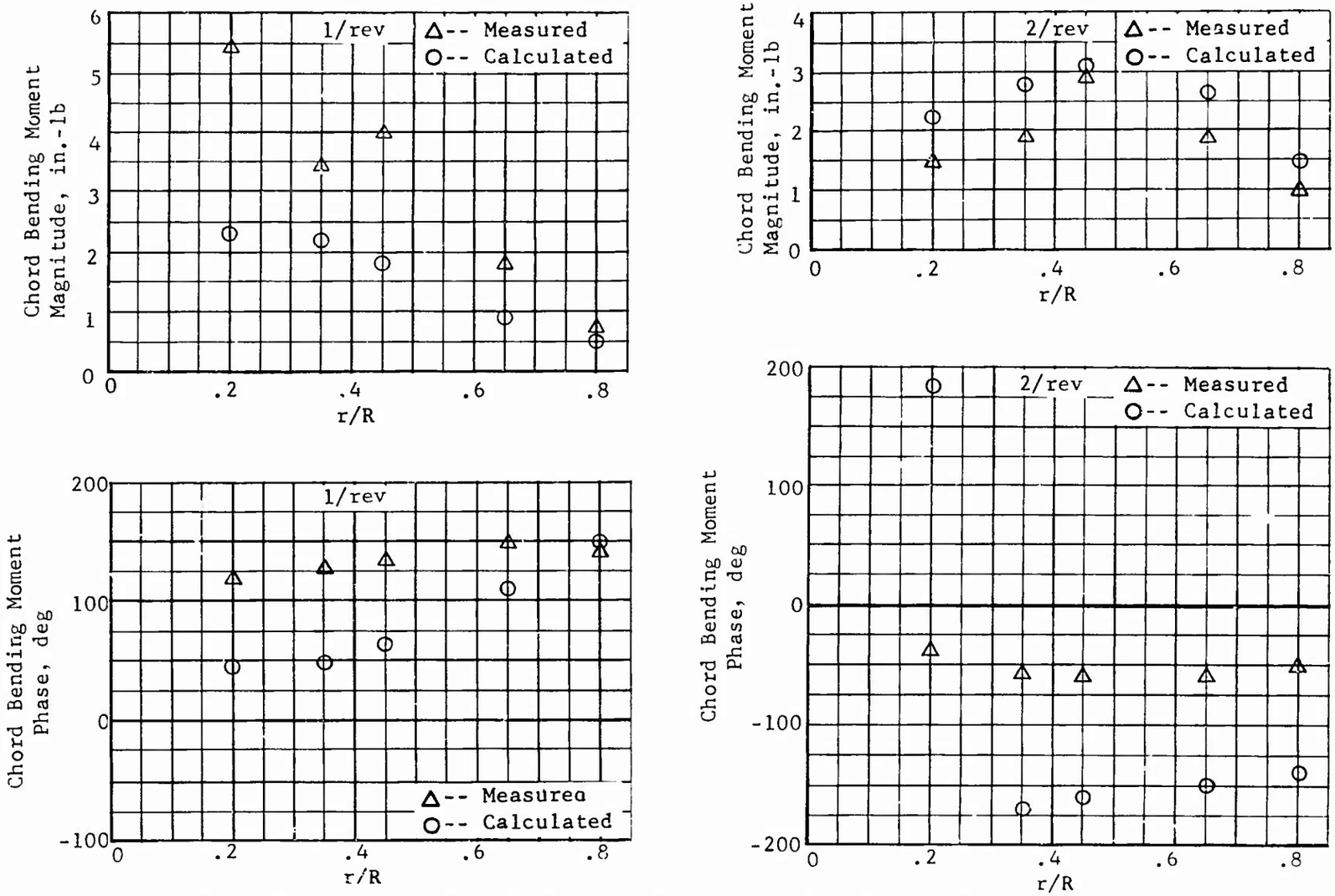

Figure 84. Measured and Calculated Chord Bending Moment Harmonics, Fiberglass Blade, -8° Twist, $\mu = 0.502$, $M_{1,90} = 0.467$, $\alpha_m = 5°$ (Cond. 44).

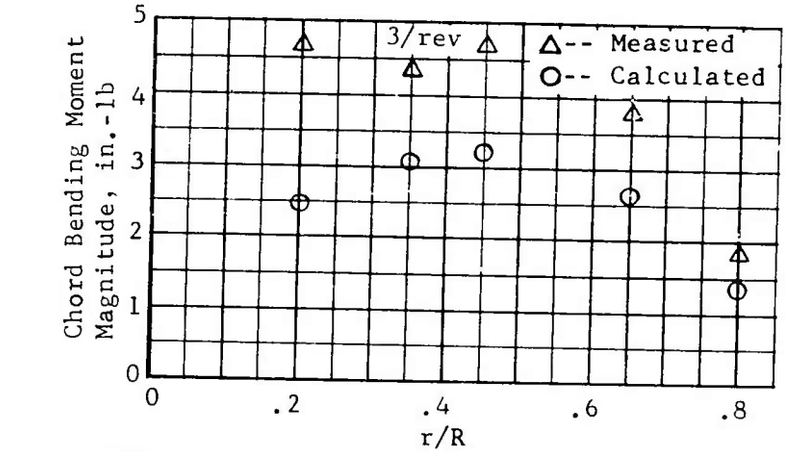

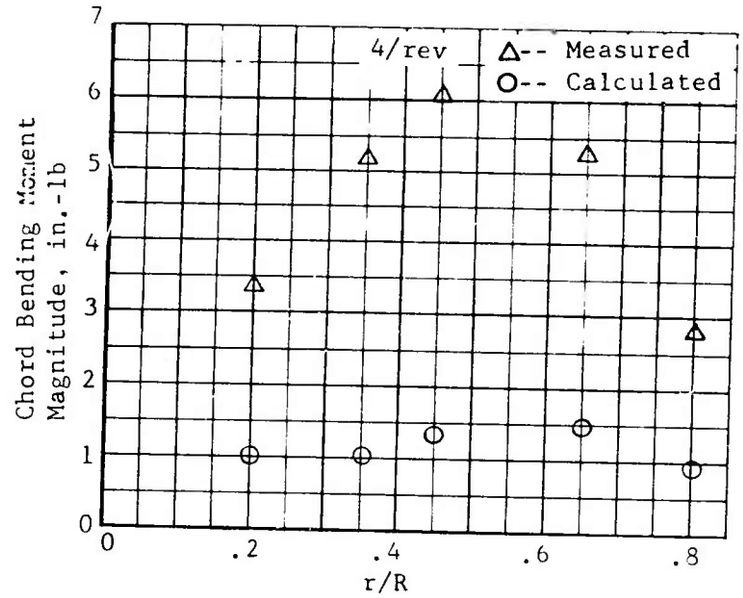

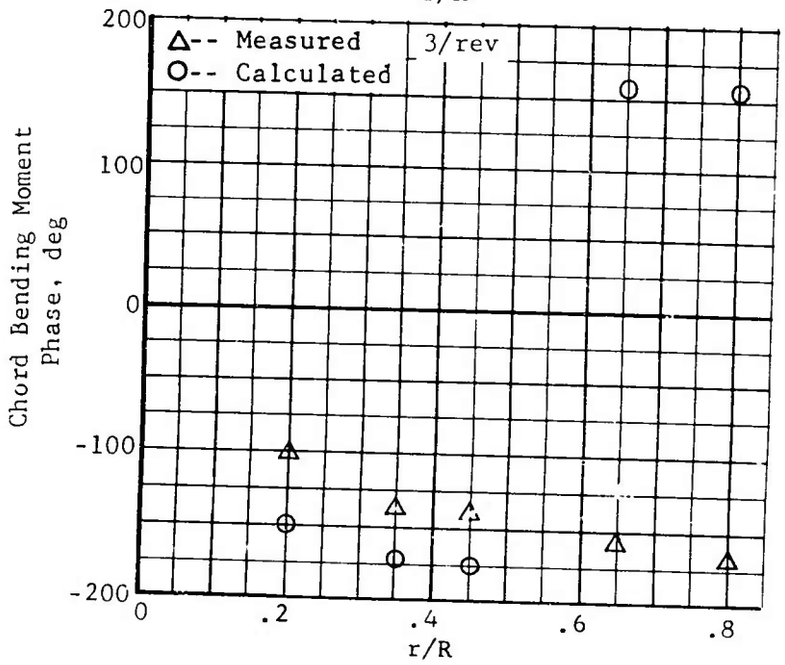

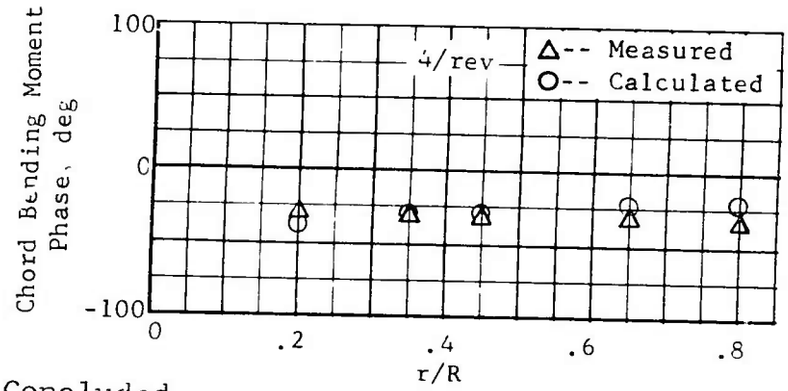

Figure 84. Concluded.

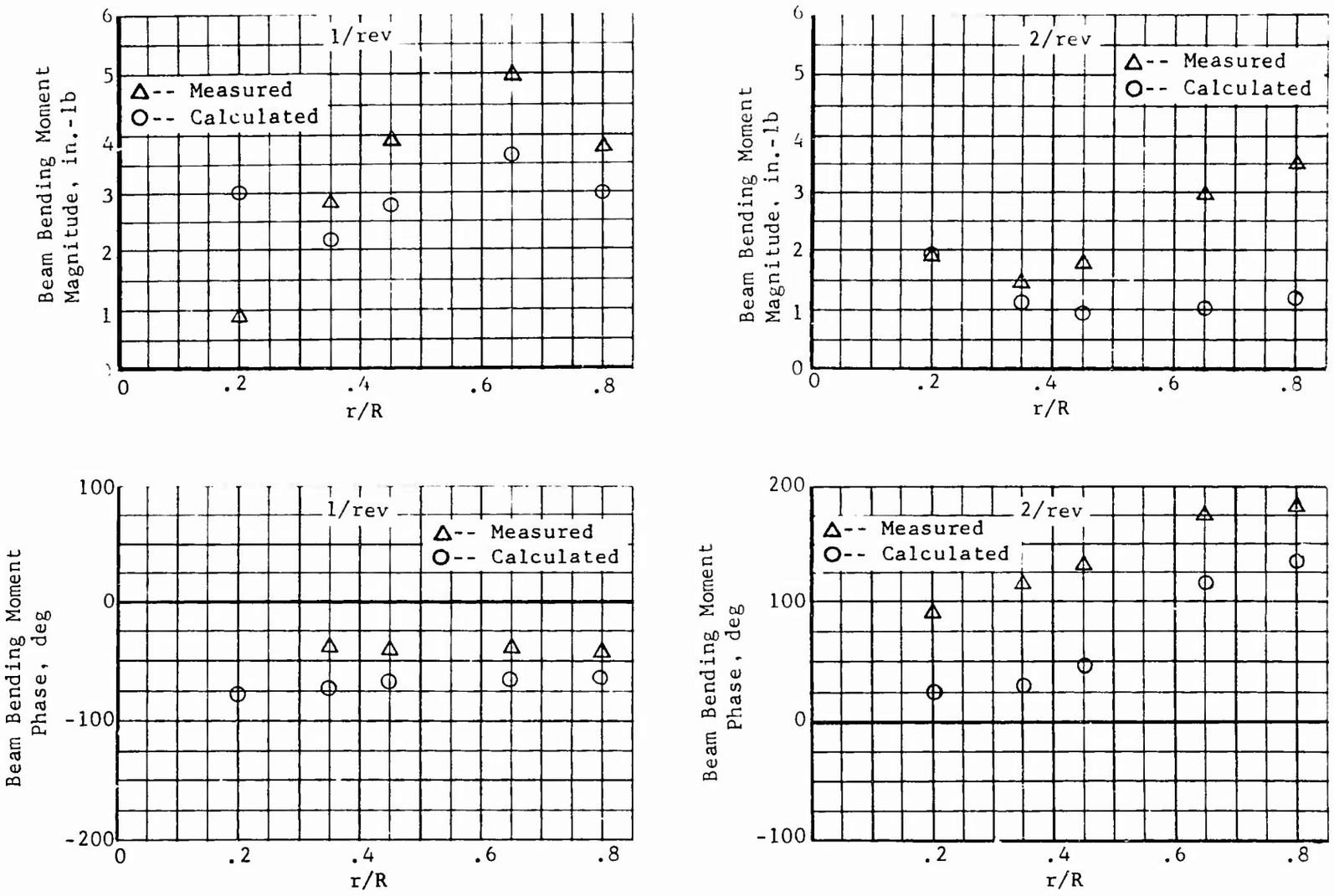

Figure 85. Measured and Calculated Beam Bending Moment Harmonics, Fiberglass Blade, -8° Twist, $\mu = 0.299$, $M_{1,90} = 0.408$, $\alpha_m = 0°$ (Cond. 68).

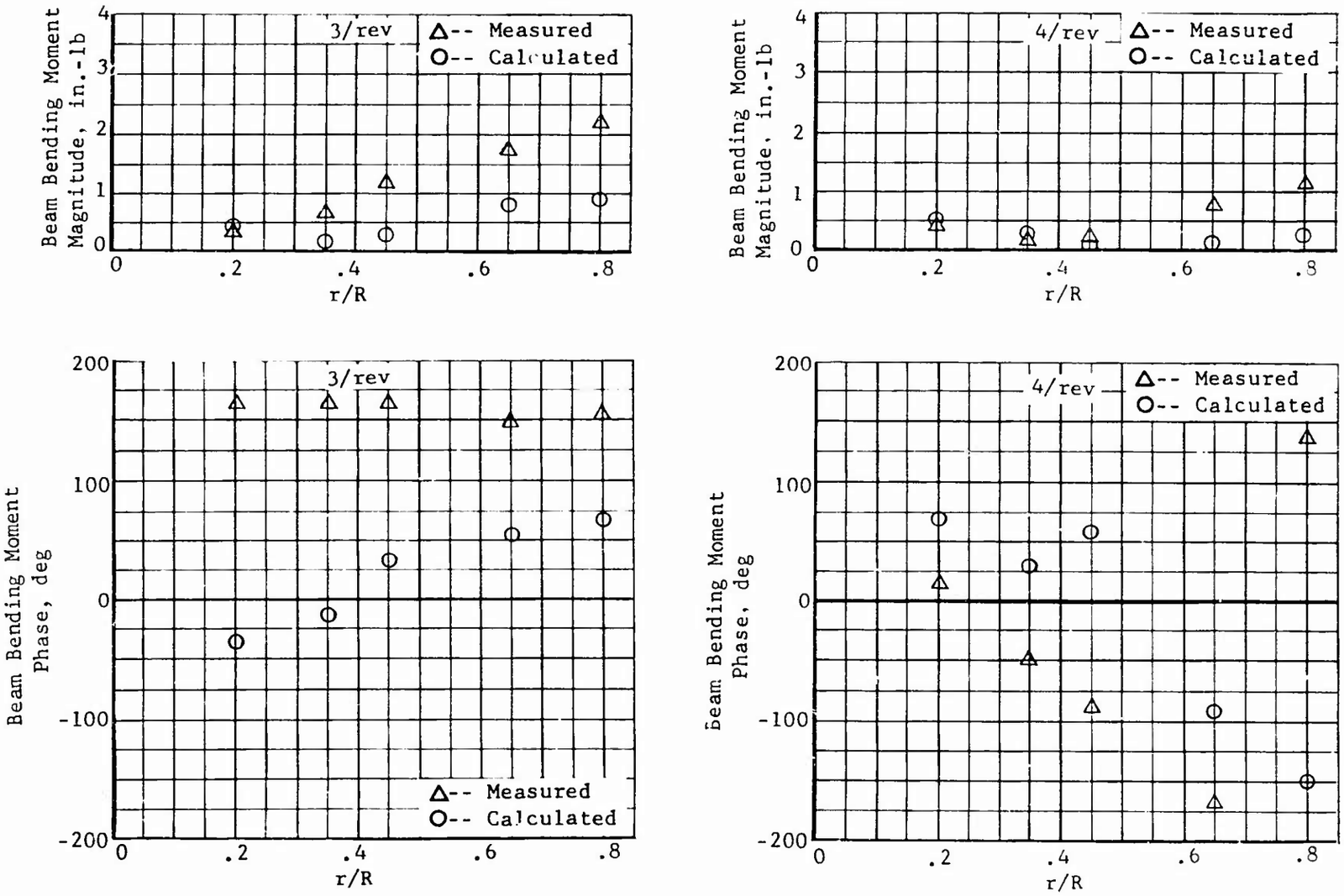

Figure 85. Concluded.

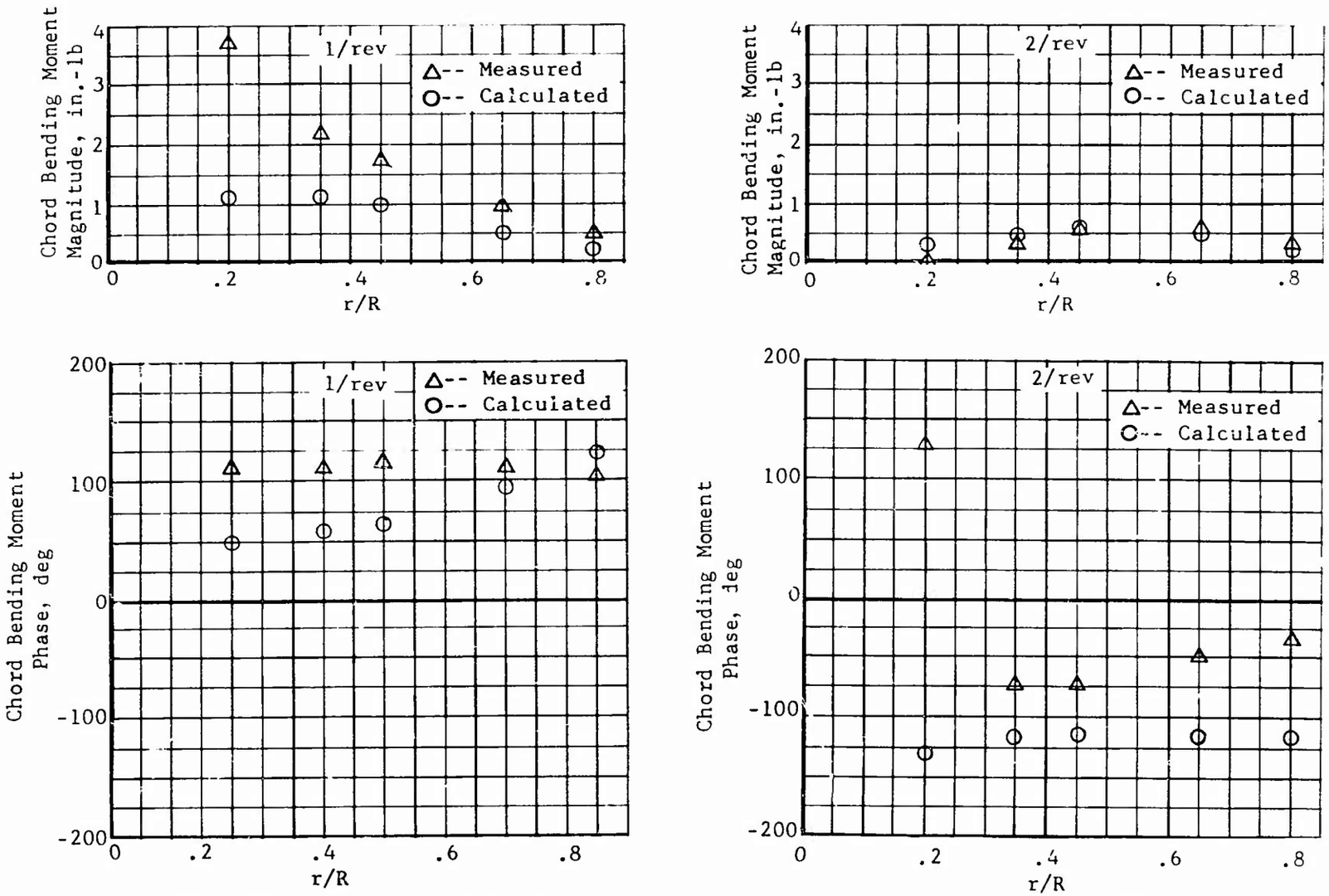

Figure 86. Measured and Calculated Chord Bending Moment Harmonics, Fiberglass Blade, -8° Twist, $\mu = 0.299$, $M_{1,90} = 0.408$, $\alpha_m = 0°$ (Cond. 68).

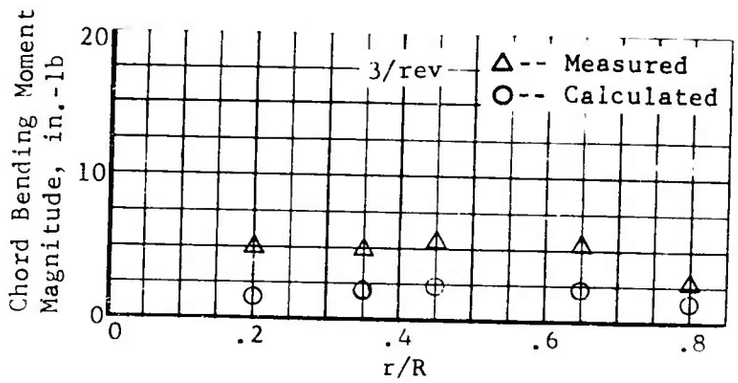

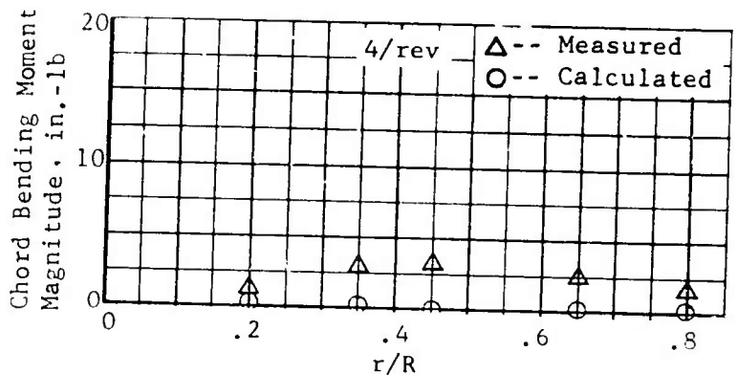

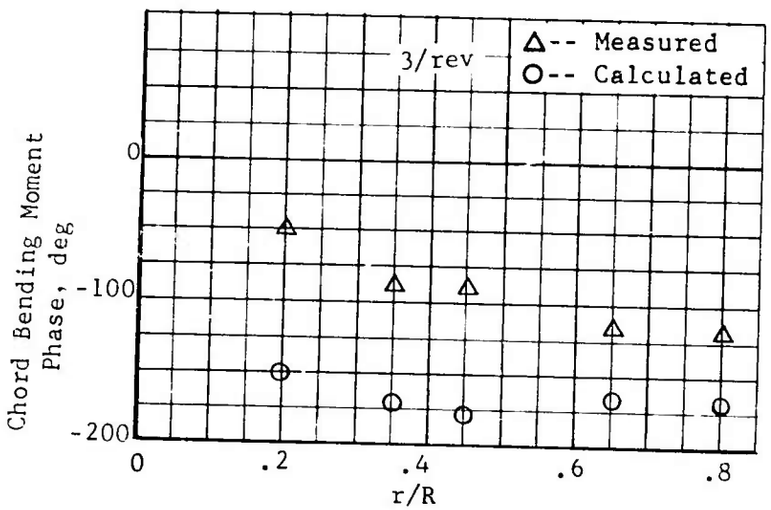

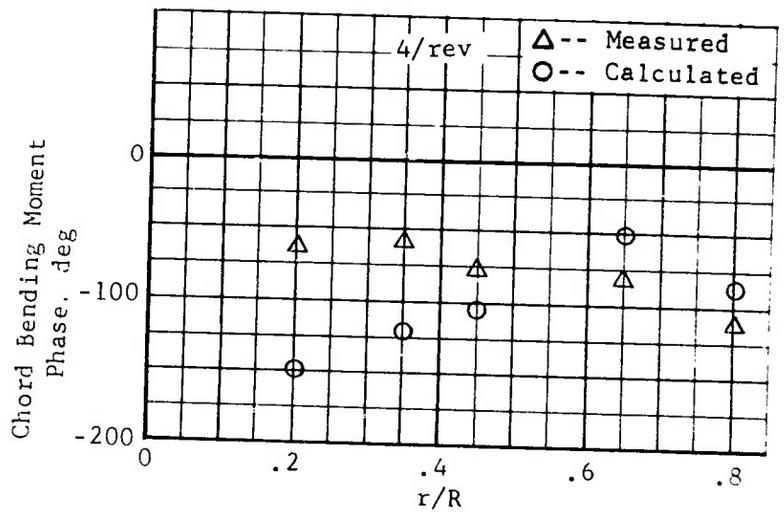

Figure 86. Concluded.

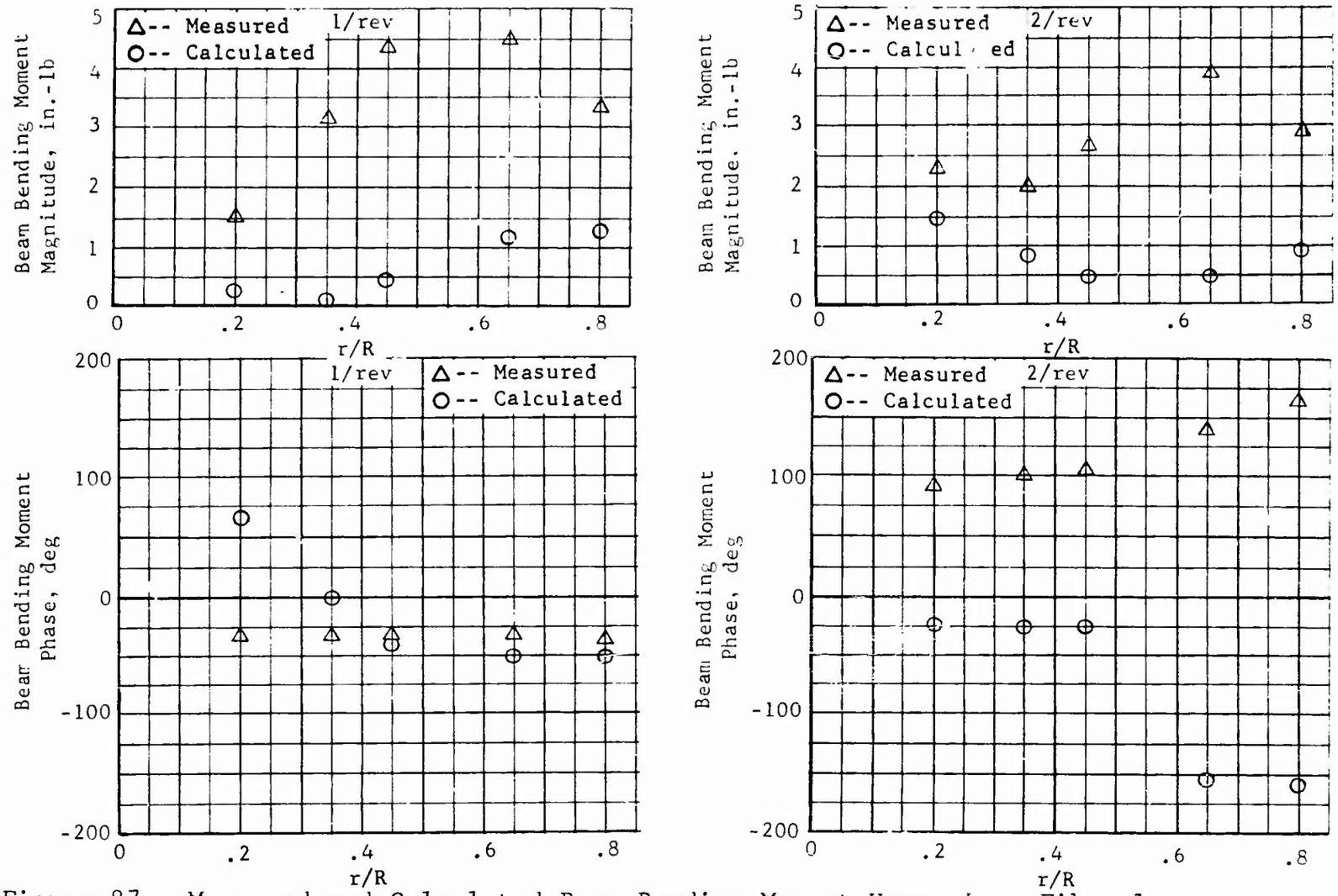

Figure 87. Measured and Calculated Beam Bending Moment Harmonics, Fiberglass Blade, 0° Twist, $\delta_F = 5°$, $\mu = 0.399$, $M_{1,90} = 0.434$, $\alpha_m = 0.5°$ (Cond. 25).

Figure 87. Concluded.

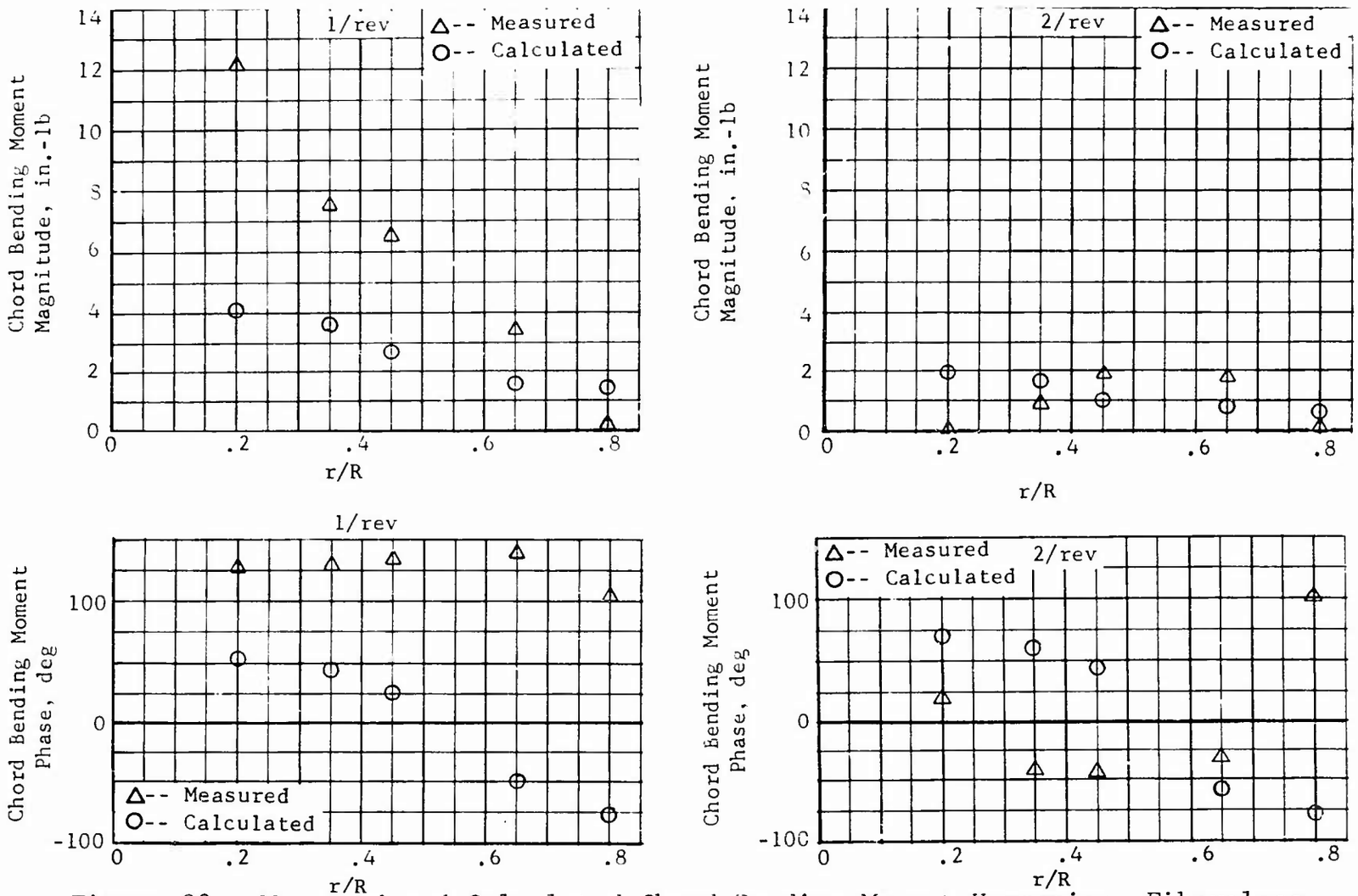

Figure 88. Measured and Calculated Chord Bending Moment Harmonics, Fiberglass Blade, 0° Twist, $\delta_F = 5°$, $\mu = 0.399$, $M_{1,90} = 0.434$, $\alpha_m = 0.5°$ (Cond. 25).

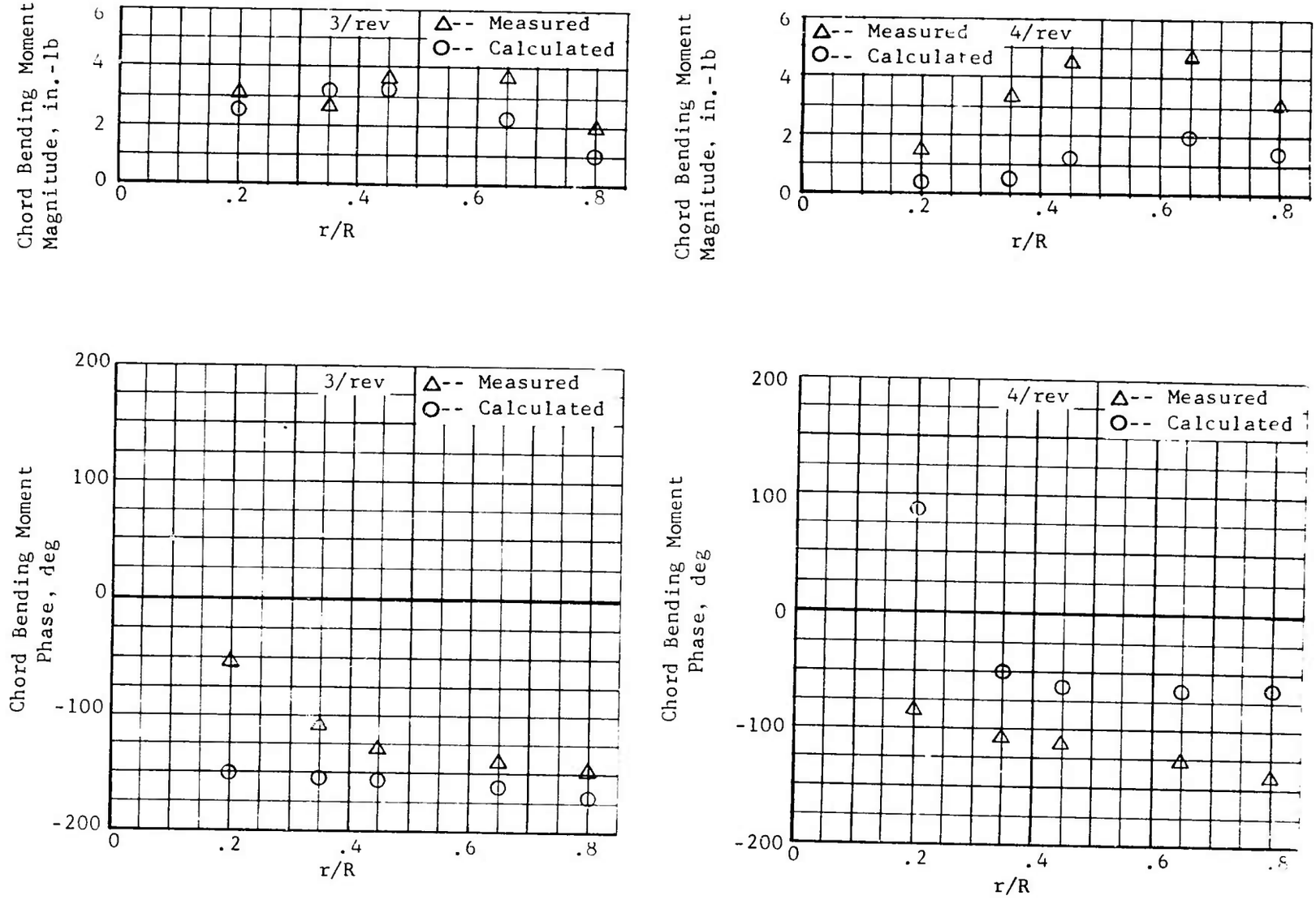

Figure 88. Concluded.

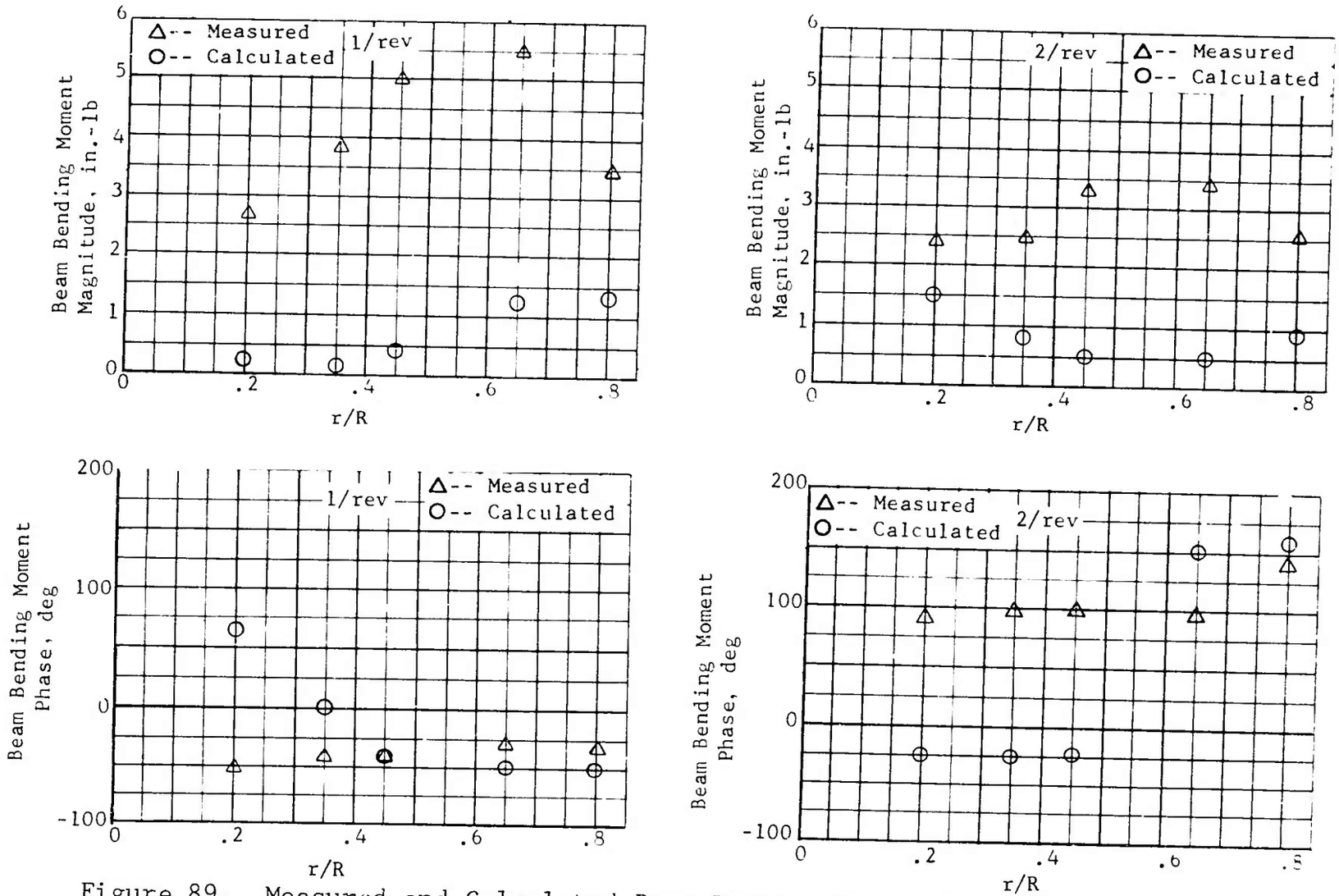

Figure 89. Measured and Calculated Beam Bending Moment Harmonics, Fiberglass Blade, 0° Twist, $\delta_F = 5°$, $\mu = 0.502$, $M_{1,90} = 0.467$, $\alpha_m = 5°$ (Cond. 44).

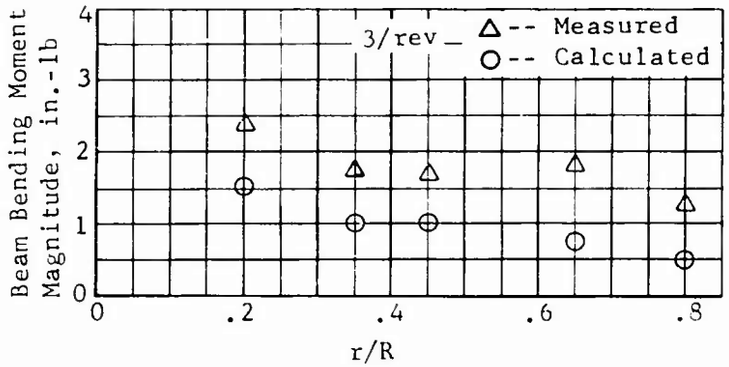

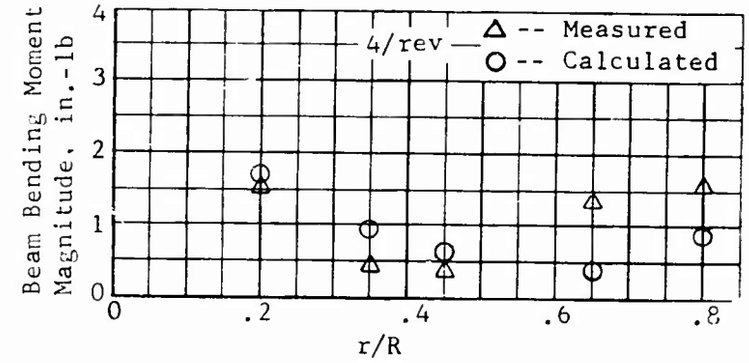

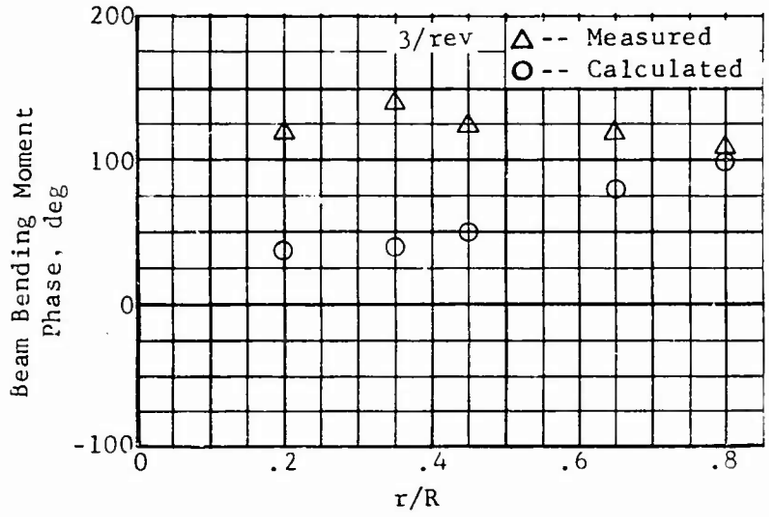

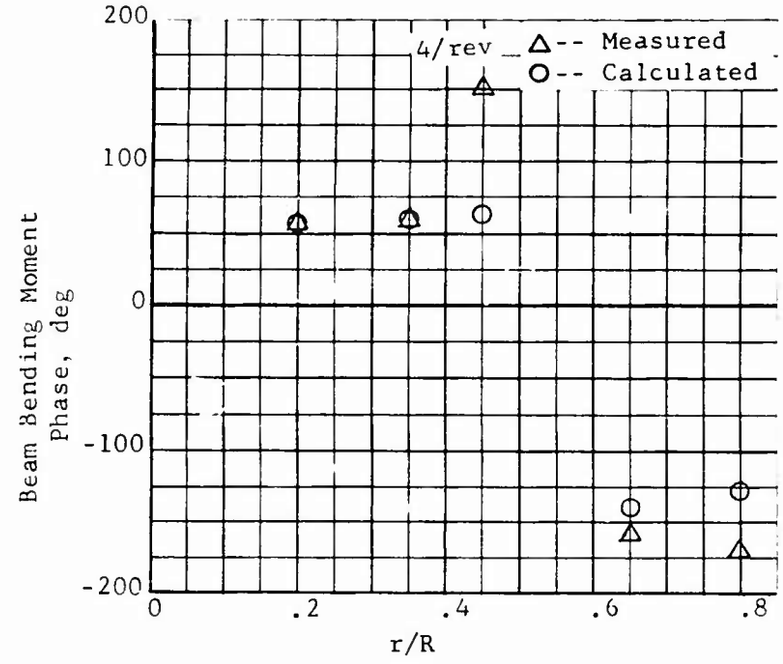

Figure 89. Concluded.

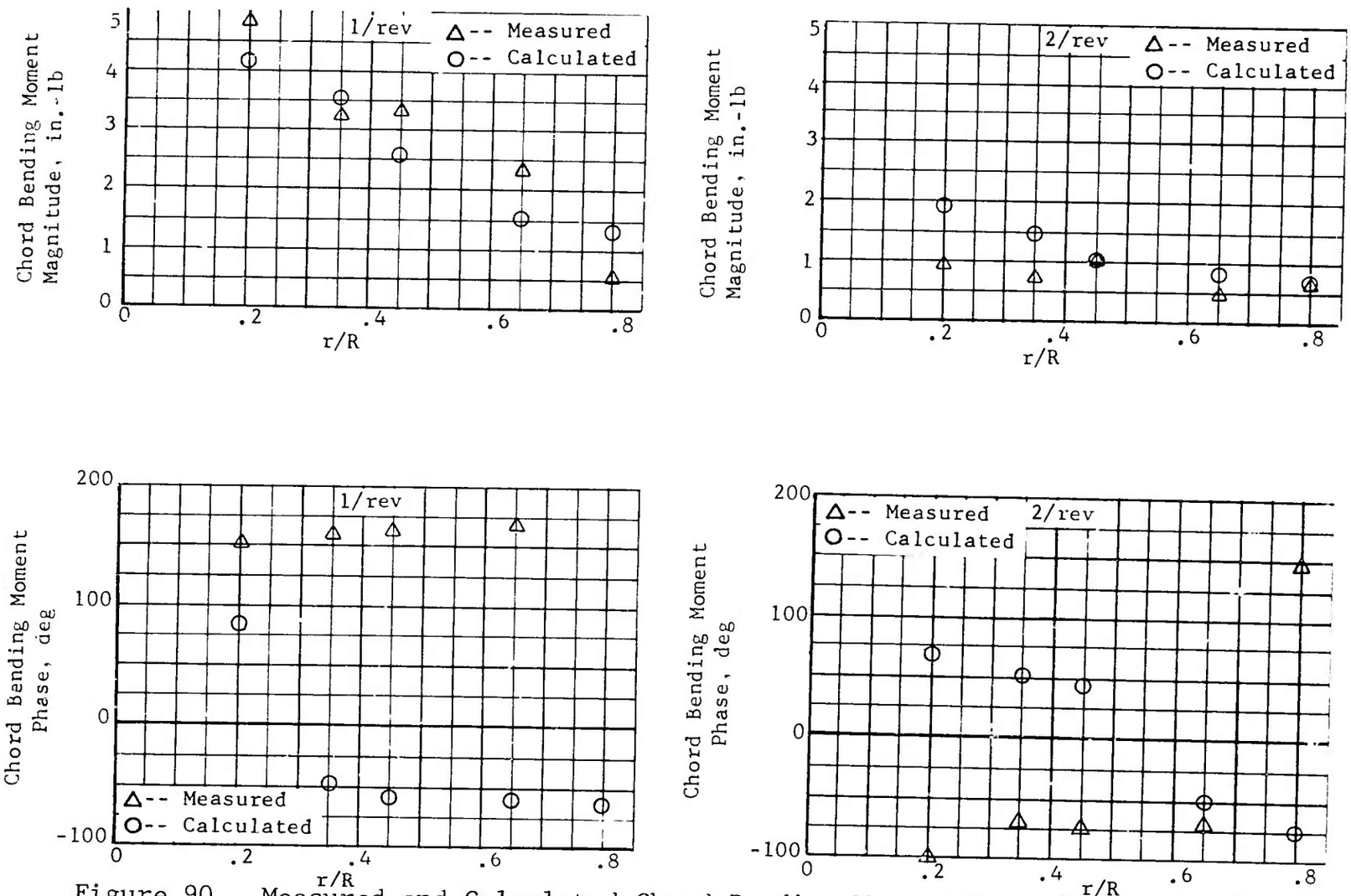

Figure 90. Measured and Calculated Chord Bending Moment Harmonics, Fiberglass Blade, 0° Twist, $\delta_F = 5°$, $\mu = 0.502$, $M_{1,90} = 0.467$, $\alpha_m = 5°$ (Cond. 44).

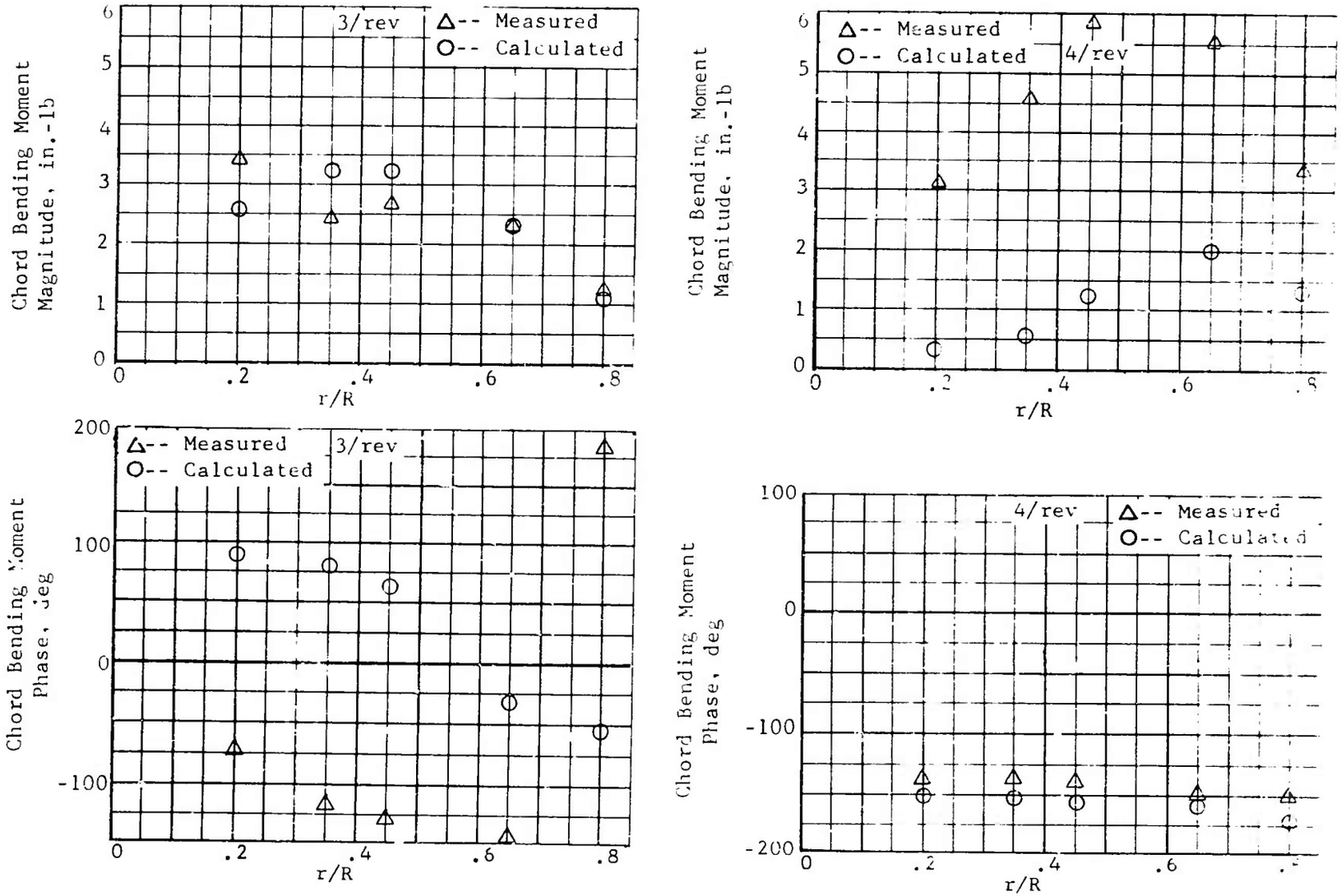

Figure 90. Concluded.

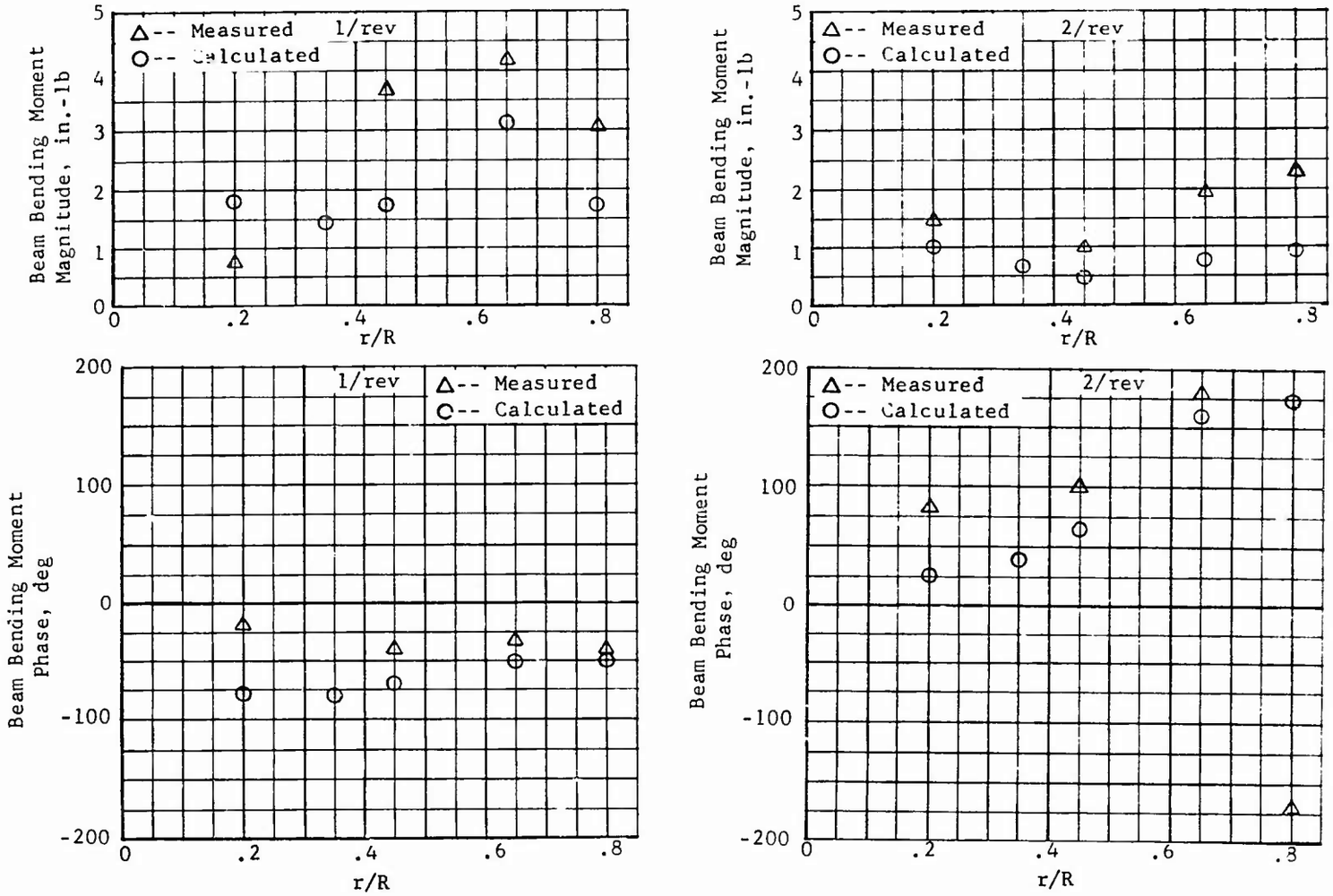

Figure 91. Measured and Calculated Beam Bending Moment Harmonics, Fiberglass Blade, 0° Twist, $\delta_F = 5°$, $\mu = 0.299$, $M_{1,90} = 0.408$, $\alpha_m = 0°$ (Cond. 68).

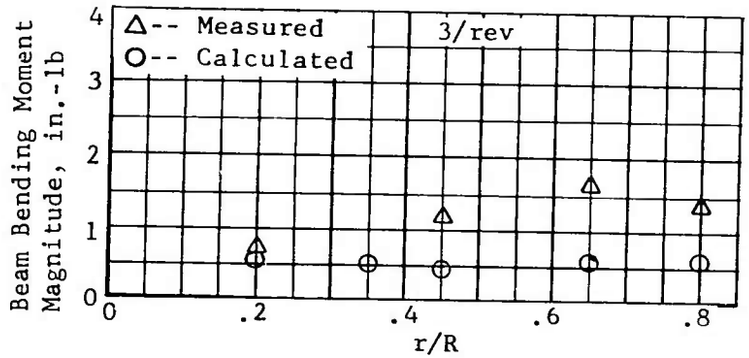

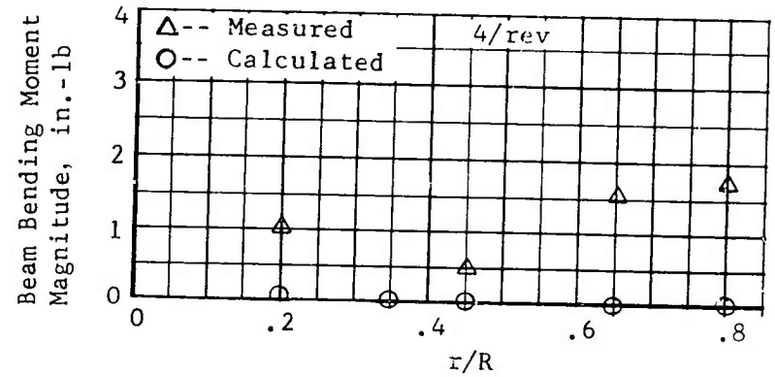

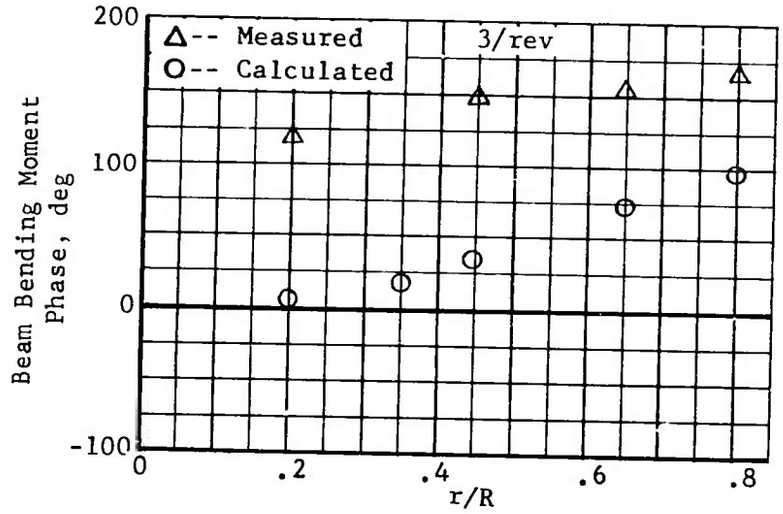

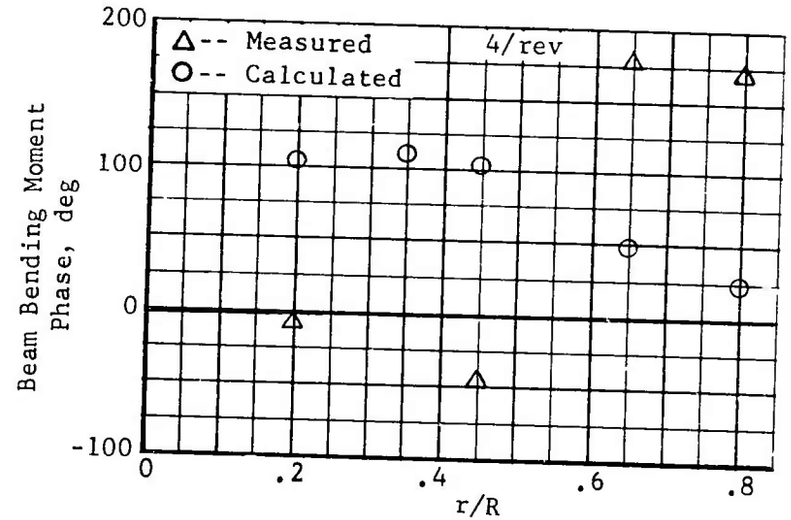

Figure 91. Concluded.

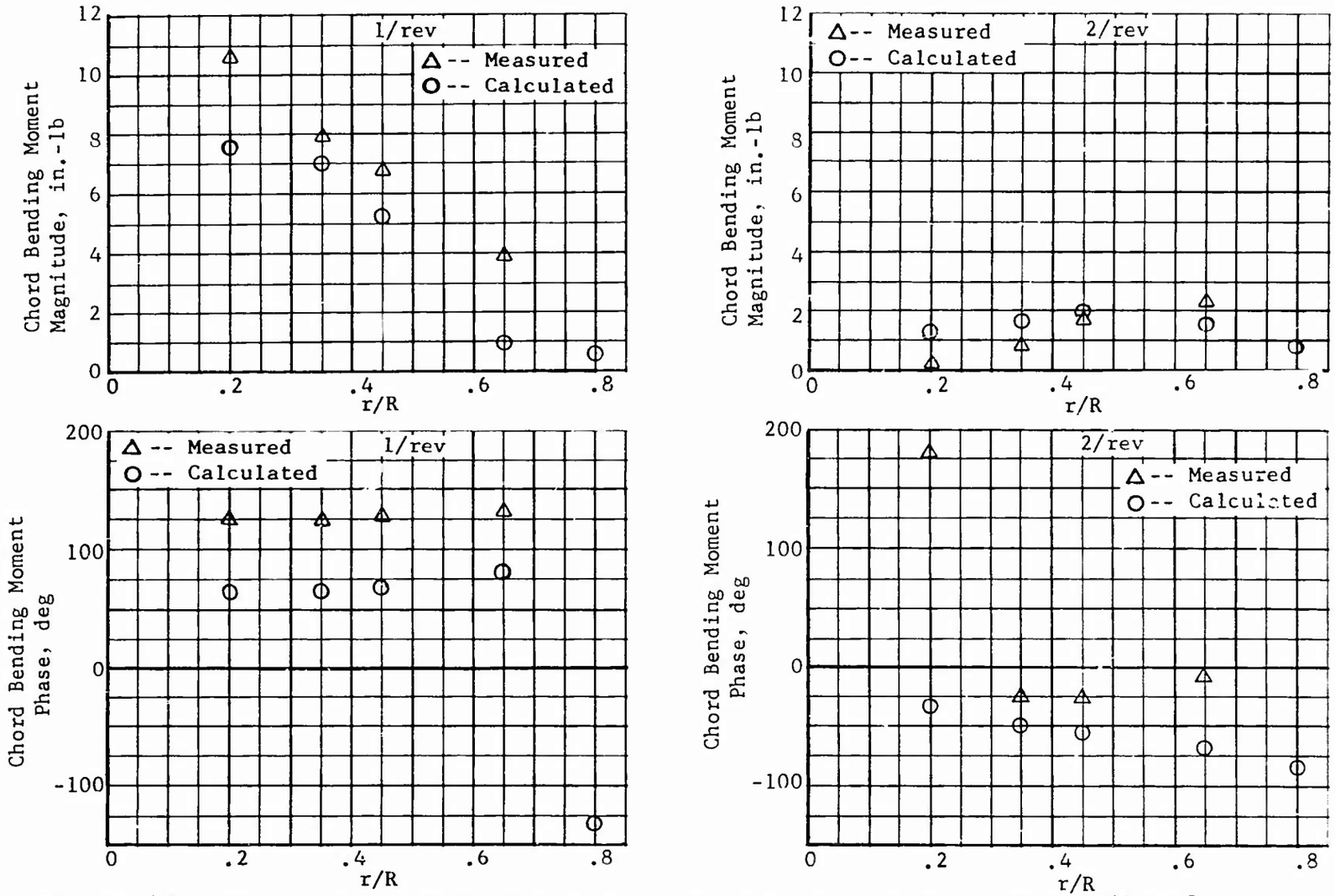

Figure 92. Measured and Calculated Chord Bending Moment Harmonics, Fiberglass Blade, 0° Twist, $\delta_F = 5°$, $\mu = 0.299$, $M_{1,90} = 0.408$, $\alpha_m = 0°$ (Cond. 68).

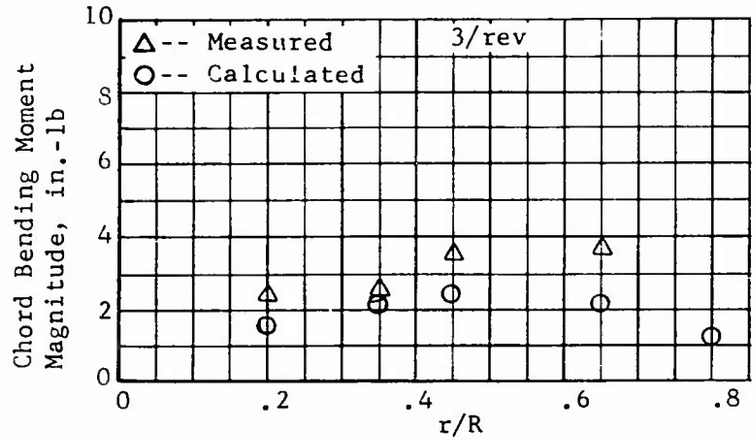

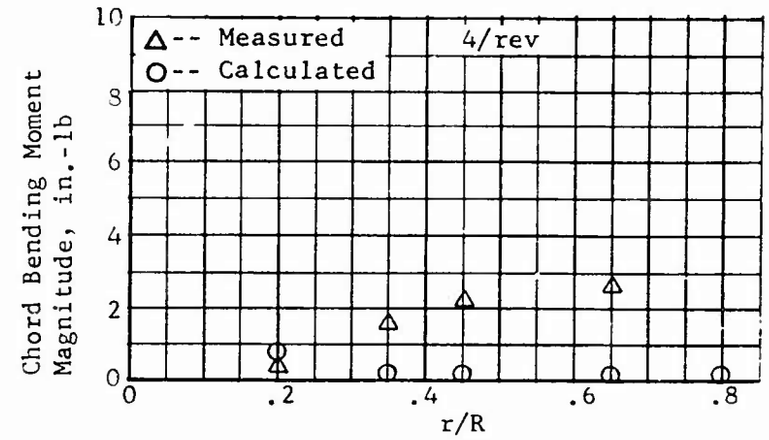

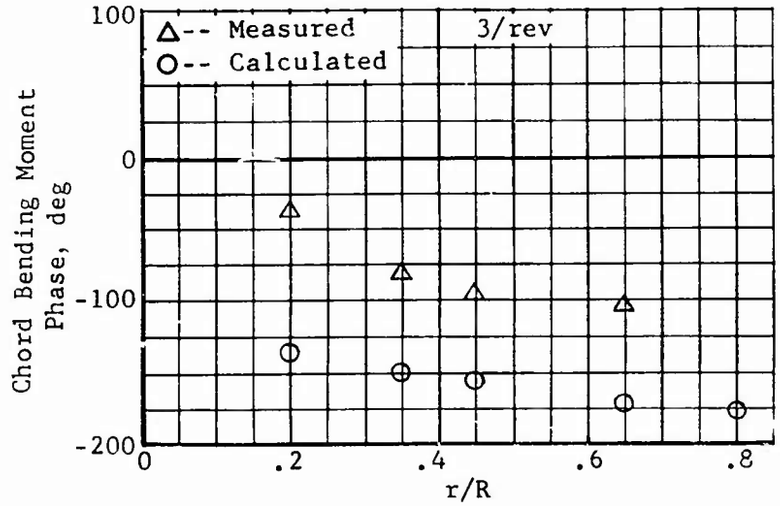

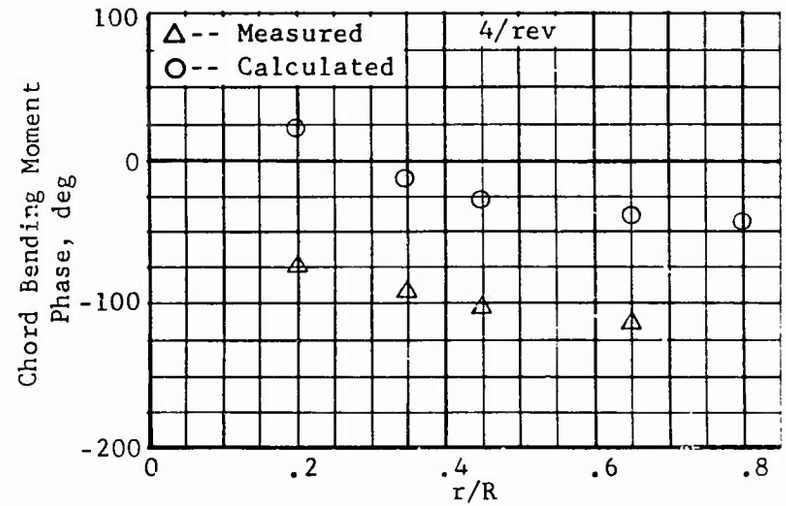

Figure 92. Concluded.

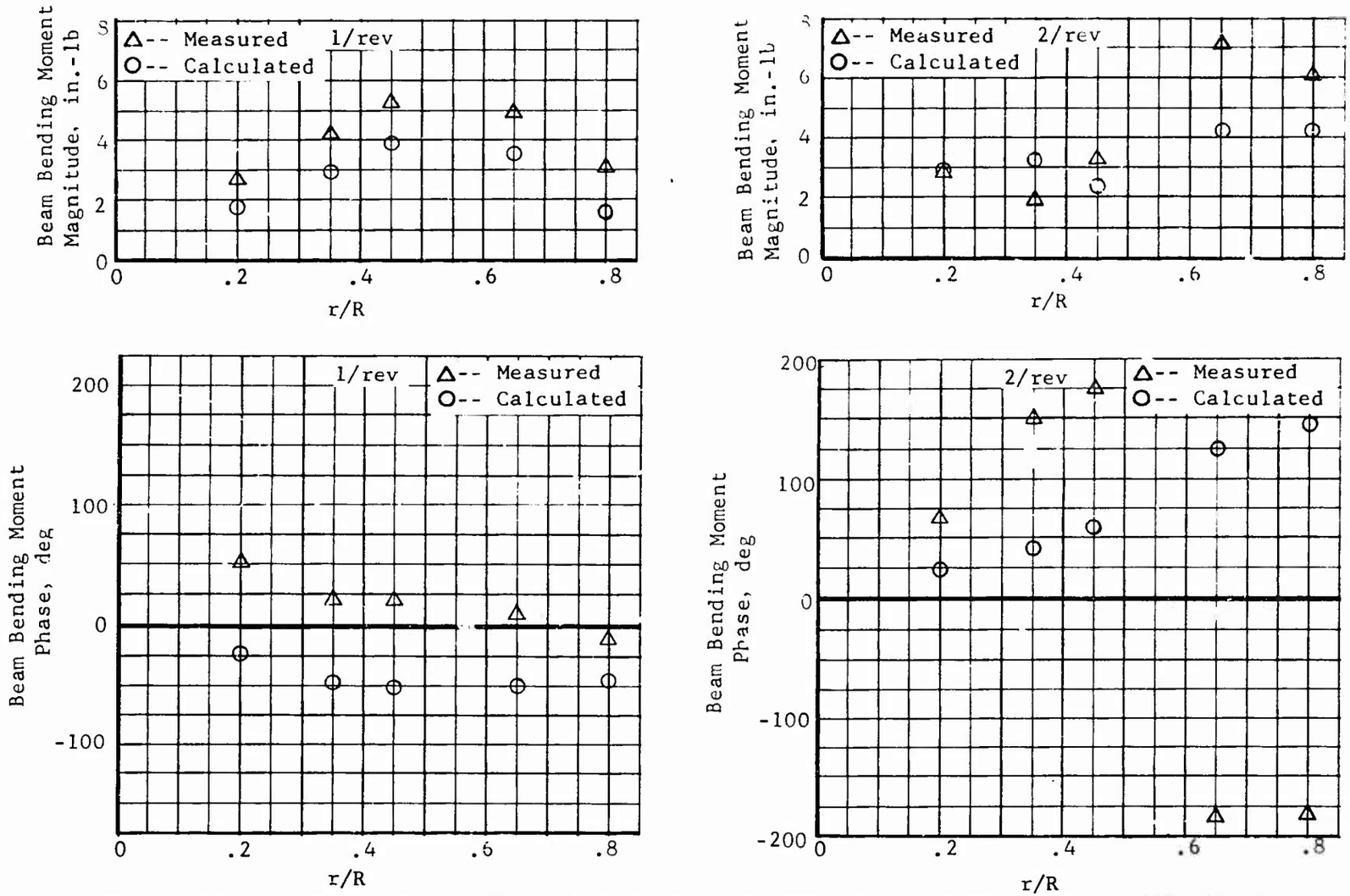

Figure 93. Measured and Calculated Beam Bending Moment Harmonics, Aluminum Blade, 0° Twist, $\mu = 0.399$, $M_{1,90} = 0.434$, $\alpha_m = 0.5°$ (Cond. 25).

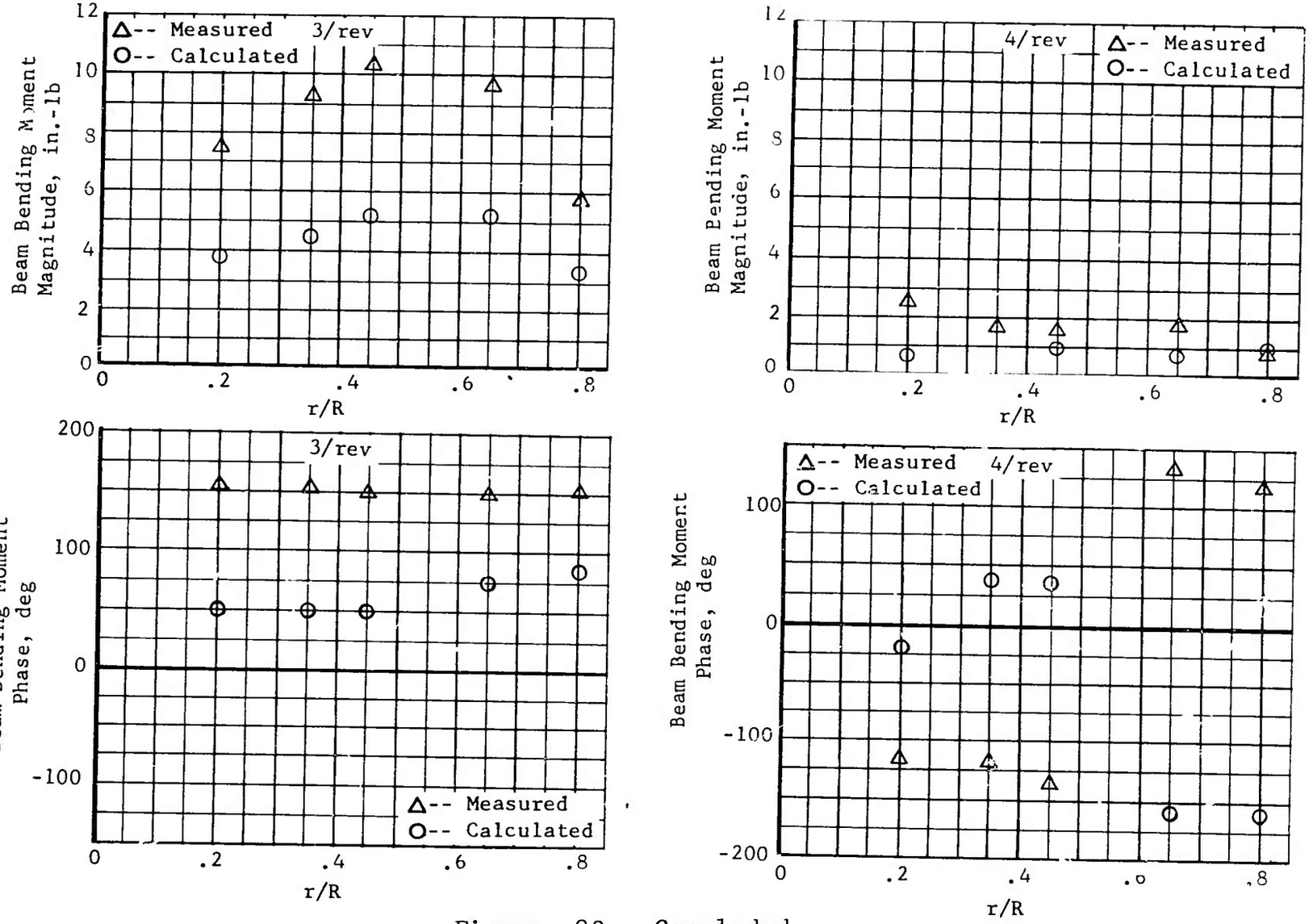

Figure 93. Concluded.

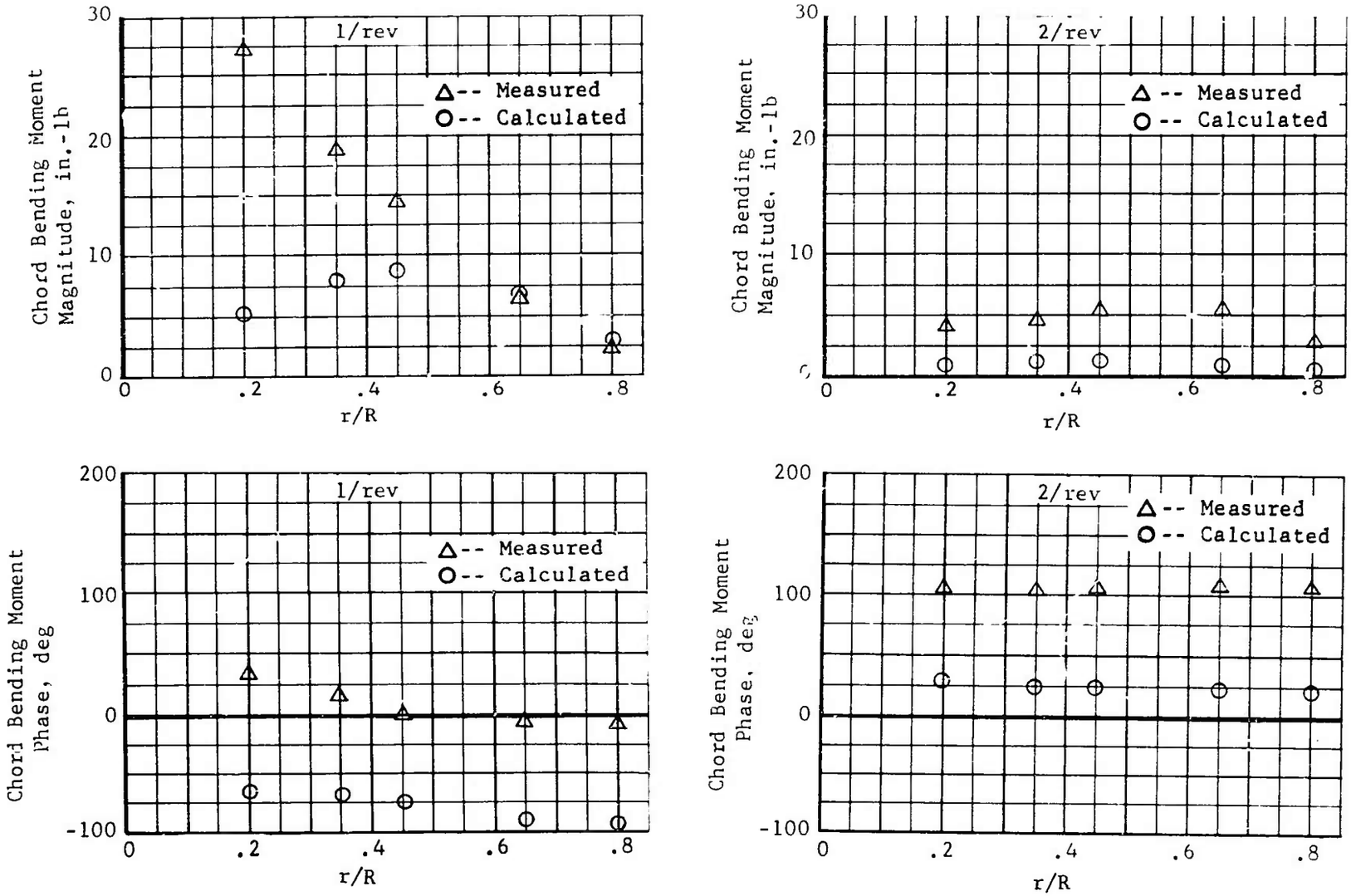

Figure 94. Measured and Calculated Chord Bending Moment Harmonics, Aluminum Blade, 0° Twist, $\mu = 0.399$, $M_{1,90} = 0.434$, $\alpha_m = 0.5°$ (Cond. 25).

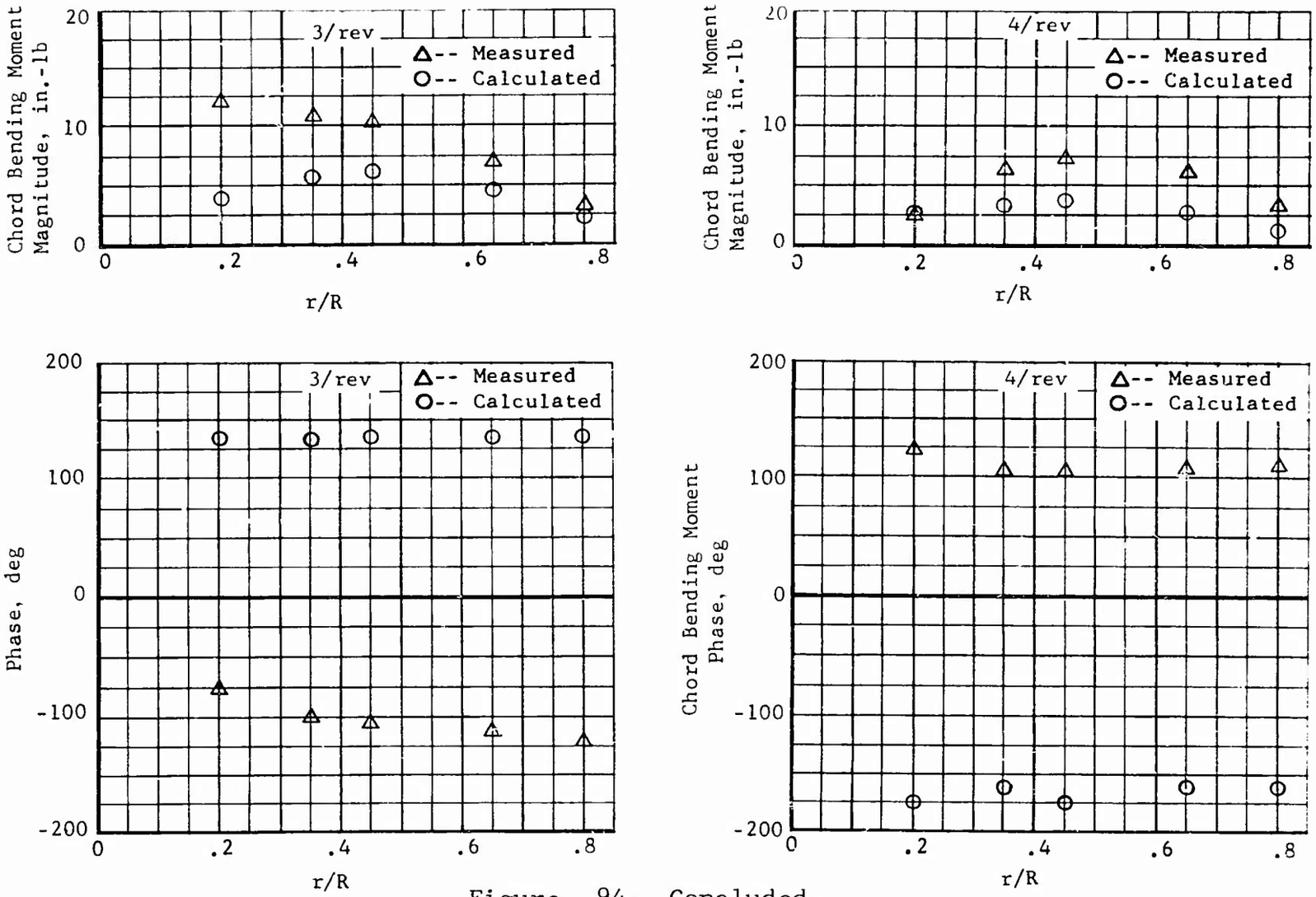

Figure 94. Concluded.

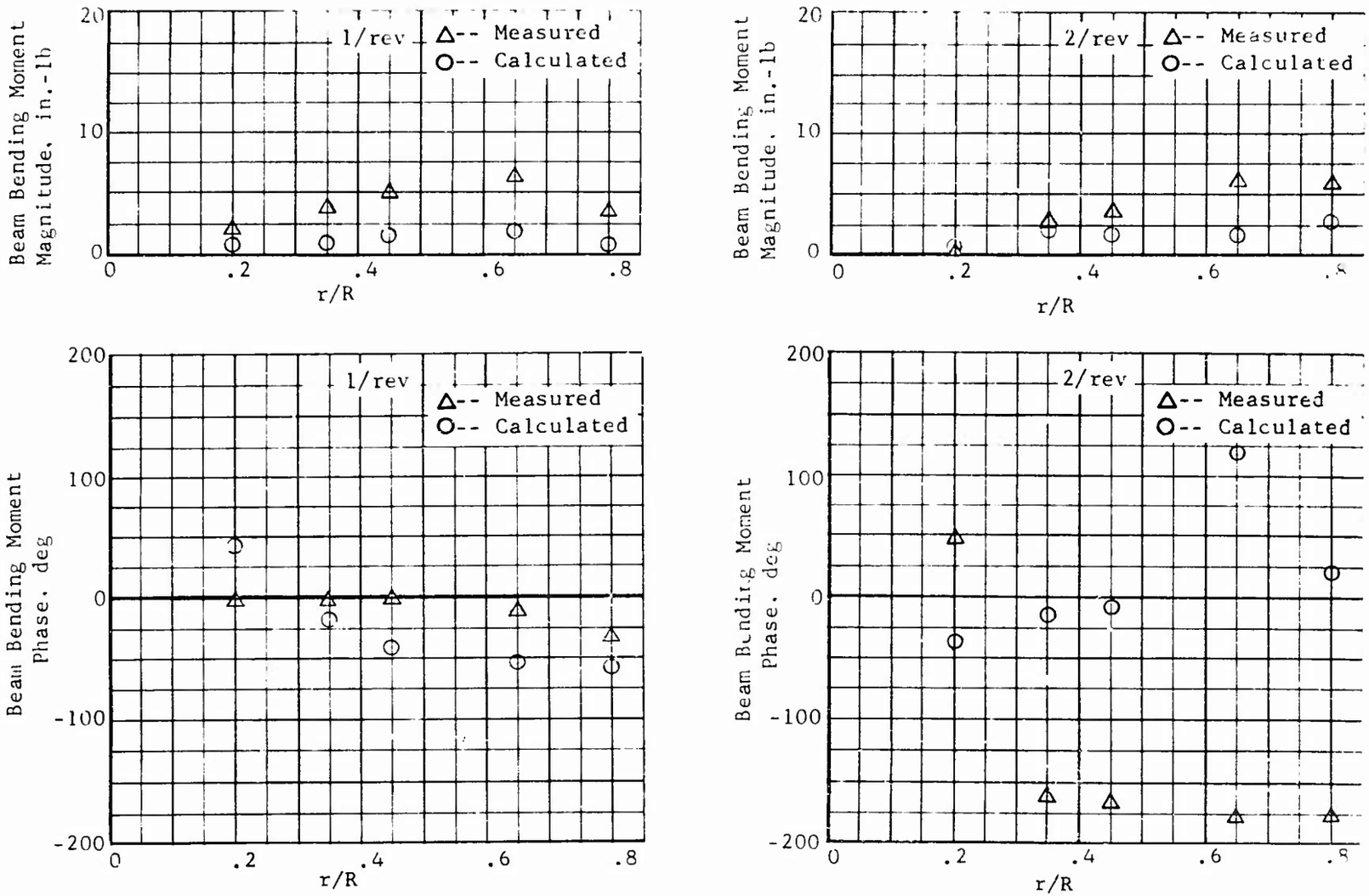

Figure 95. Measured and Calculated Beam Bending Moment Harmonics, Aluminum Blade, 0° Twist, $\mu = 0.502$, $M_{1,90} = 0.467$, $\alpha_m = 5°$ (Cond. 44).

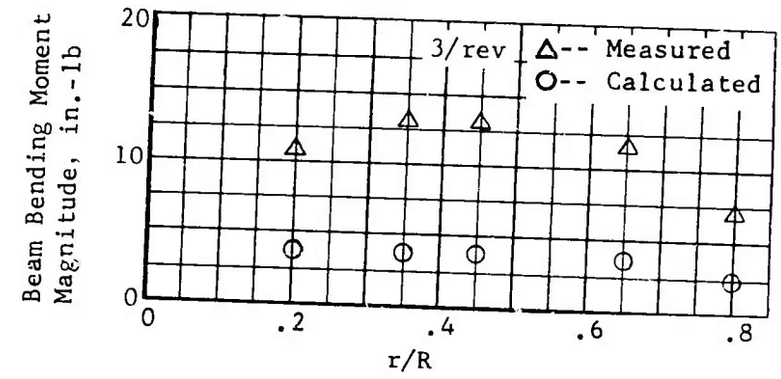

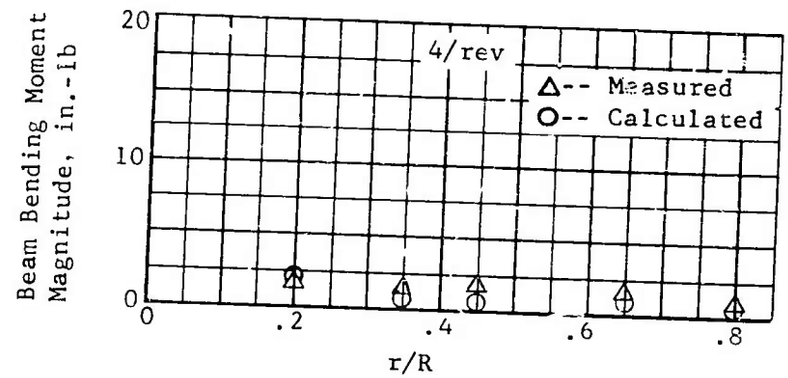

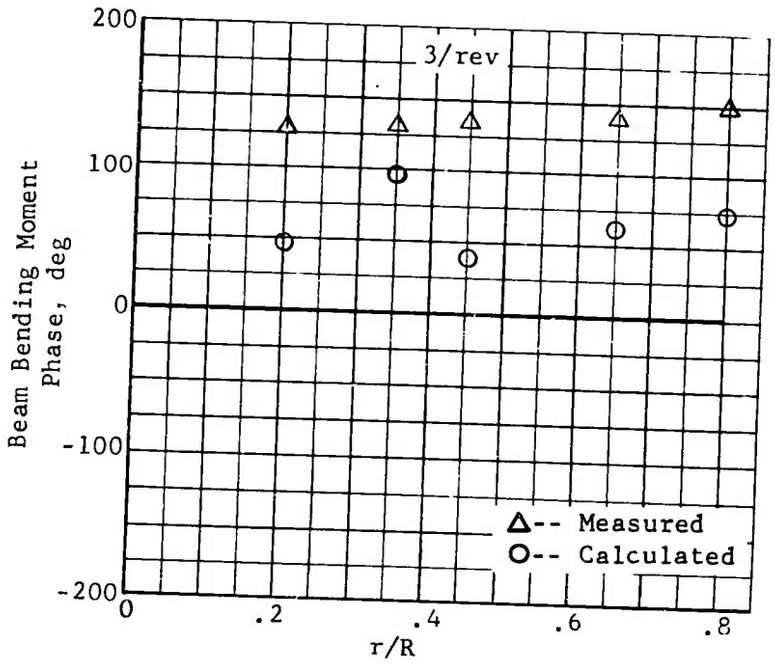

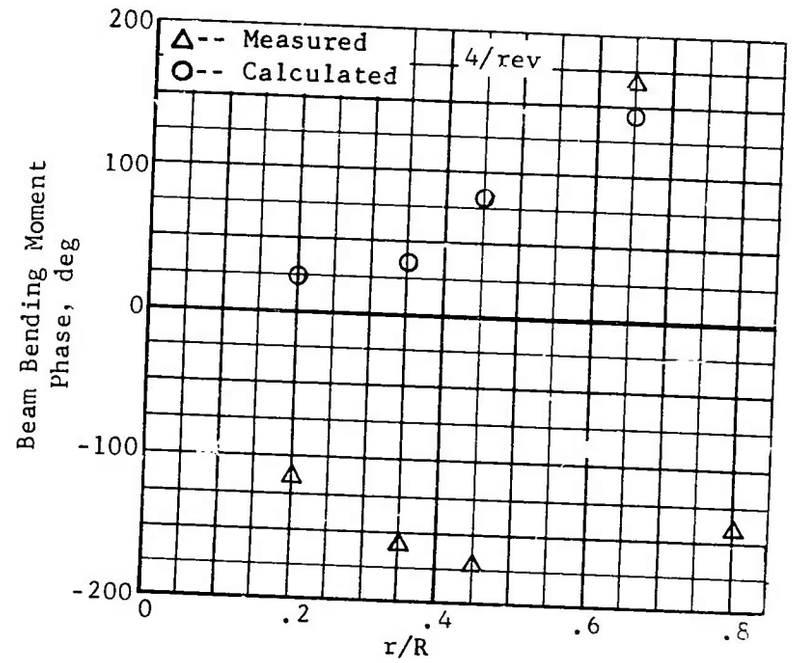

Figure 95. Concluded.

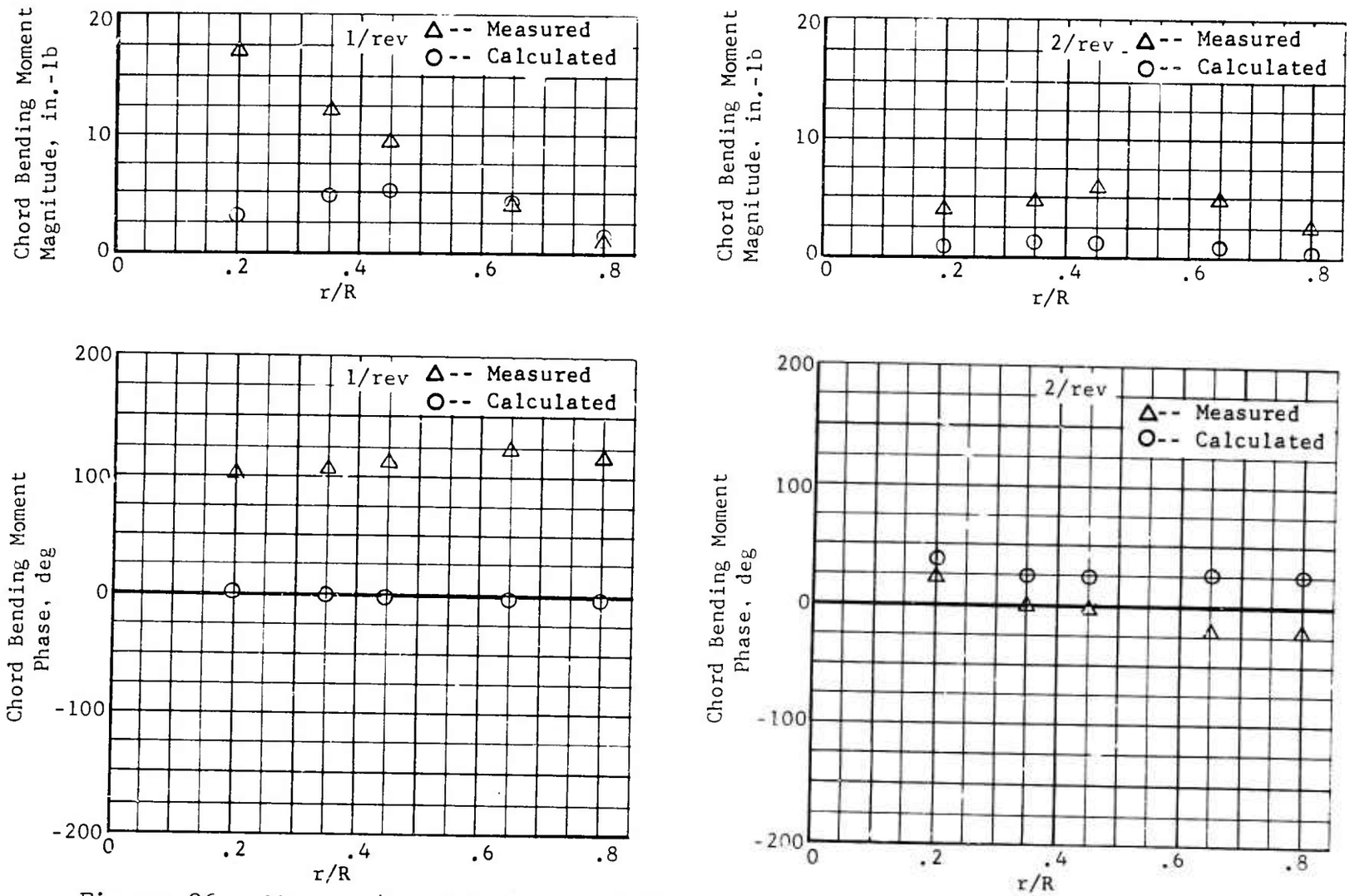

Figure 96. Measured and Calculated Chord Bending Moment Harmonics, Aluminum Blade, 0° Twist, $\mu = 0.502$, $M_{1,90} = 0.467$, $\alpha_m = 5°$ (Cond. 44).

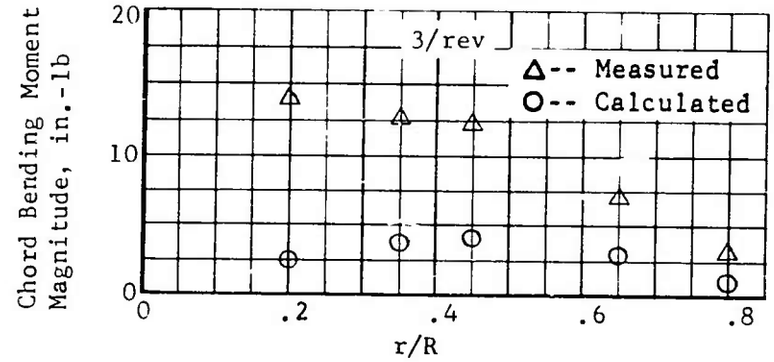

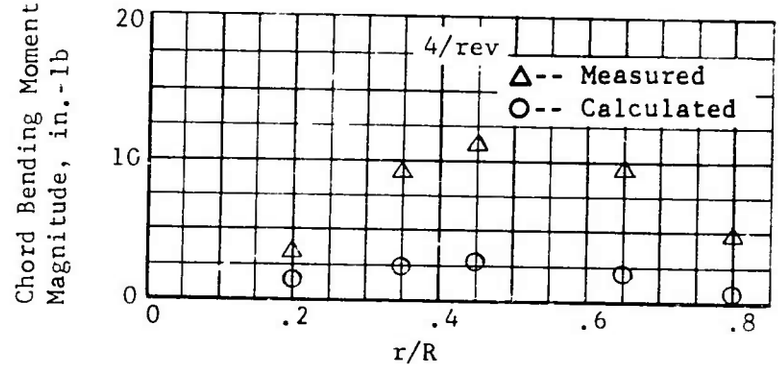

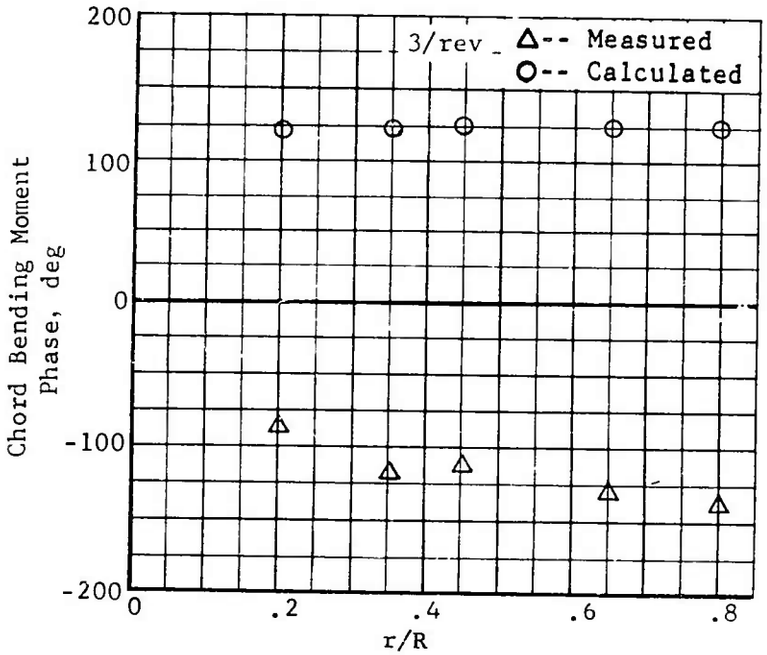

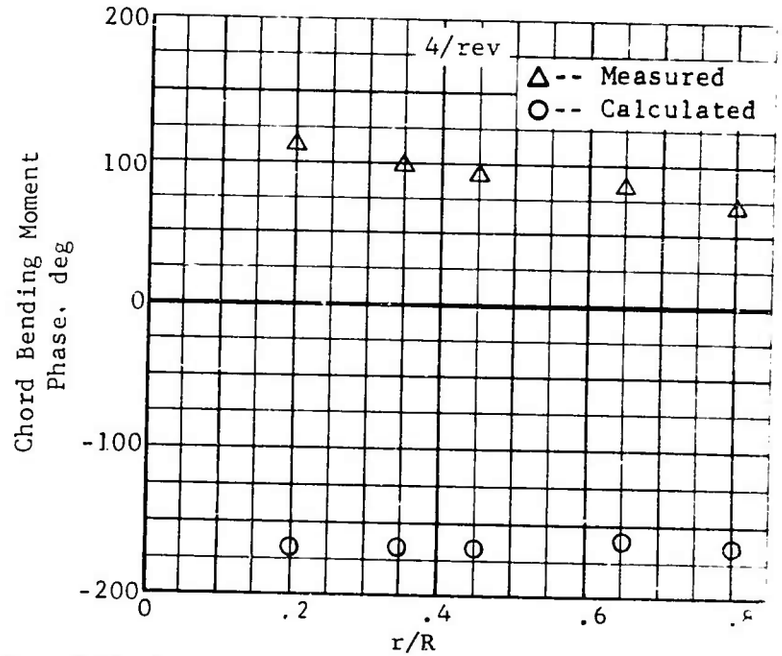

Figure 96. Concluded.

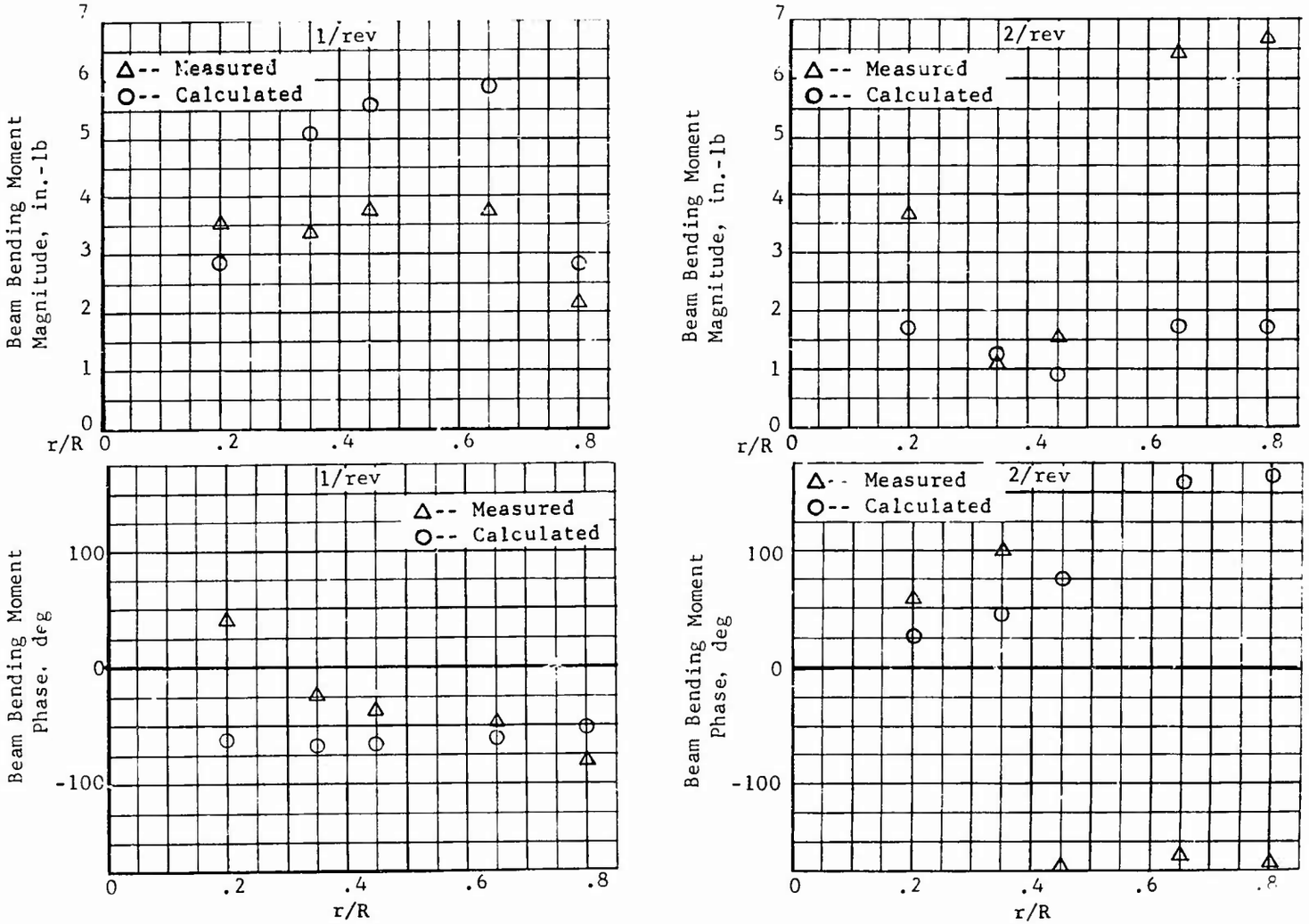

Figure 97. Measured and Calculated Beam Bending Moment Harmonics, Aluminum Blade, 0° Twist, $\mu = 0.299$, $M_{1,90} = 0.408$, $\alpha_m = 0°$ (Cond. 68).

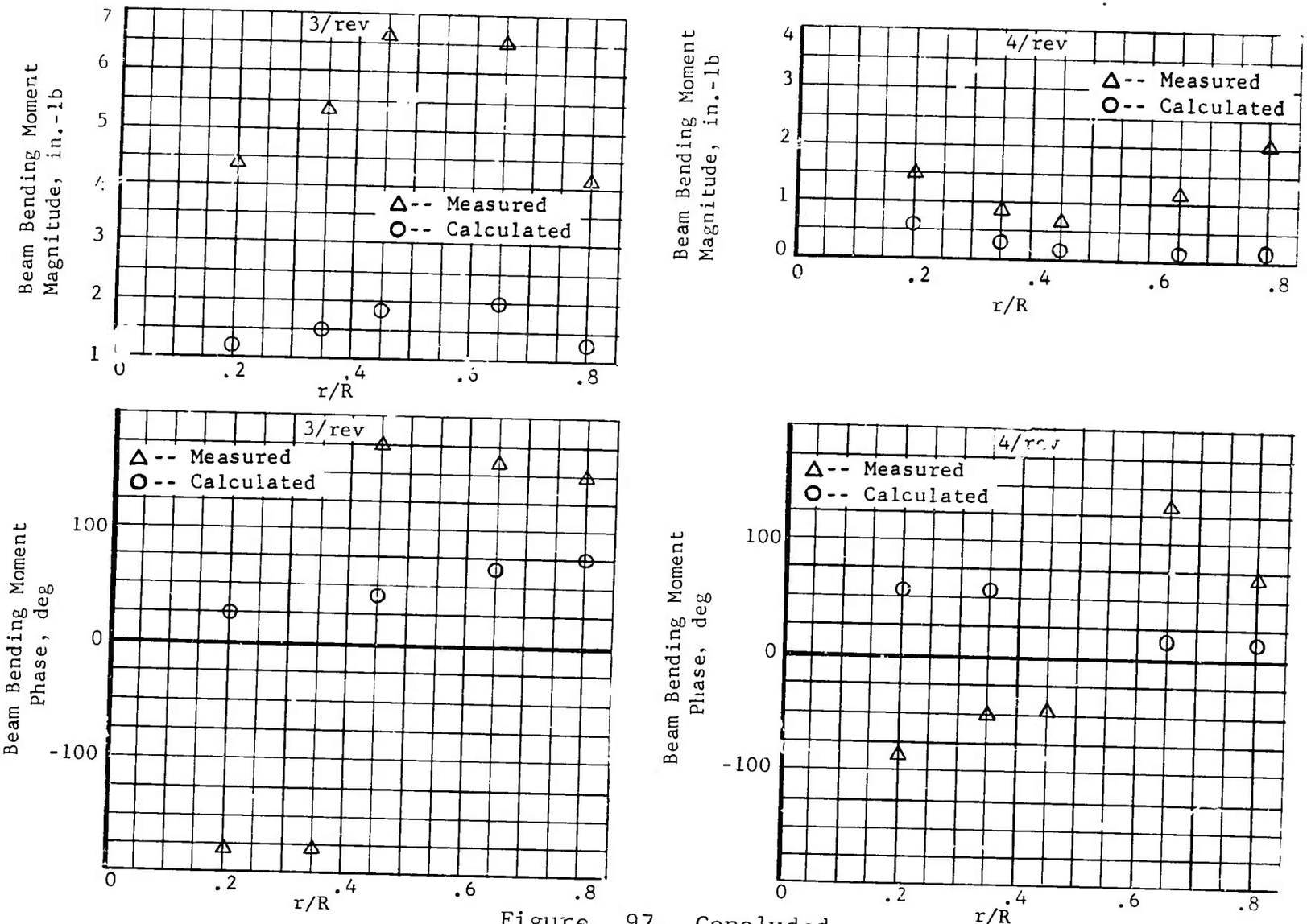

Figure 97. Concluded.

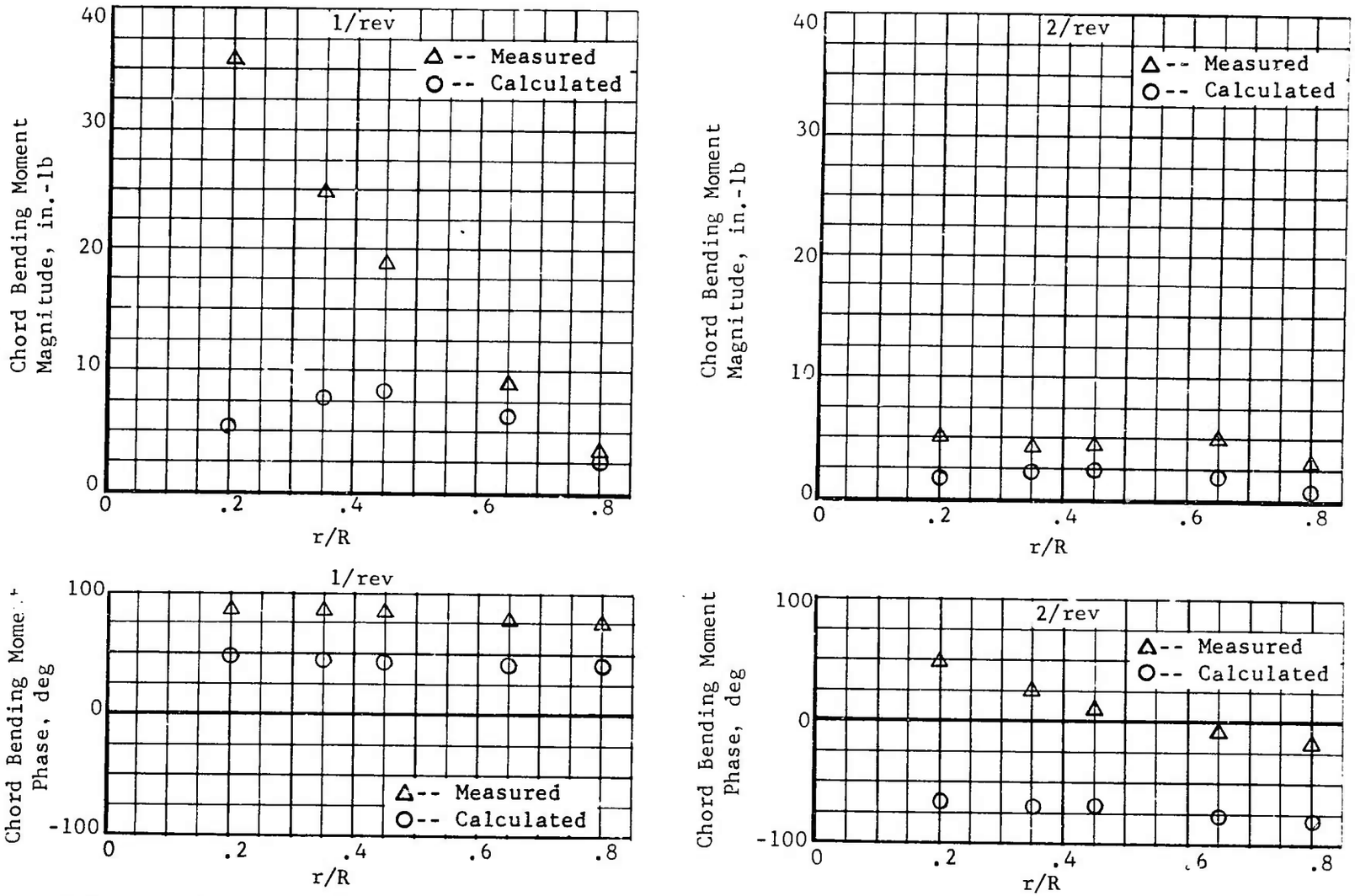

Figure 98. Measured and Calculated Chord Bending Moment Harmonics, Aluminum Blade, 0° Twist. $\mu = 0.299$, $M_{1,90} = 0.408$, $\alpha_m = 0°$ (Cond. 68).

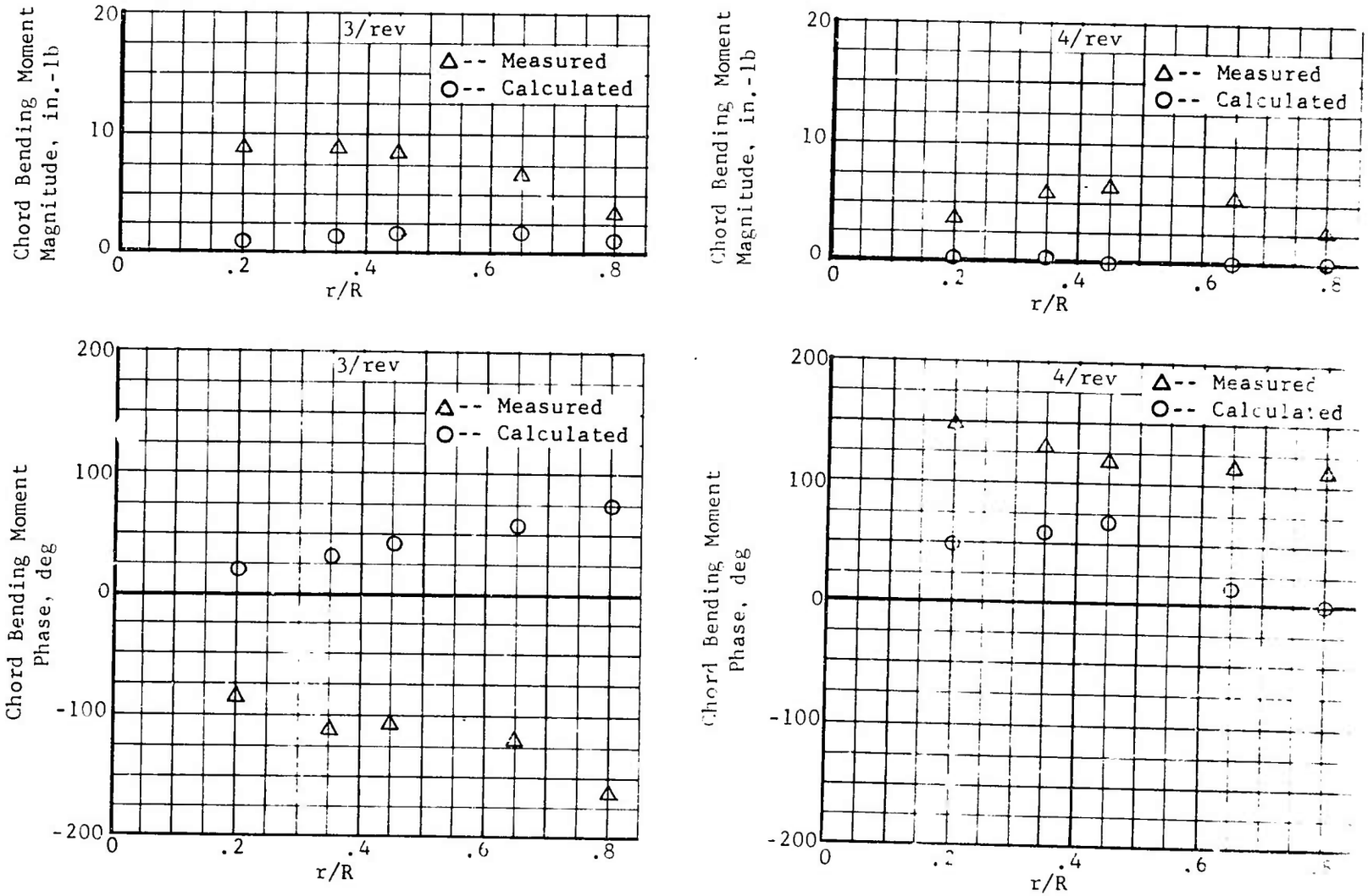

Figure 98. Concluded.

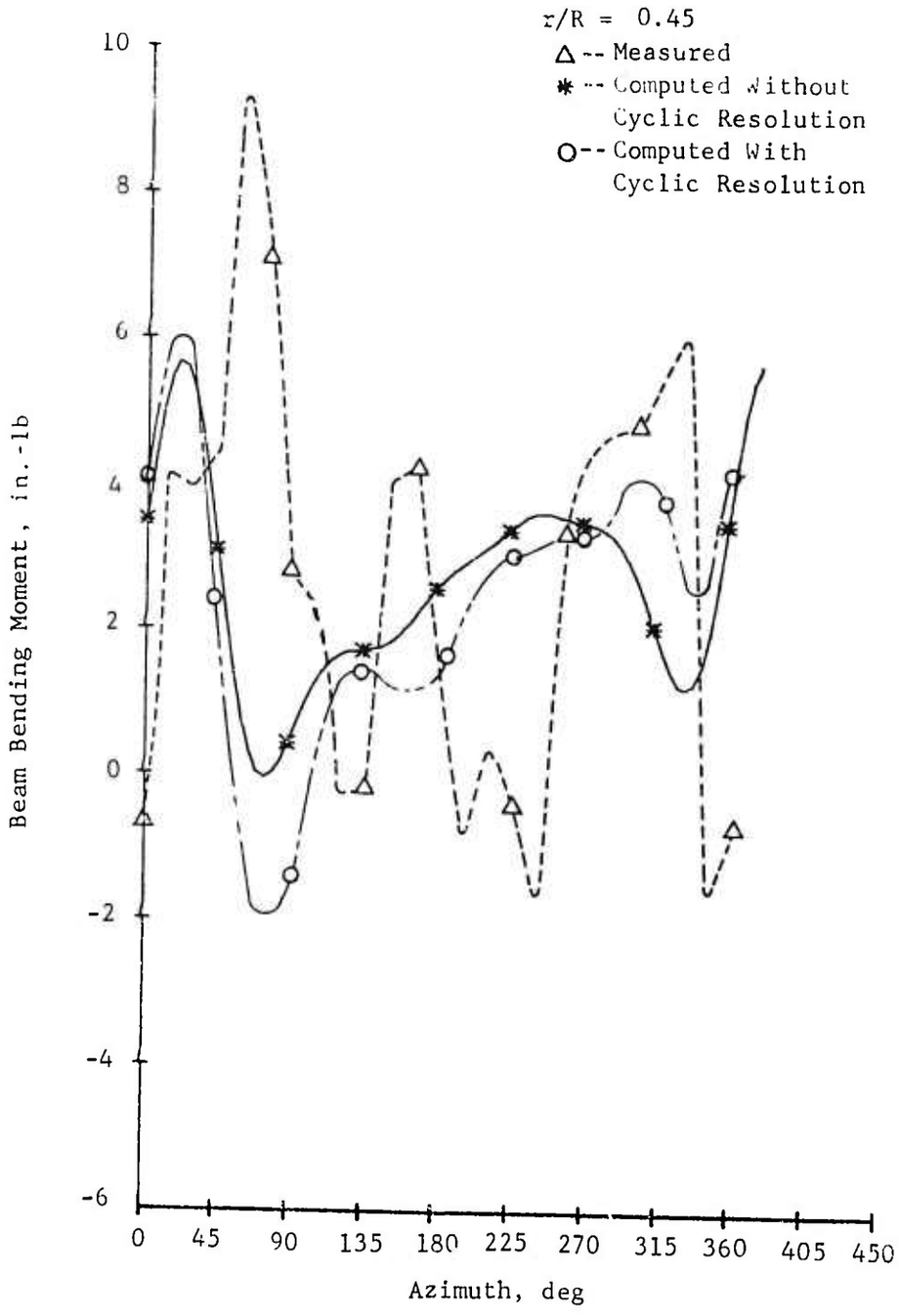

Figure 99. Example of Effect of Cyclic Pitch Resolution Angle Change in Beam Bending Moment of Fiberglass Blade, 0° Twist, $\mu = 0.399$, $M_{1,90} = 0.434$, $\alpha_m = 0.5°$ (Cond. 25).

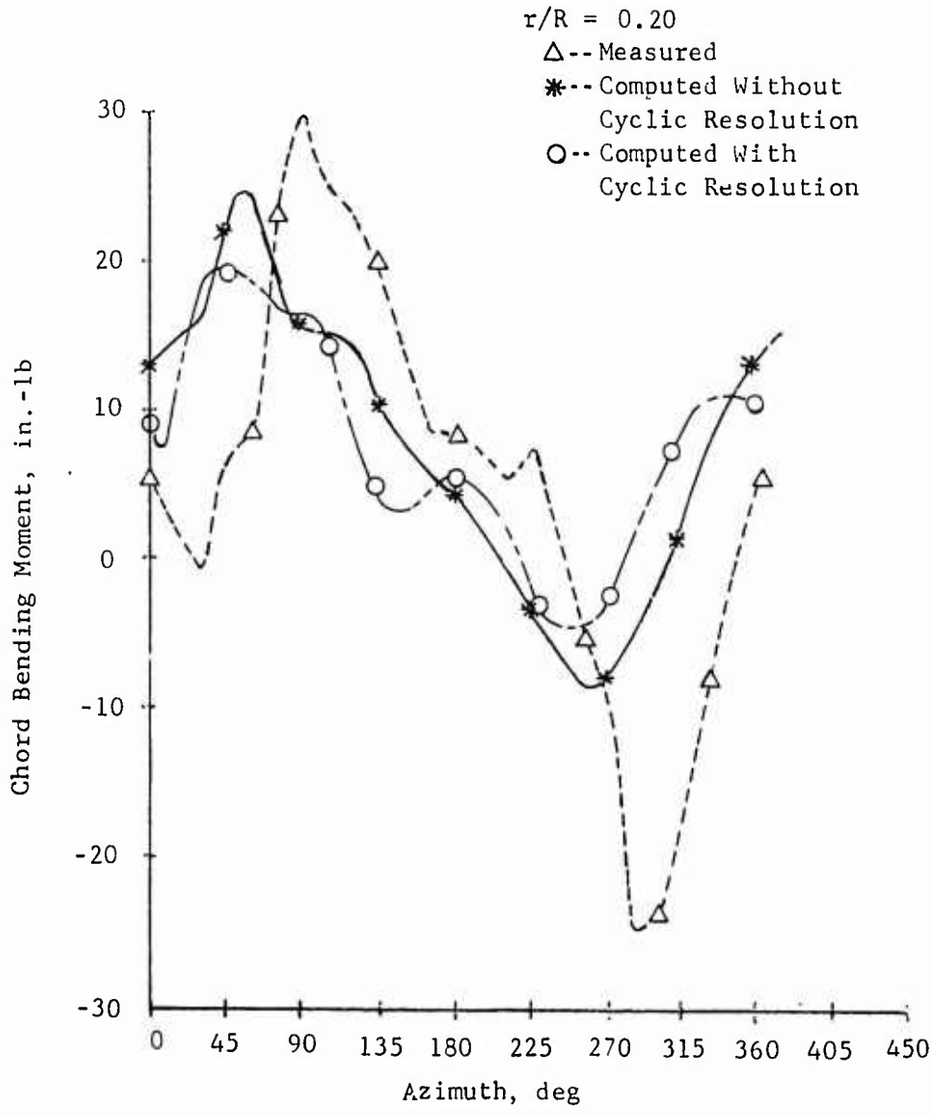

Figure 100. Example of Effect of Cyclic Pitch Resolution Angle Change on Chord Bending Moment of Fiberglass Blade, 0° Twist, $\mu = 0.399$, $M_{1,90} = 0.434$, $\alpha_m = 0.5°$ (Cond. 25).

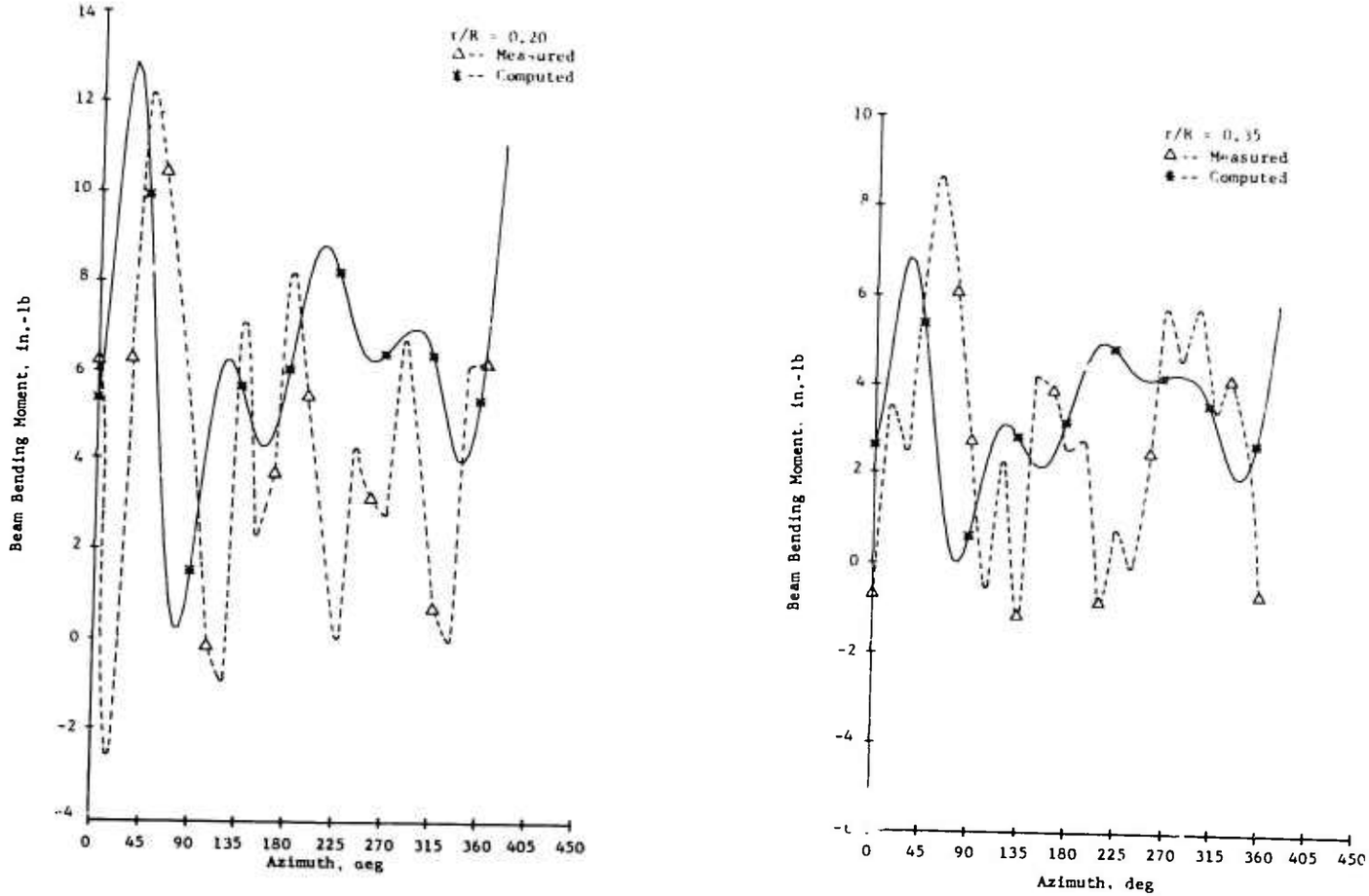

Figure 101. Measured and Calculated Beam Bending Moment Time Histories, Fiberglass Blade, 0° Twist, $\mu = 0.399$, $M_{1,90} = 0.434$, $\alpha_m = 0.5°$ (Cond. 25). Unsteady Aerodynamics Effects Activated.

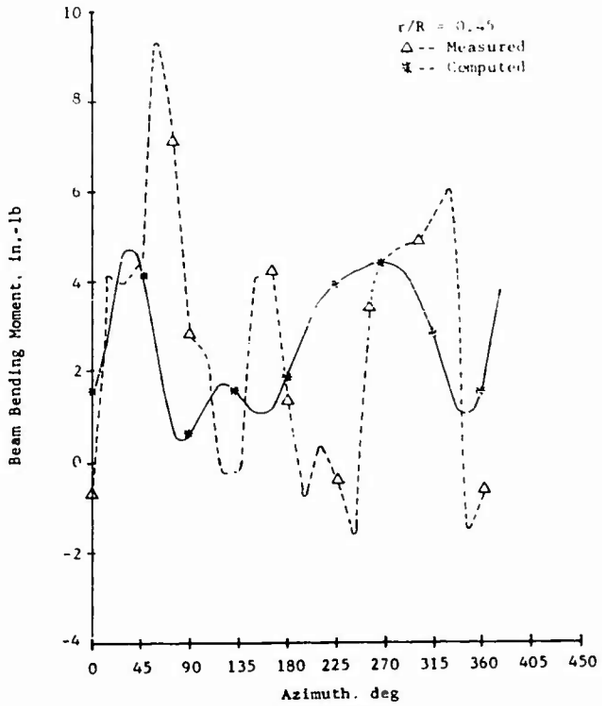

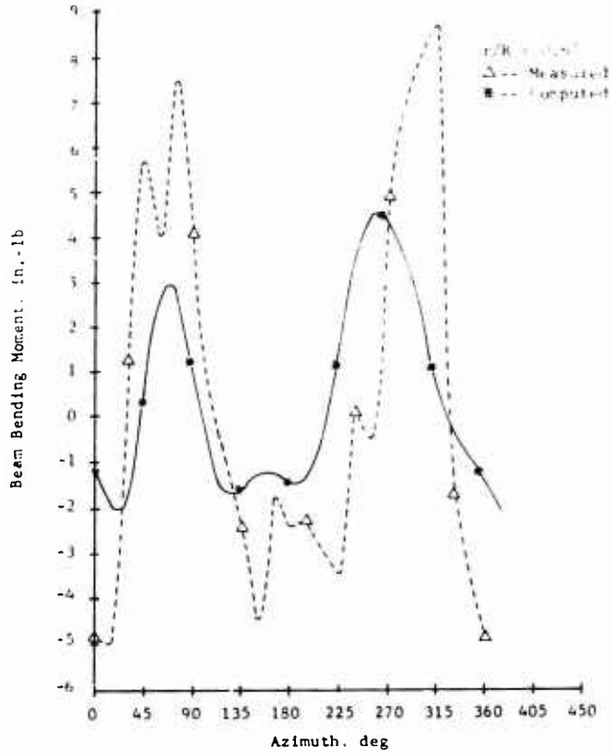

Figure 101. Continued.

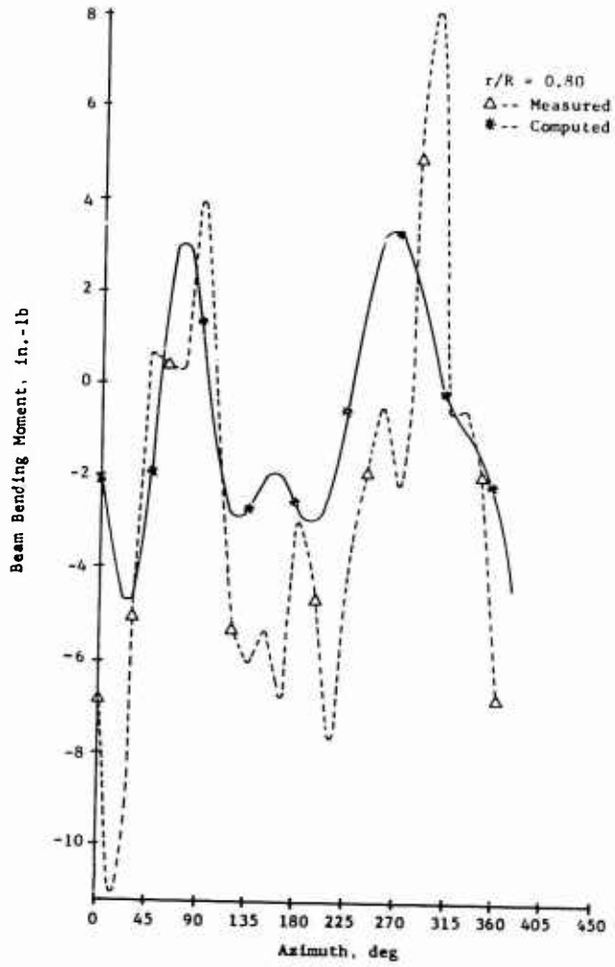

Figure 101. Concluded.

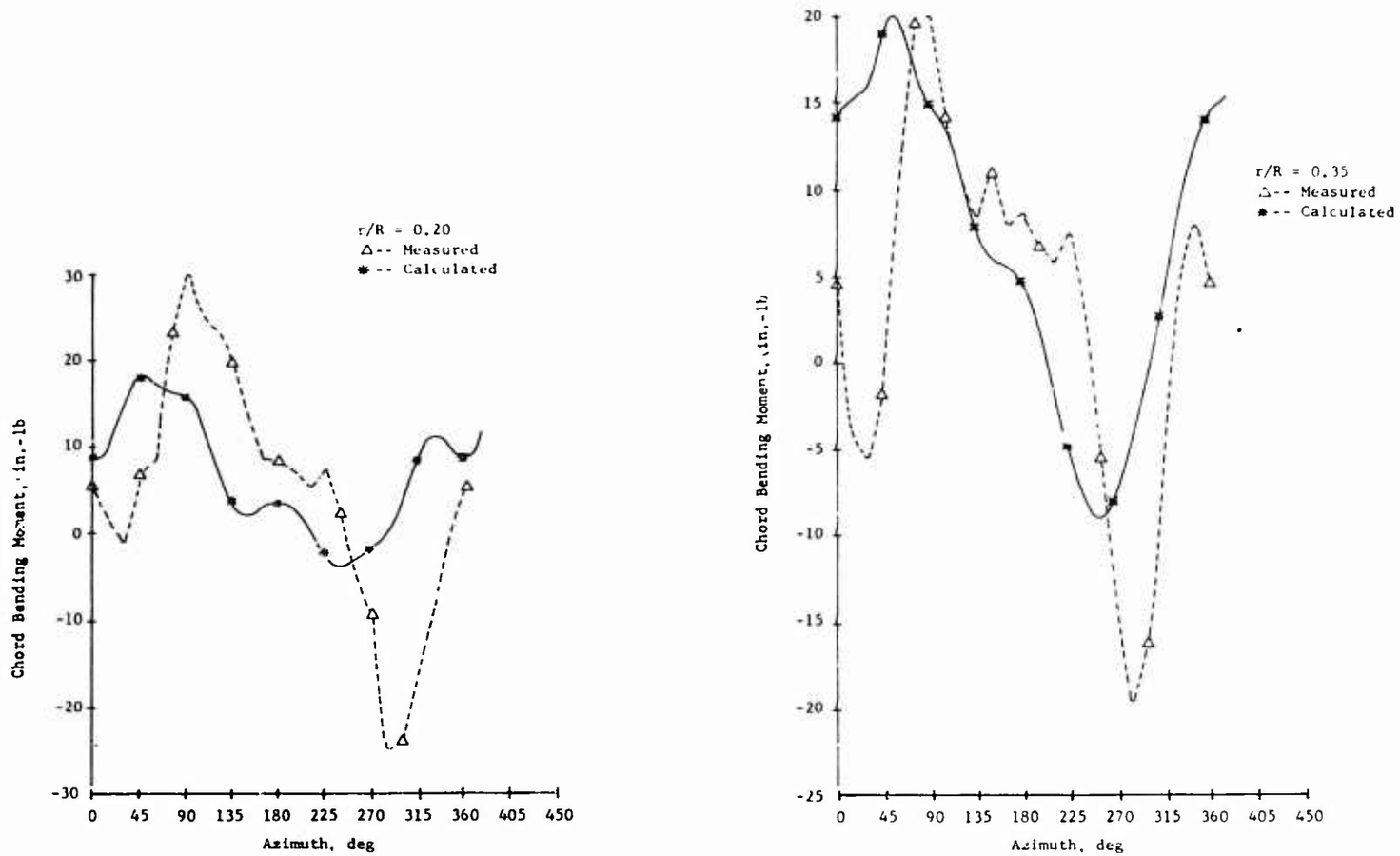

Figure 102. Measured and Calculated Chord Bending Moment Time Histories, Fiberglass Blade, 0° Twist, $\mu = 0.399$, $M_{1,90} = 0.434$, $\alpha_m = 0.5^\circ$ (Cond. 25) Unsteady Aerodynamics Effects Activated.

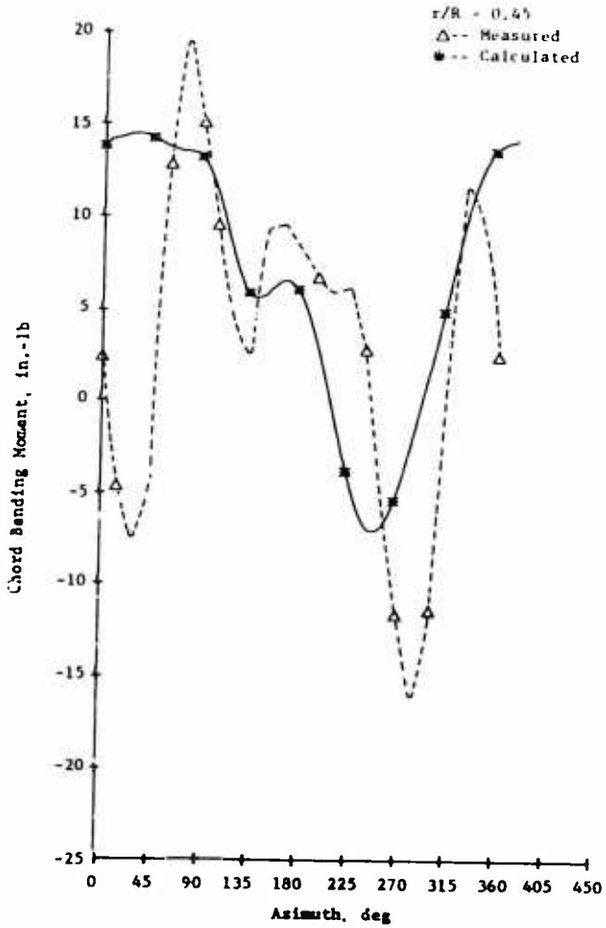

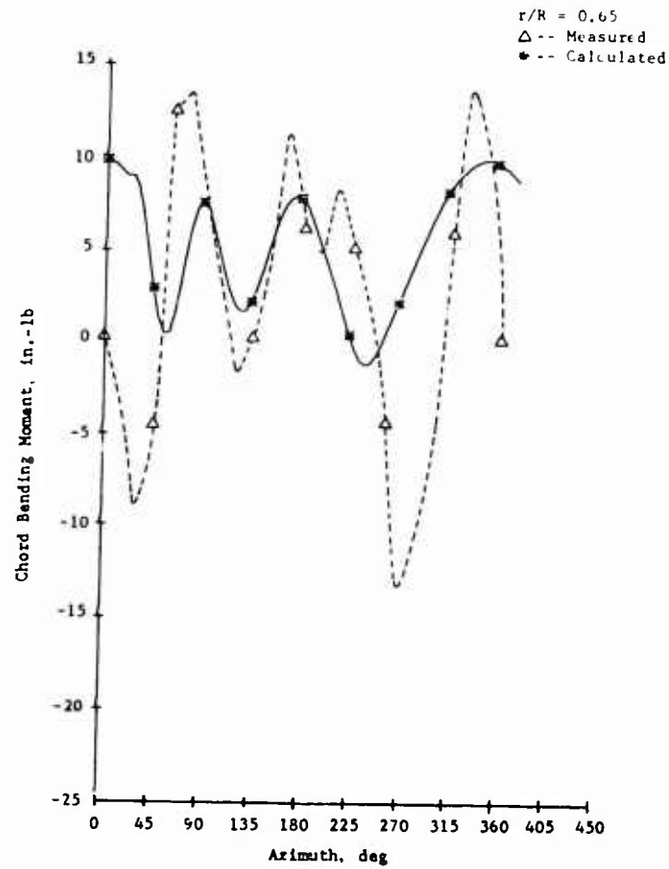

Figure 102. Continued.

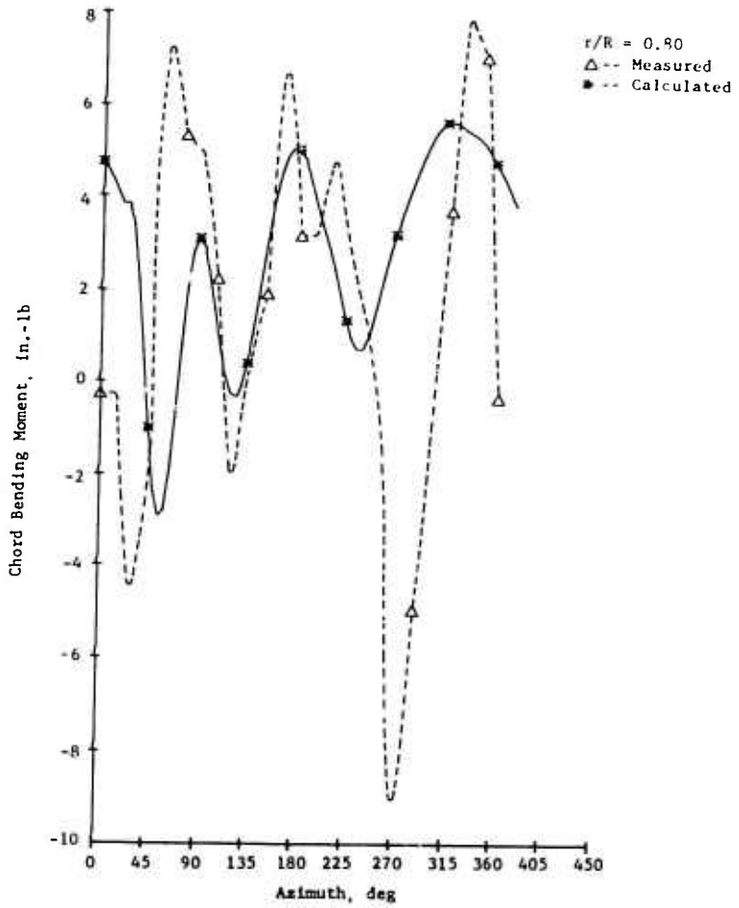

Figure 102. Concluded.

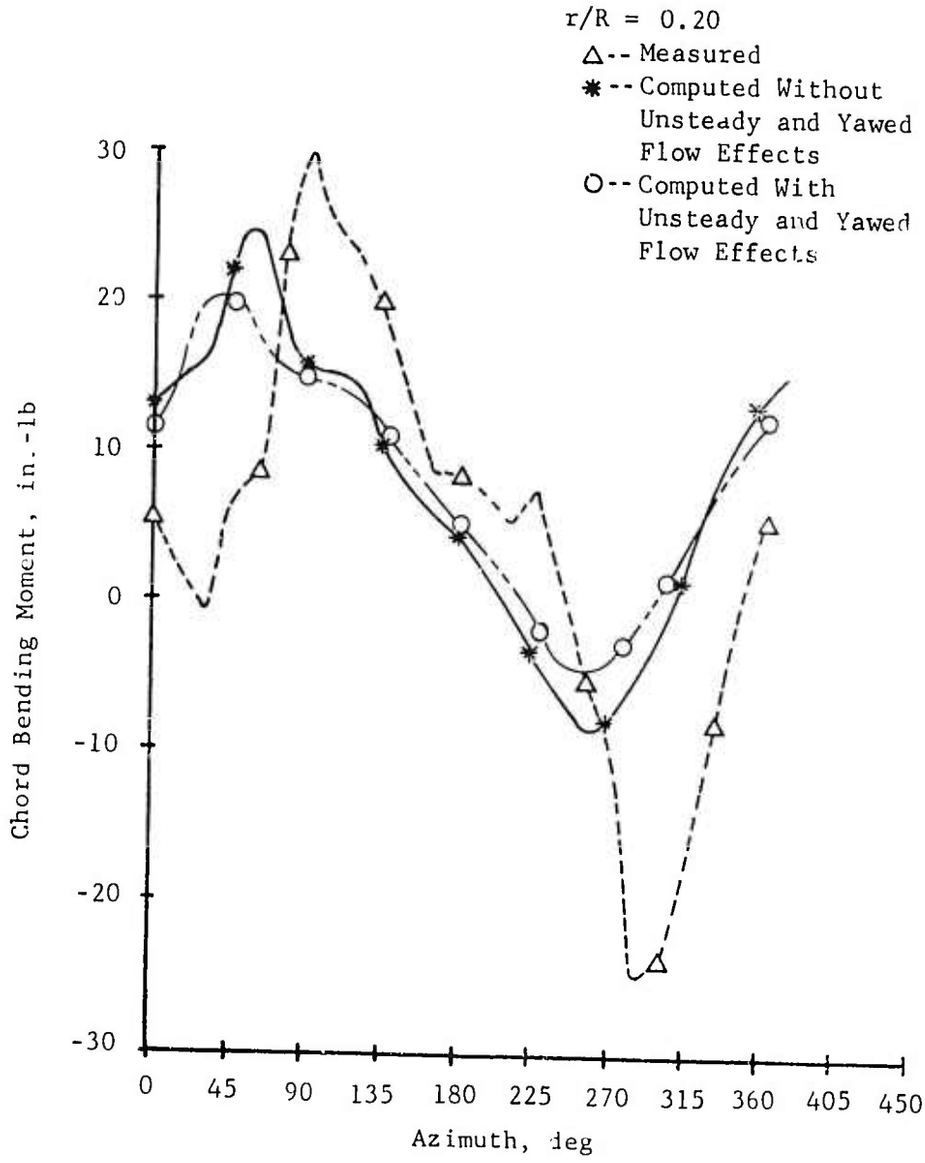

Figure 103. Example of Effect of Unsteady Aerodynamics and Yawed Flow Effects on Chord Bending Moment Fiberglass Blade, 0° Twist, $\mu = 0.399$, $M_{1,90} = 0.434$, $\alpha_m = 0.5°$ (Cond. 25).

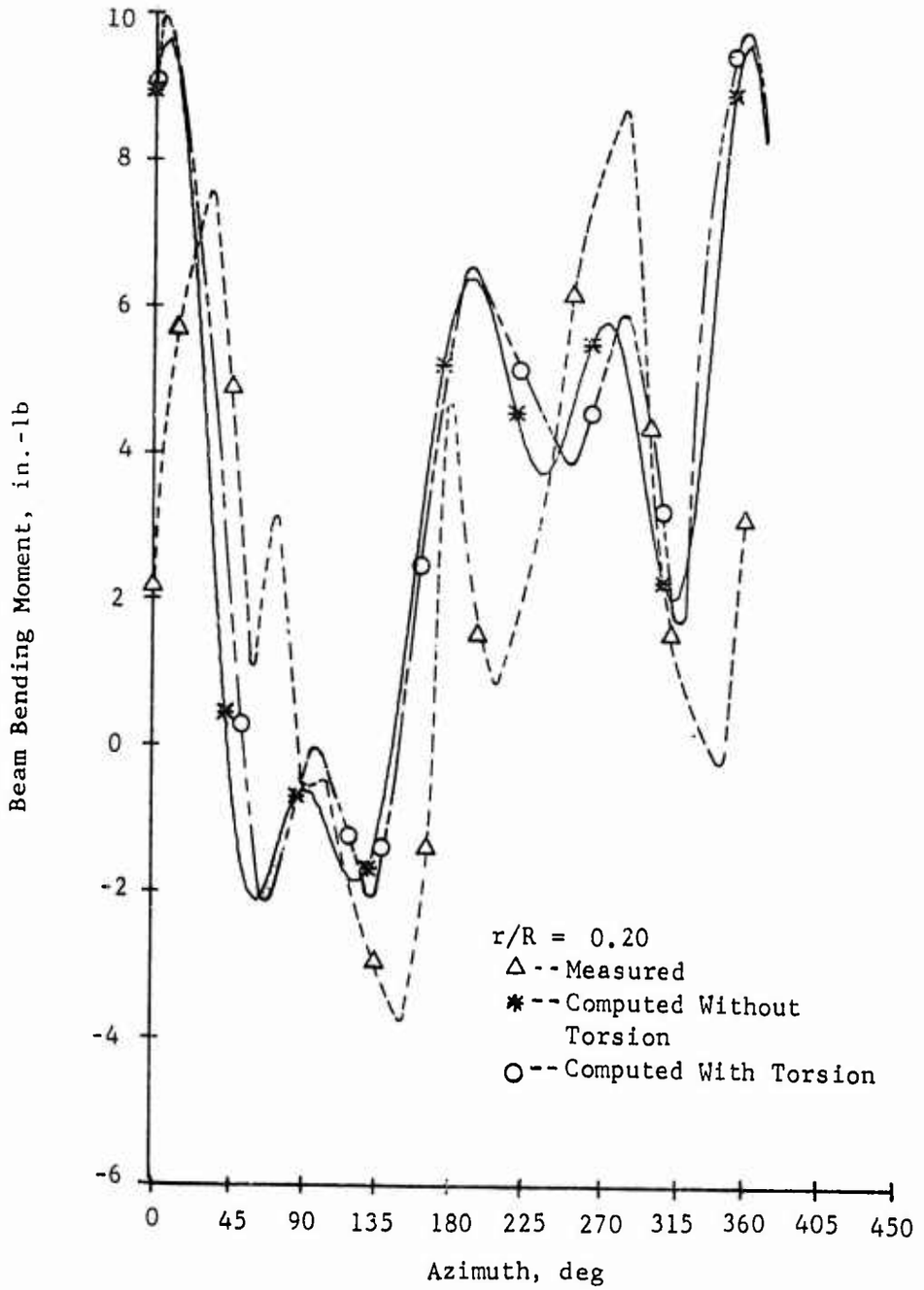

Figure 104. Example of Effect of Addition of Torsional Mode Shape Fiberglass Blade, -8° Twist, $\mu = 0.502$, $M_{1,90} = 0.467$, $\alpha_m = 0.5°$ (Cond. 25).

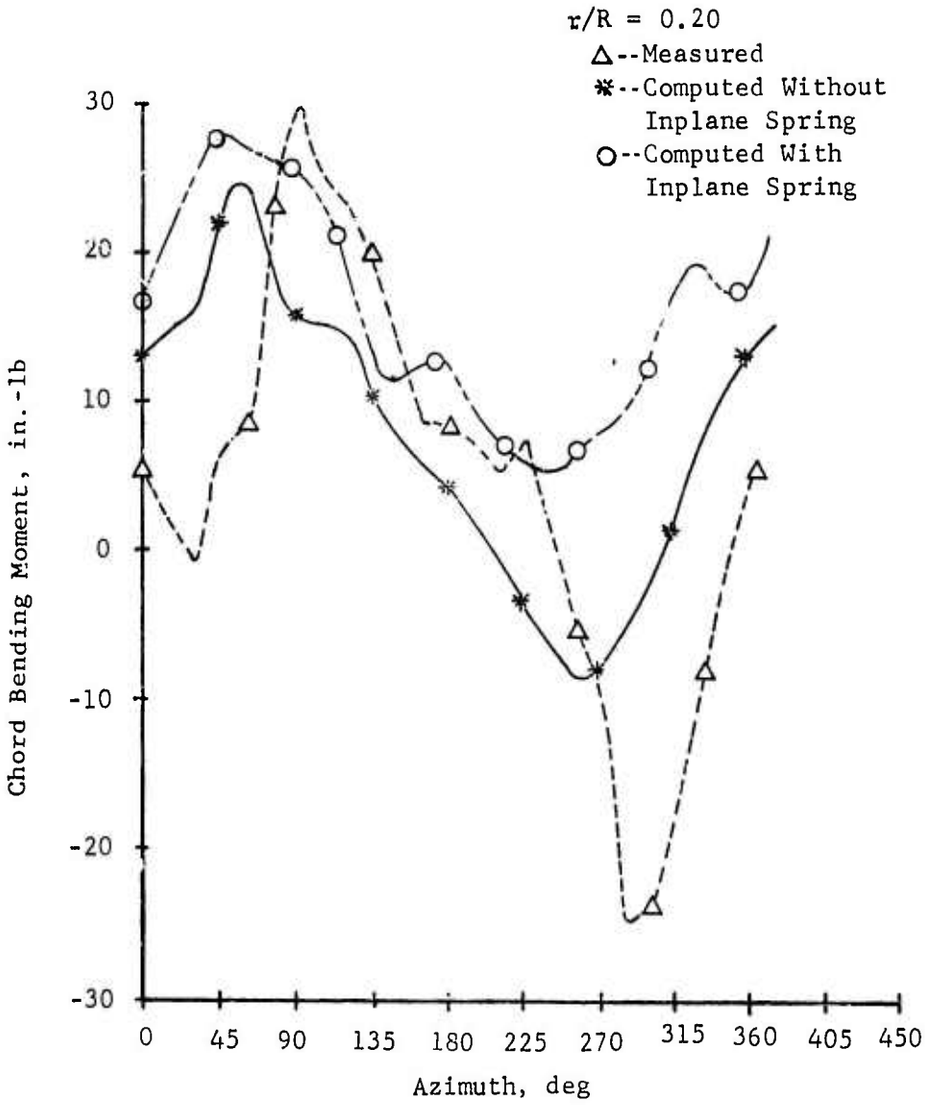

Figure 105. Example of Effect of Inplane Spring Fiberglass Blade, 0° Twist, $\mu = 0.399$, $M_{1,90} = 0.434$, $\alpha_m = 0.5°$ (Cond. 25).

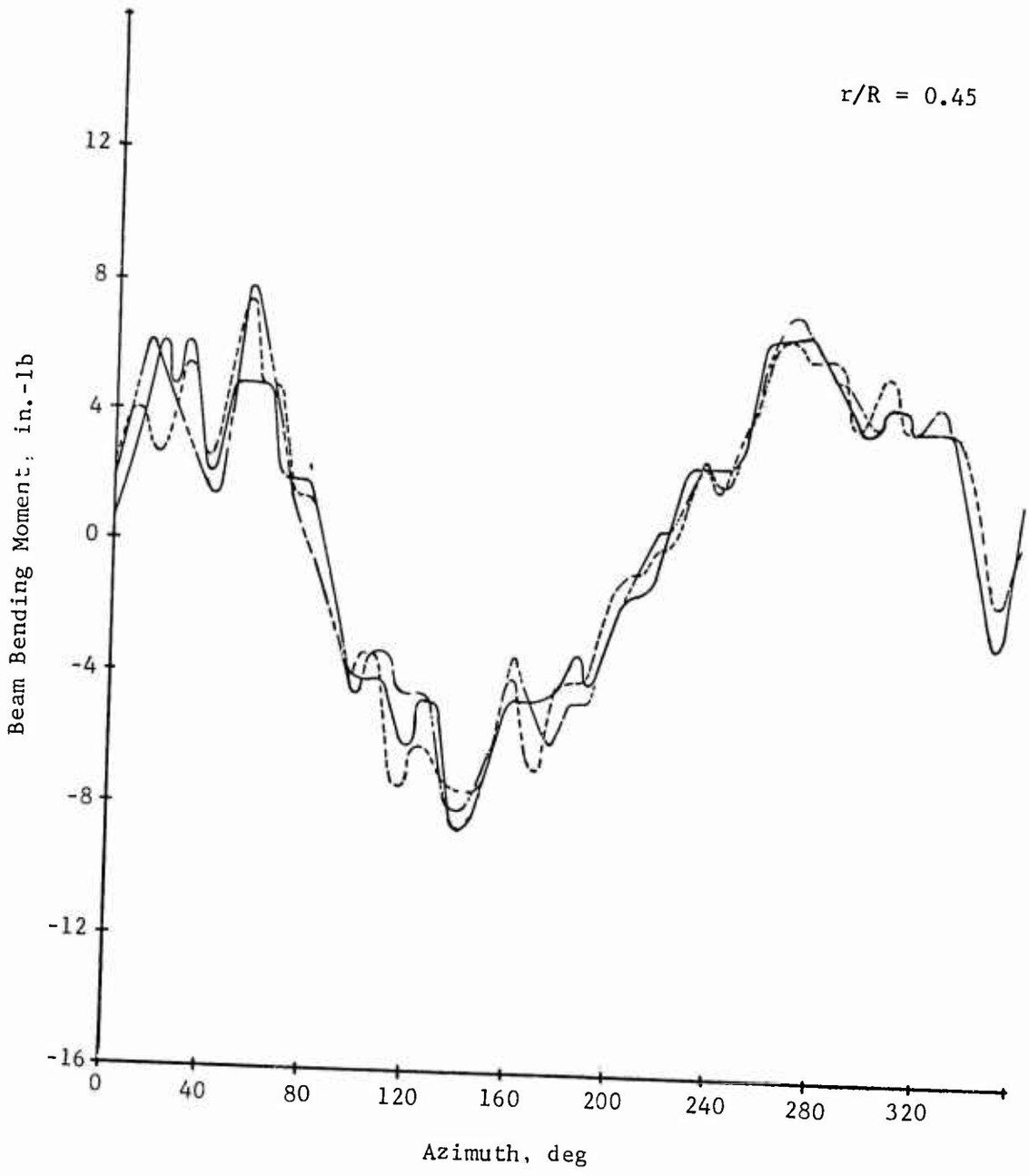

Figure 106. Three Successive Revolutions of Beam Bending Moment Time History, Fiberglass Blade, -8° Twist, $\mu = 0.399$, $M_{1,90} = 0.43$, $\alpha_m = 0.5°$ (Cond. 25).

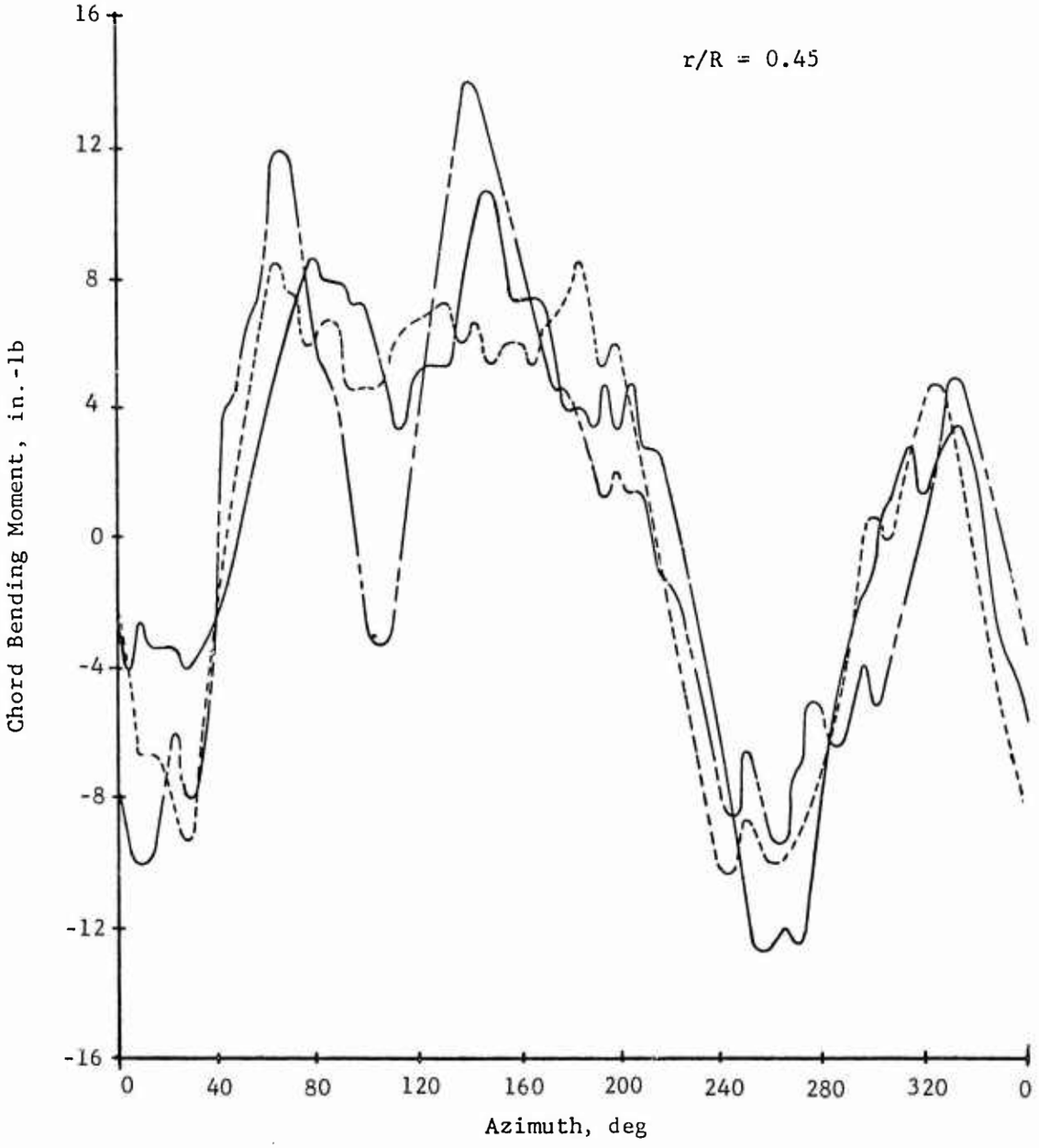

Figure 107. Three Successive Revolutions of Chord Bending Moment Time History, Fiberglass Blade, -8° Twist, $\mu = 0.399$, $M_{1,90} = 0.434$, $\alpha_m = 0.5°$ (Cond. 25).

TABLE 1. H-34 FIBERGLASS MODEL ROTOR BLADE STIFFNESS PROPERTIES

Δr (in.)	r_{in} (in.)	I_x (in.^{4})	I_y (in.^{4})	J (in.^{4})
.23	3.00	.466	2.68	2.37
.52	3.23	.578	3.54	
.28	3.75	1.870	5.32	
.30	4.03	.268	.268	
.45	4.33	1.600	1.600	2.37
.62	4.78	1.030	1.030	1.36
.63	5.40	.814	.814	1.36
.22	6.03	1.120	1.129	1.99
.28	6.25	.330	.359	.52
.54	6.53	.336	.332	.50
.56	7.07	.1907	.1497	.36
.65	7.63	.0711	.0712	.0440
.125	8.28	.003148	.02190	.0070
.495	8.405	.00916	.01730	.00427
3.630	8.900	.001236	.01240	.00370
.270	12.53	.001236	.01240	.00343
41.035	12.80	.001060	.01152	.00319
.320	53.835	.00057	.00625	.00174
.845	54.155	.00057	.00625	.00174

NOTE: The following values of E and G should be used to obtain bending and twisting stiffnesses for the fiberglass blades:

$$E = 2.50 \times 10^6 \text{ lb/in.}^2$$
$$G = 1.01 \times 10^6 \text{ lb/in.}^2$$

TABLE 2. H-34 ALUMINUM MODEL ROTOR BLADE STIFFNESS PROPERTIES

Δr (in.)	r_{in} (in.)	I_x (in.^{4})	I_y (in.^{4})	J (in.^{4})
.23	3.00	.117	.670	.600
.52	3.23	.145	.885	
.28	3.75	.468	1.330	
.30	4.03	.0670	.0670	
.45	4.33	.400	.400	.600
.62	4.78	.258	.258	.344
.63	5.40	.204	.204	.344
.22	6.03	.280	.280	.503
.28	6.25	.0825	.0898	.132
.54	6.53	.0840	.0830	.127
.56	7.07	.0477	.0374	.0911
.65	7.63	.05456	.0574	.0367
.125	8.28	.002415	.0177	.00583
.495	8.405	.001504	.0140	.00356
3.630	8.90	.000948	.0100	.00308
.270	12.53	.000948	.0100	.00286
41.035	12.80	.000813	.00929	.00266
.320	53.835	.000437	.005041	.00145
.845	54.155	.000437	.005041	.00145

NOTE: The following values of E and G should be used to obtain bending and twisting stiffnesses for the aluminum blade:

$E = 10.0 \times 10^6$ lb/in.^{2}

$G = 4.00 \times 10^6$ lb/in.^{2}

The values of I_x, I_y, and J between r = 8.28 in. and r = 53.835 in. have been corrected to reflect the stiffness test results for the aluminum blade.

TABLE 3. H-34 MODEL ROTOR BLADE INERTIA AND CENTER OF GRAVITY DATA

Δr (in.)	r_{in} (in.)	w (lb/in.)	ρI_x (10^{-3} lb-sec^2)	ρI_y (10^{-3} lb-sec^2)	Y_{cg} (in.)
.23	3.00	.147	.0036	.177	.33
.52	3.23	.147	|	|	.33
.28	3.75	.475	|	|	.10
.20	4.03	.149	|	|	.33
.10	4.23	.162	.0036	.177	.30
.17	4.33	.180	.0801	.254	.27
.14	4.50	.273	.0801	.254	.18
.14	4.64	.343	.0801	.254	.14
.62	4.78	.343	.0928	.266	.14
.17	5.40	.343	.0892	.0892	0.0
.07	5.57	.295	|	|	|
.27	5.64	.112	|	|	|
.12	5.81	.169	.0892	.0892	|
.22	6.03	.169	.0645	.0645	|
.23	6.25	.048	.0177	.0177	|
.54	6.53	.0822	.0193	.0199	|
.56	7.07	.0588	.0111	.00955	|
.65	7.63	.0414	.0042	.00504	|
.125	8.28	.0176	.00037	.00314	|
.495	8.405	.0081	.00025	.00268	|
3.630	8.90	.0094	.00013	.0086	|
.270	12.53	.0106	.00014	.0089	|
40.135	12.80	.0121	.00018	.0114	|
.72	52.935	.0202	.00034	.0221	|
.18	53.655	.0178	.00034	.0221	|
.32	53.835	.0276	.00034	.0221	|
.845	54.155	.0044	.00009	.00571	0.0

NOTES:
1. Mass moments of inertia are with respect to the local chord line and an axis normal to it at the feathering axis.
2. Mass moments of inertia include parts at the root that flap, lag, and pitch with the blade. Parts that flap and lag but do not pitch are excluded.
3. The flapwise position of the blade center of gravity is on the chord line for all blade stations.

TABLE 4. H-34 MODEL ROTOR BLADE MISCELLANEOUS DATA

Item	Parameter or Description	Value	Units
1	Radius	55.0	in.
2	Blade Airfoil Chord Outboard of 8.9" Radial Station	2.69	in.
	Blade Shank Chord Inboard of 8.9" Radial Station	1.19	in.
3	Blade Linear Twist From Center of Rotation to Tip		
	Blade Sets a, c, d	0.0	deg
	Blade Set b	-8.0	deg
5	Blade Shear Center Locations		
	Beamwise With Respect to Feathering Axis	0.0	in.
	Chordwise With Respect to Feathering Axis	0.0	in.
6	Location of Blade Hinges		
	Radial Station of Coincident Flapping and Lead-Lag Hinge	3.0	in.
	Feathering Bearing Outboard End Radial Station	5.60	in.
	Feathering Bearing Inboard End Radial Stations	4.64	in.
	(The feathering, flapping and lag bearing axes intersect at the same poin.)		
7	Location of Lead-Lag Damper		
	Rotary Damper on Blade Lead-Lag Hinge		
8	Pitch Flap Coupling Ratio	0.0	
9	Damping Coefficient of Lead-Lag Damper (Expressed as a damping moment about the hinge)	17.0	in.-lb-sec
10	Tabs or Flaps		
	Blade Set c Deflection Over the Aft 20% of the Airfoil Chord	5.0	deg

TABLE 4. H-34 MODEL ROTOR BLADE MISCELLANEOUS DATA (Cont'd.)

Item	Parameter or Description	Value	Units
11	Pitch Control Geometry		
	At 0° Collective and Cyclic Input:		
	Distance Aft Along Flapping Hinge Axis to Pushrod Upper End	1.43	in.
	Radius on Swashplate of Pushrod Lower End	1.95	in.
	Distance of Plane of Swashplate Below Plane of Flapping Hinges	6.31	in.
	Angle on Swashplate Between Pushrod Lower End and Plane of Shaft and Lead-Lag Axis	40.5	deg
	Pitch Control Spring Rate	21,000	in.-lb/rad
	Airfoil Section - NACA 0012		

TABLE 5. H-34 FIBERGLASS MODEL ROTOR BLADE EQUAL SEGMENT STIFFNESS PROPERTIES

Station No.	EI_x (10^6 lb-in.^{2})	EI_y (10^6 lb-in.^{2})	GJ (10^4 lb-in.^{2})
1	1.7	2.59	194.4
2	1.7	2.59	194.4
3	.460	.438	15.6
4	.00345	.0337	.396
5	.00292	.0302	.351
6	.00265	.0288	.322
7			
8			
9			
10			
11			
12			
13			
14			
15			
16			
17			
18			
19	.00265	.0288	.322
20	.00194	.0212	.238

TABLE 6. H-34 ALUMINUM MODEL ROTOR BLADE
EQUAL SEGMENT STIFFNESS PROPERTIES

Station No.	EI_x (10^6 lb-in.^{2})	EI_y (10^6 lb-in.^{2})	GJ (10^4 lb-in.^{2})
1	1.70	2.59	196.3
2	1.70	2.59	196.3
3	.757	.709	35.0
4	.0106	.109	1.30
5	.00896	.0975	1.67
6	.00813	.0930	1.07
7			
8			
9			
10			
11			
12			
13			
14			
15			
16			
17			
18			
19	.00813	.0930	1.07
20	.00595	.0685	.793

TABLE 7. H-34 MODEL ROTOR BLADE EQUAL SEGMENT INERTIA AND CENTER OF GRAVITY DATA

Station No.	w (lb/in)	ρI_x (10^{-3} lb-sec^2)	ρI_y (10^{-3} lb-sec^2)	Y_{cg} (in.)
1	.261	.0904	.209	0.0
2	.261	.0904	.209	-0.178
3	.0905	.0311	.0311	0.0
4	.00989	.000207	.00725	
5	.0105	.000148	.00960	
6	.0121	.000180	.0114	
7				
8				
9				
10				
11				
12				
13				
14				
15				
16				
17				
18				
19	.0121	.000180	.0114	
20	.0140	.000223	.0144	0.0

TABLE 8. H-34 MODEL ROTOR BLADE MODE TYPES, FREQUENCIES, AND INERTIAS

Fiberglass Blade, 0° Twist

Mode No.	Mode Type	Natural Frequency ω_n (per rev)	Generalized Inertia (lb-ft^2)
1	B	1.045	0.00660
2	C	0.305	0.00664
3	B	2.588	0.00455
4	C	3.171	0.00554
5	B	4.381	0.00546
6	C	7.538	0.00614

Fiberglass Blade, -8° Twist

1	B	1.045	0.00660
2	C	0.305	0.00664
3	B	2.594	0.00437
4	C	3.164	0.00535
5	B	4.387	0.00536
6	C	7.556	0.00589

Aluminum Blade, 0° Twist

1	B	1.045	0.00661
2	C	0.305	0.00668
3	B	2.769	0.00495
4	C	4.497	0.00561
5	B	5.282	0.00593
6	B	9.000	0.00606

B = Beamwise Mode
C = Chordwise Mode

Rotor Speed = 730 RPM
Root Collective Pitch = 12°

TABLE 9. CORRELATION CRITERIA

A. Mean Load and Rotor Performance

Excellent	0/5
Good	5/10
Fair	10/15
Poor	15/

B. Overall Amplitude or Phase

Excellent	0/10
Good	10/20
Fair	20/30
Poor	30/

C. Harmonic Amplitude

Scale/Harmonic	1	2	3	4	5
Excellent	0/10	0/20	0/30	0/35	0/40
Good	10/20	20/40	30/60	35/70	40/80
Fair	20/30	40/60	60/90	70/105	80/120
Poor	30/	60/	90/	105/	120/

D. Harmonic Phase

Scale/Harmonic	1,2	3,4,5
Excellent	0/10	0/20
Good	10/20	20/40
Fair	20/30	40/60
Poor	30/	60/

Note: 10/15 implies $10 < q \leq 15$, etc.

TABLE 10. PRESENTATION AND GRADING OF POST TEST PERFORMANCE PARAMETERS

1. Fiberglass Blade, -8° Twist, $\mu = 0.299$, $M_{1,90} = 0.408$

Lift	Power
$C_L/\sigma_{meas} = -0.00778 + 1.40\ C_L/\sigma_{comp}$	$C_P/\sigma_{meas} = 0.000771 + 0.755\ C_P/\sigma_{comp}$
$r = 0.977$	$r = 0.975$
$q_a = 39.7\%$ (poor)	$q_a = 24.5\%$ (poor)
$q_b = 12.8\%$ (fair)	$q_b = 29.5\%$ (poor
$q_r = 3.4\%$ (excellent)	$q_r = 2.5\%$ (excellent)

2. Fiberglass Blade, -8° Twist, $\mu = 0.400$, $M_{1,90} = 0.435$

Lift	Power
$C_L/\sigma_{meas} = -0.00613 + 1.33\ C_L/\sigma_{comp}$	$C_P/\sigma_{meas} = 0.000725 + 0.902\ C_P/\sigma_{comp}$
$r = 0.975$	$r = 0.997$
$q_a = 32.5\%$ (poor)	$q_a = 9.8\%$ (good)
$q_b = 12.3\%$ (fair)	$q_b = 17.5\%$ (poor)
$q_r = 2.5\%$ (excellent)	$q_r = 0.3\%$ (excellent)

3. Fiberglass Blade, -8° Twist, $\mu = 0.502$, $M_{1,90} = 0.467$

No curve fit was made because too few points were available for a statistical analysis.

TABLE 10. Continued

4. Fiberglass Blade, 0° Twist, $\mu = 0.299$, $M_{l,90} = 0.408$

Lift

$C_L/\sigma_{meas} = 0.0062 + 1.19\ C_L/\sigma_{comp}$

$r = 0.975$
$q_a = 18.5\%$ (poor)
$q_b = 11.3\%$ (fair)
$q_r = 2.5\%$ (excellent)

Power

$C_P/\sigma_{meas} = 0.000876 + 0.685\ C_P/\sigma_{comp}$

$r = 0.945$
$q_a = 31.5\%$ (poor)
$q_b = 31.6\%$ (poor)
$q_r = 5.5\%$ (good)

5. Fiberglass Blade, 0° Twist, with 5° Trailing Edge Flap, $\mu = 0.299$, $M_{l,90} = 0.408$

Lift

$C_L/\sigma_{meas} = 0.00291 + 1.264\ C_L/\sigma_{comp}$

$r = 0.992$
$q_a = 26.4\%$ (poor)
$q_b = 5.68\%$ (good)
$q_r = 0.8\%$ (excellent)

Power

$C_P/\sigma_{meas} = 0.0000510 + 1.45\ C_P/\sigma_{comp}$

$r = 0.916$
$q_a = 44.8\%$ (poor)
$q_b = 2.20\%$ (excellent)
$q_r = 8.4\%$ (good)

TABLE 11. H-34 MODEL ROTOR MEASURED AND CALCULATED LIFT AND POWER (CONDITIONS 25, 44, AND 68)

Condition No.		25		44		68	
μ		0.399		0.502		0.299	
$M_{T,90}$		0.434		0.467		0.407	
α_m		0.5		5.0		0.0	
		C_L/σ	C_P/σ	C_L/σ	C_P/σ	C_L/σ	C_P/σ
Fiberglass Blade 0° Twist	M	.0789	.00779	.0518	.00746	.0915	.00848
	C	.0757	.00806	.0488	.00748	.0908	.00634
Fiberglass Blade -8° Twist	M	.0794	.00692	.0507	.00592	.0929	.00767
	C	.0793	.00509	.0489	.00515	.0919	.00543
Fiberglass Blade 0° Twist $\delta_F = 5°$	M	.0824	.00660	.0522	.00590	.0943	.00565
	C	.0825	.00599	.0496	.00699	.0948	.00562
Aluminum Blade 0° Twist	M	.0752	.00791	.0504	.00805	.0949	.01099
	C	.0754	.00807	.0487	.00758	.0937	.00649

M = Measured
C = Calculated

TABLE 12. MEASURED BEAM AND CHORD BENDING MOMENTS, FIBERGLASS BLADE, 0 TWIST
$\mu = 0.399$, $M_{1,90} = 0.434$, $\alpha_m = 0.5°$ (COND. 25).

MEASURED BEAM MOMENT(IN-LBF)

STA/HARM		0	1	2	3	4	5	6	7
80%	SIN	0.0	-1.08	-0.92	-1.10	-0.33	0.24	-1.22	-2.19
	COS	-2.35	1.36	-3.81	-2.71	-0.07	-0.26	0.67	-0.15
65%	SIN	0.0	-0.28	-0.45	-0.08	0.32	0.44	0.17	-0.29
	COS	0.72	2.10	-4.11	-3.52	-0.62	-0.35	0.22	0.04
45%	SIN	0.0	0.65	-0.13	0.78	-0.76	0.29	0.45	1.38
	COS	2.83	1.61	-1.28	-2.54	-0.29	0.09	-0.64	0.25
35%	SIN	0.0	0.35	0.07	0.78	-0.80	-0.40	-0.04	0.63
	COS	3.03	1.31	-0.82	-2.36	0.05	0.09	-0.02	-0.08
20%	SIN	0.0	1.00	1.63	1.04	-1.15	-1.86	-0.59	-2.10
	COS	4.13	0.49	0.10	-2.42	0.05	0.71	1.21	-0.23

MEASURED CHORD MOMENT(IN-LBF)

STA/HARM		0	1	2	3	4	5	6	7
80%	SIN	0.0	1.50	-0.23	-3.95	-2.76	0.61	-0.11	0.36
	COS	1.63	-0.40	1.84	-1.02	-0.53	0.21	0.18	0.19
65%	SIN	0.0	3.24	-0.65	-7.24	-5.30	0.82	0.12	1.27
	COS	2.59	-1.67	2.66	-1.64	-0.32	0.59	0.07	0.08
45%	SIN	0.0	6.75	-0.02	-7.75	-5.89	0.36	0.26	0.88
	COS	3.17	-3.15	2.13	0.02	0.68	0.57	-0.33	-0.36
35%	SIN	0.0	9.53	0.76	-6.94	-4.68	0.33	0.33	-0.11
	COS	3.44	-4.83	1.46	2.65	1.22	0.41	-0.23	-0.41
20%	SIN	0.0	16.59	2.23	-4.75	-2.20	0.46	0.60	-0.52
	COS	4.44	-7.68	-0.13	5.80	1.47	0.14	-0.13	0.04

TABLE 13. CALCULATED BEAM AND CHORD BENDING MOMENTS, FIBERGLASS BLADE, 0° TWIST
$\mu = 0.399$, $M_{1,90} = 0.434$, $\alpha_m = 0.5°$ (COND. 25).

COMPUTED BEAM MOMENT(IN-LBF)

STA/HARM		0	1	2	3	4	5	6	7
22%	SIN	0.0	-0.89	1.18	1.19	-1.09	-0.65	-0.13	-0.02
	COS	-2.52	0.30	-1.92	-0.73	-0.15	0.13	-0.01	0.04
65%	SIN	0.0	-1.07	1.31	1.40	-0.53	-0.40	-0.08	-0.01
	COS	0.59	0.40	-1.32	-0.41	-0.15	0.01	-0.03	0.02
45%	SIN	0.0	-0.98	0.75	0.97	0.80	0.32	0.07	0.01
	COS	2.52	0.27	0.56	0.40	-0.04	-0.18	-0.03	-0.02
35%	SIN	0.0	-0.72	0.45	0.71	1.22	0.56	0.12	0.02
	COS	3.22	0.18	1.19	0.66	0.02	-0.23	-0.02	-0.04
22%	SIN	0.0	-0.93	0.45	0.82	2.22	1.07	0.23	0.04
	COS	5.96	0.40	2.22	1.14	0.09	-0.41	-0.04	-0.07

COMPUTED CHORD MOMENT(IN-LBF)

STA/HARM		0	1	2	3	4	5	6	7
82%	SIN	0.0	-1.51	-1.26	-0.35	-0.86	0.53	0.26	0.04
	COS	2.53	0.02	0.24	-1.43	1.20	0.99	0.27	-0.11
65%	SIN	0.0	-0.75	-1.87	-1.10	-1.30	0.76	0.34	0.03
	COS	4.67	1.46	0.43	-2.68	1.82	1.25	0.32	-0.14
45%	SIN	0.0	3.73	-0.98	-2.15	-0.87	0.29	0.05	-0.04
	COS	5.67	4.74	0.32	-3.09	1.11	0.12	-0.03	-0.01
25%	SIN	0.0	5.75	-0.25	-2.37	-0.46	-0.05	-0.13	-0.07
	COS	5.87	5.77	0.17	-2.77	0.48	-0.58	-0.24	0.07
22%	SIN	0.0	6.94	0.57	-2.15	0.06	-0.39	-0.29	-0.10
	COS	6.75	5.68	0.04	-1.93	-0.26	-1.21	-0.41	0.14

TABLE 14. MEASURED BEAM AND CHORD BENDING MOMENTS, FIBERGLASS BLADE, 0° TWIST
$\mu = 0.502$, $M_{1,90} = 0.467$, $\alpha_m = 5.0°$ (COND. 44).

MEASURED BEAM MOMENT(IN-LBF)

STA/HARM		0	1	2	3	4	5	6	7
80%	SIN	0.0	-0.92	-0.82	-0.20	-0.92	0.17	-0.77	0.21
	COS	-0.95	1.65	-3.53	-3.80	-0.82	0.76	0.35	-2.32
65%	SIN	0.0	-0.06	-1.10	0.50	-0.62	0.03	-0.04	0.29
	COS	2.45	3.19	-3.12	-4.53	-0.83	0.22	0.03	-0.43
45%	SIN	0.0	1.09	-0.89	1.84	-0.31	-0.22	0.45	-0.55
	COS	3.48	1.61	-1.48	-2.94	-0.73	-0.04	-0.50	1.75
35%	SIN	0.0	0.72	-0.89	2.33	-0.15	-0.08	-0.20	-0.06
	COS	3.55	1.10	-1.16	-2.89	-0.39	-0.35	-0.12	0.71
20%	SIN	0.0	0.14	0.46	3.05	-0.00	-1.01	-0.61	0.28
	COS	3.98	0.53	-0.12	-3.01	0.45	-0.96	1.38	-2.72

MEASURED CHORD MOMENT(IN-LBF)

STA/HARM		0	1	2	3	4	5	6	7
80%	SIN	0.0	0.62	-0.39	-4.37	-4.08	0.45	-0.39	0.87
	COS	1.48	-0.23	1.55	-1.49	-1.10	0.89	0.49	-0.15
65%	SIN	0.0	1.73	-0.69	-8.36	-7.49	0.77	-0.45	1.47
	COS	2.50	-1.51	2.31	-2.50	-1.64	1.70	0.64	0.24
45%	SIN	0.0	4.13	-0.03	-9.41	-7.68	0.46	0.04	0.50
	COS	3.12	-2.86	2.17	-0.77	-0.70	1.48	0.29	0.49
35%	SIN	0.0	5.72	0.80	-9.43	-6.35	0.12	0.36	-0.37
	COS	3.19	-4.01	2.06	2.23	0.40	1.01	0.31	0.07
20%	SIN	0.0	9.86	1.82	-7.58	-3.39	-0.61	0.65	-2.04
	COS	4.77	-5.82	0.62	5.92	1.18	-0.03	-0.04	0.53

TABLE 15. CALCULATED BEAM AND CHORD BENDING MOMENTS, FIBERGLASS BLADE, 0° TWIST
$\mu = 0.502$, $M_{1,90} = 0.467$, $\alpha_m = 5.0°$ (COND. 44).

COMPUTED BEAM MOMENT(IN-LBF)

STA/HARM		0	1	2	3	4	5	6	7
80%	SIN	0.0	-0.74	0.71	0.70	-0.57	-0.17	-0.01	0.00
	COS	0.46	0.50	-0.99	-0.29	-0.44	-0.08	0.02	0.01
65%	SIN	0.0	-0.64	0.53	0.95	-0.21	-0.07	-0.00	0.00
	COS	1.69	0.57	-0.57	-0.02	-0.29	-0.07	0.01	0.01
45%	SIN	0.0	-0.11	-0.13	0.86	0.57	0.15	0.02	0.00
	COS	3.16	0.32	0.52	0.49	0.17	-0.00	-0.01	-0.00
35%	SIN	0.0	0.11	-0.36	0.73	0.80	0.23	0.02	0.00
	COS	3.59	0.19	0.87	0.62	0.33	0.03	-0.02	-0.01
20%	SIN	0.0	0.32	-0.69	1.01	1.43	0.41	0.04	0.00
	COS	6.05	0.26	1.50	1.04	0.64	0.06	-0.04	-0.02

COMPUTED CHORD MOMENT(IN-LBF)

STA/HARM		0	1	2	3	4	5	6	7
80%	SIN	0.0	-1.61	-0.68	-0.30	-1.07	0.05	0.20	0.07
	COS	1.92	0.37	0.33	-0.76	0.73	0.58	0.14	0.01
65%	SIN	0.0	-1.73	-0.53	-0.76	-1.58	0.11	0.28	0.09
	COS	3.55	1.48	0.59	-1.71	1.15	0.77	0.16	0.01
45%	SIN	0.0	0.87	1.07	-1.26	-0.91	0.14	0.08	0.01
	COS	4.48	3.39	0.58	-2.60	0.79	0.15	-0.04	-0.01
35%	SIN	0.0	2.29	1.84	-1.32	-0.34	0.13	-0.05	-0.04
	COS	4.83	3.87	0.46	-2.65	0.42	-0.24	-0.15	-0.02
20%	SIN	0.0	3.41	2.31	-1.13	0.32	0.09	-0.18	-0.09
	COS	5.93	3.58	0.27	-2.22	-0.04	-0.61	-0.23	-0.03

TABLE 16. MEASURED BEAM AND CHORD BENDING MOMENTS, FIBERGLASS BLADE, 0° TWIST
$\mu = 0.299$, $M_{1,90} = 0.408$, $\alpha_m = 0°$ (COND. 68).

MEASURED BEAM MOMENT(IN-LBF)

STA/HARM		0	1	2	3	4	5	6	7
80%	SIN	0.0	-1.46	-1.00	-0.10	2.32	-0.17	-1.07	-0.39
	COS	-1.16	1.31	-3.40	-1.79	-0.51	0.17	0.50	1.79
65%	SIN	0.0	-1.34	-1.29	-0.07	0.75	-0.63	0.02	-0.12
	COS	0.76	1.89	-2.54	-2.15	-1.04	0.01	-0.05	0.11
45%	SIN	0.0	-0.61	-0.09	-0.18	-0.74	0.21	0.34	0.16
	COS	3.13	1.40	-0.22	-1.84	0.28	-0.23	0.14	-0.57
35%	SIN	0.0	-0.61	0.34	-0.21	-0.91	0.21	0.08	-0.02
	COS	3.60	1.18	-0.02	-1.31	0.41	-0.05	-0.04	-0.35
20%	SIN	0.0	0.0	0.0	0.0	0.0	0.0	0.0	0.0
	COS	0.0	0.0	0.0	0.0	0.0	0.0	0.0	0.0

MEASURED CHORD MOMENT(IN-LBF)

STA/HARM		0	1	2	3	4	5	6	7
80%	SIN	0.0	2.44	-0.15	-3.31	-2.84	0.92	0.28	0.41
	COS	0.24	-0.63	2.93	-0.36	0.02	0.24	-0.01	0.81
65%	SIN	0.0	4.52	-0.67	-6.01	-4.28	1.39	0.07	0.65
	COS	0.26	-1.31	3.31	-0.79	1.20	0.57	0.15	1.78
45%	SIN	0.0	8.93	-0.09	-6.44	-4.81	0.83	0.26	0.36
	COS	-1.46	-2.32	1.73	0.86	2.20	0.59	-0.03	0.59
35%	SIN	0.0	10.91	0.61	-4.91	-3.66	0.43	0.05	-0.30
	COS	0.47	-3.04	0.71	2.21	2.42	0.39	-0.05	-0.66
20%	SIN	0.0	20.92	2.97	-2.99	-1.43	-0.48	-0.37	-1.05
	COS	-0.26	-5.74	-0.44	4.80	2.05	0.30	0.11	-2.00

TABLE 17. CALCULATED BEAM AND CHORD BENDING MOMENTS, FIBERGLASS BLADE, 0° TWIST
$\mu = 0.299$, $M_{1,90} = 0.408$, $\alpha_m = 0°$ (COND. 68).

COMPUTED BEAM MOMENT(IN-LBF)

STA/HARM		0	1	2	3	4	5	6	7
80%	SIN	0.0	-1.22	0.09	0.57	-0.04	-0.08	-0.02	0.00
	COS	-0.67	1.02	-0.94	-0.12	0.11	0.05	-0.02	-0.01
65%	SIN	0.0	-1.55	0.23	0.58	0.00	-0.05	-0.02	0.00
	COS	0.51	1.12	-0.68	0.07	0.05	0.02	-0.02	-0.01
45%	SIN	0.0	-1.39	0.34	0.27	0.06	0.04	0.00	-0.00
	COS	2.62	0.55	0.17	0.35	-0.07	-0.04	0.00	-0.00
35%	SIN	0.0	-1.20	0.34	0.12	0.08	0.07	0.01	-0.01
	COS	3.36	0.25	0.47	0.42	-0.10	-0.06	0.01	0.00
20%	SIN	0.0	-1.51	0.47	0.04	0.14	0.13	0.03	-0.01
	COS	0.34	0.36	0.95	0.63	-0.17	-0.10	0.03	0.01

COMPUTED CHORD MOMENT(IN-LBF)

STA/HARM		0	1	2	3	4	5	6	7
80%	SIN	0.0	-0.66	-0.92	-0.07	-0.12	-0.04	0.03	-0.06
	COS	1.97	-0.36	0.14	-0.79	0.38	0.15	0.10	0.06
65%	SIN	0.0	0.52	-1.59	-0.29	-0.12	-0.04	0.05	-0.09
	COS	3.49	0.55	0.51	-1.47	0.59	0.21	0.13	0.11
45%	SIN	0.0	4.37	-1.51	-0.63	0.10	0.02	0.05	0.02
	COS	3.83	3.09	1.00	-1.66	0.44	0.12	0.01	0.05
35%	SIN	0.0	5.89	-1.19	-0.71	0.21	0.05	0.04	0.08
	COS	3.84	4.01	1.09	-1.47	0.27	0.04	-0.06	-0.02
20%	SIN	0.0	6.47	-0.62	-0.66	0.29	0.07	0.03	0.13
	COS	4.60	4.17	1.03	-1.00	0.04	-0.05	-0.13	-0.08

TABLE 18. MEASURED BEAM AND CHORD BENDING MOMENTS, FIBERGLASS BLADE, -8° TWIST
$\mu = 0.399$, $M_{1,90} = 0.434$, $\alpha_m = 0.5°$ (COND. 25).

MEASURED BEAM MOMENT(IN-LBF)

STA/HARM		0	1	2	3	4	5	6	7
80%	SIN	0.0	-2.69	1.03	1.11	-0.87	0.06	-0.85	-1.75
	COS	-2.19	2.90	-3.46	-1.72	-1.46	-0.38	0.23	-0.05
65%	SIN	0.0	-3.33	2.23	1.16	-0.24	0.37	0.07	-0.13
	COS	-1.39	3.98	-3.49	-1.80	-1.11	-0.50	0.07	0.17
45%	SIN	0.0	-2.84	2.27	0.69	-0.17	0.05	0.33	1.04
	COS	0.63	3.98	-1.91	-1.09	-0.20	-0.00	-0.10	0.00
35%	SIN	0.0	-2.23	1.92	0.39	-0.01	-0.32	-0.07	0.37
	COS	1.21	2.98	-1.36	-0.98	0.20	0.16	-0.01	-0.18
20%	SIN	0.0	-0.80	2.20	0.38	0.03	-1.05	-0.52	-1.70
	COS	3.01	1.36	-0.57	-0.84	0.61	0.34	0.40	0.23

MEASURED CHORD MOMENT(IN-LBF)

STA/HARM		0	1	2	3	4	5	6	7
80%	SIN	0.0	1.47	-0.92	-1.00	-0.94	-0.05	0.35	0.37
	COS	1.35	-0.69	0.90	-1.87	-1.36	0.59	-0.13	-0.07
65%	SIN	0.0	3.05	-2.29	-2.00	-2.04	-0.37	0.38	0.63
	COS	1.02	-1.88	1.60	-3.71	-2.04	1.26	-0.20	-0.17
45%	SIN	0.0	6.58	-3.18	-2.83	-2.88	-0.45	-0.01	-0.06
	COS	0.71	-3.90	1.78	-3.45	-1.53	1.19	-0.01	-0.10
35%	SIN	0.0	7.65	-1.86	-3.01	-2.75	-0.09	-0.09	-0.16
	COS	2.59	-3.74	1.00	-2.17	-0.90	0.83	0.09	0.21
20%	SIN	0.0	12.14	-0.19	-3.87	-1.90	0.62	-0.18	-0.24
	COS	2.36	-6.14	0.62	1.00	0.14	-0.24	0.24	0.67

TABLE 19. CALCULATED BEAM AND CHORD BENDING MOMENTS, FIBERGLASS BLADE, -8° TWIST
$\mu = 0.399$, $M_{1,90} = 0.434$, $\alpha_m = 0.5°$ (COND. 25).

COMPUTED BEAM MOMENT(IN-LBF)

STA/HARM		0	1	2	3	4	5	6	7
80%	SIN	0.0	-3.18	1.29	1.31	-0.70	-0.29	0.01	-0.01
	COS	-2.11	1.56	-1.28	0.64	-0.26	-0.24	-0.01	0.00
65%	SIN	0.0	-3.95	1.58	1.23	-0.38	-0.16	0.00	-0.00
	COS	-1.45	1.82	-0.67	0.74	-0.10	-0.15	-0.01	0.00
45%	SIN	0.0	-3.08	1.21	0.40	0.42	0.17	-0.01	0.00
	COS	0.77	1.19	0.82	0.51	0.24	0.11	0.00	-0.00
35%	SIN	0.0	-2.46	0.95	0.05	0.69	0.27	-0.01	0.01
	COS	1.74	0.80	1.32	0.37	0.36	0.20	0.01	-0.00
20%	SIN	0.0	-3.44	1.33	-0.16	1.29	0.50	-0.02	0.01
	COS	3.84	0.84	2.38	0.52	0.68	0.39	0.01	-0.01

COMPUTED CHORD MOMENT(IN-LBF)

STA/HARM		0	1	2	3	4	5	6	7
80%	SIN	0.0	1.17	-1.40	0.96	-0.54	-0.33	0.12	0.02
	COS	1.45	-0.83	-0.93	-1.66	0.45	0.18	-0.03	0.02
65%	SIN	0.0	2.91	-2.61	1.17	-0.91	-0.46	0.14	0.02
	COS	2.99	-0.66	-1.73	-3.17	0.56	0.25	-0.05	0.02
45%	SIN	0.0	4.63	-2.84	0.11	-0.90	-0.21	-0.04	-0.02
	COS	4.09	1.34	-2.15	-3.65	-0.05	0.04	-0.03	-0.01
35%	SIN	0.0	4.73	-2.41	-0.56	-0.69	-0.01	-0.13	-0.03
	COS	4.46	2.29	-1.92	-3.25	-0.38	-0.08	-0.02	-0.03
20%	SIN	0.0	4.10	-1.55	-1.07	-0.47	0.15	-0.21	-0.05
	COS	4.77	2.84	-1.55	-2.25	-0.72	-0.23	-0.00	-0.05

TABLE 20. MEASURED BEAM AND CHORD BENDING MOMENTS, FIBERGLASS BLADE, -8° TWIST
$\mu = 0.502$, $M_{1,90} = 0.467$, $\alpha_m = 5.0°$ (COND. 44).

MEASURED BEAM MOMENT(IN-LBF)

STA/HARM		0	1	2	3	4	5	6	7
82%	SIN	0.0	-2.67	1.45	2.61	-1.37	-0.61	0.03	0.35
	COS	-0.78	3.14	-2.86	-1.21	-2.16	-0.13	0.31	-0.83
65%	SIN	0.0	-3.69	2.64	2.33	-1.69	-0.30	0.03	0.05
	COS	-0.39	4.73	-2.36	-1.39	-1.43	-0.15	0.09	-0.05
45%	SIN	0.0	-3.34	3.02	1.65	0.39	-0.69	-0.23	-0.36
	COS	0.44	4.02	-1.80	-1.04	-0.24	-0.23	-0.18	0.59
35%	SIN	0.0	-2.88	2.41	1.50	0.91	0.14	-0.18	-0.62
	COS	0.85	3.04	-1.70	-1.05	0.33	-0.14	-0.16	0.19
20%	SIN	0.0	-2.21	2.14	1.66	1.27	0.15	0.12	-0.33
	COS	2.30	1.64	-0.81	-0.95	1.18	-0.55	0.24	-0.86

MEASURED CHORD MOMENT(IN-LBF)

STA/HARM		0	1	2	3	4	5	6	7
82%	SIN	0.0	0.48	-0.84	-0.27	-2.10	-0.68	-0.24	0.21
	COS	0.78	-0.59	0.44	-1.80	-1.69	0.62	-0.18	0.12
65%	SIN	0.0	1.05	-1.68	-0.86	-4.09	-1.03	-0.43	0.35
	COS	0.14	-1.46	0.77	-3.72	-3.30	1.43	-0.12	0.22
45%	SIN	0.0	2.80	-2.61	-2.35	-5.12	-0.65	-0.09	0.27
	COS	0.51	-2.86	1.30	-4.07	-3.35	1.56	0.27	-0.02
35%	SIN	0.0	2.80	-1.61	-2.83	-4.56	-0.16	0.08	-0.05
	COS	1.98	-2.05	0.92	-3.31	-2.46	0.95	0.41	0.03
20%	SIN	0.0	4.74	-0.92	-4.56	-3.14	0.43	0.20	-0.54
	COS	3.37	-2.70	1.09	-1.07	-1.32	-0.39	0.36	0.11

TABLE 21. CALCULATED BEAM AND CHORD BENDING MOMENTS, FIBERGLASS BLADE, -8° TWIST
$\mu = 0.502$, $M_{1,90} = 0.467$, $\alpha_m = 5.0°$ (COND. 44).

COMPUTED BEAM MOMENT(IN-LBF)

STA/HARM		0	1	2	3	4	5	6	7
82%	SIN	0.0	-3.01	1.53	0.67	-0.75	-0.21	-0.04	-0.01
	COS	-1.41	1.45	-0.63	0.82	-0.91	-0.22	0.01	0.00
65%	SIN	0.0	-3.66	1.79	0.78	-0.41	-0.11	-0.02	-0.01
	COS	-0.85	1.68	-0.05	0.92	-0.50	-0.14	0.00	0.00
45%	SIN	0.0	-2.60	1.24	0.54	0.44	0.14	0.02	0.00
	COS	0.82	1.14	1.04	0.58	0.53	0.10	-0.01	-0.00
35%	SIN	0.0	-2.16	0.90	0.39	0.73	0.22	0.03	0.01
	COS	1.55	0.80	1.35	0.40	0.66	0.18	-0.02	-0.00
22%	SIN	0.0	-2.97	1.17	0.53	1.38	0.41	0.07	0.02
	COS	3.07	0.90	2.36	0.61	1.07	0.36	-0.02	-0.01

COMPUTED CHORD MOMENT(IN-LBF)

STA/HARM		0	1	2	3	4	5	6	7
82%	SIN	0.0	0.28	-0.86	0.61	-0.68	-0.16	0.14	0.05
	COS	1.47	-0.47	-1.15	-1.25	0.09	0.23	0.04	-0.02
65%	SIN	0.0	0.86	-1.38	0.74	-1.42	-0.23	0.16	0.06
	COS	2.98	-0.55	-2.29	-2.54	-0.02	0.30	0.05	-0.03
45%	SIN	0.0	1.64	-0.96	-0.02	-1.21	-0.13	-0.03	-0.02
	COS	4.10	0.64	-2.96	-3.28	-0.56	0.02	-0.03	-0.01
35%	SIN	0.0	1.74	-0.51	-0.46	-0.81	-0.04	-0.14	-0.06
	COS	4.49	1.40	-2.73	-3.09	-0.72	-0.14	-0.07	-0.00
22%	SIN	0.0	1.02	0.04	-0.85	-0.40	0.03	-0.23	-0.09
	COS	4.93	1.70	-2.22	-2.36	-0.94	-0.32	-0.09	0.01

TABLE 22. MEASURED BEAM AND CHORD BENDING MOMENTS, FIBERGLASS BLADE, -8° TWIST
$\mu = 0.299$, $M_{1,90} = 0.408$, $\alpha_m = 0°$ (COND. 68).

MEASURED BEAM MOMENT(IN-LBF)

STA/HARM		0	1	2	3	4	5	6	7
80%	SIN	0.0	-2.54	0.09	0.90	0.75	0.39	-0.44	-0.95
	COS	-2.52	2.76	-3.52	-2.03	-0.89	0.34	-0.05	0.81
65%	SIN	0.0	-3.21	0.45	0.60	-0.22	-0.25	0.01	-0.30
	COS	-0.83	3.77	-2.98	-1.65	-0.77	-0.03	-0.05	0.05
45%	SIN	0.0	-2.57	1.28	0.32	-0.24	0.09	0.09	0.50
	COS	1.30	2.94	-1.19	-1.15	-0.00	-0.18	0.48	-0.22
35%	SIN	0.0	-1.78	1.25	0.05	-0.01	-0.11	-0.01	0.21
	COS	1.76	2.18	-0.71	-0.70	0.19	-0.02	0.06	-0.04
20%	SIN	0.0	0.26	1.91	0.10	0.13	0.01	-0.28	-0.75
	COS	4.12	0.82	-0.12	-0.39	0.39	0.23	-0.77	0.38

MEASURED CHORD MOMENT(IN-LBF)

STA/HARM		0	1	2	3	4	5	6	7
80%	SIN	0.0	2.19	-1.06	-2.49	-1.45	0.05	-0.14	-0.13
	COS	1.30	-0.65	1.29	-1.65	-0.34	0.43	0.10	0.30
65%	SIN	0.0	4.46	-2.44	-4.36	-2.02	-0.10	-0.02	0.12
	COS	0.67	-1.78	1.77	-3.19	0.28	0.92	0.11	0.41
45%	SIN	0.0	8.64	-2.91	-5.13	-3.20	-0.16	0.31	0.27
	COS	0.78	-3.42	1.19	-2.10	1.08	0.97	-0.08	0.17
35%	SIN	0.0	10.42	-1.71	-4.78	-2.67	-0.02	0.16	0.34
	COS	5.92	-3.79	0.43	-0.61	1.21	0.77	-0.07	-0.13
20%	SIN	0.0	17.63	0.41	-4.20	-1.10	0.06	-0.17	-0.30
	COS	0.21	-6.43	-0.38	2.63	0.87	0.12	0.12	-0.34

TABLE 23. CALCULATED BEAM AND CHORD BENDING MOMENTS, FIBERGLASS BLADE, -8° TWIST
$\mu = 0.299$, $M_{1,90} = 0.408$, $\alpha_m = 0°$ (COND. 68).

COMPUTED BEAM MOMENT(IN-LBF)

STA/HARM		0	1	2	3	4	5	6	7
80%	SIN	0.0	-2.69	0.70	0.91	-0.31	-0.12	0.02	-0.00
	COS	-2.42	1.39	-1.00	0.24	0.01	-0.10	-0.00	0.00
65%	SIN	0.0	-3.33	0.94	0.82	-0.17	-0.07	0.01	-0.00
	COS	-1.49	1.62	-0.56	0.32	0.03	-0.06	-0.00	0.00
45%	SIN	0.0	-2.62	0.83	0.21	0.19	0.07	-0.01	0.00
	COS	1.27	1.04	0.57	0.29	0.05	0.04	-0.00	-0.00
35%	SIN	0.0	-2.15	0.71	-0.04	0.31	0.11	-0.02	0.00
	COS	2.43	0.68	0.94	0.25	0.05	0.06	-0.00	-0.00
20%	SIN	0.0	-2.97	1.05	-0.23	0.56	0.20	-0.02	0.00
	COS	3.19	0.64	1.72	0.38	0.10	0.15	-0.01	-0.00

COMPUTED CHORD MOMENT(IN-LBF)

STA/HARM		0	1	2	3	4	5	6	7
80%	SIN	0.0	1.09	-1.24	0.63	-0.12	-0.17	0.08	-0.00
	COS	1.27	-0.79	-0.63	-1.33	0.00	0.07	-0.07	0.01
65%	SIN	0.0	2.85	-2.31	0.72	-0.25	-0.24	0.09	-0.01
	COS	2.06	-0.41	-1.12	-2.43	0.08	0.10	-0.09	0.01
45%	SIN	0.0	4.84	-2.58	-0.13	-0.38	-0.11	-0.04	-0.01
	COS	3.66	2.02	-1.29	-2.60	0.05	0.02	-0.02	-0.02
35%	SIN	0.0	5.08	-2.23	-0.53	-0.38	-0.06	-0.11	-0.04
	COS	4.11	3.08	-1.09	-2.21	-0.15	-0.03	0.03	-0.03
20%	SIN	0.0	4.54	-1.49	-0.91	-0.36	0.08	-0.16	-0.08
	COS	4.55	3.61	-0.86	-1.42	-0.05	-0.09	0.07	-0.03

TABLE 24. MEASURED BEAM AND CHORD BENDING MOMENTS, FIBERGLASS BLADE, 0° TWIST, $\delta_F = 5°$, $\mu = 0.399$, $M_{1,90} = 0.434$, $\alpha_m = 0.5°$ (COND. 25).

MEASURED BEAM MOMENT(IN-LBF)

STA/HARM		0	1	2	3	4	5	6	7
80%	SIN	0.0	-2.00	0.68	0.48	-0.41	-0.08	-0.90	-1.02
	COS	-1.98	2.67	-2.79	-1.21	-1.41	-0.61	0.29	1.29
65%	SIN	0.0	-2.40	2.48	0.95	0.02	0.08	0.11	-0.07
	COS	-0.48	3.77	-3.02	-1.74	-1.50	-0.41	0.19	0.07
45%	SIN	0.0	-2.33	2.47	0.92	-0.34	0.11	0.37	0.75
	COS	1.27	3.67	-0.94	-1.33	-0.05	0.13	-0.37	-0.68
35%	SIN	0.0	-1.74	1.97	0.65	-0.26	-0.17	-0.11	0.29
	COS	1.52	2.60	-0.56	-1.24	0.48	-0.02	-0.06	-0.28
20%	SIN	0.0	-0.80	2.30	0.81	-0.06	-0.75	-0.69	-1.15
	COS	3.47	1.28	-0.10	-1.39	0.91	-0.02	0.44	1.15

MEASURED CHORD MOMENT(IN-LBF)

STA/HARM		0	1	2	3	4	5	6	7
80%	SIN	0.0	0.23	0.11	-1.01	-1.99	-0.14	-0.20	-0.38
	COS	0.37	-0.06	-0.02	-1.67	-2.31	0.26	-0.27	0.36
65%	SIN	0.0	2.24	-1.05	-2.42	-3.76	-0.45	0.01	0.14
	COS	0.76	-2.64	1.54	-2.78	-2.90	1.31	-0.40	-0.09
45%	SIN	0.0	4.72	-1.35	-2.82	-4.10	-0.68	-0.23	-0.08
	COS	0.94	-4.43	1.30	-2.36	-2.04	1.42	0.05	0.07
35%	SIN	0.0	5.82	-0.63	-2.42	-3.23	-0.29	-0.18	0.02
	COS	1.85	-4.74	0.73	-1.03	-1.01	1.05	0.26	0.15
20%	SIN	0.0	9.54	0.07	-2.54	-1.51	0.66	0.24	0.85
	COS	-0.26	-7.52	0.15	1.83	0.15	0.24	0.44	-0.25

TABLE 25. CALCULATED BEAM AND CHORD BENDING MOMENTS, FIBERGLASS BLADE, 0° TWIST, $\delta_F = 5°$, $\mu = 0.399$, $M_{1,90} = 0.434$, $\alpha_m = 0.5°$ (COND. 25).

COMPUTED BEAM MOMENT(IN-LBF)

STA/HARM		0	1	2	3	4	5	6	7
80%	SIN	0.0	-1.03	0.36	0.47	-0.65	-0.23	-0.05	-0.01
	COS	0.52	0.80	-0.86	-0.12	-0.51	-0.11	0.02	0.00
65%	SIN	0.0	-0.93	0.22	0.74	-0.26	-0.11	-0.03	-0.01
	COS	1.68	0.81	-0.48	0.21	-0.30	-0.09	0.01	0.00
45%	SIN	0.0	-0.27	-0.21	0.80	0.57	0.16	0.02	0.01
	COS	3.02	0.33	0.49	0.69	0.26	0.02	-0.01	-0.00
35%	SIN	0.0	0.06	-0.35	0.74	0.82	0.25	0.04	0.01
	COS	3.40	0.11	0.79	0.79	0.45	0.06	-0.02	-0.00
20%	SIN	0.0	0.25	-0.58	1.05	1.46	0.46	0.08	0.02
	COS	5.76	0.11	1.38	1.21	0.88	0.13	-0.03	-0.01

COMPUTED CHORD MOMENT(IN-LBF)

STA/HARM		0	1	2	3	4	5	6	7
80%	SIN	0.0	-1.53	-0.70	-0.19	-1.21	-0.20	0.07	-0.03
	COS	1.63	0.30	0.16	-1.09	0.54	0.58	0.12	0.00
65%	SIN	0.0	-1.27	-0.67	-0.61	-1.78	-0.23	0.10	-0.03
	COS	2.99	1.59	0.43	-2.25	0.66	0.80	0.16	0.08
45%	SIN	0.0	1.18	0.69	-1.23	-1.02	0.06	0.04	0.02
	COS	3.74	2.36	0.71	-3.03	0.01	0.29	0.02	0.03
35%	SIN	0.0	2.45	1.38	-1.37	-0.38	0.22	-0.01	0.04
	COS	4.09	2.69	0.73	-2.94	0.34	-0.07	-0.07	-0.01
20%	SIN	0.0	3.34	1.85	-1.25	0.36	0.35	-0.05	0.06
	COS	5.27	2.44	0.66	-2.30	0.01	-0.42	-0.14	-0.04

TABLE 26. MEASURED BEAM AND CHORD BENDING MOMENTS, FIBERGLASS BLADE, 0° TWIST, $\delta_F = 5°$ $\mu = 0.502$, $M_{1,90} = 0.467$, $\alpha_m = 5.0°$ (COND. 44).

MEASURED BEAM MOMENT(IN-LBF)

STA/HARM		0	1	2	3	4	5	6	7
80%	SIN	0.0	-1.82	1.35	1.22	-0.71	-0.27	-0.28	-0.25
	COS	-0.72	2.98	-2.14	-0.35	-1.39	0.07	-0.06	-0.75
65%	SIN	0.0	-2.65	3.09	1.61	-0.69	-0.40	0.01	0.15
	COS	0.54	4.80	-1.53	-0.77	-1.18	0.07	0.14	-0.14
45%	SIN	0.0	-3.04	3.26	1.38	0.08	-0.15	0.01	-0.08
	COS	1.01	3.98	-0.52	-1.04	-0.34	-0.15	-0.06	0.59
35%	SIN	0.0	-2.55	2.46	1.32	0.43	0.25	-0.14	0.01
	COS	1.05	2.87	-0.51	-1.24	0.19	-0.31	-0.22	0.18
20%	SIN	0.0	-2.09	2.38	1.90	0.94	0.31	-0.22	-0.40
	COS	2.44	1.72	-0.00	-1.44	1.21	-0.94	-0.07	-0.86

MEASURED CHORD MOMENT(IN-LBF)

STA/HARM		0	1	2	3	4	5	6	7
80%	SIN	0.0	-0.56	0.37	0.39	-2.02	-0.41	-0.14	0.26
	COS	0.14	0.09	-0.55	-1.13	-2.65	0.52	-0.30	-0.29
65%	SIN	0.0	0.52	-0.43	-0.37	-3.76	-0.58	-0.14	0.49
	COS	0.05	-2.26	0.21	-2.28	-4.05	1.11	-0.32	-0.02
45%	SIN	0.0	1.01	-1.00	-1.32	-4.34	-0.52	-0.04	0.18
	COS	0.35	-3.20	0.42	-2.33	-3.97	1.21	0.14	-0.11
35%	SIN	0.0	1.12	-0.68	-1.80	-3.68	-0.39	0.06	-0.19
	COS	1.41	-3.05	0.34	-1.63	-2.80	0.84	0.40	0.04
20%	SIN	0.0	2.21	-0.99	-3.41	-2.70	-0.62	0.00	-0.51
	COS	0.20	-4.36	-0.11	-0.00	-1.66	0.55	0.63	0.70

TABLE 27. CALCULATED BEAM AND CHORD BENDING MOMENTS, FIBERGLASS BLADE, 0° TWIST, $\delta_F = 5°$ $\mu = 0.502$, $M_{1,90} = 0.467$, $\alpha_m = 5.0°$ (COND. 44).

COMPUTED BEAM MOMENT(IN-LBF)

STA/HARM		0	1	2	3	4	5	6	7
80%	SIN	0.0	-1.03	0.36	0.48	-0.65	-0.23	-0.05	-0.01
	COS	0.52	0.80	-0.86	-0.12	-0.51	-0.11	0.02	0.00
65%	SIN	0.0	-0.93	0.22	0.74	-0.26	-0.11	-0.03	-0.01
	COS	1.68	0.82	-0.48	0.21	-0.30	-0.09	0.01	0.00
45%	SIN	0.0	-0.27	-0.21	0.80	0.57	0.16	0.02	0.01
	COS	3.02	0.33	0.49	0.69	0.26	0.02	-0.01	-0.00
35%	SIN	0.0	-0.00	-0.35	0.73	0.82	0.25	0.04	0.01
	COS	3.40	0.11	0.80	0.79	0.45	0.06	-0.02	-0.00
20%	SIN	0.0	0.25	-0.58	1.05	1.46	0.46	0.08	0.02
	COS	5.76	0.11	1.38	1.21	0.87	0.13	-0.03	-0.01

COMPUTED CHORD MOMENT(IN-LBF)

STA/HARM		0	1	2	3	4	5	6	7
80%	SIN	0.0	-1.33	-0.70	-0.19	-1.21	-0.20	0.07	-0.03
	COS	1.63	0.30	0.16	-1.10	0.54	0.58	0.12	0.06
65%	SIN	0.0	-1.27	-0.67	-0.61	-1.78	-0.23	0.10	-0.03
	COS	2.99	1.09	0.43	-2.25	0.86	0.80	0.16	0.08
45%	SIN	0.0	1.18	0.69	-1.23	-1.02	0.06	0.04	0.02
	COS	3.75	2.38	0.71	-3.03	0.61	0.29	0.02	0.03
35%	SIN	0.0	2.43	1.38	-1.37	-0.38	0.22	-0.01	0.04
	COS	4.09	2.69	0.73	-2.94	0.34	-0.07	-0.07	-0.01
20%	SIN	0.0	3.34	1.85	-1.25	0.36	0.35	-0.05	0.06
	COS	5.27	2.44	0.66	-2.30	0.01	-0.42	-0.14	-0.04

TABLE 28. MEASURED BEAM AND CHORD BENDING MOMENTS, FIBERGLASS BLADE, 0° TWIST, $\delta_F = 5°$ $\mu = 0.299$, $M_{1,90} = 0.408$, $\alpha_m = 0°$ (COND. 68).

MEASURED BEAM MOMENT(IN-LBF)

STA/HARM		0	1	2	3	4	5	6	7
80%	SIN	0.0	-1.98	-0.28	0.24	0.28	0.25	-0.14	0.76
	COS	-2.19	2.38	-2.28	-1.37	-1.72	-0.05	1.24	1.99
65%	SIN	0.0	-2.30	0.02	0.70	0.02	-0.16	0.26	-0.00
	COS	0.00	3.49	-1.91	-1.52	-1.61	0.17	-0.12	-0.24
45%	SIN	0.0	-2.37	0.95	0.63	-0.37	-0.10	0.02	-0.61
	COS	2.11	2.83	-0.13	-1.00	0.36	-0.20	-0.38	-0.77
35%	SIN	0.0	0.0	0.0	0.0	0.0	0.0	0.0	0.0
	COS	0.0	0.0	0.0	0.0	0.0	0.0	0.0	0.0
20%	SIN	0.0	-0.22	1.43	0.67	-0.16	-0.02	-0.45	1.02
	COS	4.18	0.70	0.21	-0.38	1.06	-0.02	0.78	1.23

MEASURED CHORD MOMENT(IN-LBF)

STA/HARM		0	1	2	3	4	5	6	7
80%	SIN	0.0	0.0	0.0	0.0	0.0	0.0	0.0	0.0
	COS	0.0	0.0	0.0	0.0	0.0	0.0	0.0	0.0
65%	SIN	0.0	2.93	-0.36	-3.67	-2.42	-0.22	-0.55	0.03
	COS	1.62	-2.66	2.35	-0.91	-1.12	0.42	0.49	1.71
45%	SIN	0.0	5.41	-0.71	-3.59	-2.21	-0.34	-0.29	0.18
	COS	0.13	-4.16	1.52	-0.50	-0.62	0.67	0.19	0.37
35%	SIN	0.0	6.44	-0.40	-2.59	-1.61	-0.10	0.02	0.06
	COS	2.21	-4.69	0.74	0.33	-0.11	0.52	0.04	-0.63
20%	SIN	0.0	9.48	0.02	-1.50	-0.38	0.26	0.79	-0.55
	COS	-1.17	-6.98	-0.34	1.98	0.10	0.31	-0.48	-2.35

TABLE 29. CALCULATED BEAM AND CHORD BENDING MOMENTS, FIBERGLASS BLADE, 0° TWIST, $\delta_F = 5°$ $\mu = 0.299$, $M_{1,90} = 0.408$, $\alpha_m = 0°$ (COND. 68).

COMPUTED BEAM MOMENT(IN-LBF)

STA/HARM		0	1	2	3	4	5	6	7
80%	SIN	0.0	-1.32	0.09	0.57	-0.01	-0.04	-0.01	0.00
	COS	-0.78	1.11	-0.92	-0.07	0.03	0.01	-0.00	-0.01
65%	SIN	0.0	-1.70	0.25	0.59	0.02	-0.01	-0.00	0.00
	COS	0.40	1.23	-0.67	0.17	0.02	-0.01	-0.00	-0.01
45%	SIN	0.0	-1.60	0.37	0.32	0.06	0.03	0.01	-0.00
	COS	2.58	0.61	0.17	0.47	-0.02	-0.03	0.00	-0.00
35%	SIN	0.0	-1.43	0.37	0.18	0.07	0.04	0.01	-0.00
	COS	3.33	0.28	0.47	0.52	-0.03	-0.04	0.00	0.00
20%	SIN	0.0	-1.74	0.49	0.10	0.11	0.08	0.01	-0.01
	COS	6.37	0.36	0.96	0.72	-0.04	-0.06	0.00	0.01

COMPUTED CHORD MOMENT(IN-LBF)

STA/HARM		0	1	2	3	4	5	6	7
80%	SIN	0.0	-0.47	-0.91	-0.08	-0.11	-0.14	-0.01	-0.03
	COS	1.77	-0.39	0.13	-1.21	0.12	0.10	-0.06	0.03
65%	SIN	0.0	0.94	-1.60	-0.44	-0.16	-0.19	-0.02	-0.04
	COS	3.08	0.10	0.52	-2.17	0.20	0.17	-0.07	0.05
45%	SIN	0.0	4.96	-1.60	-1.06	-0.09	-0.05	-0.03	-0.00
	COS	3.21	2.04	1.08	-2.26	0.19	0.16	0.01	0.01
35%	SIN	0.0	6.46	-1.30	-1.22	-0.03	0.05	-0.03	0.02
	COS	3.14	2.79	1.20	-1.90	0.15	0.13	0.06	-0.01
20%	SIN	0.0	6.88	-0.73	-1.16	0.03	0.14	-0.02	0.04
	COS	3.83	2.99	1.15	-1.17	0.08	0.07	0.10	-0.03

TABLE 30. MEASURED BEAM AND CHORD BENDING MOMENTS, ALUMINUM BLADE, 0° TWIST
$\mu = 0.399$, $M_{1,90} = 0.434$, $\alpha_m = 0.5°$ (COND. 25).

MEASURED BEAM MOMENT(IN-LBF)

STA/HARM		0	1	2	3	4	5	6	7
80%	SIN	0.0	-1.82	-0.49	1.62	0.61	-0.82	-1.72	-0.14
	COS	-2.56	2.49	-6.14	-5.47	-0.60	0.58	0.99	-0.03
65%	SIN	0.0	-1.44	-0.01	3.89	0.79	-0.86	-0.25	0.05
	COS	2.24	4.72	-7.11	-8.85	-1.73	0.82	1.57	0.34
45%	SIN	0.0	-0.63	0.32	5.13	-1.30	0.54	0.26	-0.16
	COS	7.23	5.17	-3.28	-8.97	-1.00	-0.04	-0.42	0.44
35%	SIN	0.0	-0.23	0.82	4.18	-1.69	0.26	-0.05	0.05
	COS	8.11	4.26	-1.76	-8.28	-0.45	-0.86	-0.75	-0.31
20%	SIN	0.0	1.24	2.74	2.87	-2.50	-0.69	-0.07	-0.24
	COS	8.66	2.42	0.83	-6.86	-0.74	-1.20	-0.97	-1.36

MEASURED CHORD MOMENT(IN-LBF)

STA/HARM		0	1	2	3	4	5	6	7
80%	SIN	0.0	2.40	-0.23	-3.08	3.05	-2.20	-0.23	0.83
	COS	2.52	-0.74	2.93	-1.55	-1.53	2.38	0.24	0.33
65%	SIN	0.0	6.29	-0.47	-4.89	5.87	-4.84	-0.45	1.78
	COS	4.43	-2.32	5.38	-2.40	-2.27	4.88	-0.09	0.40
45%	SIN	0.0	13.75	0.15	-10.77	8.95	-6.29	-0.21	1.93
	COS	5.24	-4.12	5.47	-1.18	-2.87	6.29	-0.13	-0.14
35%	SIN	0.0	18.45	1.46	-11.02	5.44	-5.29	0.09	1.38
	COS	6.17	-4.61	4.50	-0.57	-3.14	6.25	-0.35	-0.35
20%	SIN	0.0	26.67	3.07	-11.68	1.79	-2.56	0.49	-0.10
	COS	5.38	-5.71	3.20	3.26	-1.92	4.30	-0.15	-0.16

TABLE 31. CALCULATED BEAM AND CHORD BENDING MOMENTS, ALUMINUM BLADE, 0° TWIST, $\mu = 0.399$, $M_{1,90} = 0.434$, $\alpha_m = 0.5°$ (COND. 25).

COMPUTED BEAM MOMENT(IN-LBF)

STA/HARM		0	1	2	3	4	5	6	7
80%	SIN	0.0	-1.61	2.07	3.46	-0.61	-1.46	-0.01	-0.22
	COS	-1.63	0.60	-3.64	-0.24	-1.62	-2.78	-0.64	0.11
65%	SIN	0.0	-3.53	3.35	5.19	-0.26	-1.20	-0.19	-0.07
	COS	1.68	0.93	-2.56	0.96	-0.79	-2.38	-0.54	0.10
45%	SIN	0.0	-3.87	2.92	4.64	1.00	0.65	-0.10	0.17
	COS	7.53	1.04	1.65	2.48	0.63	0.94	0.16	-0.05
35%	SIN	0.0	-2.87	2.13	3.90	1.45	1.32	0.16	0.13
	COS	8.28	1.05	2.49	2.42	1.16	2.14	0.37	-0.11
20%	SIN	0.0	-1.31	1.20	3.36	1.95	1.94	0.62	-0.04
	COS	8.82	1.25	2.46	1.96	1.65	3.23	0.51	-0.15

COMPUTED CHORD MOMENT(IN-LBF)

STA/HARM		0	1	2	3	4	5	6	7
80%	SIN	0.0	1.40	-0.49	1.32	-0.42	-0.65	-0.03	0.00
	COS	2.44	3.08	-0.00	-2.02	-1.43	-0.41	0.05	-0.04
65%	SIN	0.0	2.97	-1.08	2.67	-0.83	-1.26	-0.07	0.02
	COS	5.93	0.30	0.23	-4.15	-2.93	-0.68	0.15	-0.09
45%	SIN	0.0	4.09	-1.47	3.39	-1.01	-1.53	-0.08	0.04
	COS	10.01	8.11	0.57	-5.38	-3.74	-0.66	0.24	-0.12
35%	SIN	0.0	3.99	-1.39	3.14	-0.91	-1.38	-0.06	0.04
	COS	11.13	7.45	0.61	-5.02	-3.46	-0.54	0.24	-0.12
20%	SIN	0.0	3.05	-0.95	2.16	-0.58	-0.89	-0.02	0.02
	COS	11.30	4.85	0.53	-3.43	-2.32	-0.28	0.18	-0.09

TABLE 32. MEASURED BEAM AND CHORD BENDING MOMENTS, ALUMINUM BLADE, 0° TWIST
$\mu = 0.502$, $M_{1,90} = 0.467$, $\alpha_m = 5.0°$ (COND. 44).

MEASURED BEAM MOMENT(IN-LBF)

STA/HARM		0	1	2	3	4	5	6	7
80%	SIN	0.0	-1.79	-0.51	3.89	0.23	-1.43	-0.66	0.22
	COS	0.20	3.15	-6.19	-5.95	-0.80	-0.74	-0.48	0.61
65%	SIN	0.0	-1.12	-0.84	7.16	0.44	-2.28	-0.51	0.14
	COS	5.76	6.41	-6.33	-9.20	-1.30	-0.94	-0.01	0.27
45%	SIN	0.0	-0.04	-1.12	9.70	-0.31	-0.21	0.14	-0.87
	COS	9.40	5.25	-3.94	-8.98	-1.73	0.05	-0.24	-0.25
35%	SIN	0.0	-0.05	-1.18	9.39	-0.59	1.26	-0.17	-0.16
	COS	9.62	3.89	-2.82	-8.82	-1.42	0.00	-0.14	-0.10
20%	SIN	0.0	0.00	0.58	7.98	-1.42	1.83	0.30	0.54
	COS	8.64	2.45	0.41	-7.67	-0.98	-0.73	0.96	-0.27

MEASURED CHORD MOMENT(IN-LBF)

STA/HARM		0	1	2	3	4	5	6	7
80%	SIN	0.0	1.01	-0.54	-2.66	4.73	-5.96	-2.25	0.90
	COS	2.05	-0.55	2.75	-2.06	0.24	-3.06	0.45	0.65
65%	SIN	0.0	3.45	-0.71	-6.53	9.72	-12.37	-4.21	1.73
	COS	3.60	-2.38	4.99	-3.78	0.12	-5.95	0.94	1.09
45%	SIN	0.0	8.77	-0.25	-12.00	11.39	-15.84	-3.80	1.77
	COS	4.55	-3.84	6.19	-3.76	-0.53	-7.54	1.64	1.01
35%	SIN	0.0	11.72	0.59	-12.30	9.42	-14.93	-2.16	1.11
	COS	5.61	-3.65	5.54	-3.44	-1.50	-6.12	1.40	0.46
20%	SIN	0.0	16.59	2.18	-14.13	3.01	-8.90	0.93	-0.57
	COS	5.79	-4.41	3.92	0.56	-1.52	-3.28	-0.12	-0.53

TABLE 33. CALCULATED BEAM AND CHORD BENDING MOMENTS, ALUMINUM BLADE, 0° TWIST
$\mu = 0.502$, $M_{1,90} = 0.467$, $\alpha_m = 5.0°$ (COND. 44).

COMPUTED BEAM MOMENT(IN-LBF)

STA/HARM		0	1	2	3	4	5	6	7
82%	SIN	0.0	-1.12	1.77	2.53	0.30	-0.01	0.15	-0.01
	COS	0.15	0.77	-2.56	0.45	-0.66	-0.67	0.07	0.12
65%	SIN	0.0	-1.80	1.58	3.43	0.43	-0.02	0.11	0.05
	COS	4.69	1.45	-1.08	1.51	-0.76	-0.69	-0.03	0.03
45%	SIN	0.0	-1.19	-0.08	3.11	0.71	0.23	-0.03	0.07
	COS	10.16	1.48	2.08	2.46	0.11	0.10	-0.12	-0.10
35%	SIN	0.0	-0.30	-0.52	2.98	0.93	0.44	-0.04	0.02
	COS	13.34	1.15	2.10	2.36	0.70	0.46	-0.07	-0.06
20%	SIN	0.0	0.82	-0.64	3.33	1.34	0.77	0.00	-0.09
	COS	16.13	0.74	0.98	2.09	1.50	0.92	0.06	0.05

COMPUTED CHORD MOMENT(IN-LBF)

STA/HARM		0	1	2	3	4	5	6	7
82%	SIN	0.0	-0.07	0.35	1.08	-0.43	-0.32	0.13	0.04
	COS	1.87	2.07	0.40	-1.24	-1.03	0.17	0.07	0.01
65%	SIN	0.0	-0.16	0.68	2.21	-0.90	-0.66	0.28	0.08
	COS	4.56	4.30	0.93	-2.57	-2.13	0.39	0.13	0.01
45%	SIN	0.0	-0.01	0.84	2.87	-1.18	-0.86	0.36	0.10
	COS	7.96	5.52	1.32	-3.36	-2.75	0.54	0.17	0.00
35%	SIN	0.0	0.06	0.77	2.67	-1.09	-0.79	0.33	0.09
	COS	9.11	5.05	1.25	-3.14	-2.55	0.52	0.16	0.00
20%	SIN	0.0	0.24	0.53	1.85	-0.73	-0.53	0.23	0.06
	COS	9.72	3.25	0.90	-2.15	-1.72	0.37	0.11	0.00

TABLE 34. MEASURED BEAM AND CHORD BENDING MOMENTS, ALUMINUM BLADE, 0° TWIST
$\mu = 0.299$, $M_{1,90} = 0.408$, $\alpha_m = 0°$ (COND. 68).

MEASURED BEAM MOMENT(IN-LBF)

STA/HARM		0	1	2	3	4	5	6	7
80%	SIN	0.0	-2.11	-0.90	2.05	2.09	-1.60	-1.14	-0.05
	COS	-4.09	0.34	-6.57	-3.63	0.28	-1.47	-0.01	0.01
65%	SIN	0.0	-2.76	-1.91	2.27	0.78	-1.53	-0.71	-0.53
	COS	1.80	2.46	-6.10	-6.25	-0.88	-1.57	0.07	-0.16
45%	SIN	0.0	-2.25	-0.14	1.10	-0.44	0.55	-0.17	0.03
	COS	7.63	3.01	-1.57	-6.57	0.51	0.42	0.33	-0.05
35%	SIN	0.0	-1.24	1.04	0.24	-0.70	1.07	0.44	0.10
	COS	8.78	3.10	-0.31	-5.35	0.53	1.59	-0.12	0.12
20%	SIN	0.0	2.35	3.11	-0.30	-1.58	1.89	1.07	0.08
	COS	10.17	2.62	1.89	-4.36	0.13	2.28	-0.95	0.27

MEASURED CHORD MOMENT(IN-LBF)

STA/HARM		0	1	2	3	4	5	6	7
80%	SIN	0.0	3.49	-0.49	-2.69	2.70	-1.73	-0.49	0.59
	COS	2.47	0.85	2.92	-2.33	-1.60	0.84	-0.26	0.76
65%	SIN	0.0	8.96	-0.60	-5.59	4.79	-3.63	-0.68	1.18
	COS	6.57	1.40	4.89	-3.65	-2.94	1.30	-0.44	1.60
45%	SIN	0.0	18.70	0.59	-8.18	4.74	-4.62	-0.70	1.27
	COS	9.05	1.76	4.36	-2.63	-4.72	1.16	-0.64	1.39
35%	SIN	0.0	24.81	2.06	-8.90	3.26	-3.86	-0.66	1.03
	COS	10.48	1.75	3.75	-2.45	-4.88	1.09	-0.46	0.53
20%	SIN	0.0	35.89	4.02	-9.10	0.69	-2.25	-0.25	0.06
	COS	12.32	2.50	2.91	-0.11	-3.92	-0.30	-0.35	-1.11

TABLE 35. CALCULATED BEAM AND CHORD BENDING MOMENTS, ALUMINUM BLADE, 0° TWIST
$\mu = 0.299$, $M_{1,90} = 0.408$, $\alpha_m = 0°$ (COND. 68).

COMPUTED BEAM MOMENT(IN-LBF)

STA/HARM		0	1	2	3	4	5	6	7
80%	SIN	0.0	-2.24	0.30	1.35	0.05	-0.42	0.01	-0.01
	COS	-2.56	1.76	-1.72	0.23	0.21	-0.42	-0.23	0.00
65%	SIN	0.0	-5.17	0.63	1.86	0.04	-0.26	-0.04	0.01
	COS	1.67	2.97	-1.62	0.80	0.14	-0.42	-0.16	-0.00
45%	SIN	0.0	-6.01	0.91	1.32	0.17	0.25	-0.06	0.02
	COS	8.63	2.81	0.20	1.31	0.03	0.14	0.10	-0.07
35%	SIN	0.0	-4.07	0.92	0.91	0.31	0.35	-0.03	0.00
	COS	9.31	2.17	0.87	1.26	0.10	0.43	0.15	-0.04
20%	SIN	0.0	-2.54	0.94	0.56	0.53	0.34	0.04	-0.04
	COS	9.64	1.45	1.40	1.10	0.29	0.77	0.16	0.05

COMPUTED CHORD MOMENT(IN-LBF)

STA/HARM		0	1	2	3	4	5	6	7
80%	SIN	0.0	2.08	-0.91	0.73	-0.39	-0.25	0.07	-0.02
	COS	1.36	2.26	0.16	-0.70	0.01	-0.04	0.06	0.05
65%	SIN	0.0	4.36	-1.90	1.38	-0.82	-0.47	0.14	-0.03
	COS	3.86	4.65	0.48	-1.44	0.01	-0.06	0.15	0.09
45%	SIN	0.0	5.91	-2.48	1.72	-1.06	-0.56	0.18	-0.04
	COS	7.19	5.89	0.84	-1.87	-0.00	-0.01	0.23	0.11
35%	SIN	0.0	5.72	-2.30	1.56	-0.98	-0.51	0.17	-0.04
	COS	8.21	5.36	0.85	-1.74	0.00	0.01	0.22	0.11
20%	SIN	0.0	4.26	-1.54	1.07	-0.65	-0.34	0.12	-0.03
	COS	8.65	3.45	0.69	-1.18	0.02	0.05	0.15	0.08

LIST OF SYMBOLS

A_n	Harmonic coefficient of cosine terms
a	Vertical intercept of regression line
B_n	Harmonic coefficient of sine terms
b	Slope of regression line
C_D	Drag coefficient
C_D/σ	Rotor drag coefficient
C_L	Lift coefficient
C_ℓ	Rolling moment coefficient
$C_{L_{max}}$	Maximum lift coefficient
C_m	Pitching moment coefficient
C_n/σ	Yaw moment coefficient
C_P/σ	Rotor power coefficient
C_{P_i}/σ	Induced power coefficient
C_{P_p}/σ	Parasite power coefficient
C_Q/σ	Rotor torque coefficient
C_L/σ	Rotor lift coefficient
C_Y/σ	Rotor side force coefficient
E	Modulus of elasticity, lb/in.^{2}
I	Area moment of inertia, in.^{4}
I_{EQ}	Equivalent area moment of inertia, in.^{4}
ℓ	Segment length, in.
L	Rotor lift, lb
M	Bending moment magnitude, in.-lb
M	Mach number

$M_{1,90}$	Advancing tip Mach number
q	Quality factor
R	Blade radius, in.
r	Multiple correlation coefficient
r	Blade radial location, in.
R_N	Reynolds number
t	time, sec
w	Blade segment weight distribution, lb/in.
Y_{cg}	Distance from blade segment quarter chord to blade segment center of gravity, in. (positive forward)
α	Angle of attack, deg
α_m	Mast angle of attack, deg
α_{TPP}	Tip path plane angle of attack, deg
δ_F	Flap angle on trailing edge flap airfoil, deg
μ	Advance ratio
ρI_x	Blade segment mass moment of inertia in out-of-plane direction, lb-sec^2
ρI_y	Blade segment mass moment of inertia in in-plane direction, lb-sec^2